2009-11-01

Optimizing the Release and Methylation of Bacterial Endospore Dipicolinic Acid

Aaron N. Nackos
Brigham Young University - Provo

OPTIMIZING THE RELEASE AND METHYLATION OF

BACTERIAL ENDOSPORE DIPICOLINIC ACID

by

Aaron N. Nackos

A dissertation submitted to the faculty of

Brigham Young University

in partial fulfillment of the requirements for the degree of

Doctor of Philosophy

Department of Chemical Engineering

Brigham Young University

December 2009

BRIGHAM YOUNG UNIVERSITY

GRADUATE COMMITTEE APPROVAL

of a dissertation submitted by

Aaron N. Nackos

This dissertation has been read by each member of the following graduate committee and by majority vote has been found to be satisfactory.

Date	Calvin H. Bartholomew, Chair
Date	Milton L. Lee, Member
Date	Richard A. Robison, Member
Date	William G. Pitt, Member
Date	Dean R. Wheeler, Member

BRIGHAM YOUNG UNIVERSITY

As chair of the candidate's graduate committee, I have read the dissertation of Aaron N. Nackos in its final form and have found that (1) its format, citations, and bibliographical style are consistent and acceptable and fulfill university and department style requirements; (2) its illustrative materials including figures, tables, and charts are in place; and (3) the final manuscript is satisfactory to the graduate committee and is ready for submission to the university library.

_____   _____
Date   Calvin H. Bartholomew
                                                               Chair, Graduate Committee

Accepted for the Department

                                                          _____
                                                          Dean R. Wheeler
                                                          Graduate Coordinator

Accepted for the College

                                                          _____
                                                          Alan R. Parkinson
                                                          Dean, Ira A. Fulton College of Engineering
                                                          and Technology

ABSTRACT

OPTIMIZING THE RELEASE AND METHYLATION OF

BACTERIAL ENDOSPORE DIPICOLINIC ACID

Aaron N. Nackos

Department of Chemical Engineering

Doctor of Philosophy

Rapid, portable detection of biological threat agents such as *Bacillus anthracis*
endospores ("spores") is extremely important given the real and perceived threats of
bioterrorism. Gas chromatography-mass spectrometry (GC-MS) is an excellent general
means for chemical detection, although special sample preparation and specialized
equipment are required to employ GC-MS for detecting biological agents such as spores
in the field.

A GC sample introduction probe consisting of a helical wire that can be retracted
inside a syringe needle, called a coiled wire filament (CWF), was employed as a simple,
passively-heated means to introduce the mixture of spores plus reagents for
thermochemolysis methylation (TCM) into the pre-heated GC inlet. There, reactions

between spore biomarkers and the TCM reagent mixture occur between 250-290°C. At these conditions, monomethyl sulfate salt mixtures are convenient and efficient TCM reagents for the rapid conversion of a key unique spore biomarker, dipicolinic acid (DPA), to its dimethyl ester (Me_2DPA).

By this process, Me_2DPA yields from spores were quantitatively assessed for different combinations of tetramethylammonium hydroxide (TMA^+OH^-), sodium hydroxide (Na^+OH^-), and hydrogen monomethyl sulfate ($H^+MeSO_4^-$). The best reagent mixture was found by varying the combinations of the ions within the neutral or basic system containing TMA^+, Na^+, OH^-, and $MeSO_4^-$ according to a novel scheme for design of experiments termed *ionic mixtures design of experiments* (IMDOE). A combination of the above ions was found that is near-quantitative in its methylation of DPA to Me_2DPA; this mixture contained a 1:3:1:3 mole ratio of TMA^+:Na^+:OH^-:$MeSO_4^-$. This yield of Me_2DPA was approximately a ten-fold increase over the best performance observed at the same conditions with tetramethylammonium hydroxide alone, the TCM reagent widely-used for GC.

The reactions involving $MeSO_4^-$ and TMA^+ as methylating reagents, plus relevant hydrolysis and methylation reactions involving acid and base plus water and methanol, were investigated. An overall model is presented and mechanisms are proposed for reasons why basic mixtures of $MeSO_4^-$ salts are more effective in methylating DPA compared to TMA^+ salts at the conditions employed.

ACKNOWLEDGMENTS

TABLE OF CONTENTS

LIST OF TABLES

LIST OF FIGURES

1 INTRODUCTION

1.1 *Motivation*

Throughout history, much devastation has been caused by bacteria, bacterial toxins, fungi, and viruses [see 1, 2-4], and the threat of biological warfare or epidemics still exists, particularly with anthrax. For example, anthrax attacks occurred in the United States in 2001, leaving 5 people dead and 17 others infected [5]. Other occurrences of anthrax infections have been documented throughout the world [6-9]. More recently, local anthrax "scares" have occurred, for example, a white powder was mailed to the Utah Governor's Office [10], delivered to the LDS temple in Salt Lake City [11], and apparently "deliberately placed" on the surfaces of tables at Utah Valley University in Orem [12, 13].

The etiological (disease-causing) agent of anthrax is the gram-positive bacterium *Bacillus anthracis*. Appropriately grown and prepared (e.g., into the infamous "white powder" form), weaponized endospores ("spores") of *B. anthracis* (Figure 1-1) disperse easily into the air, where they may be inhaled and cause anthrax infections in people. Thus, *B. anthracis* is a particularly lethal biological weapon, although other closely-related sporulating bacteria may be beneficial (e.g., *B. thuringiensis* is a natural pesticide). Confusing them with *B. anthracis* (and vice versa) can have detrimental, costly consequences.

To deal with the possible threat of an anthrax attack, research and development have been focused on devices and techniques for rapid, accurate differentiation and identification of multiple types of microorganisms. Attention has recently been directed at technology that is portable and/or capable of point detection. Existing technologies for rapid identification of *B. anthracis* and other pathogens have been reported and reviewed by many [e.g., 14, 15-24].
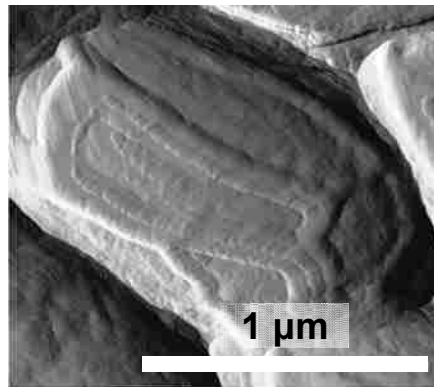
Figure 1-1. Atomic force microscopy image of a *B. anthracis* endospore [25].

Gas chromatography-mass spectrometry (GC-MS) is a versatile analytical tool for identifying a whole range of chemicals present in a mixture. Sampling of "simple" chemicals of low molecular mass and low polarity is relatively straightforward for GC-MS, particularly if an easy means of sample collection and introduction is available. In contrast, analysis of virtually anything suspected to be a biological weapon (e.g., material obtained from a mysterious package, swiped from a surface, or collected from the atmosphere) requires chemical and often physical modifications.

This author's research group is developing simple, rapid, *field-portable* methods and equipment intended to provide a small, portable gas chromatograph-mass

spectrometer instrument (also GC-MS) with ancillary capabilities related to biological warfare agent detection. The overall methodology involves thermal and chemical reactions that release and prepare "small" (i.e., less than several hundred amu) chemical biomarkers in an unknown sample for identification and quantitation using the GC-MS system. The information provided by the resultant chromatogram is examined to extract a biomarker profile, which is compared against a library database using an established algorithm. Inferences regarding the sample's identity are then made.

Although bacterial endospores of the anthrax-causing bacterium, *Bacillus anthracis* ("BA") are of primary interest, the research program has involved other spore types including *B. thuringiensis* ("BT") and *B. cereus* ("BC"; all three together are often referred to as the *Bacillus cereus* group) as well as *B. atrophaeus* spores (formerly *B. globigii* and *B. subtilis* var. *globigii*, hence the designation "BG"). BG is widely-accepted as a surrogate for *B. anthracis* spores in biodefense studies. The various studies undertaken have focused on the biochemical differences between these organisms that are readily discernible by GC-MS.

Although biochemical differences do exist, the dormant spore forms of these organisms are remarkably similar. For example, all possess robust, protective outer proteinaceous and peptidoglycan-based layers that protect their DNA contained within a dehydrated core; all have similar fatty acids and sugars that may differ significantly and reliably in their composition depending on species, strain, and growth conditions; and all contain a high abundance (5-15 wt%) of the spore-specific biomarker chemical, dipicolinic acid (DPA; see Figure 1-2). These features are reviewed in greater detail in Chapter 2.

Because of its general importance as a biomarker, sensitive DPA detection by GC-MS under a variety of chemical and procedural constraints constitutes the main topic of this dissertation. However, most aspects of the approach taken for DPA are generally applicable for any biomarker. It is anticipated that this dissertation will serve as a guide for other biomarker studies.

1.2 *Objectives*

The broad objective guiding this work is to contribute knowledge and develop technology for safe, simple, rapid, and sensitive detection of B. anthracis endospores (and other pathogenic bacteria) using portable GC-MS. With this objective in mind, the work documented in this dissertation has been directed toward a more specific objective: to optimize the yield of the dimethylated form of dipicolinic acid (DPA), a key bacterial endospore biomarker (Figure 1-2) using a protocol that is simple and compatible with GC-MS. Although DPA (as its calcium salt, CaDPA) is the "natural" form of this spore biomarker, its dimethyl ester, Me_2DPA ("Me" denotes the methyl group), is more amenable to GC-MS analysis and is more thermally stable.

Pursuit of the above objectives materialized three additional objectives: (1) to understand the endospore structure and its important relationships to the spore's chemical susceptibility for DPA release and methylation; (2) to rapidly methylate DPA with simple processes, equipment, and chemicals that are inexpensive, relatively safe and easy to handle, stable for weeks-months, and compatible with GC; and (3) to develop and demonstrate a novel chemical optimization methodology for conducting experiments

involving ionic reagents (since the most relevant chemical mechanisms were found to involve mixtures of reactive salt compounds).
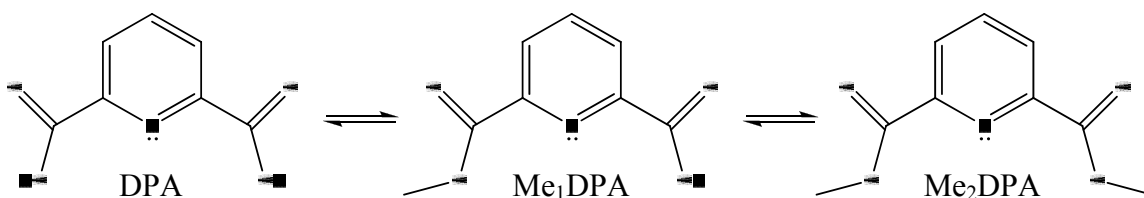
Figure 1-2. Overall reaction scheme studied for optimization. The desired product is Me₂DPA.

The foregoing objectives are justified by three key needs. First, spore detection limits must be as low as possible for field sampling where only minute sample quantities may be available, in contrast to the laboratory where samples are often abundant. Second, in the field, rapidity and simplicity are important due to equipment and power limitations. Third, biomarker-based differentiation relies upon qualitative and (often) quantitative consistency in the data. Since sensitivity, speed, and accuracy of information often compete against one another, it is important to conduct relevant research (both literature and laboratory) in order to understand the properties and interactions of spore biomarkers (DPA) with chemicals.

1.3 *Methods and approach*

The above objectives greatly influenced the approaches taken in these investigations. *Sequential design* was the guiding philosophy for making decisions about which experiments to pursue and which ones to abandon. That is, as information was acquired, attention was focused or redirected as necessary.

The most important methods and the overall approach to this research are briefly summarized below to orient the reader regarding the topics and organization of this work.

1.3.1 Multidisciplinary training

The areas of research covered in this dissertation are indicated by Figure 1-3. Due to the multi-disciplinary nature of the problems related to detecting spore DPA (many of which were outside the areas of expertise held by members of the author's research group), numerous publications spanning literally more than a century were consulted in order to seek out information relevant to the general problems, chemical properties, and experimental approach.

1.3.2 Samples

Both model compound DPA and representative *Bacillus* spores were studied. Investigations reported in this dissertation involved *B. anthracis* Sterne, *B. thuringiensis*, and *B. atrophaeus* spores with the assumption that the thermo-chemical behavior of important, shared biomarkers (e.g., the percent conversion of DPA to Me_2DPA during the procedures) is similar among these organisms, and thus results from one organism are reasonably applicable to another. From the literature, this assumption appears to be valid at high temperature where phenomena such as spore decomposition and biomarker release is rapid (usually, above 150°C). Thus, the optimal conditions that effect DPA biomarker release and conversion in one species are assumed to apply to other species (even though the relative absolute amounts of DPA may differ between organisms).
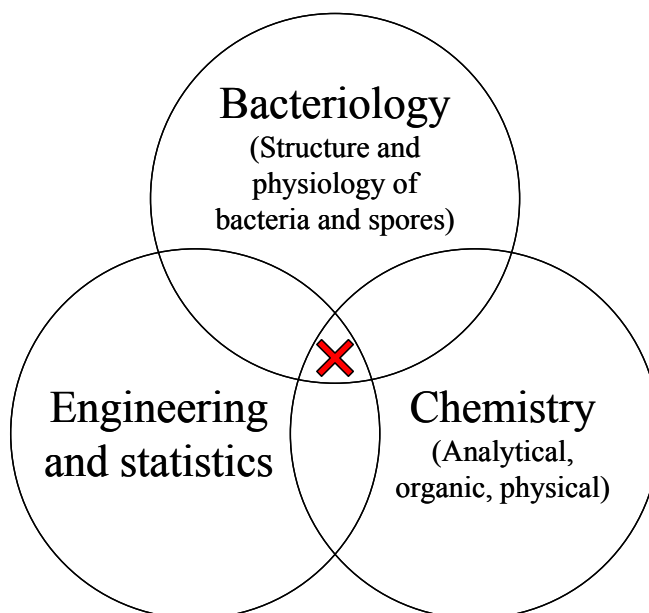
Figure 1-3. Disciplines forming the basis for this dissertation. The "X" indicates the purview of this work.

1.3.3 Instrumentation

The overall analytical approach is based on chromatographic analysis of bacterial endospore DPA and its methylated derivatives using both gas- and liquid-chromatography (LC). Other analytical methods and instrumentation (e.g., scanning electron and visible microscopy, flow cytometry, and pH measurements) were also employed.

Coiled wire filament (CWF) sampling probe. A unique means to introduce spores (and virtually any solid sample) into a GC was adopted to rapidly and easily sample bacterial spore suspensions [26]. A tiny, coiled platinum wire filament was attached to a retractable socket sized to fit inside a syringe needle housing (Figure 1-4). A small sample (< 1 μL) is collected by dipping the coiled wire filament in a liquid containing spores plus reagents that function to chemically release and modify spore

biomarkers so they are suitable for GC-MS analysis. The solvent is then air-dried

(evaporated) from the sample, the coil is withdrawn inside the needle, the needle is

pushed through the GC injection port septum, and finally the coil is rapidly extended

inside the injection port where thermally-driven reactions occur to release and convert

biomarkers to volatile, thermally stable forms that are convected into the GC separation

column. Because the CWF was invented "in-house," its performance as a GC sampling

device is given detailed attention.
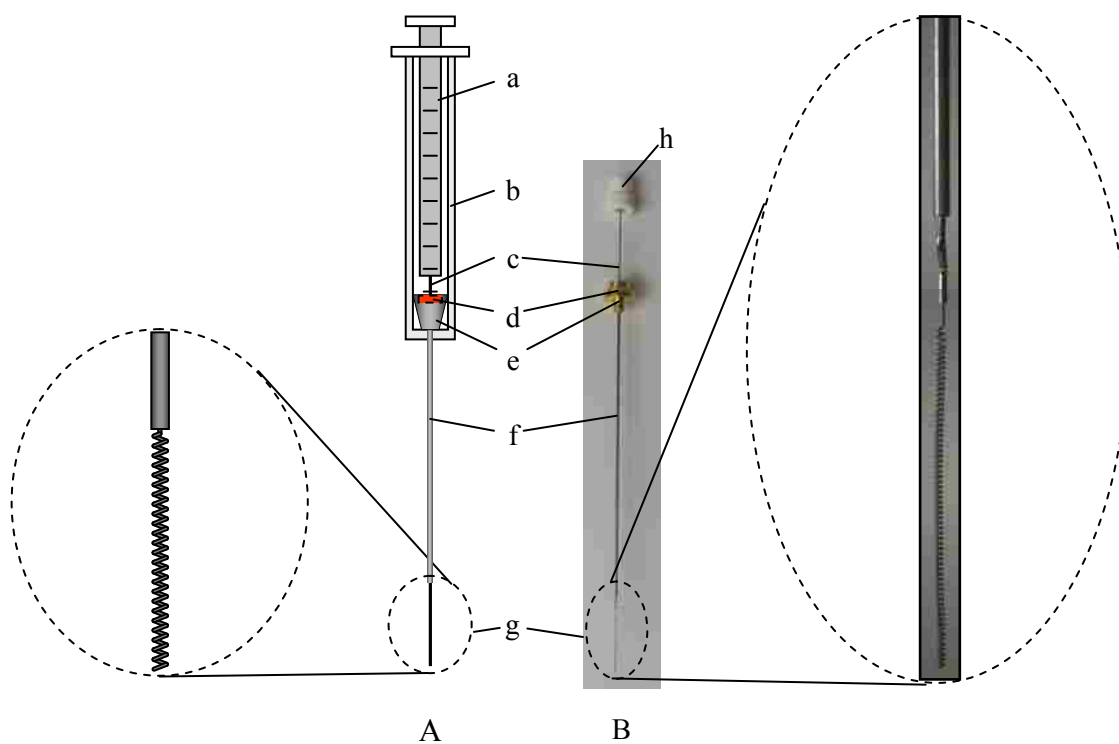
Figure 1-4. Schematic (A) and photograph (B) of the coiled wire filament assembly. (a) Syringe-like plunger pushing means, (b) syringe barrel, (c) in-needle plunger, (d) sealing septum, (e) brass compression fitting/needle base, (f) needle, (g) coiled wire filament sampling probe, (h) hub for attaching the in-needle plunger to the syringe-like plunger.

Gas chromatography-mass spectrometry (GC-MS). Based on other

publications and our experience, a general analytical protocol was adopted as the broad

basis for bench-top laboratory investigations of spores and model compounds using gas chromatography. A detailed description of the protocol is presented in Section 3.4.1. Briefly, it involves combining spores with methanolic sulfuric acid, tetramethylammonium hydroxide, and possibly other alkali hydroxides, which are collected by the CWF and analyzed by GC-MS as discussed above.

Liquid chromatography (LC). Analysis of DPA and its methyl esters by LC was conducted (1) to investigate the kinetics of some possible reactions of DPA that might occur in methanol/water solution and (2) to quantify the total amount of DPA in a given spore sample.

1.3.4 Computations

General. Since most computations were straightforward and could be accomplished using conventional desktop software tools available in Microsoft Excel, MathCAD, and R, they do not merit attention here. However, a few problems required noteworthy modeling software and development of a novel statistical method.

Modeling. Chemical and kinetics models for acid-catalyzed esterification of organic acids and base-driven hydrolysis of these esters were developed following a careful review of the literature on this topic. First-order models were fit to kinetics data obtained for DPA methylation and for hydrolysis of DPA methyl esters. In addition, the first-order kinetics of formation of a strong methylation reagent, $HMeSO_4$ (hydrogen methyl sulfate), were calculated from experimental data. A simple model for the heating rate of the CWF was also produced according to the "lumped capacitance" method.

Statistics. Of particular interest was finding a relationship between the composition of the chemical derivatization reagents and the yields of biomarker products in the gas chromatograph. This objective motivated the development of a special way to design experiments involving mixtures of *ions*, generally referred to here as IMDOE for Ionic Mixtures Design of Experiments.[1] Being charged, ions are physically restricted in how they may be combined (unlike neutral species). To deal with this problem, an approach reliant upon convex mathematical set theory was established and carried out. The details and mathematical justifications of the method are included in Appendix A and Appendix B and will be expanded and published elsewhere.

The work presented in this dissertation is, so far as this author is aware, unlike anything ever done before in gas chromatography, yet it parallels established methods for DOE involving multicomponent constraints on the mixtures [27]. A collection of studies by Schrevens, De Rijck, and (in some cases) Cornell [28-34], of which this author was unaware until after the bulk of his work, describe an almost identical, mixtures-based approach for investigating the effects of different combinations of dissolved salts on plant growth. Because the methodology is general, IMDOE is useful for many situations where complex mixtures of ions or salts are studied.

Variations of the GC-MS instrument operating parameters were <u>not</u> included in any experimental design for several reasons. Early work by a fellow graduate student established the optimal conditions for spore DPA and fatty acid methyl ester analysis for a specific chemical derivatization mixture. Because these conditions became the *de facto* standard method and since there were already many variables to explore relating to the

---

[1] The term DOE, for Design of Experiments, is commonly used in the field of statistics.

composition of chemical reagents, no significant modifications to the general
chromatographic parameters were made. However, the knowledge gained from this
dissertation invites additional studies for further optimization of GC-MS operational
details.

1.3.5   Summary of overall approach

In conclusion, this work's specific objectives were addressed through a
combination of searching prior literature, experimentation using GC-MS and LC, and
implementation of chemical, physical, and statistical models. The myriad phenomena that
underlie the general approaches taken have provided ample research opportunities
covering a wide variety of disciplines (Figure 1-3). The information gathered here
demonstrates the importance of a systems-based approach to solving problems.

1.4   *Overview of research progression*

The work performed towards this dissertation involved many detours and dead
ends. One set of lessons learned is mentioned here in order to clarify the reasons for some
of the experiments reported. At some early point in the research, a method was
established in which bacterial endospores were combined with tetramethylammonium
hydroxide (TMA-OH), a chemical known from the literature to be active in DPA
methylation when heated (cf. Figure 1-2). This reaction was carried out by transporting
the spores + TMA-OH into the GC inlet using the CWF. It was later discovered that
addition of methanolic sulfuric acid (H_2SO_4 in MeOH) to the spores prior to addition of
TMA-OH greatly improved yields of Me_2DPA, which improves detection sensitivity.

Although literature publications provided many important insights regarding the important reactions, the reasons for enhanced Me_2DPA yields, being initially unknown, formed the basis for some investigations conducted in this dissertation. Specific topics investigated include (1) acid catalysis by H_2SO_4 as a possible contributor to increased Me_2DPA yields, (2) base hydrolysis upon TMA-OH addition as an antagonist to Me_2DPA formation, and (3) thermal methylation reactions (i.e., thermochemolysis methylation, or TCM) which function as rapid means for Me_2DPA production from DPA when the latter is heated in the GC injection port in the presence of appropriate reagents. Because the processes occurring during solvent evaporation from the CWF are complicated and were thought to be relatively (although not entirely) insignificant compared to what occurs during the heating step, they were not investigated in detail, but are discussed in the context of present knowledge.

The initial hypothesis for the effect of sulfuric acid on the DPA conversion efficiency ("**Paradigm A**") was tested and revised twice to become "**Paradigm B**" and ultimately "**Paradigm C**" as more information was gained in the laboratory and gleaned from the literature. The literature studies and experimental results included in this dissertation reflect this process and validate the conclusions.

> **Paradigm A:** H_2SO_4 catalyzes methylation of DPA in methanol.
>
> **Paradigm B:** H_2SO_4 breaks up or permeabilizes the spore to release DPA, and SO_4^{2-} additionally sequesters calcium, a known poison to the reaction of carboxylic acids with TMA^+
>
> **Paradigm C:** In methanol, H_2SO_4 self-methylates to form $HMeSO_4$ ("monomethyl hydrogen sulfate"), which, in acidic or salt form (e.g., TMA-MeSO_4, NaMeSO_4), is much more highly active in methylating DPA than is TMA-OH. In addition, the features of **Paradigm B** still operate.

Since these general ideas formed the basis for the experiments, they are referenced periodically in the dissertation and are given particular discussion in Section 10.1 and Appendix C.

1.5 *Roadmap for remainder of dissertation*

In Chapter 2, a thorough literature review is presented in which pertinent aspects of the three broad topics indicated by Figure 1-3 are covered in turn to provide the background necessary to justify and interpret the experiments that have been performed. Chapter 3 covers the details of the experimental methods and Chapter 4 aspects of modeling and design of experiments. Chapters 5-9 presents the results and discussion for a variety of relevant topics. Chapter 10 presents an overall conceptual model based on the experimental results and information available in the literature. Finally, Chapter 11 brings together the overall conclusions and recommendations for future work. The material in the Appendix chapters provides additional information and learning about relevant subjects that could not be included in the body of the dissertation. Of particular importance is Appendix A, the methodology (equations and code) used to justify experiments with mixtures of ions.

2 BACKGROUND

This chapter reviews the structure and composition of bacterial endospores, mechanisms for methylating carboxylate-containing biomarkers (of which DPA is a key example) in preparation for GC-MS, and methods for modeling those reactions.

2.1 *Biology*

2.1.1 Chemotaxonomy

Chemotaxonomy entails the identification and measurement of chemical *biomarkers* present in organisms for classification, the latter term referring to compounds (usually organic) that are either by themselves unique or present as a group of similar compounds in a distinct combination (relative ratio) with respect to one another. Although biomarker molecules may be structurally free (e.g., metabolites), many biomarkers are integrated structural units, chemically bound within the organism's constituent oligomers or polymers [35]. Even smaller biomarkers such as individual fatty acids are covalently bonded to phospholipids and sometimes proteins. Thus, chemical, mechanical, and/or thermal treatments are usually necessary to release them.

Analysis of biomarkers by a chemical analytical technique renders possible the identification or characterization of a microorganism. Some biomarkers are species-specific, while others serve as general indicators of the presence of a living organism.

Compounds that fall in between these two extremes may be indicative of a certain class of organisms.

A discussion of the many types of biomarkers that are possessed by even a single species of bacteria is a broad topic beyond the scope of this dissertation. Briefly, fatty acids constitute an important class of biomarkers since they are generally present in all bacteria and exhibit enough diversity so as to be useful for identification [36, 37]. Dipicolinic acid (DPA) is a biomarker specific to bacterial endospores and forms the basis for the studies of this dissertation.

2.1.2   Overview of sporulation process

Certain bacteria form endospores (spores) under stress to protect their nucleic acids, enzymes, and small molecules plus the basic structure necessary for germination, all the while maintaining a state of near-zero metabolic activity until conditions that promote growth return. Figure 2-1 reveals the structural features of a mature *B. anthracis* spore as seen by cross-section. Although biological species and specific growth conditions have a significant effect on structural features such as spore size and thickness of spore integuments, the structure is generally the same for all species of spore formers. Spores are prolate spheroids usually around 1-2 μm in size, weigh on the order of a few picograms (0.25 to 10 pg, depending on the species) [38-40], and have bulk densities of about 1.2 to 1.4 g/cm^3, depending on several factors including moisture [41] and DPA [42] content. Despite their small size, spores are remarkably resistant to heat, chemicals, and radiation, a resistance due in large part to very unique structural features.

Initiation of sporulation is affected by a cell's growth environment (which includes nutrients, vitamins, minerals, pH, temperature, and extent of aeration) and is organism-specific. Depending on the particular organism, sporulation may be induced by limitation of carbon, nitrogen, and/or phosphorous sources [43], and the physiological state (e.g., growth phase, metabolic state, and thus gene expressions) of the spore plays a significant role [44]. Sporulation may be induced either by direct *starvation* (a bacterial culture depletes all nutrients in its growth medium) or by *endotrophic* means, where vegetative organisms are transferred from a complete nutrient medium into another medium lacking growth nutrients [44-48].
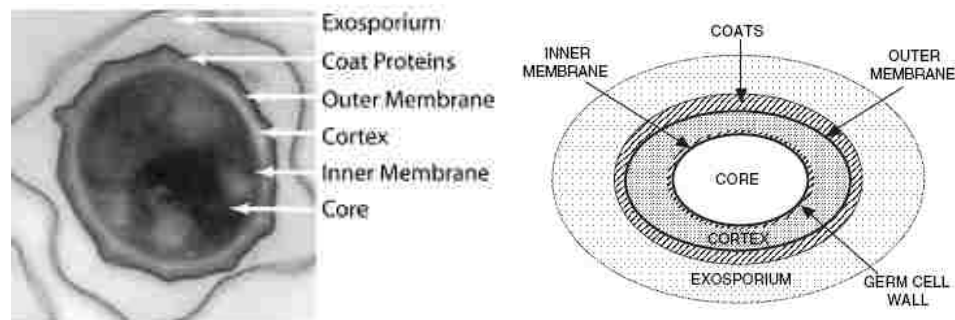
Figure 2-1. TEM of cross-section of *Bacillus anthracis* endospore, left [49], and schematic representation of this structure, right [50].

Development of a *single* spore proceeds more slowly than a vegetative cell, requiring from 6-10 h under typical laboratory conditions [44, 51-53]. The sporulation process entails a series of events involving tight genetic control to regulate the alteration of the cell. Despite the complexity, the process has been divided into seven stages based on the cytological changes that occur as the spore is formed, each stage occurring approximately at hourly intervals [44]. The stages, listed in Table 2-1 below, are not

necessarily discrete or isolated events but overlap to some degree. Figure 2-2 illustrates

some of these steps.

Table 2-1. Stages of spore formation.

Stage	Description
0	At the end of logarithmic growth (i.e., stationary phase or transition state [54]), a cell commits to sporulation following sensing of a variety of parameters, including nutrient levels.
I	*N/A* (This stage is no longer considered a distinct morphological state, and developing cells go from stage 0 to Stage II.)
II	The cell is divided into a *forespore* compartment (in which the spore develops) and a *sporangium* (mother cell) compartment.
III	The forespore is engulfed by the mother cell and converted into a *protoplast* (a bacterium with its cell wall removed), surrounded by two membranes.
IV	Peptidoglycan structures of the spore (the germ cell wall and cortex) are formed between the membranes and the developing spore becomes refractile.
V	Inner spore coat protein is deposited on the outer forespore membrane.
VI	Formation of the spore coat continues, with the outer coat proteins being deposited, and overall spore maturation continues. Uptake of large amounts of minerals occurs during Stages IV, V, and VI [55].
VII	The sporangium releases the mature spore by autolysis.
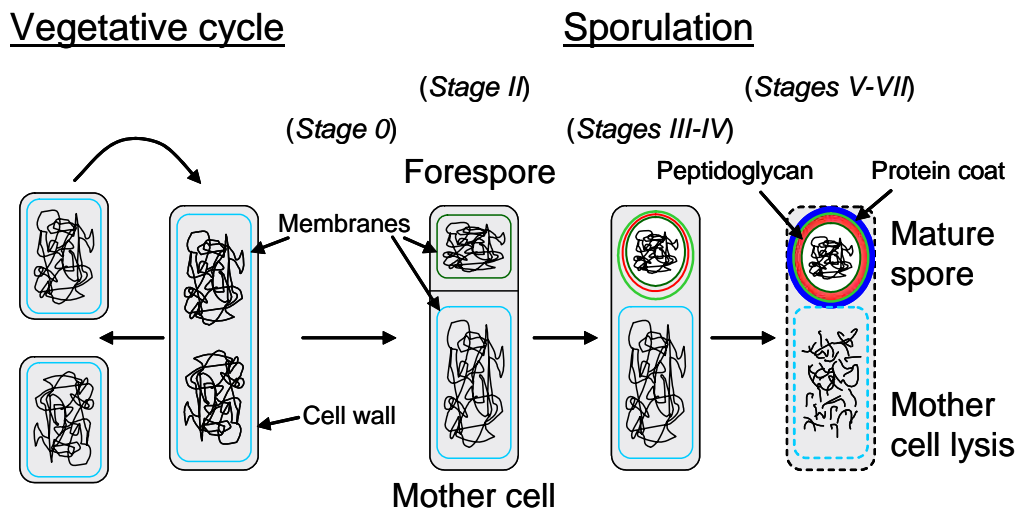
Figure 2-2. Life cycle of bacterial endospores [44, 56, 57].

2.1.3   Spore composition

The structure of the spore is unique and is responsible for its ability to resist chemicals, heat, desiccation, and radiation, only later to germinate and become a viable vegetative cell again. Here, each of these structural features is discussed in turn, from the inside outward.

2.1.3.1   *Core*

The spore core, referred to as a "vegetative bud" [58], contains a relatively dehydrated mixture of DNA, enzymes, proteins, ribosomes, dipicolinic acid (DPA) [59-62], divalent metals (most notably Ca^{2+}),[2] and other small molecules [61]. The mixture of these components results in a variety of polar and nonpolar interactions (hydrogen, electrostatic, and noncovalent bonding), including close association of DPA with DNA [61], due in part to binding by intercalation [64, 65] as well as protection of the spore's DNA by small acid-soluble proteins (SASPs; [50, 66-69]). Chelation between Ca^{2+} (or other divalent metals) and anionic small molecules [70] also occurs,[3] the most notable interaction being that of Ca^{2+} and DPA, although other small, anionic Ca^{2+}-chelators exist, e.g., L-glutamic acid, D-phosphoglyceric acid, and (in some species) L-sulfolactic acid [72, 73].

Core material has been termed "spore cement" [74] or gel [61, 75]. In this mixture, the spore constituents crucial for its future outgrowth (DNA and enzymes) are

---

[2] Ca^{2+} and DPA, which dominate the spore's ionic composition, vary at ratios ranging from 0.67 to 1.09 for various species of *Bacillus* [63], but are usually present at near-stoichiometric amounts.

[3] The topic of Ca^{2+} binding was given an excellent treatment by Levine [71].

protected [76], at least in part, because of the low content of mobile water. Some water is immobilized, being called "structured" [77, 78], "unfreezable," or "bound" [79]. As a result, complete dehydration is prevented [79]. Low mobile water content reduces the diffusivity of chemicals within the viscous, dehydrated core [80]. Maintaining such a low water concentration in the presence of hydrophilic solutes that would absorb large quantities of water in wet or humid environments is accomplished by a strong mechanical counterforce supplied by the external spore structures (called *integuments*), most notably the cortex, as described in the relevant sections below.

Of all small molecules in a spore, DPA is the most abundant and is generally unique to spores.[4] Although individual spores show variation in DPA levels [89], DPA is generally present at amounts between 5-15 wt% of the dry spore [90] and exists at "concentrations" (i.e., moles DPA per volume occupied) between 0.8 to 1 M, depending on species and growth media.[5] Specific per-spore DPA quantities for *B. subtilis* and *B. atrophaeus* have been reported to be about 1-5 $\times 10^{-16}$ moles/spore [89, 95, 96], while the amount is greater in larger *B. megaterium* spores (about 1 $\times 10^{-15}$ moles/spore) [96]. Numerous factors that are not discussed here influence the amount of DPA in spores; therefore, per-spore DPA content may vary substantially with species, strain, and growth conditions. For studies involving a given batch of spores, the average amount of DPA is almost always sufficient since spores are usually analyzed collectively.

---

[4] DPA is found in bacterial endospores of *Bacillus*, *Clostridium*, and other genera of sporulating bacteria. In addition, some *nonbacterial* fungi of the genus *Penicillium* release DPA into their culture medium [81-88].

[5] For reference, the water solubility of CaDPA is ~0-20 mM, with supersaturated solutions being stable temporarily at around 40 mM in TRIS buffer [91-94] or in the presence of amino acids (~10 mM) or gelatin (0.2%) [91, 93].

2.1.3.2 *Membranes*

Unlike their vegetative cell precursors, spores have two membranes: an inner one that lies between the core and cortex, and an outer one that resides between the cortex and the coat. As with other membranes, spore membranes serve as permeability barriers [97, 98] and contain a significant amount of protein, including enzymes [70] and, in the inner membrane, germinant recognition proteins [99]. Although some have questioned whether the outer membrane remains intact in mature spores [100], it presents a loose permeability barrier (e.g., to glucose [101, 102]) and becomes more sensitive to permeation with chemical and mechanical treatments that affect the coats (and hence the coat-outer membrane interactions) [102].

The inner membrane has unique properties that greatly reduce its permeability. It is quite immobilized compared to that of vegetative cells [77], a result of low core water content brought on by constriction due to the cortex (see Section 2.1.3.3 below). The result is reduced membrane surface area [103, 104], (probably) a tightly-packed, crystalline arrangement [105], and consequently reduced rates of transport of external and internal molecules to and from the core. Small molecules may permeate through this membrane (or its proteins) depending on their (1) molecular dissociation and ionic charge, (2) lipid solubility (lipophilic compounds permeate more readily), and (3) molecular weight and shape [106]. While Ca^{2+} and DPA are readily retained in the core by the membrane in this state [50, 78], water is quite permeable [78], as apparently are other solvents (including MeOH) and even acids (discussed below).

Various chemicals have been reported to damage or disrupt the permeability barrier of the inner membrane. Such treatments include ethanol (70 vol% at 65°C), strong

acid (0.3-1 M HCl at 24°C) [107], and oxidizing agents such as hydrogen peroxide,

ozone, and sodium hypochlorite [108, 109]. In contrast to the above chemicals, alkali is

rather ineffective in breaching this barrier [107], even though it is lethal to the spore (e.g.,

B. subtilis, *B. cereus*, and *B. megaterium* spores are "killed" or lose viability by exposure

to 1N NaOH for 1 h, although they remain refractile and stain resistant following this

exposure [110]).

2.1.3.3   *Cortex*

Enclosed by the two spore membranes, the cortex consists of two types of

peptidoglycan: an inner layer called the *primordial* cell wall (which ultimately becomes

the vegetative cell's wall upon germination and outgrowth), and a thicker outer layer

known as the cortex [111].[6] Both types of peptidoglycan consist of alternating *N*-acetyl-

glucosamine and *N*-acetyl-muramic acid sugar residues[7] cross-linked by peptides [57],

the primordial cell wall having a much greater extent of cross-linking than the cortex

proper [57, 114-117]. The result of reduced cross-linking within the cortex is a higher net

negative charge and increased elasticity relative to vegetative peptidoglycan [118].

A key function of the cortex is to maintain the low water content of the core by

applying pressure against this body to counteract the osmotic or turgor pressure. The

cortex may also present a diffusion barrier to chemicals [80, 119]. In this way, spore heat

resistance and other spore properties are influenced [120, 121]. Various models for the

pressure have been proposed (outward swelling against the coats, inward swelling against

---

[6] Unless specified otherwise, "cortex" refers to both types of peptidoglycan in this dissertation.

[7] Muramic acid is found nowhere else in nature except in bacteria [112, 113].

22

the core, and contraction due to tension), with evidence for and against each of them, although the latter appears most likely [61, 122-131].

From a variety of assumptions and models, values of 20-30 [126, 132], 200 [133] or even 500 [131] atm have been given for the pressure inside the spore core maintained by the cortex. Under such conditions, the tensile stress on the cortex is enormous—around 900 atm by one estimate [133]. The developing forespore may be under 10-20 atm prior to mature cortex formation [55]. The high pressure inside the spore core influences the spore's behavior in the presence of certain chemicals (and possibly heat).

2.1.3.4 *Coat*

Surrounding the outer spore membrane is the spore coat, a structure that consists largely of protein with smaller amounts of complex carbohydrate, lipid, and significant amount of phosphorous in some species [68, 134]. The coat differs significantly in complexity (e.g., thickness, number of different proteins, and their assembly) for different spores [135, 136]. It protects the spore from predation and the cortex against degradative enzymes (e.g., lysozyme), and can keep surfactants and other toxic molecules from reaching the core [61, 70, 119, 137-141]. Discovery of specific enzymatic or other activity of coat proteins is still in its infancy.[8,9] As judged by its porosity, the coat does not provide a significant permeability barrier to small molecules (such as germinants and sporicidal agents), but does serve as a sieve for larger molecules such as lysozyme [146,

---

[8] Even 5 and 10 years ago, an expert in the 50+ year-old field of sporology stated that no specific coat protein functionality, other than spore protection, had been discovered [135, 142].

[9] Some proteins in the coat are now known to be involved in the assembly of other coat proteins during sporulation [140] including a second coat-associated protein, CwlJ, which is a CaDPA-activated cortex lytic enzyme [143-145].

147]. The coat may protect the inner membrane from damage by some chemicals such as oxidizers [50, 109], and it may impede water absorption at high water activity [148]. Coats are often chemically disintegrated or permeabilized by reducing chemicals that break disulfide bonds such as dithiothreitol [149], mercaptoethanol [150], and thioglycolic acid [151, 152], usually with the addition of denaturants such as urea or sodium dodecyl sulfate.

2.1.3.5 *Exosporium*

Some spores (notably *B. anthracis*, *B. cereus*, and *B. thuringiensis* [153] but also *B. megaterium* [154] and even *Clostridium botulinum* [155]) contain a thin, loose-fitting layer external to the coat called the exosporium. Although debated, a more tight-fitting exosporium is probably present in other species such as *B. subtilis* [135, 156, 157]. The hydrophobic exosporium assists in binding to surfaces, including hosts [140, 158]. Exosporia of *B. megaterium* may have apical openings [101, 134, 154].

The *B. cereus* exosporium has been most thoroughly characterized because it is very loose-fitting and consists of protein, polysaccharide, neutral lipid, and phospholipid molecules [159, 160]. Some exosporium proteins are enzymatically active [161-163] and are known to contain spore-specific antigens [163]. For example, the exosporium of *B. anthracis* contains a distinctive oligosaccharide with a unique sugar monomer called *anthrose*, which is very specific to this spore type [164, 165], although it was recently shown to be present in lower abundance in some strains of *B. thuringiensis* and *B. cereus* [166]. A recent review on the spore coat and exosporium [140] is recommended for further details. The exosporium is not considered to be a significant permeability barrier.

2.1.3.6 *Mineral content*

Spores contain a considerably larger concentration and quantity of metal cations than vegetative cells. Divalent organic ions are of particular importance in sporulation (frequently, the higher the divalent cation level, the more heat resistant the spore) [61, 90, 167-172]. Of these, Ca^{2+} is almost always the most prominent, comprising 1.5-3.0 dry wt% of spores [93] and being about 20 times more concentrated in spores than in vegetative cells [173]. Depending on the growth medium, spores accumulate Zn, Ni, Cu, and Co [168]; Mn [168, 174, 175]; Mg [176]; and Sr and Ba [46] to different degrees (and minor amounts of other metals [49, 177]), depending not only on spore species and strain [38, 43], but also on absolute and relative concentrations of metals in the medium during sporulation [43, 178-180]. A preponderance of calcium is usually reported because conventional media contain high amounts of this cation. Ca^{2+} appears to impart the best overall heat resistance [e.g., see 72, 123, 167, 168, 176]. A large portion of the Ca^{2+} is chelated with DPA (and perhaps other components) in the spore core, as may also be Mg^{2+} and Mn^{2+} [93, 181, 182].

2.1.4 Representative *Bacillus* species

Although many members of *Bacillus* produce endospores, only a small number of species are of particular interest for investigation in our laboratory for various reasons. First and foremost, *B. anthracis*, as the non-virulent Sterne strain, is (likely) most similar in chemical composition to the virulent forms of the same organism that cause the disease anthrax. Second, *B. thuringiensis* (genetically similar to *B. anthracis* [183]) produces insecticidal toxins during sporulation [184], the mixture of which (spores + toxins) is

often distributed outdoors in powdered, granulated, or liquid-suspended form to protect

crops [185].[10] Third, *B. atrophaeus* (formerly, *B. globigii*) spores are frequently used as a

surrogate for *B. anthracis* endospores [188], although they are genetically and

morphologically different from members of the *B. cereus* group (e.g., *B. atrophaeus*

spores are significantly smaller than those of the *B. cereus* group and do not possess an

exosporium [189]).

2.2 *Chemistry*

2.2.1 **Overview of sampling approaches for GC**

It has been stated that "introduction of a sample into a GC column probably calls

for more attention of the analyst than any other part of the technique" [190]. This section

is dedicated to describing the coiled wire filament (CWF) that has been developed in-

house to introduce a variety of sample types (including spores + chemical reagents) into a

standard split/splitless GC inlet[11] with minimal user intervention and virtually no

requirement for sample cleanup steps.

The split/splitless (SS) inlet into which most GC samples are presented must

briefly be reviewed. It is standard on most instruments (including Torion's portable GC-

MS, the GUARDION-7[TM]; www.torion.com) and is designed to accommodate direct

---

[10] *B. anthracis* and *B. thuringiensis* belong to what is often called the "*Bacillus cereus* group" since all
three species of bacteria are quite similar genetically [183] and biochemically [186, 187]. Although *B.
cereus* spores have been investigated in our laboratory, they were not studied in this dissertation.

[11] The term split/splitless describes the operational feature of most GC inlets. During "split" mode some
portion of the injected sample plus the carrier gas bypasses entry into the column and flows on the *outside*
of the liner before exiting a split vent [Figure 2-3o]. "Splitless" flow occurs when the sample is carried into
the column in its entirety due to closing of the split vent. Each mode has advantages that cannot be
enumerated here.

injection of gas or liquid samples via a small hypodermic syringe or thermal desorption of a sample contained on/in a transportable body sized to be inserted in the inlet. SS inlets (ideally) rapidly effect volatilization of the sample and any solvent used to introduce it in an evaporation chamber (often a removable, high thermal mass, chemically deactivated fused SiO_2 "liner") before the sample is swept onto the column by the carrier gas [190-194] (see Figure 2-3). One feature of the SS inlet is that it is designed to remain hermetically sealed during sample introduction, which is usually accomplished by installing a compressed rubber or silicone-based septum (or some other means of sealing such as a Merlin Microseal® [195]). Although the SS inlet is a simple design that may be customized for use with a variety of sample introduction methods, it is ideally suited for sample introduction using some form of small needle.

Figure 2-3i identifies what is termed an "extendable body" to carry a sample into the GC inlet. The extendable body is most frequently employed in cases where solvent is not used (often called "dry sampling"). The extendable bodies designed for use with syringes have taken a variety of forms. Hollowed out plungers possessing a small side vent were developed for capillary uptake and carrier gas expulsion of a sample [196, 197]. Other extendable bodies intended mostly for solid samples have included straight [198], flattened and twisted [199, 200], or coiled [26, 201] wires or plungers with grooves [202] as well as tubes with "tongues" [203, 204], needles with troughs [205], or needles with "windows" [206]. Sorbent materials have been installed on the inside of capillary tubes or on fibers or hollow bodies that can be extended from within syringe needles [207-209], including helical-shaped metal wires extendable from within a syringe [210-213].
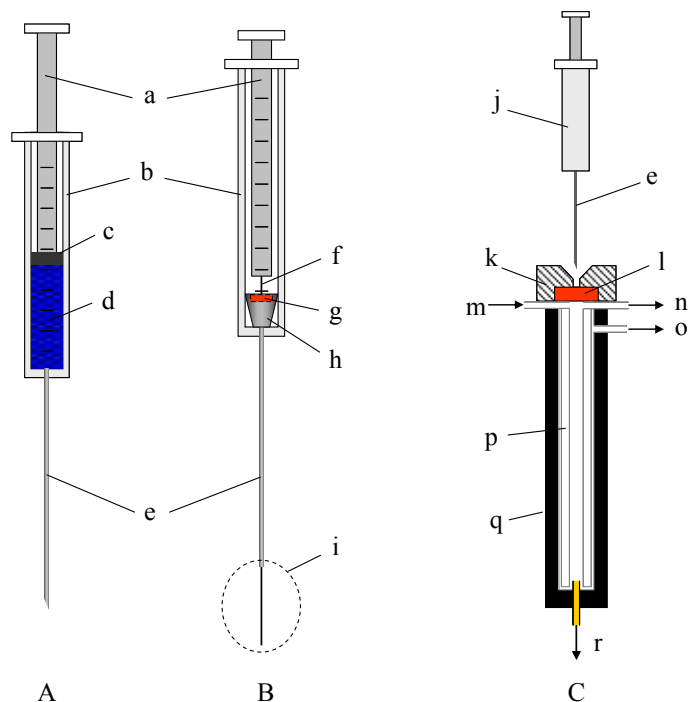
Figure 2-3. Common designs for sampling (A) liquids or (B) dry solid or sorbed samples in which a syringe penetrates a septum of (C) a split/splitless GC inlet. (a) Manually operated plunger, (b) syringe barrel, (c) gas-tight plunger, (d) liquid sample, (e) needle, (f) in-needle plunger, (g) sealing septum, (h) compression fitting/needle base, (i) extendable body carrying sample, (j) syringe or syringe-like sample introduction device, (k) septum cap, (l) GC inlet septum, (m) carrier gas inlet, (n) septum purge outlet, (o) split vent outlet, (p) liner, (q) heated injector block, (r) GC column entrance.

The coiled wire filament (CWF) employed for these experiments is another form of an extendable body that consists of a helical wire constructed of a sufficiently stiff, inert, refractory metal (e.g., PtIr) that can collect a wide variety of liquid-based samples by capillarity (capillary uptake), rapidly facilitate solvent evaporation (if desired), and enable sample introduction into any standard GC inlet with very little inlet contamination, even with "dirty" solid samples that contain large quantities of nonvolatiles. The coil is sized for compatibility with syringe-like devices used with split/splitless GC inlets, such as Supelco's commercial solid-phase microextraction (SPME) devices housed in 23-gauge needles. The dimensions of the CWF used in this study are presented in Figure 2-4.
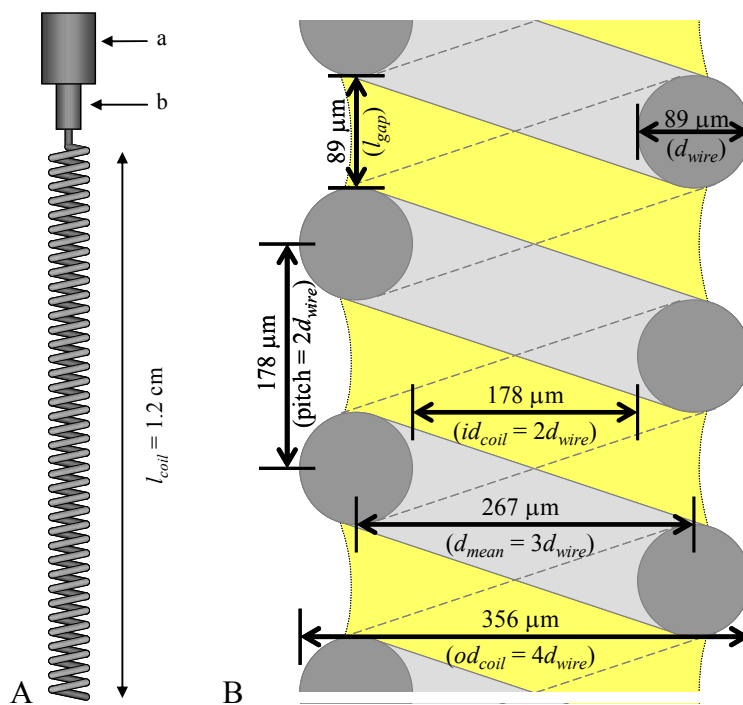
Figure 2-4. Schematics of coiled wire filament showing (A) an overall drawing (a indicates the needle and b indicates the movable plunger) and (B) an enlarged cutaway of the coil with specific dimensions.

The main objective in developing the CWF GC sampling tool was to produce a simple, rapid, sensitive, and reliable method for collecting, derivatizing, and transferring bacterial endospore biomarkers in a form suitable for chromatography to the GC column using as few steps as possible while avoiding excessive chemical "wear-and-tear" to the GC inlet and column. This objective is important because the method will be used in field scenarios by persons without extensive training in GC who are likely wearing restrictive personal protective equipment and thus cannot interact much with small samples, complex equipment, or involved procedures.

When dipped in a liquid-based sample, the liquid proceeds up the coil by capillarity. Liquids (including those with non-volatile components and solids) may be sampled directly because the non-volatiles or solids remain adhered to the wire surface

and exit the GC injection port with the wire. A dirty filament is easily and rapidly cleaned by rinsing with appropriate solvents and exposing it to a flame. The noble metal filament can be directly exposed to harsh or caustic samples, notably thermochemolysis-methylation reagents such as tetramethylammonium hydroxide, without damage.

Although ours appears to be the first syringe-extendable coiled wire for *capillary* sampling [26], other similar devices with coils have been utilized for GC sample introduction. For example, one end of a 1-mm diameter silver thread was tapered to a point of 200 μm and twisted into a 1 mm diameter, 7 mm [214, 215] or 12 mm [216, 217] long spiral. A 1-μL sample was applied to the coil with a microliter syringe [216, 217] or sample was collected by dipping [214, 215], the solvent was evaporated after 2-5 min at ambient conditions, and the silver thread was moved into the heated zone of the GC [214-217]. Additionally, free glass and metal spirals [218] were used as sample carriers, in one case with glass wool installed inside a Pt coil (1.5-2 mm o.d., 3 mm long) to allow it to retain more sample [219]. After the solvent was evaporated, the free coil was manually [219] or automatically [218] transferred inside a flash evaporator near the column inlet. Quite recently, a coiled stainless steel wire (2 cm long, 250 μm wire o.d., <1.35 mm coil o.d.) was used to introduce a sample plus derivatizing reagent (explained in the following paragraph) into a GC inlet, although the 5-μL liquid sample it carried was manually transferred to the wire [201].

2.2.2 Chemical requirements for GC-MS analysis

With low polarity separation columns often employed for GC, an analyte mixture separates well with good chromatographic peak shapes when it consists of thermally

30

stable chemicals generally of low polarity and small enough size so as to be sufficiently volatile (usually less than several hundred amu). However, most organic compounds in biological specimens ("biomarkers") are large and polar since they contain an appreciable quantity of electronegative heteroatoms (e.g., S, N, O) that are bonded with hydrogen.[12] Large biomarker molecules may be fragmented into smaller (hopefully still unique) biomarker products by chemical and/or thermal means. However, in addition to surviving polar functionalities, additional polar groups may be generated. In such cases, satisfactory chromatographic results are obtained only after these polar moieties are chemically converted to less polar forms, a process referred to as *derivatization*.[13] One of the most common derivatizations for GC is *methylation*, a process whereby biomarker polarity is attenuated by replacing hydrogens attached to polar moieties with a *methyl* ("Me" or "-CH$_3$") group. While reducing a molecule's polarity and increasing its volatility, methylation adds little mass to the derivatized molecule compared to other possible derivatizations, resulting in rapid chromatographic elution and oftentimes improved thermal stability of the molecule.

The carboxylate (-COOH) group is a common polar functionality in molecules of biological origin, and it is usually exposed by hydrolysis of esters (e.g., fatty acids in di/triglycerides) or amides (e.g., peptide bonds in amino acids). Since DPA contains two unesterified carboxylate groups, the mechanisms by which methylation on the carboxylate functionality may be brought about are now reviewed.

---

[12] It is often the identity and location of polar constituents that make the biomarkers diagnostic.

[13] A myriad of chemicals and procedures for releasing biomarkers and derivatizing them in preparation for characterization by GC are documented [37, 39, 220-235]. Many of these methods require lengthy, multistep workup procedures that are conducted in the liquid phase, and some employ dangerous or toxic reagents.

2.2.3 Mechanisms of carboxylate methylation and ester hydrolysis

There are two main categories of mechanisms by which carboxylate groups are either methylated or already-formed esters are hydrolyzed: (1) a multi-step tetrahedral mechanism and (2) a single-step substitution mechanism. Both of these reactions involve "attack" of a nucleophile (essentially a chemical with one or more unshared electron pairs—a Lewis base [236]) against a center of positive charge, but they differ in whether the carboxylate is the nucleophile or is the substrate attacked by a nucleophilic reagent.

2.2.3.1 *Tetrahedral mechanisms*[14]

2.2.3.1.1 Acid-catalyzed methylation reactions

Figure 2-5 presents the *reversible* Brønsted acid-catalyzed mechanism for the conversion of a carboxylic acid to a methyl ester [225]. The first step is protonation of the carbonyl oxygen—the atom with the highest electron density—which draws electrons from the carbonyl carbon. Next, MeOH (the nucleophile) attacks the carbonyl group and a tetrahedral intermediate is formed that is altered via proton exchange. Although there are three possible tetrahedral intermediates, only two of them (labeled as I and II in the figure) can eject a proton-stabilized leaving group (H_2O or MeOH). The reaction is quite reversible (H_2O and MeOH have a similar tendency to leave the tetrahedral intermediate) and so must be driven forward by addition of excess MeOH reagent and/or removal of H_2O. Water removal is important at high carboxylic acid concentrations because H_2O is

---

[14] An excellent summary of this mechanism in a more general sense than the present discussion has been provided by Adler and coworkers [237] and by Jencks and Gilbert [238].

released as the reaction proceeds [239, 240]. Water influences both the equilibrium and the kinetics since it solvates H^+ more strongly than does MeOH and may form structured clusters around H^+, inhibiting protonation of the carbonyl oxygen [241].

2.2.3.1.2 Kinetics of acid-catalyzed reactions

The rate determining step of this scheme is nucleophilic attack on the carbonyl carbon (all other steps involve relatively rapid proton transfers) and so the reaction kinetics proceed according to Eq. (2-1) [241], where C indicates concentration[15] and the subscripts A, AH^+, and B indicate, respectively, the carboxylic acid-containing moiety, the protonated carbonyl ($C=OH^+$), and the attacking nucleophile (for methylation, MeOH; for hydrolysis, H_2O).

$$-\frac{dC_A}{dt} = kC_{AH^+}C_B \qquad (2\text{-}1)$$

The concentration of C_{AH^+} may be computed assuming quasi-equilibrium occurs between unprotonated A and H^+ concentration (activity), resulting in a model of the form in Eq. (2-2).

$$C_{AH^+} = K_{eq}\, C_A\, C_{H^+} \qquad (2\text{-}2)$$

Eqns. (2-1) and (2-2) are combined and rewritten as Eq. (2-3), which may be simplified to a first-order form with rate constant k_1 if B is present in excess and k, K_{eq}, C_{H^+}, and C_B are approximately constant [Eq. (2-4)]. The deactivating effects of

---

[15] Concentrations are used in place of activities, although the latter are more precise in their description of the reaction, particularly for H^+ behavior. Further discussion on activity is given in Appendix E.

water on the catalyst activity are not included in this model but are mathematically

addressed elsewhere [241].
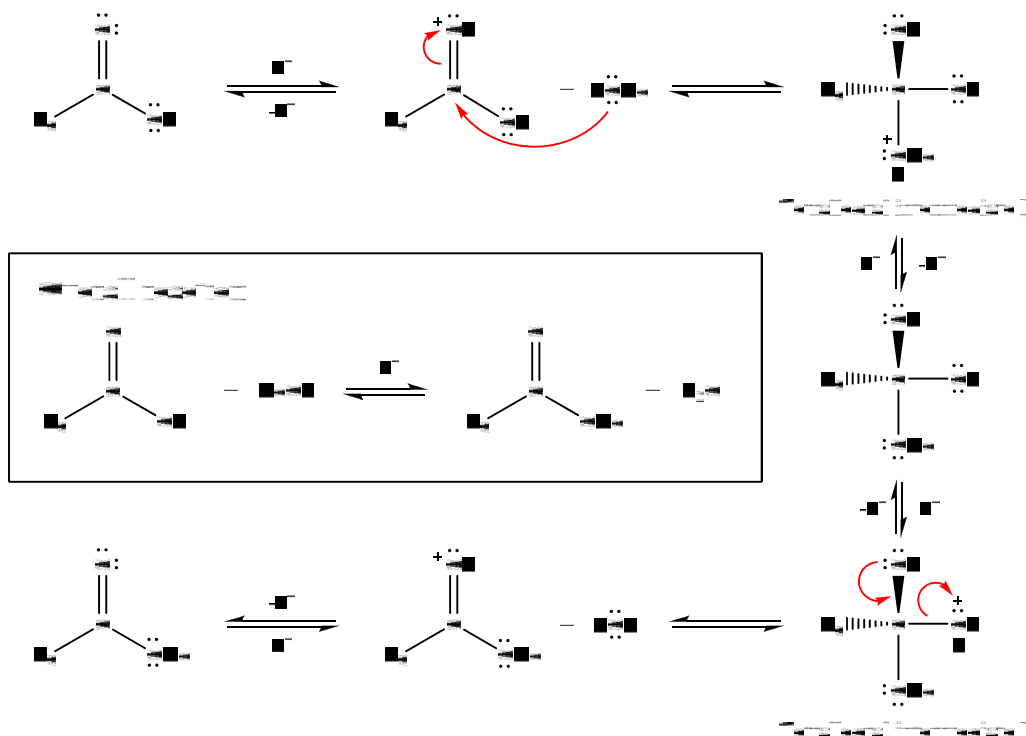
Figure 2-5. Tetrahedral mechanism for acid-catalyzed methylation of a carboxylic acid (clockwise) and hydrolysis of the methyl ester (counterclockwise).

$$-\frac{dC_A}{dt} = kK_{eq}\, C_A\, C_{H^+} C_B \qquad\qquad (2\text{-}3)$$

$$-\frac{dC_A}{dt} = k_1\, C_A \qquad\qquad (2\text{-}4)$$

2.2.3.1.3   Alkaline hydrolysis and transmethylation reactions

Alkali converts nucleophiles to more electron-rich, deprotonated forms (e.g., OH⁻

and MeO⁻) that are much more active for nucleophilic attack than their protonated

34

counterparts (e.g., H_2O or MeOH) [236]. Importantly, free carboxylic acids are deprotonated under basic conditions, so the carbonyl carbon of carboxylate anions is *not* attacked by nucleophiles (Figure 2-6) [239]. Consequently, hydrolysis of esters by OH⁻ in basic media is irreversible (Figure 2-7), although existing esters (e.g., di/triglycerides) that are not negatively charged at the carbonyl group in basic media are converted into methyl esters by methanolysis (i.e., *transmethylation*) with MeO⁻, which is reversible (Figure 2-8) [242].
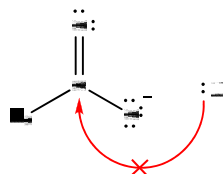
Figure 2-6. Carboxylate ions are not attacked by nucleophiles.
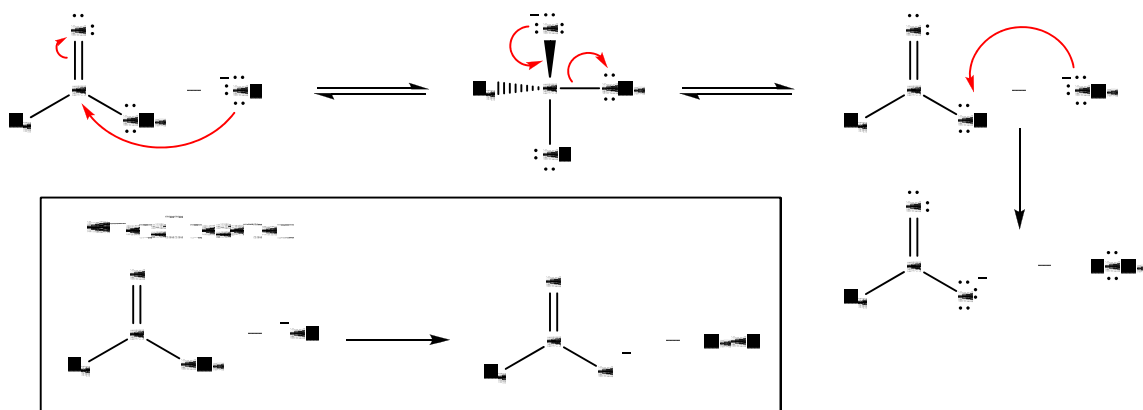
Figure 2-7. Hydroxide-promoted hydrolysis of a methyl ester.

Technically, hydrolysis via OH⁻ is appropriately termed *promoted* rather than *catalytic* since OH⁻ is consumed in the process, while in acid-catalyzed methylation and hydrolysis processes, H⁺ is regenerated [239]. Direct transmethylation by MeO⁻ *is*

35

catalytic because MeO⁻ is regenerated [Eq. (2-5); further pertinent discussion on this

reaction is given in Section 2.2.3.1.5 below].

$$OH^- + MeOH \rightleftharpoons H_2O + MeO^- \tag{2-5}$$
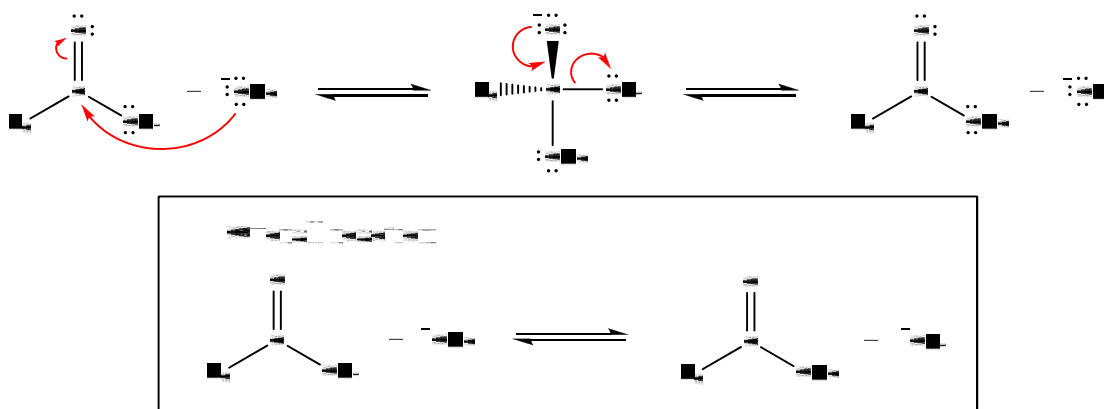
Figure 2-8. Methoxide-catalyzed transmethylation of an ester (i.e., *direct* transmethylation) [243].

Considered together, the overall reaction network involving OH⁻ and MeO⁻ is

complicated (Figure 2-9). The various reactions in Figure 2-9 correspond to the chemistry

already reviewed; *viz*, A and D correspond to irreversible hydrolysis (Figure 2-7), B

corresponds to Eq. (2-5), C corresponds to transmethylation (Figure 2-8), and E

corresponds to a proton exchange reaction similar to Eq. (2-5) (not shown).

Although the net reaction is irreversible hydrolysis (reactions A and D in Figure

2-9), direct transmethylation is fast enough compared to hydrolysis that esterified

molecules may form, albeit temporarily, in high abundance [244]. Some have found the

rate of methanolysis to be ~1500 times that of hydrolysis [245], which feature allows

methylation by methoxide to be conducted in the presence of water-containing samples at

room temperature in under 5 min, although the reaction must be quenched before the

extent of hydrolysis becomes significant [244, 246, 247].
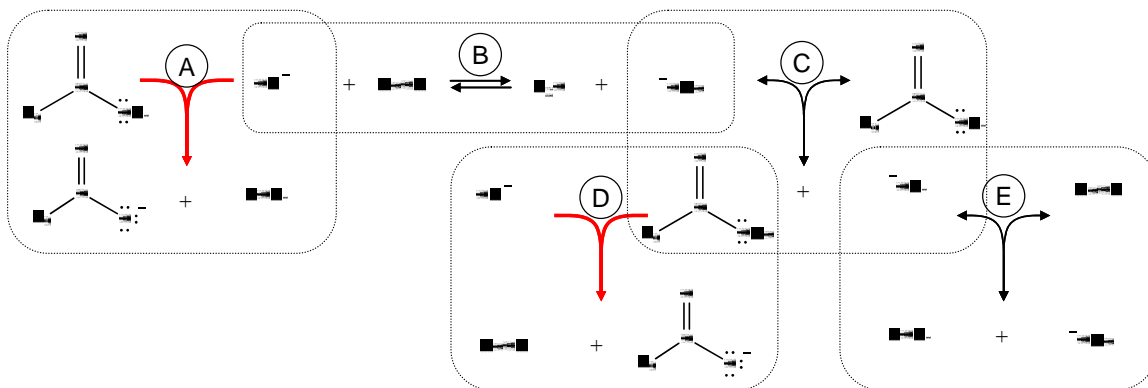
Figure 2-9. Combined hydrolysis and saponification of an ester in alcoholic base. Note reactions A and D are irreversible [adapted from 242].

2.2.3.1.4 Kinetics of base-catalyzed and promoted reactions

The rate of base-catalyzed/promoted reactions is modeled by Eq. (2-6), where C

indicates concentration[16] and the subscripts A and B indicate, respectively, the carboxylic

acid-containing moiety and the attacking nucleophile (e.g., OH⁻ or MeO⁻). In excess base

and when the solvent's composition and basic strength are fairly constant, the reaction is

nearly first-order in A, and k and C_B may be lumped together into k_1 [Eq. (2-7)].

$$-\frac{dC_A}{dt} = kC_A\,C_B \tag{2-6}$$

$$-\frac{dC_A}{dt} = k_1\,C_A \tag{2-7}$$

---

[16] Again, replacement of concentration with activity describes the reaction more exactly.

2.2.3.1.5 Implications of the OH$^-$ $\leftrightarrows$ MeO$^-$ equilibrium

The hydroxide ion, OH$^-$, is often obtained by dissolving an easily-dissociated hydroxide salt (e.g., NaOH, KOH, TMA-OH) in H$_2$O, is also produced by dissolving Na or K metal directly in H$_2$O. Likewise, the basic methoxide ion, MeO$^-$, may be generated by dissolving Na or K metal in MeOH. Another option is to dissolve the very strong base tetramethylguanidine (pK$_a$ = 13.6) in H$_2$O or MeOH, which not only converts water to hydroxide or methanol to methoxide for hydrolysis or transmethylation reactions, respectively, but even activates *free* fatty acids for attack by the alcohol [235, 248].

Regardless of how the hydroxide/methoxide is prepared, the equilibrium of Eq. (2-5) governs the relative abundances of these species. Because Eq. (2-5) lies mostly to the right [242, 249-252], in MeOH solutions with little water, essentially all OH$^-$ becomes MeO$^-$ [242]. Although a variety of different values for this equilibrium constant have been reported [see citations in 252], the results of Bender and Glasson [251], who quantified the fraction of hydroxide in dilute (~5-10 mM) NaOH in 0-100% H$_2$O (see Figure 2-10), are used for computations in this dissertation.
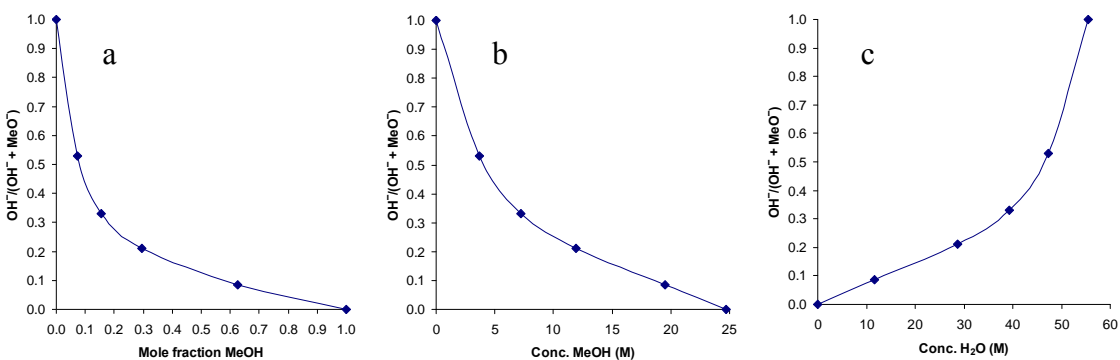
Figure 2-10. Fraction of total base (MeO$^-$ + OH$^-$) that is OH$^-$ (relative error ±15%) vs. solvent composition in H$_2$O-MeOH solutions. (a) MeOH mole fraction, (b) MeOH molar concentration, and (c) H$_2$O molar concentration (data are from [251]).

The key ramification of the results of Eq. (2-5) and Figure 2-10 is that the

concentration of OH$^-$ in a methanol/water solution is *not* equal to the concentration of a

hydroxide-containing reagent (corrected for any acid-base neutralizations) and so must be

measured or calculated.

2.2.3.2 *Direct substitution (direct methylation) mechanism, i.e., S$_N$2*

Figure 2-11 shows a generic alternative pathway to methylation in which

nucleophilic substitution occurs at a methyl (–CH$_3$, or "Me") group. An electron-rich

nucleophile, Y (e.g., a carboxylate oxygen), attacks the back side of the methyl group

substrate, displacing the leaving group, X (the *nucleofuge*) to which the methyl group is

initially bound. Seen in another way, the *attacked* group is an electrophile that readily

accepts one pair of electrons from Y and releases a second pair to X. This mechanism is

often abbreviated as S$_N$2 to indicate substitution nucleophilic bimolecular reaction [236].

Nucleophilic substitution reactions are first order each in the nucleophile and the

substrate, although cases with an excess of reagent, such as when the solvent serves as a

nucleophile, are pseudo-first order in the substrate [236]. An important feature of S$_N$2

reactions is the dependence of their rates on the basicity of both the attacking nucleophile

(Y) and the leaving nucleofuge (X), which is indicated by the pK$_a$ values of the non-

methylated/non-protonated nucleophile and nucleofuge. The more basic the attacking

group, the greater strength of the bond formed between it and the substrate (methyl

group). Similarly, the more basic the leaving group, the more energy is required to detach

it from the substrate to which it is bound. Although linear correlation of rate vs. pK$_a$ does

not exist for nucleophiles and nucleofuges of very different structures, the trend generally

holds that *as the pK$_a$ of the nucleophile increases, or the pK$_a$ of the nucleofuge decreases, the rate of bimolecular substitution increases.*
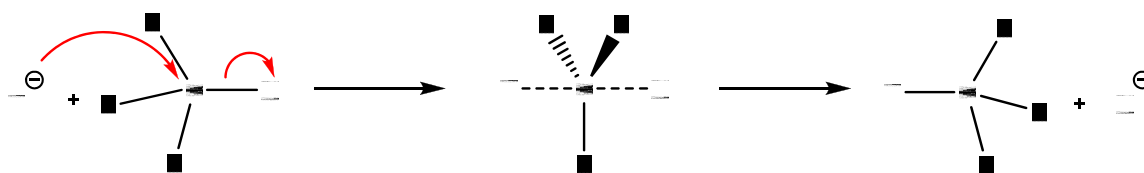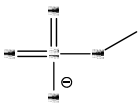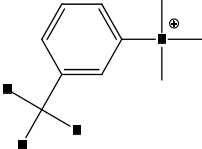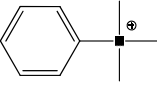
Figure 2-11. Bimolecular nucleophilic substitution on a methyl group.

Several of the many reagents active for S$_N$2 methylation are included in Table 2-2, the last three of which are commonly used to prepare samples by TCM for GC analysis [253]. Here, a somewhat arbitrary division is made by categorizing S$_N$2-acting reagents as "strong," "intermediate," or "weak" in terms of methyl donating activity if their pK$_a$ values are below 0,[17] between 0 and 3, or above 3, respectively. Strong methyl donors are often esters of strong acids [254]. Their activity can be so great that they are very toxic and mutagenic, and one should be very careful when working with them. In contrast, weak methyl donors function appreciably rapidly only at elevated temperatures. The effectiveness of these various methyl donors is discussed again later.

---

[17] pK$_a$ values <<0 are numerically less accurate than those given on the "normal" pH scale (~1 to 14) and so are of limited utility. Here they are seen as indicating that the de-methylated form has very little nucleophilicity, although the actual numeric value may be misleading in terms of methyl group affinity.

Table 2-2. Some active methyl donors and pK$_a$ values for their demethylated forms.

ID	Me donor reagent	Structure	Acid form (Aqueous pK$_a$)	Sources(s) for pK$_a$ values
1	MeI		HI (−10)	[255]
2	Me$_3$S$^+$		HMe$_2$S (−7.0)	[256]
3	Me$_2$SO$_4$		HMeSO$_4$ (−3.4)	[257]
4	MeSO$_4^-$		HSO$_4^-$ (+2)	[258, 259]
5	(*m*-CF$_3$Ph)Me$_3$N$^+$		H(*m*-CF$_3$Ph)Me$_2$N$^+$ (+3.3)	[260]
6	PhMe$_3$N$^+$		HPhMe$_2$N$^+$ (+4.6-5.2) (5.0-5.2 in MeOH)	[260-264]
7	Me$_4$N$^+$ (TMA$^+$)		HMe$_3$N$^+$ (+9.7-9.8) (9.8 in MeOH)	[261, 262, 265]

One possible area of confusion in discussions of methylating reagents that act via the S$_N$2 mechanism stems from the grammatical assignments of what is acting and what is being acted upon. In a practical context, the reaction is frequently discussed in terms such as "the reagent 'methylates' the analyte (biomarker)" or "the biomarker is methylated by the reagent." However, it is important to note that it is an electron pair of the *biomarker* (the *nucleophile*) that attacks the *reagent* (the *substrate*). *Stated simply, the nucleophilic biomarker attacks the methyl group of a methyl donor reagent in S$_N$2 reactions.*

2.2.3.3 *Tetrahedral vs. direct substitution mechanisms*

The direct substitution (S_N2) methylation mechanism possesses advantages over the acid-catalyzed tetrahedral one (Figure 2-5), provided conditions are such that methyl transfer is sufficiently rapid (promoted by high reagent concentration, temperature, and reagent reactivity). First, the tetrahedral mechanisms are slowed by steric and structural hindrances that inhibit both directed nucleophilic attack *and* conformational changes, while direct nucleophilic substitution suffers to a lesser degree from these effects [266-269]. Second, since the S_N2 reaction does not require strong acid or alkali to function, it is less destructive to the analyte molecule. Third, appreciably rapid overall methylation of nucleophiles may occur by the S_N2 route in the presence of water, even under basic conditions [270-273]. However, direct substitution may be at a disadvantage when contact between the methyl donor and carboxylate group is inhibited or if the reagent prematurely decomposes, volatilizes, or reacts elsewhere.

When both mechanisms occur, the dominant one depends on relative nucleophile strengths (pK_a values), stabilization of reaction intermediates (influenced both by pH and solvent identity), steric hindrances, activation energy barrier differences, and so forth. Particularly in the gas phase, reactions may differ greatly from solvated processes. Not only are thermodynamics of association in gas very different than in liquid [265, 274], but so are reaction rates, often because different mechanistic pathways are opened up [275]. The S_N2 pathway generally dominates (1) when the methyl donor is "strong" (i.e., the pK_a of the conjugate acid is very low) and (2) at elevated temperatures in the absence of solvent (since the tetrahedral transition state is less stabilized and protons are donated/removed with greater energy costs and lower probability of occurrence).

2.2.4 Reagent selection for GC derivatization reactions

The above mechanisms apply generally for preparing methyl esters prior to GC analysis. Literally hundreds of unique protocols have been published, which fall into two general categories: "off-line" and "on-line." Off-line involves mixing, heating, and analyte extraction/cleanup in a separate sealed container prior to GC. On-line (i.e., "on-column" [276], "intra-injector" [277, 278], or "at-line" [279]) entails conducting the reactions in or nearby the injector port. Tetrahedral mechanisms are always conducted off-line so the methylated products can be extracted from reagents prior to injection so as to prevent the introduction of GC column-damaging acids or bases. Although derivatizations involving the direct S_N2 mechanisms may be conduced with the off-line approach [e.g., 280], such methylations are usually done on-line since the entire reaction may be conducted with fewer steps. Direct liquid injection [281, 282] or solvent-less thermal decomposition from a solid probe have been employed as means for introducing the sample + reagent. The direct liquid injection technique is not commonly used due to reproducibility problems [283] and to deposition of residues inside the GC injector or column. Solvent-less introduction utilizes a probe that is heated either inside or just upstream of the injector [279, 284]. Almost without exception [e.g., 26, 201, 284] the probe is an actively heated analytical pyrolyzer.

The literature describing "on-line" derivatizations of carboxylates for GC has focused primarily on cationic methyl donors that are usually quaternary ammonium ions (items 5, 6, and 7 in Table 2-2) since they form salt complexes with carboxylate groups. The tertiary sulfonium cation (item 2 in Table 2-2) has received considerable attention as a methylation agent as well [253, 285]. Often, though not always, the anion of the methyl

donor reagent is a hydroxide, which can hydrolyze molecules having functionalities sensitive to cleavage by alkali (such as esters, amides, carbonates, and ethers) [286-294]—a key advantage for producing small molecules of biological origin. Although thermally-driven hydrolysis may mimic pyrolytic degradation, it occurs at lower temperatures [295] and greatly (usually desirably) alters the mechanisms and locations of bond cleavages compared to thermolysis alone [294], thus preserving functionalities. These features have led to the term *thermally assisted hydrolysis and methylation*, or THM [285, 296], sometimes referred to as *thermochemolysis* [297, 298]. A variation on the latter term, *thermochemolysis/methylation* (TCM), is preferred since it is a more general label for the process and is more accurate when chemical reagents effect more than scission by hydrolysis [297]. However, inclusion of "thermo" in thermochemolysis may be somewhat misleading since chemical lysis occurs at low temperatures as well.

2.2.5 Quantitative methylation of spore DPA by TCM

2.2.5.1 *Overview*

Specific experimental data regarding yields of Me_2DPA by TCM are lacking, although difficulty in obtaining spore core biomarkers has been recognized by a variety of studies. For example, significantly lower quantities of methylated DNA derivatives were obtained from *B. anthracis* spores than from vegetative cells by pyrolysis with TMA-OH at 450°C (presumably, both have the same quantity of DNA) [299]. By heating alone (in the absence of TCM chemicals), temperatures exceeding 250°C were required to sufficiently "release the majority of the DPA" [300-302] (although DPA begins to decompose around this temperature [181, 303]). In solution at room temperature,

mechanical disruption of spores via bead beating or sonication enhances extraction of amino acids and DNA [304-306].

2.2.5.2 *Summary of issues pertaining to TCM using TMA-OH*

The issues affecting quantitative conversion of spore TPA by TCM using TMA-OH are summarized in the following seven categories. The principles are generalizable to other reagents.

1. The chemical functionality of a compound to be derivatized has a significant impact on its extent of methylation by TMA-OH. The pK_a values of the sites where methylation may occur influence the relative amounts of products [253, 290]. The pK_a values for the first and second carboxylates of DPA are 0.5 and 2.2, respectively ([74, 173, 307-309]; see Appendix E for further details), much lower than the pK_a of Me_3N (~9.8 [261, 262, 265]), indicating that (at least in solution) the thermodynamic driving force for methyl exchange from TMA^+ to DPA is especially small relative to other biomarkers (e.g., the aqueous pK_a of isolated fatty acids is about 5 [310]).

2. The greater the number of sites where methylation may occur, the greater the variety in products due to partially-methylated compounds. Amino acids and oligopeptides [299, 311, 312] as well as nucleic acids and nucleotides [312, 313] are biomarkers with more than one functionality recognized to exhibit mixtures of partially methylated products. The same is true for DPA (see Figure 2-12), which may be unmethylated, singly methylated to the mono-ester (Me_1DPA), or dimethylated to the di-ester (Me_2DPA). Its decarboxylation product, monopicolinic acid (MPA), may be un- or singly methylated (as MeMPA). Although Me_2DPA, MeMPA (methylated monopicolinic

acid), and pyridine are readily detected by GC, only the first two indicate DPA since pyridine is also formed by thermal decomposition of DNA and proteins [314].

3. The TMA-OH-analyte ratio influences the yield of methylated products. For example, the maximum extent of methylation for each nucleotide belonging to a 16-base pair oligonucleotide model compound occurs at a different concentration of TMA-OH [312, 313]. For complete DPA methylation, the Me-donor:DPA ratio must be ≥ 2.

4. Both maximum temperature and temperature ramp rate affect observed TCM products. In practice, optimal temperature determination is based on trial-and-error [253] and whether or not pyrolysis processes are required to cleave bonds [285], which can require balancing minimizing secondary products against thermal dissociation and volatilization [315]. Thermochemolysis and pyrolysis are generally conducted at lower temperatures as the number and strength of required bond cleavages decrease.
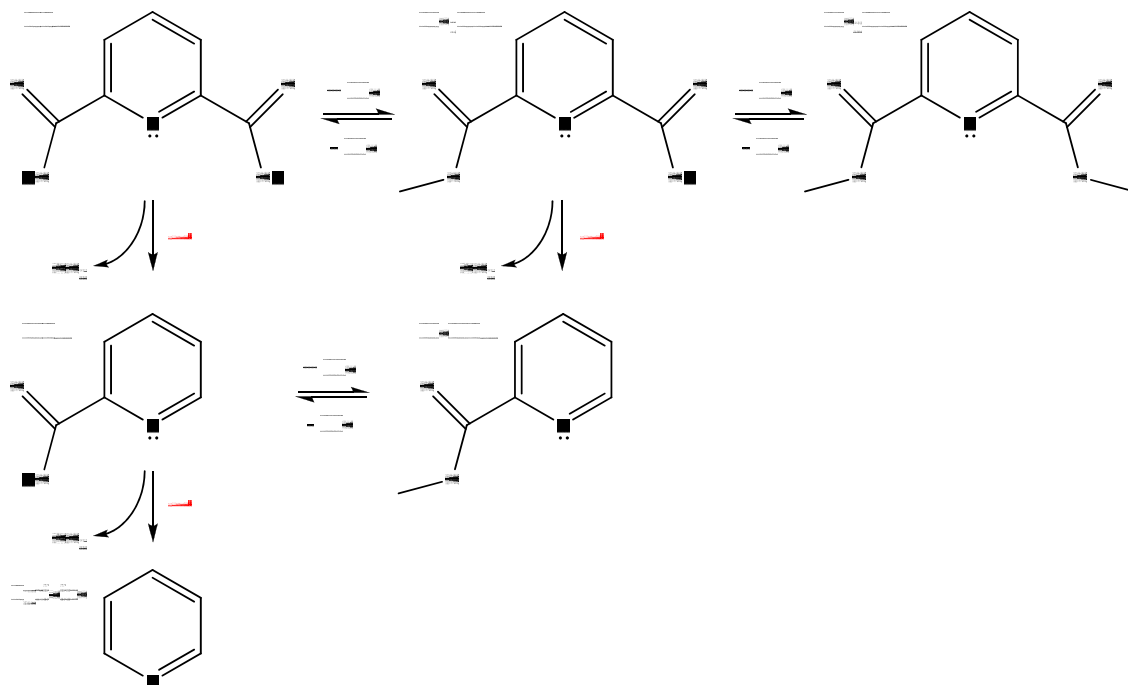
Figure 2-12. Possible methylated and decomposition products from DPA.

The thermal behavior of DPA is complex. Pure DPA sublimes at about 200°C [302] and decomposes between about 230-240°C [181, 303], releasing CO_2 and producing monopicolinic acid (MPA), pyridine [299, 316-319], and monopicolinic acid methyl ester (Me_1MPA) [39] (see Figure 2-12). Evidently, the spore structure [300] and/or the Ca^{2+} salt form of DPA [302] increase its thermal stability and decrease its volatility, as significant amounts of DPA and its decomposition products appear from spores above 250°C. DPA is protected from decarboxylation by methylation [299].

5. *The degree of mixing and degree of reagent access to potentially reactive sites influence yields.* Adequate wetting of the sample is necessary to produce "good interaction between the reagent and the reactive sites" in a sample [290], which may be enhanced by sonication and/or extending the contact time [279, 320], or choosing a solvent that will dissolve the sample [321]. Premature evaporation of solvent may lead to separation of TMA-OH from the analyte [285].

The spore's structure inhibits mixing of TMA-OH with DPA in solution. TMA-OH diffusion into the spore is slowed by features such as the inner membrane's very low permeability to alkali [107] and the core's viscous, dehydrated material [80] (which remains under pressure by the alkaline-hydrolysis/methanolysis-resistant cortex) that is stable under basic conditions due to (1) Ca^{2+} chelation structures, especially CaDPA [322], and (2) base-insoluble proteins.

6. *The solvent employed affects observed product distribution*, particularly with polymers and other samples that retain solvent after drying [253, 283]. Methanol is itself a reagent for methanolysis/transmethylation [288, 289] and apparently effects methylation via even more complex reactions [323]. Water may strongly impact the

chemistry, as different TCM products are observed in samples treated with aqueous TMA-OH than with methanolic TMA-OH [283, 324]. Peaks in addition to the desired FAMEs were found in chromatograms when bacterial samples were not completely dried of water before adding methanolic $Me_3S^+OH^-$. The extra peaks were "attributed to chemolysis products of proteins, sugars, and/or other cell constituents" [279]. Penetration into the spore core is more rapid at high temperature and at higher water activity [325], and water assists transport of charged species and/or hydrolysis reactions.

7. The ionic constituents of the mixture influence observed TCM products. Certain metal cations (e.g., alkali and alkaline earth metals) poison S_N2 methylation reactions by binding more strongly to carboxylate groups than TMA^+, reducing the substrate's nucleophilic strength and physically blocking the reaction [284, 323, 326]. Even in the difficult-to-come-by case of a well-homogenized mixture/solution of CaDPA and TMA-OH (cf. item 5 above), the stability of the former ion pair inhibits direct methylation of DPA because the nucleophilic activity of DPA carboxylates is reduced by DPA's chelation with Ca^{2+}.

In all the publications reviewed for this dissertation, only one [327] addressed the issue presented by Ca-DPA chelation as a possible inhibitor to the thermal methylation reaction (using Me_3PhN^+—item 6 in Table 2-2). Spores were hydrolyzed in 1.5 M H_2SO_4, the SO_4^{2-} (presumably) removed Ca^{2+} by precipitation of $CaSO_4$, then the DPA was solvent-extracted and finally injected with Me_3PhN^+ into a GC inlet at 310°C. Use of sulfuric rather than phosphoric acid for hydrolysis greatly increased recovery of Me_2DPA [327]. Whether the improved recovery was due to enhanced extraction of non-Ca-chelated DPA into the organic liquid or resulted from removal of Ca^{2+} was not indicated.

The foregoing facts all indicate that sub-quantitative yields of Me$_2$DPA are to be expected when TMA-OH is added alone to spores and the two are heated together in the GC inlet.

2.2.5.3 *Possible remedies to TMA-OH problems*

In addition to altering process temperature, time, solvent, etc., a different methylating reagent or counter ion may be employed. For example, TMA-HSO$_4$ increased FAME yields for certain FA samples relative to TMA-OH [328]. Degradation of polyunsaturated fatty acids was reduced by using a counter ion to TMA$^+$ of much lower basicity than OH$^-$ such as acetate [329, 330] (obtainable by addition of acetic acid [283, 331]), fluoride, or cyanide [276, 330]; adding short chain methyl esters such as methyl propionate [332, 333] or methyl acetate [334]; exchanging water for methanol as the solvent to reduce the apparent basicity of a given reagent [253]; and using a cation more active than TMA$^+$ at releasing a methyl group to a nucleophile so that the reaction may be performed at lower temperatures [253, 276, 330, 335].

2.2.5.4 *MeSO$_4^-$ as an alternative S$_N$2 methylation reagent*

One possible alternative methylating reagent is MeSO$_4^-$, either in acid or salt form. The pK$_a$ value of its acid form, HSO$_4^-$ (Table 2-2), should reflect its activity for transferring its methyl group to carboxylate nucleophiles. A thorough search of the literature did not reveal any use of MeSO$_4^-$ for GC derivatizations, although one 1960s paper reported the use of potassium *ethyl* sulfate (KEtSO$_4$) to ethylate carboxylic acids by "flash exchange gas chromatography." The reaction was carried out by mixing solid

potassium carboxylate salts with $KEtSO_4$ and heating at 300°C for 10 s in a capillary tube attached to a GC inlet. Equimolar ratios of the two gave the maximum yield with no side reactions, although low overall amounts of sample (3.5 mg) gave erratic degrees of ester formation for reasons that were not identified [336]. In a non-GC application, $NaMeSO_4$ methylated $NaNH_2$ and acetamide when they were ground together dry (or in a small amount of benzene) between 180-200°C [337]. Anhydrous salts of organic acids heated to 200°C in the presence of $HMeSO_4$ or $KMeSO_4$ produced methyl esters [338].

The literature on methylation by $HMeSO_4$ in a solvent is more prolific (although none of the publications discussed this reaction for GC, probably because the non-volatile residual sulfates would need to be removed prior to GC injection). For example, it was used (at various concentrations) to methylate the S atom in methionine when both were heated in MeOH in an ampoule from 73-115°C [339]; carboxylate groups of amino acids with heating to 80-90°C for 4 h [340] or refluxing at 69-75°C for 30 min [341]; and aromatic acid groups after reacting for 16 h at 20-25°C [342]. The foregoing examples were generally for the hydrogen form of $HMeSO_4$, although methylation proceeds quite well under basic conditions. N-functionalities of alkaloids were methylated by $HMeSO_4$ under reflux in *aqueous* NaOH or in fusel oils [270]. Phenoxide was methylated in the presence of basic $NaMeSO_4$ and $KMeSO_4$ (the former seemed to proceed more rapidly) [271]. A patent claims that basic (NH_4^+, alkali metal, and alkaline earth) salts of alkyl sulfates methylate dicarboxylic acids in 1-50% H_2O at elevated temperatures. The pK_a of the acids to be esterified must be higher than about 4 [272].

Monoalkyl sulfates were efficient alkylating agents of O and N nucleophiles (including NH_3, $MeNH_2$, Me_2NH, Me_3N, HPO_4^{2-}, PO_4^{3-}, $MeOPO_3^{2-}$, NH_2OH, SO_3^{2-}, and

$S_2O_3^{2-}$) in water at temperatures between 40-110°C [273]. Specifically, in water at 25°C, methyl sulfate was approximately 10^2 and 10^6 times more active in transferring methyl groups to dimethylamine (Me_2NH) than were trimethylsulfonium (Me_3S^+) and tetramethylammonium (TMA^+), respectively [273, 343]. In fact, $HMeSO_4$ will methylate Me_2S, producing $Me_3^+HSO_4^-$ [344].[18]

2.2.5.5 *$MeSO_4^-$ safety concerns*

The high methylation activity of $MeSO_4^-$ salts presents a possible danger. At present, they are not known carcinogens, although a related chemical, dimethylsulfate (Me_2SO_4), is reasonably anticipated to be so [345]. For example, although monomethyl sulfate was harmless, Me_2SO_4 was mutagenic and cytotoxic to Chinese hamster ovary cells [346]. Also, although manufacturers of $MeSO_4^-$ salts do not list it as a carcinogen on their MSDSs, it is generally given toxin and irritant status. A $KMeSO_4$ reagent recently received by this author included a "may cause cancer" label, although this possibility is probably not due to $MeSO_4^-$ itself but rather to the presence of some Me_2SO_4 formed either during its manufacture or upon storage. One MSDS lists a Me_2SO_4 content of 0.1% in $KMeSO_4$ [347], possibly a byproduct formed according to Eq. (2-8).

$$2KMeSO_4 \text{ (s)} \leftrightarrows Me_2SO_4 \text{ (l)} + K_2SO_4 \text{ (s)} \qquad (2\text{-}8)$$
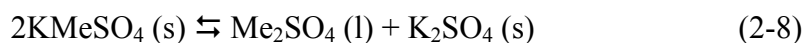
A bottle of (aged) $TMA^+MeSO_4^-$ received by this author contained a liquid, which (although not tested) may have been Me_2SO_4 formed by Eq. (2-9).

$$Me_4^+MeSO_4^- \text{ (s)} \rightarrow Me_3N \text{ (g)} + Me_2SO_4 \text{ (l)}. \qquad (2\text{-}9)$$

---
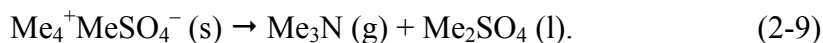
[18] The relatively strong affinity of Me_2S for the methyl group indicates that the relative pK_a of HSO_4^- and Me_2S are not accurate indicators of the relative reactivity.

Conditions that are known to produce Me_2SO_4 include evaporation of solvent MeOH from $HMeSO_4$ [348], applying a vacuum to $HMeSO_4$ [349, 350], and distillation of $HMeSO_4$ [350, 351]. Adding a neutral salt (e.g., NaCl) during distillation of $HMeSO_4$ to form Me_2SO_4 reduces hydrolysis of the latter, promoting higher yields [350, 351].

Since $HMeSO_4$ forms by mixing H_2SO_4 and MeOH [352-354], the presence of Me_2SO_4 in a MeOH/H_2SO_4 solution is suspected, although its content is generally negligible at low acid concentrations [355]. In solutions ≤ 5 wt% H_2SO_4 (≤ 2.2 vol%), Me_2SO_4 does not form [356]. Some authors have concluded that Me_2SO_4 formation requires H_2SO_4 in excess of > 75 wt% [357] (diethyl sulfate was formed in traces only at > 95 wt% acid in EtOH [358]), although other reports did not find Me_2SO_4 in any detectible amounts at -15, 23, or 82°C with MeOH and 95 wt% H_2SO_4 [359].

Curiously, formation of dimethyl sulfate *was* observed in methanol solutions of ~0.1-0.3 wt% H_2SO_4, $NaHSO_4$, and $KHSO_4$ following 20 min of ultrasonication at room temperature [360]. Perhaps ultrasonication increased the reaction rate. Catalytic processes (e.g., adding dimethyl ether) and high temperatures reportedly promote the formation of Me_2SO_4 as well [359].

2.3 *Engineering and statistics*

2.3.1 Deterministic modeling

Chemical reaction engineering relies heavily on models to estimate the best conditions in which to operate a process. Many models presume liquid- or gas-phase reactions in a homogeneous fluid that either reacts within itself or at an interface between itself and another phase. Since the properties and behavior of fluid portions are readily

measured or predicted from established physical principles and empirical data, such *deterministic* models are powerful. Deterministic modeling relies upon the assumption that at some scale one or more volume portions of the mobile/reactive fluid behave either as a uniform body or as a body with one or more well-defined gradients in chemical and physical properties. The body thus has characterized intensive properties (i.e., temperature, pressure, and concentration/composition), clear extensive properties (e.g., volume or mass), and predictable reactive behavior. The result of the foregoing is that, in the reaction engineering sense, a knowledge of the properties of a fluid, reactants, and catalyst plus type of reaction enclosure allow for prediction of the products exiting a process, the amount of energy required for it, etc. The kinetics equations reported above for acid-catalyzed methylation [Eqns. (2-1) through (2-4)] or base-promoted hydrolysis reactions [Eqns. (2-6) to (2-7)] are excellent examples of useful deterministic models.

2.3.2   Statistical approach to modeling

Many physical phenomena are so complex or involve unknown mechanisms that producing a deterministic model of them from first principles or even established correlations is arduous or essentially impossible. The thermochemical methylation reactions of pure DPA and TCM of bacterial endospore DPA are instances where an exact deterministic model is painstaking because it involves transient processes within solid, liquid, and gaseous phases in quantities or portions that are not easily characterized.

In the absence of an established deterministic model of known mathematical form and with known constants, recourse is made to statistically-based experimental design and interpretation of data (often called DOE for *design of experiments*). Like

deterministic modeling, DOE relies upon some function to relate dependent variables (observed data) to other variables that may be measured or controlled; however, the *form* of the function must be chosen (and tested) by the experimenter and the function's so-called "best-fit" constant parameters must be determined from data. Given a function plus its parameters, future behavior of the system may be predicted or some optimal condition determined.

A statistical approach is taken for modeling Me$_2$DPA yield as a function of TCM reagent composition. Since this approach is complex and employs features unique to this dissertation, it is discussed in detail in Section 4.4, Appendix A, and Appendix B.

2.4 *Summary*

Portable GC-MS can potentially provide critically vital information in the form of positive identification of potential chemical or biological threat agents. Consequently, many publications relative to chemical and biodefense have (justifiably) focused on interpreting chromatographic and mass spectral information for species identification/differentiation. Relatively few papers discuss the chemical reactions employed in derivatization procedures in great detail, and even fewer comment on *quantitative* topics (e.g., percent released, converted, and detected).

Efforts to optimize conditions for maximum TCM yields [e.g., 279, 361] provide a few quantitative assessments [e.g., 362, 363] (including comparisons of rapid TCM procedures to standardized laboratory protocols such as those for FAMEs analysis [289, 319, 363], which methods generally produce comparable FAME profiles, as this biomarker class is easily methylated). However, these few examples are exceptions to the

norm. Additionally, although the robust structure of the spore is recognized, no study has focused on the degree to which conversion of spore DPA to Me$_2$DPA is quantitative.

The lack of quantitative analysis has been recognized and rarely addressed in other publications, as illustrated by the following statements: The use of TMA-OH is "inadequate for quantitative purposes" [364]; "Comprehensive methodological studies with fatty acids (including quantification) have not been carried out up to now" [365]; and "We are not aware of any literature reports of quantification of TMA-OH thermochemolysis experiments, either on model compounds or polymeric organic matter" [366].

TCM sampling has usually involved a "sledgehammer," e.g., an actively-heated pyrolyzer or a complex GC inlet system (such as a direct thermal desorption inlet [279, 363, 367, 368]). To date, the methods for *in situ* derivatization of spore DPA to Me$_2$DPA (relevant to rapid, portable spore detection) have (so far as this author is aware) involved TMA-OH exclusively with some type of actively heated pyrolyzer at temperatures in the range of 360-610°C [39, 289, 299, 312, 319, 369-372]. A single paper involving a non-field-portable method described the direct liquid injection of spore-extracted and purified DPA (as a PhMe$_3$N$^+$ salt) [327]. No other study involved other direct methylation (S$_N$2) reagents for DPA, such as the largely overlooked methylation reagent, MeSO$_4^-$. Very few studies have involved a passively heated sample probe to introduce a sample + TCM reagent into a heated GC inlet [201, 284], and none has been used with bacterial endospores. The coiled wire filament (CWF) provides a tool for simple, solvent-less sample introduction into gas chromatographs equipped with the standard split/splitless

GC inlet, and seems to be the smallest device of its kind. The result is a simple, clean means for conducting TCM analysis of bacterial samples directly.

The IMDOE method pursued in this work for organizing, in a systematic way, mixtures of ionic reagents that accompany a biological sample for TCM-based derivatization has never been done before with GC. Usually, *in situ* GC derivatization reactions use single ion pairs at a time. For example, in a recent publication [373] TMA-OH by itself was compared to $Me_3S^+OH^-$ by itself, but mixtures of TMA-OH and $Me_3S^+OH^-$ were not investigated.[19]

In Chapter 1 it was explained how adding methanolic H_2SO_4 to spores before adding TMA-OH and heating on the CWF in the GC inlet greatly increased Me_2DPA peak area. This effect was initially hypothesized to result from acid catalysis (referred to as "**Paradigm A**"). Literature reports of acid-catalyzed DPA esterification are not only few (e.g., entire spores were refluxed in a strong mineral acid dissolved in methanol, ethanol, or isopropanol to give methyl, ethyl, and isopropyl di-esters, respectively [374], and pure DPA was esterified in *n*-butanol by a tungstophosphoric superacid at reflux temperature to form the *n*-butyl di-ester [375]), but involve high temperature reactions. Therefore, no information useful for predicting the rate of Me_2DPA formation by H_2SO_4 catalysis at ambient temperatures is available in the literature.[20] Additionally, no previous literature was available concerning the rate of Me_2DPA hydrolysis in H_2O-MeOH solutions—a reaction relevant since OH^- (from TMA-OH) is added to the spores prior to

---

[19] The addition of certain acidic compounds to attenuate the basicity of hydroxide salts of methyl donors [283, 331] is essentially the same idea as IMDOE, although it has been done in a comparatively un-systematic way without careful consideration of the combinatorial aspects of the ions involved.

[20] That the protocol for methylation of spore DPA involved 1 h of reflux in MeOH with HCl gas continuously bubbled through it [374] suggests the reaction is not fast at room temperature in the sub-molar H_2SO_4 concenterations relevant to the standard protocol.

their being heated in the GC inlet (again, OH^- releases other biomarkers via thermally-assisted hydrolysis of spore structures). Therefore, data on the rate of hydrolysis of Me_2DPA to DPA in a MeOH solution representative of a standard protocol are useful.

Given that small quantities of spores are likely to be encountered in the field, it is important to understand and (if necessary) improve the extent to which spore DPA is converted to Me_2DPA by simple means. The reward for such efforts is a lower spore detection limit and thus improved sensitivity. Models of the processes involved in these methylation reactions (deterministic and statistical) serve as tools for quantitative interpretation, prediction, and optimization.

3 EXPERIMENTAL

3.1 *Chemicals and materials*

Tetramethylammonium hydroxide pentahydrate (TMA-OH·5H$_2$O) was purchased from Alfa Aesar (98%) or Sigma (>97%); 2,6-pyridinedicarboxylic acid (dipicolinic acid, DPA, or H$_2$DPA) from Aldrich (99%); dimethyl 2,6-pyridinedicarboxylic acid (Me$_2$DPA) from Aldrich (99%); Ca(OH)$_2$ from EMD chemicals (>96%) or Sigma-Aldrich (>95%); NaMeSO$_4$ (>99%), KMeSO$_4$ (>99%), and TMA-MeSO$_4$ (purity unavailable) salts from Acros; concentrated H$_2$SO$_4$ was from Mallinckrodt (95-98%); HCl (12.1 nominal molarity) in H$_2$O from EMD; pyrene and chrysene (internal standards for GC) from unknown sources; nitrobenzene[21] (NB; internal standard for LC work) from the chemistry department's organic stockroom (unknown source); MeOH and H$_2$O were HPLC-grade from Sigma-Aldrich or Fisher Scientific; formic acid (>88%) from CCI; and trifluoroacetic acid (99.7%) from Fisher Scientific.

Calcium-complexed dipicolinic acid (CaDPA) was prepared according to a method previously reported [376] by addition of a stoichiometric amount of Ca(OH)$_2$ to aqueous DPA at sub-boiling temperature. Upon mixing, the Ca(OH)$_2$ dissolved, and CaDPA was precipitated by chilling in a refrigerator at ~2°C for 48 h. The amount of hydration of the resultant crystalline material was uncertain, but was likely near three

---

[21] Nitrobenzene is a probable carcinogen and should be handled accordingly [345].

waters of hydration (i.e., CaDPA·3H$_2$O) based on the method employed to synthesize it [376]. The precipitate was washed and centrifuged twice at 0°C with HPLC grade water, from which a diluted aqueous solution and a methanol suspension of CaDPA[22] was produced at a concentration of ~0.01M (by centrifuging and washing of CaDPA with cold methanol three times). The sodium and tetramethylammonium forms of DPA (Na$_2$DPA and TMA$_2$DPA, respectively) were prepared in a similar manner.

Hydrogen methyl sulfate (HMeSO$_4$) was prepared by adding about 10 vol% sulfuric acid to methanol [354, 359, 377, 378] and allowing that reagent to stand at room temperature (approx. 22°C) until further decrease in acid strength was not observed (requiring approximately 8 days). Aqueous sulfuric acid was prepared by mixing concentrated sulfuric acid with water. Aqueous 1 N standard HCl and NaOH solutions were prepared by appropriate dilutions of standard 10 N samples from Fisher Scientific sold specifically for preparing standardized titration solutions.

Alkali (Li$^+$, Na$^+$, K$^+$, Cs$^+$) and tetramethylammonium (TMA$^+$) salts of MeSO$_4$ were prepared by combining known concentrations of the aqueous hydroxides with stoichiometric amounts of methanolic HMeSO$_4$. Sufficient water and methanol were then added to obtain final solution concentrations of 50 mM in 50/50 vol% H$_2$O/MeOH. Some of these (TMA-MeSO$_4$ and NaMeSO$_4$) were dried by lyophilization for use in thermogravimetric studies (see below).

Pt wires (99.99%, ~100 and 125 μm o.d.) were from MWS Wire Industries (Westlake Village, CA, USA), and Pt-Ir wire (90% Pt, 10% Ir, ~89 μm o.d.) was obtained

---

[22] At neutral pH, CaDPA is quite insoluble in MeOH but is slightly H$_2$O soluble.

from California Fine Wire Company (Grover Beach, CA; www.calfinewire.com). Empty

solid-phase microextraction (SPME) assemblies were kindly donated by Supelco[®].

3.2   *Bacterial endospores*

Bacterial endospore samples studied included *B. anthracis* Sterne 1043 ("BA"),

B. thuringiensis var. *kurstaki* ("BT"), *B. cereus* ATCC 14579 ("BC"), and *B. atrophaeus*

ATCC 51189 ("BG"). BA and BG were studied specifically for chemical optimization

purposes. Ten microliters of a thawed stock suspension (stored at −80°C) were streaked

out into quadrants onto a Columbia agar isolation plate and incubated at 37°C overnight.

An isolated colony was taken from the isolation plate and streaked onto the surface of a

solid agar-based growth plate containing either a Leighton-Doi or Columbia growth

medium.[23] These growth plates were incubated at either 32 or 37°C for approximately

two weeks (growth time depended on species and growth media). At some point during

cell growth, the nutrients were consumed, leading to conversion of cells into spores

(sporulation).

Once sporulation was near-complete (about 90-95% of all visible bodies were

spores, as judged by phase-contrast microscopy), the spores were scraped from their

growth plates using a sterile plastic inoculation loop, which was dip-rinsed after each

scraping inside a 50 mL conical centrifuge tube filled with 10 mL sterile water. The

centrifuge tube containing the spore suspension was then placed in a 65°C water bath

(Brinkman, Lauda RM20) for 30 min to kill the remaining vegetative cells.

---

[23] Although liquid broth and solid growth plates were used to grow spores, the latter was employed for the majority of samples utilized in these studies and is thus described in detail here.

The endospores were separated from vegetative cells by a variation of the "daily water wash" procedure [379] that involved centrifugation at 3500 g for 10 min (using a Beckman GS-15R centrifuge), decanting the supernatant into a biological waste container, and resuspending the remaining endospore pellet in autoclaved HPLC water for overnight storage at 4°C (which lyses any residual vegetative cells). This rinsing/centrifugation procedure was repeated three times (i.e., it required 3 days). Endospore purity was verified by phase-contrast microscopy. Spore samples were generally delivered as wet pellets in an Eppendorf tube, obtained by centrifugation of a 1 mL aqueous suspension (measured by micropipette) and removal of the majority of the supernatant by micropipette so as not to disturb the spore pellet.

A detailed description of the spore preparation protocol is found in Appendix F.

3.3 *Instrumentation and equipment*

3.3.1 GC-MS system

An Agilent 6890 gas chromatograph (Agilent, San Jose, CA) with a split/splitless injector fitted with a 0.75 mm i.d. (3.175 mm o.d., 79 mm long) deactivated fused SiO_2 liner (Restek) was coupled with an Agilent 5793 MS using electron ionization and quadrupole analyzer. The transfer line to the mass spectrometer was kept at 270°C for all experiments, and the mass spectrometer was tuned to scan over the 33-550 m/z range. The majority of experiments were conducted using a Restek Rtx®-5 column (5-10 m x 0.1 mm x 0.4 μm), although some initial studies were conducted on similar 5% diphenyl-95% dimethyl polysiloxane columns such as the J&W Scientific DB-5, 30 m x 0.25 mm x 0.25 μm column. A typical temperature program was as follows: hold at 65°C, then

ramp to 300°C at 30-33°C/min. This procedure was modified to reduce the chromatographic run times for studies whose focus was on DPA methylation (e.g., begin at 80°C, and ramp to 260°C).

All experiments were conducted at a GC injection port setpoint of 290°C. This temperature was employed because another student had previously determined it to be optimal for obtaining maximum yields of spore Me_2DPA using TMA-OH alone and because several hundred spore samples had already been analyzed at this temperature prior to the work in this dissertation.

The inlet was run splitless for the first 1-2 min before the split vent was opened to purge the inlet with helium. The inlet pressure was held constant between 30-80 psig helium, depending on the column used and the purposes of the particular experiment. The typical flow rate at the initial column temperature ranged from 0.6 to 1.0 mL/min, as indicated by the instrument. For some experiments, the septum purge vent was purposely plugged so that the only point of exit for the sample would be the column.

3.3.2 LC-UV-MS system

DPA-containing samples (including mono- and diesters of the same) were separated and analyzed with an Agilent 1100 series liquid chromatograph system configured with a UV-Vis diode array detector and a time-of-flight mass spectrometer (TOF-MS). A Synergi 4 μm MAX-RP 80 Å 75 x 3.0 mm x 4 μm column was employed for separating DPA, Me_1DPA, Me_2DPA, and NB (nitrobenzene) using programmed solvent gradient LC-MS. The mobile phase was produced by blending HPLC-grade H_2O and MeOH (each with 0.1% v/v trifluoroacetic acid) using the liquid chromatograph's

binary pump according to the program summarized by Table 3-1. Total flow was 1

mL/min, and injection volume was 10 μL. The column was kept at ambient temperature

(21-23°C). UV absorbance from 250-350 nm was used to obtain chromatographic data,

while the mass spectrometric data were collected from m/z 105 to 1000 to verify peak

identity.

Table 3-1. Liquid chromatographic conditions for analysis of DPA, Me$_1$DPA, Me$_2$DPA, and NB.

Time (min)	Vol. % MeOH‡	Comments
-1.50	31	Pre-condition column
0	31	Inject sample, begin data acquisition
1.40	31	Increased MeOH content to reduce retention times of Me$_2$DPA, NB
1.42	73	
1.70	73	
1.72	51	Reducing MeOH to 51% before restoring it to 31% minimizes a solvent "ghost" peak that may obscure the NB signal
2.80	51	
2.82	31	Restore original column conditions
5.00	31	End data acquisition

‡Percentage is v/v; balance is H$_2$O.

Trifluoroacetic acid (TFA) performs two important functions: First, it protonates

DPA and Me$_1$DPA while they are in solution, preventing them from acquiring a negative

charge. With a negative charge, they interact too strongly with the polar mobile phase and

elute much too soon. Protonated, they are neutral and their interaction with the C$_{12}$ carbon

chains on the reversed phase column is greatly increased, resulting in the desired

separation. Second, the presence of TFA assists in producing positively charged species

in the electrospray ionization source, which is required for analysis of a sample by TOF-

MS in positive ion mode.

3.3.3 Thermogravimetric analyzer (TGA)

A Perkin Elmer TGA 7 thermogravimetric mass analyzer was equipped with a controlled atmosphere cell through which He or N_2 was flowed at approximately 100 cm^3/min (to flush away volatilized components). This TGA was coupled with a Perkin Elmer thermal analysis controller (Model TAC 7/DX). Heating and cooling were programmed via Pyris software (v5.00.02), with which data was also acquired.

An empty, flame-cleaned platinum sample pan was weighed to zero the instrument, following which approximately 5-15 mg of sample was placed in the pan. Spores present as aqueous suspensions were first dried to constant weight at 80 or 90°C for at least 1 h. All samples (spores and chemicals) were heated via linear temperature ramps from room temperature to final temperatures up to 800°C (or lower) at experiment-specific rates ranging from 10-200°C/min, following which the samples were cooled to room temperature. Percent weight loss as a function of temperature was then recorded. The platinum pan was cleaned between runs with solvent rinsings (water and acetone) and with a small butane flame.

3.3.4 Volumetric liquid measurement

Precision syringes (e.g., Hamilton GASTIGHT® and MICROLITER™ syringes) were used for accurate and precise measurements of a variety of liquid volumes. Thorough cleaning of the syringes between uses to remove residual materials and entrained air bubbles was accomplished by multiple rinsings in aqueous and organic media along with frequent replacement of the detachable needles. Syringes were adopted after micropipettes were deemed to be disadvantageous for at least two reasons: first, they

were quite irreproducible (especially when different solvents were used), and second, it was much easier to sequentially measure a variety of volumes using the syringe, while the same task required adjustment of a set screw in the micropipettes for each sample.

3.3.5 pH Meter and probes

Titration data were taken using an Oakton pH 510 bench top pH meter with automatic temperature compensation for pH. Two pH probes were used: either an Oakton WD-35805-10 single-junction, calomel reference pH electrode with an epoxy body or an all-glass Cole-Parmer Accumet 55500-00 Ag/AgCl all glass refillable electrode. The probes were calibrated at 5 points using different buffers: two Fisher Scientific certified buffers for pH 4.00 ±0.01 and pH 10.00 ±0.02 at 25°C); a Ricca Chemical Company pH 7.00 ±0.01 at 25°C; a home-made pH 1.68 buffer consisting of 0.05 molal $KH_3(C_2O_4)_2$ [380], made by combining equimolar amounts of oxalic acid (Spectrum Chemical Manufacturing Company, >98%) and potassium binoxalate (Fisher Scientific, 99.6%); and a home-made pH 12.45 buffer of saturated $Ca(OH)_2$ (Sigma, >95%) in water [380].

3.3.6 Temperature measurement

A stainless steel-clad, 240 μm o.d., 17 cm long type K thermocouple (Omega Engineering, Inc.) was employed to measure the temperature of the inlet of the Agilent 6890 GC. The fiber-holding plunger of a Supelco® SPME assembly needle was removed and the thermocouple was installed in its place by inserting it through the compressed septum in the back portion of the brass hub-needle assembly (the septum prevents gas leakage through the back side of the assembly; see Figure 1-4 and Figure 2-3). The

needle was then held vertically and used to penetrate the GC inlet's septum, with both the distance that the needle was inserted as well as the extent to which the thermocouple extended outside of the needle being recorded.

The voltage generated by the thermocouple was read using a National Instruments NI cRIO-9211, 4 channel 24-bit thermocouple module that was interfaced to a personal computer's USB connection via a NI USB-9161 USB carrier. The signal was then converted to a measurement in °C via a National Instruments LabVIEW code written for this purpose. The thermocouple signal was updated at 4 Hz (the maximum acquisition rate of the particular USB hardware employed). The thermocouple was moved upwards in 0.25 cm increments as the temperature was recorded when the temperature had stabilized to the nearest 0.1°C at each position.

To ensure its accuracy, the thermocouple was calibrated against three other temperature measurement devices by installing all of them simultaneously at the same location inside a GC oven (Hewlett Packard 5890). These three devices included two standard laboratory thermometers (Fisher Scientific Fisherbrand® 14-985G and 15-041-4E having operational temperature ranges of –10 to 400°C, and –10 to 200°C, respectively) and a Vaisala HMI41 humidity and temperature sensor equipped with a NIST-traceable HMP42 probe having a temperature measurement range of –40 to +100°C.

The conditions of the inlet during measurement using the thermocouple alone were similar to those employed for the experiments: a 5 m x 0.1 mm x 0.4 μm column was installed, the oven was held at constant temperature of 50°C, the inlet pressure was fixed at 30 psig, the septum purge vent was blocked, and total He flow was 0.6 mL/min.

3.3.7 Microscopy

Light microscopy (including phase-contrast mode) was performed with a Zeiss Axioskop 2 equipped with an AxioCam HRc digital camera or a Zeiss Axio Imager.A1 with an AxioCam ICc1. Spore counting using the hemocytometer was accomplished with the latter at 400x magnification.

Scanning electron microscopy (SEM) was performed using a Philips (now FEI) XL30 ESEM FEG. Samples were placed on electrically-conductive tape attached to microscope stubs, and the top surface was sputter-coated with gold using a Polaron E5300 freeze dryer with a sputter attachment. Further details regarding the conditions of the instrument are included in the SEM micrograph images.

3.3.8 Coiled wire filaments

Some initial studies utilized hand-wound coils of 100% Pt wire, although in most cases, coiled wire filaments (CWFs) for solids sampling of bacteria using GC were prepared by deflection coiling 90 μm o.d. Pt-Ir wires by Motion Dynamics Corporation (Fruitport, MI; www.motiondc.com). Pt-Ir was chosen because of its increased stiffness relative to platinum, which allowed for better control and reproducibility in the coiling process. This family of materials generally exhibits high strength and oxidation resistance [381]. The length of the coiled section was 1.2 cm, the coil outer diameter was approximately 360 μm, and the coil pitch was approximately 180 μm. A 0.5-cm straight "nib" was left on one end of the coil so that it could be inserted inside the empty socket of the Supelco® SPME assembly and mechanically held in place by compressing the socket against the nib with a DMC crimping tool (Orlando, FL; www.dmctools.com).

3.4 *Procedures*

3.4.1 GC liner deactivation

Two deactivation procedures were used to restore the passivation coating to used, contaminated fused silica liners, which differ only at the 7th step:

Cleaning and deactivation protocol:
1. Soak used liners in MeOH to assist removal of organics.
2. Bake liner in air at 500°C for ~24 h. Heat and cool slowly (e.g., 1°C/min).
3. After cooling, soak liner in 10 N NaOH for at least 1 h.
4. Rinse off NaOH, then soak in 6 N HCl for at least 1 h.
5. Rinse off HCl with HPLC H_2O, then with HPLC MeOH.
6. Dry liner at 110°C in GC oven.
7. Immerse liner in 3:1:9 volume ratios of HDMS:TMCS:pyridine for 30 min (HDMS = hexamethyldisilazane, TMCS = trimethylchlorosilane), **or** Immerse liner in 1:9 volume ratios of HDMS:toluene + 1 vol% trifluoroacetic acid for 30 min.
(*Note: both procedures produce a white precipitate, which is normal.*)
8. Remove liner and rinse well with pyridine.
9. Rinse with MeOH.
10. Dry in GC oven at 110°C for 30 min.

3.4.2 GC sampling

The overall sampling protocol for gas chromatography generally involves mixing chemical reagents (and sometimes spores) in methanolic solution, applying a small volume of the solution to the CWF, allowing the solvent to evaporate at ambient conditions, and inserting the coil (protectively housed within a needle) inside the heated GC inlet, at which point the coil is re-extended from within the needle in order for volatiles to rapidly pass into the GC carrier gas and ultimately to the head of the column in which they were separated.

For the first step identified in the previous paragraph, addition of dissolved chemical reagents for both model compound and spore studies was conducted by careful measurement of liquid reagents of known concentrations using Hamilton GASTIGHT® and MICROLITER™ precision syringes. A constant volume of DPA-containing solution (or similar pelleted masses of bacterial endospores) were combined with reagents, diluent solvents, and internal standards (chrysene or pyrene) in amounts that were experiment-specific. The mixing was accomplished using 0.5 dram glass vials (for model compounds) or 1.5 mL Eppendorf-type microfuge tubes (for spores) to make up a consistent total final volume ranging between 0.5 to 1.0 mL.

A small volume of the sample(1-3 μL) was either placed drop-wise via a MICROLITER syringe onto the coiled wire filament, or the coiled wire filament was dipped inside the solution, resulting in the uptake of approximately 0.6-0.7 μL of solution. Following air drying (about 1 min for methanolic samples, and 10 min for aqueous samples with forced air blowing), the coiled wire was retracted inside the needle, and an injection was made. The retracted wire was inserted into the GC injector port (290°C set point), and the wire was immediately extended. The GC program was begun, and the wire was left in the injection port for 60 s. Following the injection, the wire was cleaned by rinsing in HPLC-grade water and by thermal cleaning in a Bunsen burner flame.

Because many of the experimental results of this dissertation center around a "standard" or "reference" spore derivatization protocol (summarized in Table 3-2) that was developed by a peer, the protocol is covered in detail here. It involves a series of batch processes. First, 500 μL of 375 mM (2 vol%) sulfuric acid in methanol is added to

a sample of spores, which are suspended by agitation and/or physical dislodgment (**Step 1**). Next, one min is allowed to transpire (**Step 2**). Then 200 μL of 2 M methanolic TMA-OH·5H$_2$O plus 100 μL of a methanolic internal standard (100 ppm chrysene or pyrene) are added (**Step 3**) and the mixture is re-agitated to re-suspend the spores.[24] A small volume (< 1 μL) of the suspension is collected by the coiled wire filament (CWF) by capillary action and air-dried (**Step 4**), and finally heated to 290°C in the GC injection port for one min (**Step 5**).

A single step version of this protocol was also explored (not illustrated in) in which all reagents were blended together *prior* to mixing with spores and were added to the spores (**Step 1'**). The mixture was then agitated (**Step 2'**), collected by the CWF (**Step 3'**), and injected into the heated GC inlet for 1 min (**Step 4'**).

3.4.3 LC sampling

Liquid chromatography is a very accurate and reproducible means for quantifying soluble compounds, particularly those with strong UV absorption behavior such as DPA (since it contains an aromatic ring). Published reports stated that boiling or autoclaving spores in acid quantitatively releases their DPA [303, 382, 383], so samples of spores (approximately 1×10^{10} mL^{-1}) were transferred to capped test tubes and autoclaved at 15 psi (~121°C) for 30 min in 3N (1.5 M) aqueous H$_2$SO$_4$. After cooling, the suspensions were clarified with a 0.2 μm pore size, 25 mm diameter Sartorius Stedim Minisart$^{®}$ cellulose acetate syringe filter with three 1-mL rinsings of the test tubes being passed

---
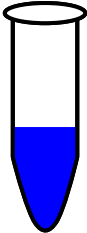
[24] The time allowed to elapse between **Step 3** and **Step 4** is not considered significant.

through the filter. All liquid was transferred directly into 5 mL volumetric flasks. One mL

of 1 mM nitrobenzene (NB; an internal standard) was added to the flask, and the

remaining volume was made up with water to produce a solution of exactly 5 mL. A

series of standardized concentrations of DPA (0.5 to 10 mM) plus NB were prepared in a

similar manner for quantifying the unknown spore DPA concentrations.

Table 3-2. Summary of events during the 5-step standard spore biomarker derivatization protocol.
All species are dissolved in MeOH.

Step #	Brief description of event	Chemical species identity	Chemical species concentration	Volume added	Reaction "vessel"
1	Add methanolic sulfuric acid at room T	H_2SO_4 (+ $HMeSO_4$)[‡]	375 mM (=2 vol% H_2SO_4)	500 μL	
2	Wait 1 min	*N/A*	*N/A*	*N/A*	
3	Add TMA-OH·5H$_2$O	TMA-OH·5H$_2$O	2 M	200 μL	(Vial or test tube)
	Add internal standard	Chrysene or Pyrene	100 ppm m/v (0.44 or 0.49 mM, respectively)	100 μL	
4	Deposit sample on CWF and air-dry	*N/A*	*N/A*	~1 μL *subtracted*	
5	Insert CWF into 290°C GC inlet for 1 min	*N/A*	*N/A*	*N/A*	(CWF)

[‡] $HMeSO_4$ is formed by the slow methylation of H_2SO_4 in acidic MeOH.

4 MODELING AND DESIGN OF EXPERIMENTS

This chapter presents the computational methods employed in the body of this dissertation. The models include entirely predictive ones with no supporting data (e.g., a simple model of the wire heating rate), deterministic models that utilize experimental kinetics data for describing first-order reaction rates (e.g., DPA methylation, Me_2DPA hydrolysis, and H_2SO_4 methylation), and models that connect arbitrary functions with no known fundamental basis (but that nonetheless work well) to sets of data (e.g., titration curve behavior and Me_2DPA yield from spore DPA as a function of a TCM reagent mixture's composition).

4.1 *Wire heating model*

Equations (4-1) through (4-4) summarize the equations associated with the "lumped capacitance" model, which predicts how rapidly a small body initially at one temperature heats or cools when placed in a fluid of a different temperature. In Eq. (4-1), $T(t)$ is the temperature of the solid body as a function of time, T_∞ is the external fluid temperature, and T_i is the initial solid temperature (all in units of °C or K). t is time and τ_t is a thermal time constant (both in s).

$$T(t) = T_\infty + (T_i - T_\infty) \cdot \exp\left(-\frac{t}{\tau_t}\right) \qquad (4\text{-}1)$$

τ_t [Eq. (4-2)] is comprised of a component describing resistance to convection, R_t (K/mW or K·s/mJ), and a lumped thermal capacitance component, C_t (mJ/K). Computation of R_t [Eq. (4-3)] requires values for the convective heat transfer coefficient (h, usually W/m^2/K, but here, mW/mm^2/K) and external surface area available for heat transfer (A_s). Estimation of C_t [Eq. (4-4)] incorporates density (ρ, in mg/mm^3), heat capacity (c_p, in mJ/mg/K), and total solid volume of the wire (v_{wire}, in mm^3). Thus, the higher the values for h or A_s or the lower the values of ρ, v_{wire}, or C_p, the more rapid the heating by convection, and vice-versa. For example, the heating rate decreases in the order: quartz (fused SiO$_2$) > Ag > Pt > Ni (C_t values of 0.55, 0.86, 1.01, and 1.41 mJ/K, respectively).

$$\tau_t = R_t \cdot C_t \tag{4-2}$$

$$R_t = \frac{1}{h \cdot A_s} \tag{4-3}$$

$$C_t = \rho \cdot v_{wire} \cdot C_p \tag{4-4}$$

4.2 *First-order kinetics reaction models*

In Sections 2.2.3.1.2 and 2.2.3.1.4, the rate laws for first-order forms of rate equations were given for acid-catalyzed methylation of carboxylates and base-promoted hydrolysis of those esters. Data on the rate of these reactions obtained as described above were fit to first-order models by minimizing sum of squared errors using Microsoft Excel's solver. Mathcad was also employed as a means for computations involving

prediction of reaction rates at various conditions. Because these methods and tools are generally well-known they are not covered in further detail here.

4.3 *Finding inflection points in titration curves*

Inflection points in titration curves for both acid- and base-titrations were found by fitting Eq. (4-5) to pH vs. volume titrant data. The predicted pH (pH_{pred}) is a function of the experimental volume ratio of titrate/titrand added (α), the fitted volume ratio at the inflection point ($\alpha_{inflection}$), the pH at inflection ($pH_{inflection}$), and four polynomial coefficients (β_i). The model's parameters (italicized) were found using Microsoft Excel's solver to minimize the sum of squared error between the measured pH and pH_{pred}.

$$pH_{pred} = pH_{inflection} + \sum_{i=1}^{4}\left[\beta_i\left(\alpha - \alpha_{inflection}\right)^{(2i-1)^{-1}}\right] \text{, where } \alpha = \frac{V_{titrant}}{V_{titrand}} \qquad (4\text{-}5)$$

4.4 *Ionic mixtures experimentation*

4.4.1 Introduction to mixtures

Arguably the best-known approach to DOE is factors analysis using *factorial designs* [384]. This method is often utilized since varying factors at different levels is easy to implement. A similar approach to DOE is *experiments with mixtures* [27], hereafter referred to as MDOE (*mixtures* DOE). MDOE is appropriate for studies of systems that consist of two or more physical components with at least one quantifiable property that can be additively combined (e.g., mass, moles/number, volume,

concentration). For clarity, the property of the ith species is denoted as p_i. Individual components of a mixture contribute to the sum total property, p_{tot} [Eq. (4-6)].

$$p_{tot} = \sum_{j=1}^{n} p_j \qquad (4\text{-}6)$$

The resultant mixture fraction (mass fraction, mole/number fraction, volume fraction, concentration fraction) is referred to as x_i [Eq. (4-7)].

$$x_i = \frac{p_i}{p_{tot}}, \ \{x_i \in \Re : 0 \leq x_i \leq 1\} \qquad (4\text{-}7)$$

For example, say a mixture of apples ($i = 1$), oranges ($i = 2$), and pears ($i = 3$) contains 5 ($p_1 = 5$), 2 ($p_2 = 2$), and 3 ($p_3 = 3$) items, respectively, giving 10 total fruit objects ($p_{tot} = 10$). The number fraction of each fruit therefore becomes $x_1 = 0.5$, $x_2 = 0.2$, and $x_3 = 0.3$.

In vector/matrix notation, all x_i and p_i are together represented by the n-element vectors $\mathbf{x}$ and $\mathbf{p}$, respectively [Eq. (4-8)].

$$\mathbf{x} = (p_{tot})^{-1} \mathbf{p}, \ \mathbf{x} \in \Re^n, \ x_i \geq 0 \ \ \forall x_i \in \mathbf{x}, \ \sum_{i=1}^{n} x_i = 1 \qquad (4\text{-}8)$$

The fact that the constituents of $\mathbf{x}$ sum to one indicates that only $n - 1$ x_i values may be chosen independently ($n - 2$ in the case of mixtures of n distinct charged ionic species where their charges must sum to zero; see Appendix A for details). Experimental design and modeling is appropriately done using an $n - 1$ (or $n - 2$) independent subsets of $\mathbf{x}$, the subset hereafter being referred to as $\boldsymbol{\chi}$ (note $\mathbf{x}$ is easily recovered from $\boldsymbol{\chi}$). One or several response variables, $\mathbf{y}$ (e.g., one or more peak areas of a chromatogram),

may be modeled as a function of χ, although some experimentally- or theoretically-

determined parameters, $\boldsymbol{\beta}$ (often written as $\hat{\boldsymbol{\beta}}$ if they are estimated from the data, though

here, $\boldsymbol{\beta}_*$ is used to indicate a best-fitting parameter set), must be supplied to the model.

Eq. (4-9) is a nondescript representation of a predictive model.[25]

$$y = f(\chi, \boldsymbol{\beta}) \qquad\qquad (4\text{-}9)$$

The right hand side of Eq. (4-9) is often chosen to be linear in $\boldsymbol{\beta}$ because this

form is easy to handle numerically when solving for $\boldsymbol{\beta}_*$ that make the model match the

data, $\mathbf{y}$, most closely. However, even nonlinear functions of $\boldsymbol{\beta}$ may be fit to data using

suitable numerical methods to minimize the errors between $\mathbf{y}$ and $f(\chi, \boldsymbol{\beta})$.

For clarity, Eqns. (4-10) and (4-11) give example linear and non-linear functions,

respectively. Note that a linear function (in the parameters $\boldsymbol{\beta}$ and not necessarily in the

independent variables χ) possesses the property $f(\chi, \boldsymbol{\alpha} + \boldsymbol{\beta}) = f(\chi, \boldsymbol{\alpha}) + f(\chi, \boldsymbol{\beta})$, while a

nonlinear one does not.

$$y = \beta_0 + \beta_1 \chi_1^2 + \beta_2 \chi_1 \chi_2 + \beta_3 \chi_2^2 + \beta_4 \chi_1 + \beta_5 \chi_2 \qquad\qquad (4\text{-}10)$$

$$y = \beta_0 \chi_1^{\beta_1} \chi_2^{\beta_2} \exp(\beta_3 \chi_1 + \beta_4 \chi_2) \qquad\qquad (4\text{-}11)$$

Because $\mathbf{x}$ is obtained by dividing $\mathbf{p}$ by some total quantity directly associated

with $\mathbf{p}$, it only contains information about the *intrinsic properties* of the system. To

recover the n values of $\mathbf{p}$, $n - 1$ values of $\mathbf{x}$ (or $n - 2$ values in charge-balanced systems)

---

[25] Sometimes, one or more process variables, $\mathbf{z}$ (e.g., temperature, pressure, time, and so forth) are also included in the predictive model (not considered in this dissertation), making Eq. (4-9) of the form $\mathbf{y} = f(\chi, \boldsymbol{\beta}, \mathbf{z})$.

must be specified along with some extrinsic quantity relating to $\mathbf{p}$ (i.e., p_{tot} or one or more values of p_i). Further details are given in Appendix A.

4.4.2 Fundamental existence theorem and model optimization

The basic problem of optimization theory is: Given a set[26] S and a real-valued function f defined on S, is there an element s_* in S such that $\mathrm{f}(s_*) \leq \mathrm{f}(s)$ [or $\mathrm{f}(s_*) \geq \mathrm{f}(s)$] for all $s \in S$? If so, what is s_*? [385]. In this dissertation, two general categories of optimization problems are encountered, labeled as **I** and **II** in Table 4-1. In **I**, the best-fit parameters, $\boldsymbol{\beta}_*$, are found (from the set $S_\boldsymbol{\beta}$) that make the predicting function, $\mathrm{f}(\boldsymbol{\chi}, \boldsymbol{\beta})$ (the "model"), best match some observed response variable, y (Me$_2$DPA yield), using the experimental conditions, $\boldsymbol{\chi}$ (e.g., mixture/mole fractions or concentrations), as independent variables for the model.[27] The second problem, **II**, comes after **I** and involves finding the value(s) of $\boldsymbol{\chi}$ (from the set S_χ) that maximize $\mathrm{f}(\boldsymbol{\chi}, \boldsymbol{\beta}_*)$.

In many statistical models, both $\boldsymbol{\beta}$ and the form of the equation $\mathrm{f}(\boldsymbol{\chi}, \boldsymbol{\beta})$ possess no direct physical meaning; that is, they are not derived from a fundamental basis. Instead, the following approach to modeling is pursued: A guess is made to the form of $\mathrm{f}(\boldsymbol{\chi}, \boldsymbol{\beta})$, the model is "fit" to data by determining the best $\boldsymbol{\beta}$ values ($\boldsymbol{\beta}_*$), and the possibility that

---

[26] In mathematics, a set is a collection of objects (usually numbers) that possess a given property. The set may be finite (e.g., integers from 1-5) or infinite (e.g., all possible numbers on the interval [0,1]). The set involved in mixtures experiments possesses an infinite number of elements since many possible values of $\mathbf{x_{des}}$ may be chosen.

[27] Note $\boldsymbol{\chi}$, referred to as "$\boldsymbol{\chi_{des}}$" in Appendix A, is the $n-2$ set of mathematically-independent elements of the n-element $\mathbf{x}$ ("$\mathbf{x_{des}}$" in Appendix A).

random error may explain the results better than the fit is evaluated. The model is finally evaluated by comparing its predictive power against new data or observations that were not employed in finding $\boldsymbol{\beta}_*$ and revised if necessary. In addition to providing predictive power, if the model and its parameters are deemed to be statistically significant, they may provide insights into the mechanics of a physical process.

4.4.3 Experimentation with ionic mixtures

The composition of chemicals (usually salts) that are co-introduced with spores or pure DPA into the heated GC inlet using the CWF influence greatly the percent conversion to Me$_2$DPA. The key objective of the "mixture" experiments conducted for this dissertation is to determine the "best" relative proportions of chemicals present in the methylating mixture. This objective is pursued via the three key steps according to the approach described in Section 4.4.2. First, the chemicals in the mixture are systematically varied by changing the volumes of "stock" reagent solutions that are combined to make an "aggregate" solution from which a small portion is sampled by GC-MS using the CWF. Second, the components of this aggregate solution are used as independent variables upon which a model of the response (Me$_2$DPA yields) is constructed. Finally, the model is validated by further experimentation.

The overall mixtures approach pursued in this dissertation is similar to work already published on mixture studies involving plant growth and ionic solutions [28-34]. However, because the author's approach had already been developed and documented by the time he became aware of this prior work, his equations, nomenclature, and organization were kept in their original form, all of which is given in detail in Appendix

A. There, the information coverage is quite different from the other publications on the subject, going into greater depth in some areas. For example, the equations that convert solution concentrations to ionic mixtures and vice-versa are derived and explained, as is the use of convex multipliers to select experimental design points.

Table 4-1. Two major types of optimization problems for this dissertation.

	Optimization problem type I: Find best-fitting parameters	**Optimization problem type II: Optimize a process**
Target/ objective function	$$g(\boldsymbol{\beta}) = \sum_{i=1}^{n}\left[y_i - f(\boldsymbol{\chi}_i, \boldsymbol{\beta})\right]^2$$ (i.e., "least-squares" optimization using observed data)	(e.g., a rate law expression or an arbitrary function selected to model a response)
Desired outcome	Find $\boldsymbol{\beta}_*$ from experimental data sets of $\mathbf{X} = \{\boldsymbol{\chi}_1, \boldsymbol{\chi}_2, \dots \boldsymbol{\chi}_i\}$ and $\mathbf{y} = \{y_1, y_2 \dots y_i\}$	Find the highest (or lowest) possible value of y via $f(\boldsymbol{\chi}, \boldsymbol{\beta}_*)$
Methodology	Minimize $g(\boldsymbol{\beta})$ by finding $\boldsymbol{\beta}_*$ such that $g(\boldsymbol{\beta}_*) \leq g(\boldsymbol{\beta})$ for all possible values of $\boldsymbol{\beta}$ for which $g(\boldsymbol{\beta})$ is defined.	Maximize $f(\boldsymbol{\chi}, \boldsymbol{\beta}_*)$ by proper selection of $\boldsymbol{\chi}_*$ such that $f(\boldsymbol{\chi}_*, \boldsymbol{\beta}_*) \leq f(\boldsymbol{\chi}, \boldsymbol{\beta}_*)$ for all values of $\boldsymbol{\chi}$ for which $f(\boldsymbol{\chi}, \boldsymbol{\beta}_*)$ is defined.
Numerical approach	Use linear or nonlinear least squares	Solve $\nabla_{\chi} f(\boldsymbol{\chi}, \boldsymbol{\beta}_*) = \mathbf{0}$, and/or examine the points on the boundary of the domain of $\mathbf{x}$. Ensure that the result is a maximum by performing a second derivative test.

4.4.4 Assumptions for mixtures of ions

Six key assumptions about solutions of ions are made for designing mixtures experiments around ionic FCs.

Assumption #1. *All thermodynamically-favored solution behavior (association kinetics, acid-base neutralizations, etc.) is fast and reproducible.* Thus, any permutation on the order of addition will produce the same final salt complexes. Precipitation of chemicals from solution as the solvent is evaporated (driven by higher salt concentrations, cooler temperatures, and random factors that seed crystallization) occurs with reproducible results.

Assumption #2. *Other than dissociation and reassociation/crystallization, no chemical reactions of FCs in solution or in the solid state on the CWF occur until heating in the GC inlet* (i.e., the reagents are stable until heated). The key challenges to this assumption involve the reactivity of OH^- and $MeSO_4^-$. Long-term storage or direct exposure of OH^--containing reagents to CO_2 (present in the atmosphere) produces carbonates [Eqns. (4-12) and (4-13)] [243, 295, 386-388].

$$OH^- + CO_2 \leftrightarrows CO_3^{2-} + H^+ \tag{4-12}$$

$$2OH^- + CO_2 \leftrightarrows CO_3^{2-} + H_2O \tag{4-13}$$

However, because the reagents are generally kept in sealed containers and since OH^- is exposed directly to air only for short durations of time while measuring reagents, opening vials, and evaporating away solvent on the coiled wire filament, it is assumed that OH^- remains unaltered.

Methyl sulfates are known to slowly hydrolyze according to Eqns. (4-14), (4-15), and (4-16) in neutral, basic, and acidic solutions, respectively. Of these, acid-catalyzed hydrolysis is the fastest [389, 390] [recall the reverse of Eq. (4-16) is what produces $HMeSO_4$ from H_2SO_4 in the first place].

Other nucleophilic methyl transfer reactions that prematurely de-methylate $MeSO_4^-$ may occur in solution at room temperature [273]. However, in the present case Eqns. (4-12)-(4-15) are presumed slow enough to be neglected for IMDOE given the short time that $MeSO_4^-$ resides in solution in the presence of high concentrations of OH^-. A rough estimate using published kinetics parameters reveals that the initial rate of hydrolysis/methyl transfer in solutions containing sub-molar concentrations of $MeSO_4^-$ in water are *at most* on the order of 10 μM/s at room temperature (this value is based on transfer of the Me group from $MeSO_4^-$ to trimethylamine). In other cases (including acid hydrolysis), the rates are 2-3 orders of magnitude lower at the same concentrations, so such reactions should only be significant at high temperatures and possibly as solvent is evaporated from the wire, which greatly concentrates all dissolved species. Hydrolysis of $HMeSO_4$ via Eq. (4-16) is not applicable since the significant amounts of water required for this reaction are only present after the addition of base, which effects a slower hydrolysis [Eq. (4-15)].

$$MeSO_4^- + H_2O \leftrightarrows H^+ + SO_4^{2-} + MeOH \qquad (4\text{-}14)$$

$$MeSO_4^- + OH^- \leftrightarrows MeOH + SO_4^{2-} \qquad (4\text{-}15)$$

$$HMeSO_4 + H_2O + H^+ \leftrightarrows MeOH + H_2SO_4 + H^+ \qquad (4\text{-}16)$$
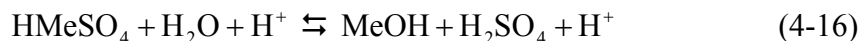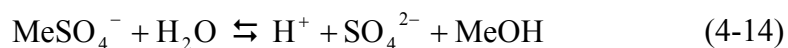
Assumption #3. *The solvent behaves as a neutral spectator both pre- and post-drying, acting only as a dispersing/solubilizing medium. Complexes formed between salts and one or more solvent molecules such as hydrates or methanolates are assumed to be chemically inert. Consequently, solvent composition and amount is not considered in these experiments.* In reality, reactions of salts and analytes with solvent molecules may

occur in solution, the solvent influences the solubility of certain species, and residual

solvent (particularly the small, polar, hydrogen-bonding water molecules [391], and

possibly MeOH under anhydrous conditions [392]) is incorporated inside the air-"dried"

salts. Many salt compounds that may be employed or produced form stable hydrates

(TMA-OH·5H$_2$O, CaDPA·3H$_2$O [376, 393, 394]), are hygroscopic (e.g., Na$_2$SO$_4$, H$_2$SO$_4$),

and are even deliquescent (e.g., NaOH, TMA$_2$CO$_3$ [295]). Thus, the solvent identity and

drying effects may alter the chemical identity and morphology of the precipitated salts

[324]. Formation of hydrate/methylate compounds is a potential source of variability in

pyrolysis products [279, 283] and premature reagent decomposition, although the

presence of polar solvent may produce positive effects (e.g., solute penetration into the

spore core is more rapid at higher water activity [325], probably because water solvation

assists transport and association/dissociation of ionic species). The role of the

hydrate/methylate compounds is addressed again in Sections 5.4 and 5.5.

Assumption #4. *The H$^+$/OH$^-$ (or H$^+$/MeO$^-$) pair combines rapidly in a 1:1 ratio
to form H$_2$O (MeOH), permanently "annihilating" each other to the extent that the
species of lesser concentration is consumed and the residual H$^+$ or (OH$^-$ + MeO$^-$)
remain in solution.*[28] Autodissociation of protic solvents is ignored since it is reversed

when the solvent evaporates on the wire at ambient conditions.

Assumption #5. *Methoxide (MeO$^-$) completely converts to hydroxide (OH$^-$)
during solvent evaporation* since (1) the reagents already possess substantial quantities of

---

[28] The notation "H$^+$" is technically inaccurate, for in a chemical mixture H$^+$ is always bound to (i.e., shares
electrons with) some other element or molecule. For example, in aqueous (H$_2$O) or methanolic (CH$_3$OH)
solutions, H$^+$-solvent structures such as the respective H$_3$O$^+$ and CH$_3$OH$_2^+$ *oxonium* ions (and even more
complex structures) form.

water if TMA-OH is supplied as a pentahydrate, (2) evaporation of the already hygroscopic MeOH cools the solvent to temperatures below water's dew point, promoting H_2O condensation during evaporation [289], and (3) MeOH is more volatile than H_2O,[29] which drives Eq. (4-17) towards OH^- [242].

$$OH^- + MeOH \leftrightarrows H_2O + MeO^- \qquad (4\text{-}17)$$

Assumption #6. *The solutions are ideal in how they mix together*; in other words, the change in total volume upon mixing, Δv_{mix}, is assumed to be negligible and so the total volume of the aggregate solution is exactly equal to the sum of all the stock solution volumes that comprise it. This assumption is justified because the maximum volumetric shrinkage of binary mixtures of H_2O and MeOH is –3.6 vol% and occurs at about 40 vol% H_2O. At lower water content it is less (e.g., -2 vol% at 15 vol% H_2O) [396].

4.4.5 Designing mixture experiments with ions

The above discussion as well as Appendix A summarize the derivations of important equations used for the design of experiments with mixtures for ions (IMDOE). In Appendix A it is shown how the mixture composition, $\mathbf{x_{des}}$ (des = design), of all (or some subset) of the ions in the aggregate solution may be computed once the concentrations, $\mathbf{c_0}$ (e.g., mM), and volumes, $\mathbf{v_0}$ (usually in µL), of the blended stock solutions are known.[30] This is referred to as the "top-down" approach.

---

[29] Note: a methanol-water azeotrope does not form [395].

[30] Although contrary to the engineering convention of using uppercase for concentration and volume (i.e., C_0 and V_0), lowercase letters are employed here because they represent 1-dimensional vectors, each of which represents a *collection* of concentrations or volumes.

Also in Appendix A are given equations, methods, and justifications relevant to the "bottom-up" approach, where c_0 and v_0 are computed from x_{des} and other information. The bottom-up approach is very important because it is the means for designing mixture experiments using ions. However, it is an involved process because (1) mixtures of ions require that charge balance requirement be met (i.e., unlike neutral species, the relative amounts of ions may <u>not</u> be arbitrarily chosen); (2) information in addition to x_{des} must be provided to compute the volumes and/or concentrations of the "stock" solutions that are blended to form the mixture; and (3) additional constraints on concentrations of or ratios between specific ions may be specified by the experimenter.

Constraints on mixtures are dealt with by invoking mathematical convex set theory, which involves the identification of *extreme points* from which any possible experimental design point (ion combination) may be exactly identified. A formal definition of an extreme point is given in Appendix A, although for practicality and simplicity here it is conveniently considered a binary combination of <u>one</u> cation with <u>one</u> anion in a numerical combination where the net charge is zero, which *usually* may be obtained simply by using one single stock solution to produce the aggregate solution. The most relevant exception is when Brønsted acid-base neutralizations occur between solutes in two stock solutions to form a "neutral" salt (nonacidic or nonbasic) plus H_2O or MeOH. In these cases, a *pair* of stock solutions—one acidic and the other basic—must be conceptually combined to obtain an extreme point.[31]

---

[31] For example, NaOH and HCl may be combined in a 1:1 ratio to yield NaCl. Although four ions (Na^+, H^+, OH^-, and Cl^-) are blended, only two (Na^+ and Cl^-) end up as mixture components since the OH^- and H^+ irreversibly neutralize one another to form water.

Two examples illustrate these points. First, use of *only* TMA-OH gives $x_{TMA^+} = x_{OH^-} = 0.5$ and addition of *only* Na-OH gives $x_{Na^+} = x_{OH^-} = 0.5$ (see Figure 4-1). Although the two solutions may be blended at any volumetric combination, being the only anion x_{OH^-} remains constant at 0.5, while the fractions of TMA$^+$ and Na$^+$ each vary continuously (though not independently) on the interval [0,0.5]. This set of any physically realizable combination of TMA$^+$-Na$^+$-OH$^-$ is shown as a line (**qr**) in a ternary mixture diagram (Figure 4-1), where **q** and **r** are extreme points between which any possible combination of ions may be realized. Although a ternary mixture, this system possesses only one degree of freedom since two were "lost" due to the mixture constraint equation (sum of the mixture components must be one) and the charge balance constraint equation (sum of charges must be zero).

For a given set of reagents, each set of ion combinations that constitutes an extreme point comprises a single row of what is called the *convex hull* matrix, Ξ (see Appendix A for further discussion). For the TMA$^+$-Na$^+$-OH$^-$ system, the convex hull matrix is

$$\Xi = \begin{bmatrix} TMA^+ & Na^+ & OH^- \\ 0.5 & 0 & 0.5 \\ 0 & 0.5 & 0.5 \end{bmatrix}. \qquad (4\text{-}18)$$

Since an abundance of H$^+$ consumes OH$^-$ (and vice-versa), Ξ must be constructed either in an "acidic" form or a "basic" one. If an "acidic" design is intended, the reagents are combined in a manner that gives only neutral or acidic mixtures. In such a case, Ξ [e.g., Eq. (4-18)] does not possess a column representative of OH$^-$. If a "basic" design is pursued, only neutral or basic mixtures (excess OH$^-$) result and no "H$^+$" column is

included. All studies in this dissertation are "basic" designs, with the fraction of $OH^- \geq 0$

(since OH^- is the active thermochemolytic component) and thus H^+ *always* is 0.
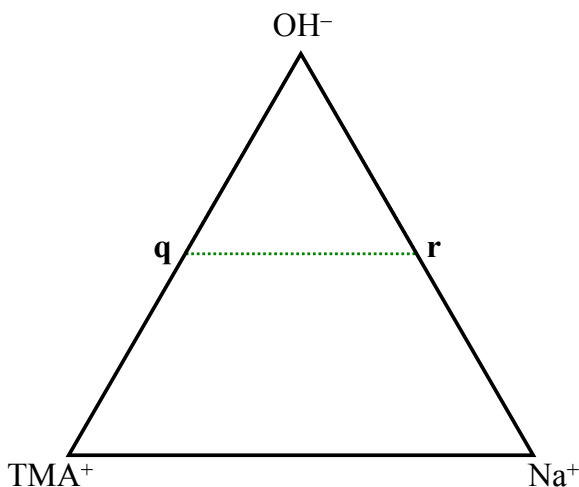
Figure 4-1. Ternary diagram of the TMA^+-Na^+-OH^- system.

The second example involves the quaternary mixture TMA^+, Na^+, OH^-, and

$MeSO_4^-$. In a tetrahedral plot, the set of possible combinations of these ions is a two-

dimensional surface (square **qrst** in Figure 4-2). The corners of square **qrst** are extreme

points (i.e., rows of Ξ in Eq. (4-19)) and are binary combinations of oppositely-charged

ions (TMA-OH, NaOH, TMA-MeSO$_4$, and NaMeSO$_4$). This second example illustrates a

case where acid-base neutralization reactions may be important. Although the indicated

mixture is intended to be neutral or basic, $MeSO_4^-$-containing mixtures may be produced

by adding pure TMA-OH, NaOH, TMA-MeSO$_4$, and/or NaMeSO$_4$ salts directly **as well**

as by combining HMeSO$_4$ plus TMA-OH and/or NaOH in amounts such that the H^+ from

HMeSO$_4$ is neutralized.
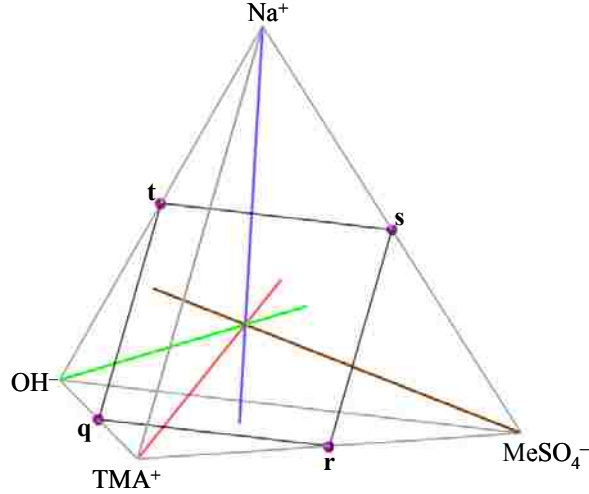
Figure 4-2. Quaternary diagram of the TMA^+-Na^+-OH^--$MeSO_4^-$ system.

$$\Xi = \begin{bmatrix} TMA^+ & Na^+ & OH^- & MeSO_4^- \\ \hline 0.5 & 0 & 0.5 & 0 \\ 0 & 0.5 & 0.5 & 0 \\ 0.5 & 0 & 0 & 0.5 \\ 0 & 0.5 & 0 & 0.5 \end{bmatrix} \qquad (4\text{-}19)$$

Any single experimental design point, $\mathbf{x}_{des}$, may be specified by a *convex multiplication* of Ξ with a *convex multiplier* vector, $\boldsymbol{\eta}$ [Eq. (4-20)]. $\boldsymbol{\eta}$ possesses two key properties: its elements sum to one and no element is ever less than zero. Thus, convex multipliers are essentially linear weighted averages of the extreme points that interpolate between them.

$$\mathbf{x}_{des} = \boldsymbol{\eta}^T \Xi \qquad (4\text{-}20)$$

Although a single value of $\mathbf{x}_{des}$ may be computed from 1-dimensional vector $\boldsymbol{\eta}$, entire *sets* of experimental points (denoted by the matrix $\mathbf{X}_{des}$) may be produced by multiplying Ξ by $\mathbf{H}$ (capital eta), which is a matrix of $\boldsymbol{\eta}$'s [Eq. (4-21)]. Each row of

$\mathbf{X_{des}}$ is a single $\mathbf{x_{des}}$ (represents a single mixture of ions), and each column of $\mathbf{H}$ is a single unique convex multiplier vector, $\mathbf{\eta}$.

$$\mathbf{X_{des}} = \mathbf{H}^{\mathrm{T}}\mathbf{\Xi} \qquad (4\text{-}21)$$

Eq. (4-21) serves as the basis for all mixtures experiments that are presented in this dissertation. Appendix A gives some example $\mathbf{\Xi}$ and $\mathbf{H}$ matrices along with visual representations of $\mathbf{X_{des}}$ obtained by Eq. (4-21) to illustrate some patterns that may be produced by this procedure.

4.4.6 Advantages of mixtures experiments

The use of mixtures provides an alternative—and often advantageous—perspective for describing the properties of any aggregate for the following reasons. First, many optimization problems depend only on intrinsic properties (e.g., the best tasting fruit punch or the optimal gasoline blend to achieve a desired octane [27]), the net quantity being irrelevant. Second, numbers given as mixture fractions $\mathbf{x}$ (i.e., percentages) are often more directly indicative of fundamentals than are absolute numerical values and may be more simple to grasp intuitively. Furthermore, the parameterization of the total amount of a quantity, p_{tot}, being a single number, is easier to remember and more straightforward to work with than is a collection of many absolute numbers. In other words, while the n values of $\mathbf{p}$ are have no mathematical upper limit (although they may have a physical one), the n values of mixture components $\mathbf{x}$ are always found either on [0,1] or some smaller subinterval thereof, making the experimental design space numerically consistent. Only one value, p_{tot}, is on the large

unbounded interval $(0,\infty)$. Third, because a mixture is described using one fewer

dimension (i.e., degree of freedom) than the number of components present, an additional

dimension is available for visual presentation of response data (**y**) and/or functions

describing them [Eq. (4-9)] (i.e., where $n \leq 4$), thereby allowing easy visualization of

trends and relationships within the mixture's "substructure." Fourth, the ability to

represent information using one fewer dimension facilitates analysis of relationships

between constituents of **x** by mathematical and visual interpolation.

The third and fourth advantages are illustrated by pointing out several common

examples of plot types familiar in chemistry and engineering. The composition of a two-

component system is described using a one-dimensional line, which may become an

abscissa for an x-y plot, the y coordinate then being available as an ordinate to record a

response or property (e.g., a binary phase diagram). Similarly, a three-component

(ternary) system may be described using a two-dimensional equilateral triangle, the space

within the triangle providing a region for making contour plots, or alternatively, the

"extra" third dimension (i.e., direction perpendicular to the plane defined by the triangle)

being used to represent the magnitude of the response. A four-component system is

visualized via a three-dimensional tetrahedron. Data obtained using such a system may be

represented as contour surfaces within the tetrahedron, or they may be indicated by

points/spheres of different colors, sizes, transparencies, etc.

These advantages are quite applicable to mixtures of ionic compounds, although

in such situations the ions belonging to the mixture, *not* their precursors, are the

chemically active species. For example, dissolving equimolar quantities of NaOH, TMA-

OH, and H_2SO_4 in water produces a solution with the exact same ionic composition as

does adding the same quantity of TMA-NaSO$_4$ salt. Also, combining NaCl and TMA-OH

is the same as combining NaOH and TMA-Cl. Once these ionic dissociations and

neutralizations are accounted for, the IMDOE approach to DOE can be used to design

experiments and model response data.

4.4.7   Drawbacks of mixtures experiments

The line, equilateral triangle, and tetrahedron are examples of 1-, 2-, and 3-

dimensional simplexes (essentially *n*-dimensional analogs of an equilateral triangle) and

thus allow for easy visualization of 2-, 3-, and 4-component mixtures, respectively.[32]

However, the most common and straightforward means for plotting data and functions is

via two- and three-dimensional Cartesian coordinate systems. Thus, one hurdle that must

be overcome in the design and analysis of mixtures is to produce a method of plotting

data within a simplex. Derivations for converting 3- and 4-component mixtures into 2-

and 3-dimensional plots using Cartesian coordinates are presented in Appendix B.

Although mixtures are readily interpreted visually, the design and analysis of

mixtures experiments is more complicated than factorial designs. Mathematically,

constructing a mixture means that one degree of freedom is lost (two degrees of freedom

with ionic mixtures), which must be accounted for in the statistical analysis [27]. Also,

customized experimental designs require additional manipulations of the dependent and

response variables, necessitate special plotting software or techniques, and demand an

---

[32] Visual representation of simplexes of higher dimensions (and thus mixtures of 5 or more components) is not straightforward, requiring projections into two- or three-space. Specific sub-plots may be generated to capture trends within data sets having dimensions ≥ 5. Mixtures of any dimensionality are readily described mathematically.

overall general knowledge of the underlying methods to be done properly. Such is the case for MDOE around the ions that make up a salt blend (e.g., TMA^+, Na^+, OH^-, and $MeSO_4^-$), where an additional special constraint exists due to the physical requirement for charge neutrality.

4.5 *Computational methods for optimization*

Both linear *and* nonlinear regressions on the percent yield of Me_2DPA data as functions of reagent mixture composition were utilized. For both cases, the R statistical package was employed (available gratis at www.r-project.org). Linear regression was performed with R's `lm` function, and nonlinear regression by the `nls` function using the Port algorithm that employs an established code generally known as `NL2SOL` [397, 398], which relies on a variation of Newton's method. Mathcad was used for numerical derivatives and other more trivial computations, including finding derivatives and plotting data and functions.

5 DPA BEHAVIOR IN ACIDIC AND BASIC METHANOL

In Section 3.4.1, an overview of the reference protocol for biomarker derivatization was given as a 5-step process. In the present chapter, the behavior of DPA during **Steps 1-4** are examined in greater detail since during these steps, DPA is in a solvent (methanol + water) that may effect both methylation and hydrolysis. The rates of each of these reactions are measured and the significance is discussed.

The conditions prevailing during **Steps 1-2** and **Step 3** are given in Table 5-1 and Table 5-2, respectively (because these tables are referenced extensively in the present chapter and because many of the values contained therein are the results of computations, they are included here rather than in Chapter 3). From these tables, it is important to note that a substantial amount of water is introduced by the reagents, spore samples, and methylation reactions of DPA and H_2SO_4 in MeOH [Eq. (5-1)]. It is also relevant that the acidity of H_2SO_4 in stoichiometric excess MeOH slowly decreases with time to half its original strength due to Eq. (5-1), which also produces water.

$$H_2SO_4 + MeOH \leftrightarrows HMeSO_4 + H_2O \qquad (5\text{-}1)$$
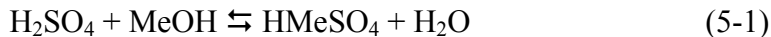
The change in acidity caused by this reaction produces two effects. First, the acidity of the solutions during **Steps 1** and **2** *decreases* with time, and second, the concentration of base after TMA-OH addition at **Step 3** is higher the greater the conversion to $HMeSO_4$. Since total amounts of H^+/OH^- and water are very influential on the reaction chemistry, these details must be taken into account for modeling.

Table 5-1. Description of protocol for <u>Steps 1-2</u> (500 μL of 2 vol% H_2SO_4 in MeOH added to spores). Total liquid volume is between 500–550 μL, depending on spore water content.

Chemical source (I)	Chemical species (II)	Original design conc. (III)	Actual concentrations	
			DPA model study (and dry spores) (IV)	Wet spores[§] (V)
H₂SO₄ (18.8 M pure) CofA[†] for stock: 4 wt% H₂O (4.1 M H₂O + 18.0 M H₂SO₄)	C_{H^+}*	750 mM (as H₂SO₄)	360-720 mM[‡,*] (360 mM catalytically "active")[$]	330-660 mM[‡,*] (330 mM "active")[$]
	$C_{SO_4^{2-}}$	375 mM	0-360 mM[‡,*]	0-330 mM[‡,*]
	$C_{MeSO_4^-}$	0 mM	0-360 mM[‡,*] $= 360\ mM - C_{SO_4^{2-}}$	0-330 mM[‡,*] $= 330\ mM - C_{SO_4^{2-}}$
H₂O (55.5 M pure)	C_{H_2O}	0 mM	82 mM (from "stock" H₂SO₄) + $C_{MeSO_4^-}{}^{‡,*} + C_{Me_1DPA} + 2\,C_{Me_2DPA}$ (up to ~460 mM) **(~300 mM nominal)**	5.1M (from spore pellet) + 0.5 M (from sources indicated in column IV) **(~5.4 M nominal)**
MeOH (24.7 M pure)	C_{MeOH}	24.7 M	~24.6 M	~22.3 M

[§] Except for H₂O, concentrations are lower in column V than those in column IV because of the H₂O addition from the wet spore pellet.

[‡] Except for H₂O, lower concentrations are reported in columns IV and V than in III because the "stock" H₂SO₄ contained about 4 wt% H₂O.

[*] The actual concentrations of H₂SO₄ and HMeSO₄ are dependent upon the degree of methylation of H₂SO₄ (unknown for this study since it predated knowledge of the H₂SO₄ → HMeSO₄ conversion reaction).

[$] See footnote 35.

[†] CofA = Certificate of Analysis.

Table 5-2. Description of protocol for <u>Step 3</u> (300 μL total volume of TMA-OH + internal standard added to mixture from <u>Steps 1-2</u>). Total liquid volume is between 800–850 μL, depending on spore water content. Table notes continued on next page.

Chemical source (I)	Chemical Species (II)	Original design conc. (III)	Actual concentrations		
			Dry spores (IV)	Wet spores[§] (V)	Me$_2$DPA model study[#] (VI)
H$_2$SO$_4$ (18.8 M pure) CofA[†] for stock: 4 wt% H$_2$O (4.1 M H$_2$O, 18.0 M H$_2$SO$_4$)	$C_{SO_4^{2-}}$	234 mM	0-225 mM[‡]	0-212 mM	0 mM
	$C_{MeSO_4^-}$	0 mM	0-225 mM[‡] (225 mM $- C_{SO_4^{2-}}$)	0-212 mM (212 mM $- C_{SO_4^{2-}}$)	166 mM
TMA-OH·5H$_2$O (2 M in MeOH)	C_{TMA^+}	500 mM	500 mM	471 mM	500 mM
	C_{base} [*,$] ($C_{OH^-}$)[◊]	32 mM[$] (0.63 mM)[◊]	50-275 mM[*,$] = 275 mM $- C_{SO_4^{2-}}$ (1.1-6.1 mM)[◊]	47-259 mM[*,$] = 259 mM $- C_{SO_4^{2-}}$ (2.1-11.7 mM)[◊]	334 mM (14.4 mM)[◊]
H$_2$O (55.5 M pure)	C_{H_2O}	2.50 M (from TMA-OH pentahydrate)	2.50 M (pentahydrate) + 51 mM (stock H$_2$SO$_4$) + 225 mM (HMeSO$_4$ formed + H$^+$ neutralized) $- C_{Me_1DPA} - 2 C_{DPA}$ (H$_2$O consumed during hydrolysis of Me$_2$DPA) (**~2.8 M nominal**)	3.27 M (from spores) + 2.35 M (pentahydrate) + 48 mM (stock H$_2$SO$_4$) + 212 mM (HMeSO$_4$ formed + H$^+$ neutralized) $- C_{Me_1DPA} - 2 C_{DPA}$ (H$_2$O consumed during hydrolysis of Me$_2$DPA) (**~5.9 M nominal**)	2.8 M (deliberately added) + 2.4 M (pentahydrate) + 38 mM (stock H$_2$SO$_4$) + 332 mM (HMeSO$_4$ formed + H$^+$ neutralized) $- C_{Me_1DPA} - 2 C_{DPA}$ (H$_2$O consumed during hydrolysis of Me$_2$DPA) (**5.6 M nominal**)
MeOH (24.7 M pure)	C_{MeOH}	~23.6 M	~23.5 M	~22.1 M	~22.2 M

[§, ‡, †] See notes in Table 5-1.

[*] The basic strength of the final solution after TMA-OH addition varies within these ranges if actual concentrations of H$_2$SO$_4$ and HMeSO$_4$ are unknown.

[$] The subscript "base" indicates OH$^-$ and MeO$^-$ concentrations together (after neutralization of acid introduced during **Step 1**).

[#] Concentrations of column VI deviate from column IV due to an oversight in computing final TMA-OH content, although the implications remain the same.

[◊] Concentration of OH$^-$ computed from fraction of total base that is OH$^-$, as reported by Bender and Glasson [251].

5.1 *Acid catalyzed methylation of DPA-results*

The rate of acid-catalyzed methylation of spore dipicolinic acid (DPA) to its

monomethyl and dimethyl ester products (Me_1DPA and Me_2DPA, respectively) during

Steps 1 and **2** was determined at room temperature (20-22°C) by measuring the

concentration of DPA, Me_1DPA, and Me_2DPA in a methanolic solution initially

containing the sodium salt of DPA (Na_2DPA; ~7 mM),[33,34] nitrobenzene (an internal

standard; 7.5 mM), and sulfuric acid[35] (360 mM), as summarized in column IV of Table

5-1. The reacting mixture was sampled by liquid chromatography at ~9 min intervals (the

turnaround time for the LC method employed). A sample chromatogram is shown in

Figure 5-1 and the overall concentration vs. time profile in Figure 5-2. The initial

concentration of DPA, 7.07 mM, was close to the 6 mM estimated to exist for a spore

suspension consisting of ~10^{12} spores per mL.[36]

The two series reactions describing DPA conversion to its mono- and di-ester

products (Me_1DPA and Me_2DPA, respectively) are summarized by Eqns. (5-2) and (5-3).

Since the concentration of MeOH is high compared to all DPA derivatives (> 24 M vs. 7

mM), and since the H_2O concentration is low, first-order kinetics may be assumed for

---

[33] Na_2DPA was used because the acidity of H_2DPA results in autocatalyzed methylation in MeOH.

[34] Solubility of Na_2DPA in MeOH was found by evaporation of the solvent from a saturated solution was approximately 15-25 mM and in water it was ~400 mM. For comparison, the literature reports the upper solubility limit of CaDPA in *water* to be about 20 mM [91, 93]; In MeOH its solubility is unknown. At room temperature, H_2DPA solubility in de-ionized water is about 200 mM [94]. Greater DPA solubility in MeOH is achieved by using organic salts such as TMA_2DPA.

[35] Although the extent of reaction of H_2SO_4 to $HMeSO_4$ in MeOH was unknown, the acidity (and hence catalytic acidity) of $HMeSO_4$ is likely very close to that of H_2SO_4 for the following reasons. First, the two chemicals are similar in structure. Second, bisulfate (HSO_4^-), a very weak acid in water compared to H_2SO_4 and $HMeSO_4$ [255, 257, 259, 399-401], and is almost completely associated in MeOH [401]. Thus, 360 mM is treated as the active "H^+" concentration regardless of relative $H_2SO_4/HMeSO_4$ amounts.

[36] Each spore weighs approximately 10^{-12} grams and is ~10 wt% DPA.

both reactions, as documented mathematically by Eqns. (5-4)-(5-6). In these equations, C denotes concentration of a subscripted species (DPA, Me$_1$DPA, or Me$_2$DPA), t is time, and k_1 and k_2 are the first-order rate constants for the methylation reactions of Eqns. (5-2) and (5-3), respectively. Further justifications for a first-order reaction of the acid-catalyzed model were given in Section 2.2.3.1.2.
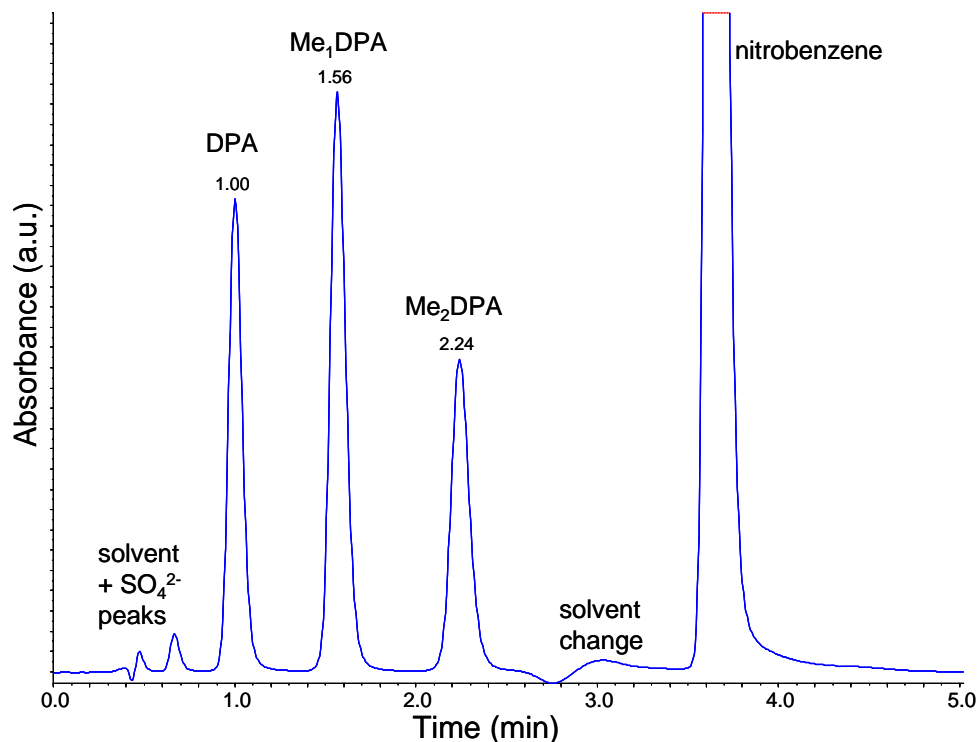
Figure 5-1. Sample chromatogram for acid-catalyzed methylation experiment (cf Figure 5-4).

$$DPA + MeOH \xrightarrow{H^+} Me_1DPA + H_2O \qquad (5\text{-}2)$$

$$Me_1DPA + MeOH \xrightarrow{H^+} Me_2DPA + H_2O \qquad (5\text{-}3)$$
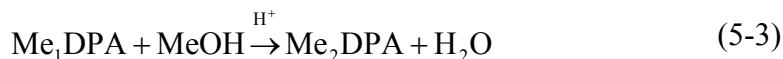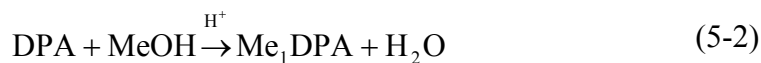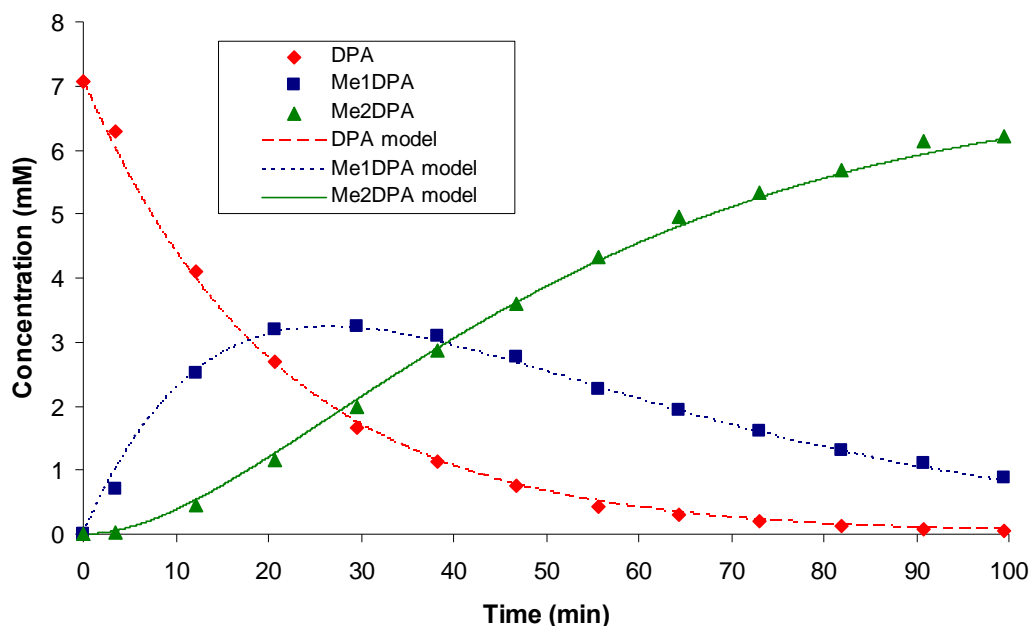
Figure 5-2. Concentration of DPA, Me₁DPA, and Me₂DPA as a function of time in acidified MeOH (data points) and fit of a first-order, irreversible kinetics model (lines).

$$-\frac{dC_{DPA}}{dt} = k_1 C_{DPA} \tag{5-4}$$

$$-\frac{dC_{Me_1DPA}}{dt} = -k_1 C_{DPA} + k_2 C_{Me_1DPA} \tag{5-5}$$

$$-\frac{dC_{Me_2DPA}}{dt} = -k_2 C_{Me_1DPA} \tag{5-6}$$

Eqns. (5-7)-(5-9) are the respective analytical solutions to Eqns. (5-4)-(5-6), where C_{DPA_0}, $C_{Me_1DPA_0}$, and $C_{Me_2DPA_0}$ are the initial concentrations of these species. The latter two species were both zero for this study. Because no mono-methylated DPA (Me₁DPA) standard was available to produce a calibration curve (i.e., conversion of the LC peak area to concentration), the concentration of Me₁DPA was obtained from a "pseudo"-calibration curve obtained from a linear fit of the observed Me₁DPA/NB peak

98

areas to $C_{\mathrm{Me_1DPA,calc}}$ calculated from a mass balance [Eq. (5-10)]. The slope of that line

(Figure 5-3) was then used to estimate $C_{\mathrm{Me_1DPA}}$. In this way, the direct mathematical

dependence of $C_{\mathrm{Me_1DPA,calc}}$ on the observed C_{DPA} and $C_{\mathrm{Me_2DPA}}$ was eliminated and

replaced with a linear correlation.

$$C_{\mathrm{DPA}}(t) = C_{\mathrm{DPA_0}}\, \mathrm{e}^{-k_1 t} \tag{5-7}$$

$$C_{\mathrm{Me_1DPA}}(t) = C_{\mathrm{DPA_0}}\, \frac{k_1}{k_2 - k_1}\left(\mathrm{e}^{-k_1 t} - \mathrm{e}^{-k_2 t}\right) + C_{\mathrm{Me_1DPA_0}}\, \mathrm{e}^{-k_2 t} \tag{5-8}$$

$$C_{\mathrm{Me_2DPA}}(t) = C_{\mathrm{DPA_0}}\left[1 + \frac{k_1}{k_2 - k_1}\left(\mathrm{e}^{-k_2 t} - \mathrm{e}^{-k_1 t}\right) - \mathrm{e}^{-k_1 t}\right]$$
$$+ C_{\mathrm{Me_1DPA_0}}\left(1 - \mathrm{e}^{-k_2 t}\right) + C_{\mathrm{Me_2DPA_0}} \tag{5-9}$$

$$C_{\mathrm{Me_1DPA,calc}} = C_{\mathrm{DPA_0}} - \left(C_{\mathrm{DPA}} + C_{\mathrm{Me_2DPA}}\right) \tag{5-10}$$
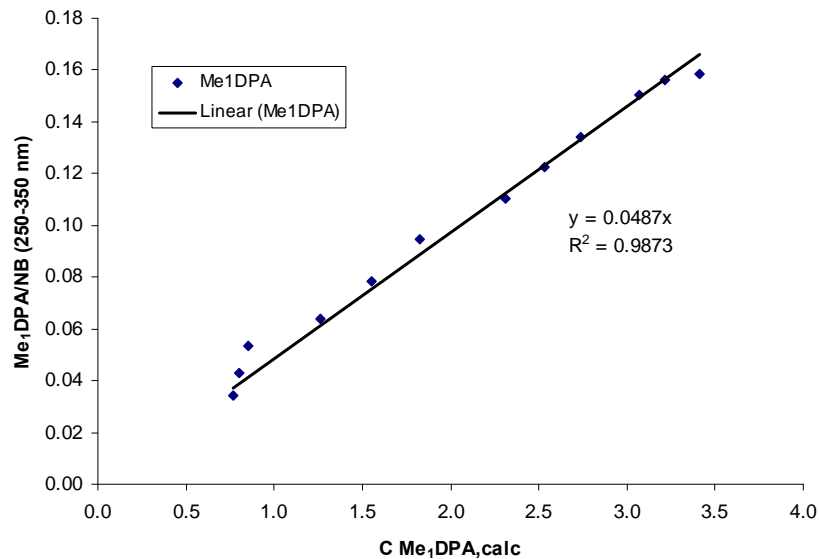
Figure 5-3. "Pseudo"-calibration curve used to determine Me$_1$DPA concentration.

Microsoft Excel's solver was used to find values of k_1 and k_2 that minimized the sum of squared errors between the concentration vs. time data and Eqns. (5-7)-(5-9), the best-fit values being 4.72 x10^{-2} min^{-1} and 2.94 x10^{-2} min^{-1}, respectively. These rate constant values and an initial DPA concentration of 7.07 mM were inserted into Eqns. (5-7)-(5-9) and plotted in Figure 5-2. Agreement of observed and calculated concentrations is excellent.

Since the spores were delivered wet (as pellets at the bottom of Eppendorf tubes) and water is known to influence reactivity, a simple determination of water content was made by weighing three "wet" spore pellet samples, drying them to constant mass over P_2O_5 at 50°C, and weighing them again. The difference in mass indicated the amount of water contained in the pellets. The average water content of three replicates was 45.6 mg (standard deviation 2.5 mg), indicating that ~5% of the original 1 mL water volume remains following supernatant abstraction. Hence, ~50 μL water is incorporated in the 500 μL of acidic MeOH during **Step 1**, making water content ~9.1 vol%, or about 5.1 M, in this mixture. When water from other sources is added, water content may be as high as 5.5 M (see column V of Table 5-1).

5.2 *Acid catalyzed methylation of DPA-discussion*

5.2.1 Comparison to published methylation rate kinetics

The results of a recent detailed kinetics study by Liu *et al.* on the H_2SO_4-catalyzed methylation of high concentrations of acetic acid (~7 M) in 2:1 MeOH:CH_3COOH at a variety of temperatures [241] serve as a useful basis for interpreting the present rate data

since the reactions are very similar (methylation of an organic acid). In the cited study, the reaction rate (excluding autocatalysis) was found to be of the form of Eq. (5-11).

$$-\frac{dC_{\text{Acetic acid}}}{dt} = k_{\text{app}} C_{\text{H}_2\text{SO}_4} C_{\text{MeOH}} C_{\text{Acetic acid}} \qquad (5\text{-}11)$$

The apparent rate constant, k_{app} (in $\text{M}_{\text{MeOH}}^{-1} \text{M}_{\text{H}_2\text{SO}_4}^{-1} \text{min}^{-1}$), was found to vary with water concentration according to Eq. (5-12).

$$k_{\text{app}} = 0.38 \text{M}^{0.83} C_{\text{H}_2\text{O}}^{-0.83} \qquad (5\text{-}12)$$

High concentrations of water (either present initially or formed by the methylation reaction) precluded exact determination of k_{app} under anhydrous conditions (hence, mathematical discontinuity in Eq. (5-12) at $C_{\text{H}_2\text{O}} = 0$ was not an issue for the authors), although from a plot of k_{app} vs. $\overline{C}_{\text{H}_2\text{O}}$ (the average water concentration during the reaction), k_{app} appeared to approach 1 $\text{M}_{\text{MeOH}}^{-1} \text{M}_{\text{H}_2\text{SO}_4}^{-1} \text{min}^{-1}$ as $\overline{C}_{\text{H}_2\text{O}}$ neared zero. The authors determined a pre-exponential factor, A_0, and activation energy, E_A, for a low water content sample (0.3 M nominal) from 30-60°C, the values being 1.46 x10^7 $\text{M}_{\text{MeOH}}^{-1} \text{M}_{\text{H}_2\text{SO}_4}^{-1} \text{min}^{-1}$ and 46 kJ/mol, respectively.

This information was used for comparison against the present study. Using A_0 and E_A at 0.3 M H$_2$O and 20°C from Liu *et al.*, the value of $k_{\text{app,20°C}}$ is 9.28 x10^{-2} $\text{M}_{\text{MeOH}}^{-1} \text{M}_{\text{H}_2\text{SO}_4}^{-1} \text{min}^{-1}$. The constant $k_{\text{app,20°C}}$ was converted to the first-order form, $k_{\text{1app,20°C}}$, seen in Eq. (5-13) [cf. Eqns. (2-4) and (5-4)] by multiplying together $k_{\text{app,20°C}}$

$(9.28 \times 10^{-2}$ $M_{MeOH}^{-1}M_{H_2SO_4}^{-1}$ $min^{-1})$, $C_{H_2SO_4}$ $(0.360 \, M)$, and C_{MeOH} $(24.6 \, M)$. At these conditions, $k_{1app,20°C}$ is 82.2×10^{-2} min^{-1} (i.e., 8.2×10^{-1} min^{-1}).

$$-\frac{dC_{Acetic\,acid}}{dt} = k_{1app,20°C}C_{Acetic\,acid} \tag{5-13}$$

This estimated value for $k'_{1,20°C}$ $(82.2 \times 10^{-2}$ $min^{-1})$ is slightly greater than one order of magnitude higher than the observed values of 4.72×10^{-2} min^{-1} and 2.94×10^{-2} min^{-1} for the first and second methylations of DPA, respectively. It follows, nevertheless, that these approximate results are consistent with acid-catalyzed methylation of carboxylate groups if differences in chemical reactivities based on molecular functionalities are considered (and differences in solvent composition ignored).[37] Therefore, all else being equal, the rate of acid-catalyzed methylation of acetic acid will be faster than for DPA for several reasons. First of all, nucleophilic attack by MeOH on acetic acid is less sterically hindered than on the carbonyl carbons of DPA. Second, aryl groups are somewhat deactivating towards nucleophilic attack because resonance diminishes the positive charge on the carbonyl carbon [236]. Third, the DPA nitrogen is basic and can attract protons, potentially deactivating the catalyst by reducing proton concentrations [375]. Fourth, in acidic methanol, the majority of DPA and Me_1DPA is positively charged (i.e., as H_3DPA^+ and $H_2Me_1DPA^+$) due to protonation at both carboxylates and at the pyridyl nitrogen (discussed further in Appendix E). This positive charge is understood to inhibit protonation at the carbonyl oxygen.

---

[37] Liu *et al.* studied a solution that was 7.3 M (not mM) acetic acid, 14.6 M MeOH, and 1 mM H_2SO_4—conditions that differed substantially from the present study, i.e., 7 mM (not M) DPA, 24.6 M MeOH, and 360 mM H_2SO_4.

However, not all features of the DPA molecule are deactivating. The presence of N should promote nucleophilic attack on the carbonyl carbon. This is substantiated by comparing the pK_a values of the carboxylate groups of DPA against other carboxylic acids. For example, while the pK_{a1} and pK_{a2} values of DPA are about 0.5 and 2.2, respectively, those of 1,3-dibenzoic acid (isophthalic acid), a DPA homologue that does not possess an aromatic nitrogen, are about 3.6 and 4.7, respectively, and the single pK_a value of acetic acid is 4.75 (see Appendix E for details). The lower pK_a values of DPA indicate greater electron deficiency in its carbonyl carbons [402] and hence higher reactivity towards nucleophilic substitution (when protonated). A direct comparison of the methylation rates of DPA and acetic acid in MeOH involves many factors.

Further discussion on the protonation behavior of isophthalic acid, DPA, Me_1DPA, and Me_2DPA is given in Appendix E. This information is relevant to (1) the methylation and hydrolysis reactions (which depend on solvent composition, solution ionic strength, sites and ease of (de)protonation, and pH [403, 404]); (2) liquid phase partitioning behavior (which relates to liquid chromatographic retention behavior as well as to the overall speed and efficiency of uptake by solid-phase microextraction, an alternative to coiled-wire-filament sampling for GC); and (3) the very low sensitivity of DPA detection by TOF mass spectrometry in the positive electrospray ionization mode.

5.2.2 Water and temperature effects on the observed rate constant

The catalytic activity of the H_2SO_4-MeOH solution is strongly inhibited by water, which is not solely a result of the reverse hydrolysis reaction, but also because water strongly attenuates catalyst activity [241]. Evidently, the acidic protons are preferentially

solvated by water, which weakens their ability to interact with the carboxylate groups (a key step in the acid-catalyzed reaction mechanism) [241]. Indeed, the apparent activation energy of acetic acid methylation increased 15 kJ/mol as water content increased from 0.3 M to 3 M, although little further changes in E_A were observed above 3 M H_2O [241].

For the dry conditions (see column IV of Table 5-1), the maximum possible water concentration from H_2SO_4 reagent, H_2SO_4 methylation, and DPA methylation reactions was approximately 460 mM (66 moles H_2O/mole DPA); however, probably less than half the H_2SO_4 (< 180 mM) was methylated at the commencement of the DPA methylation reaction, so the concentration of water was likely between 200-300 mM (29-43 moles H_2O/mole DPA), nearly reproducing the 0.3 M water concentration reported by Liu *et al.* in their low water kinetics studies [241]. In any case, the water concentration was much less than MeOH (24.6 M).

Since only 14 mM water is produced during DPA methylation and since the reaction occurs in a large excess of MeOH, deactivation from changing water composition is small compared to changes in temperature. Using the activation energy found by Liu *et al.* [241], a 2°C uncertainty in temperature from 20-22°C would influence each observed rate constant by 12-13%, while a 14 mM difference in H_2O at 300 mM nominal water concentration only changes the observed rate constant by about 4% if the same water attenuation effect reported in [241], $C_{H_2O}^{-0.83}$, is assumed.

5.2.3   Comparison to the situation of wet spores

Although insightful, these results are not directly comparable to the spore studies for at least three reasons. First, spore DPA is protected from easy release by the spore's

structure. Second, spores contain minerals, enzymes, biopolymers, etc., which may enhance or attenuate the rate of methylation depending on the degree to which they reduce acid strength/activity, inhibit, or promote the (trans)methylation reaction (e.g., metal cations are Lewis acids in solution [405]), and reduce the activity of the MeOH. Finally, because the spores were delivered as wet pellets at the bottom of Eppendorf tubes (a result of centrifugation followed by withdrawal of most, but not all of the supernatant), the water content in actual spore samples is much higher than in the model compound study just discussed.

If the kinetic inhibition effect of water found by Liu *et al.* [241] [Eq. (5-11)] is applied to the 5.1-5.5 M water in MeOH found in this study, the rate constants and hence methylation reaction rates are slowed by a factor of approximately four ($5.1^{-0.83} = 0.26$, $5.5^{-0.83} = 0.24$). Furthermore, the overall reaction rate is slowed an additional 10% because MeOH concentration drops from 24.6 to 22.3 M, and ultimately the equilibrium is slightly shifted away from Me_2DPA toward Me_1DPA and DPA.

5.2.4 Acid catalyzed DPA methylation and GC detection limits

The GC detection limit for Me_2DPA in a 1-μL sample using the CWF is approximately 1 ppm m/v, which is about 5 μM in that liquid volume. If the assumptions are made that spores are dry, weigh 10^{-12} g each, and contain 10 wt% DPA; that the DPA is entirely released from spores upon mixing with acid; and that the spore components do not inhibit or promote the DPA methylation reaction in any way, the model may be used to predict the distribution of DPA, Me_1DPA, and Me_2DPA after 1 min of reaction (the nominal time that spores are left in contact with the acidic H_2SO_4 mixture). Although

higher values are possible, an upper limit on the number of spores that are easily

suspended in 1 mL of solvent is $\sim 10^{12}$, which would contain about 6 mM DPA. After 1

min of reaction, 5.7 mM (960 ppm m/v) DPA, 0.27 mM (49 ppm m/v) Me_1DPA, and

0.0041 mM (0.79 ppm m/v) Me_2DPA are expected. Given the assumptions and results of

this upper-limit scenario, acid-catalyzed methylation alone *cannot* be responsible for the

much improved Me_2DPA yields observed in the chromatogram after prior addition of

H_2SO_4 to the spore suspension.

5.3 *Base promoted hydrolysis of Me$_2$DPA-results*

The case against acid catalysis being responsible for increased Me_2DPA yields is

strengthened by the results of a study on base-hydrolysis of the same compound. The rate

of hydrolysis of a 7 mM Me_2DPA solution was determined under conditions reported in

column VI of Table 5-2. Figure 5-4 is an example chromatogram from the hydrolysis

study[38] and Figure 5-5 displays the overall concentrations vs. time with initial Me_2DPA

concentration of 7.0 mM.

Eqns. (5-14) and (5-15) summarize the series hydrolytic reactions of Me_2DPA to

Me_1DPA and DPA in basic solution.

$$Me_2DPA + OH^- \rightarrow Me_1DPA^- + MeOH \qquad (5\text{-}14)$$

$$Me_1DPA^- + OH^- \rightarrow DPA^{2-} + MeOH \qquad (5\text{-}15)$$

---
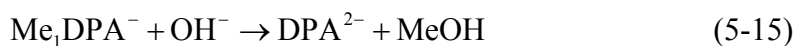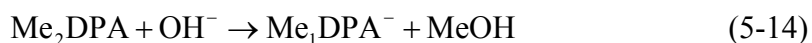
[38] The reasons for the lower retention times of DPA and Me_1DPA in Figure 5-4 compared to Figure 5-1 are explained in Appendix E.
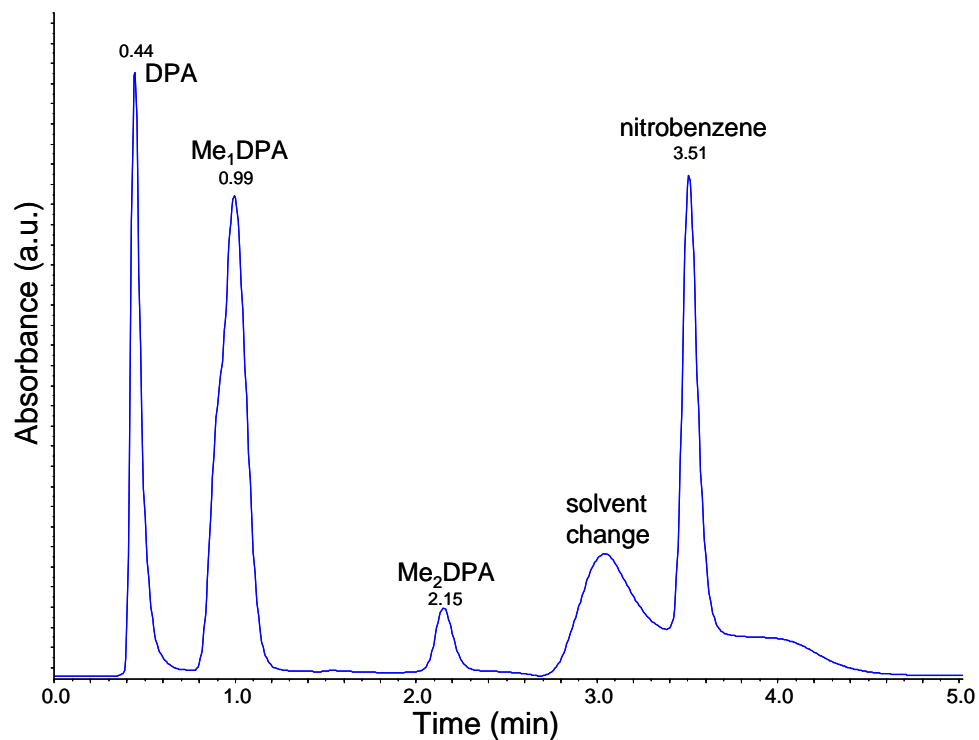
Figure 5-4. Sample chromatogram for base hydrolysis experiment (compare to Figure 5-1).
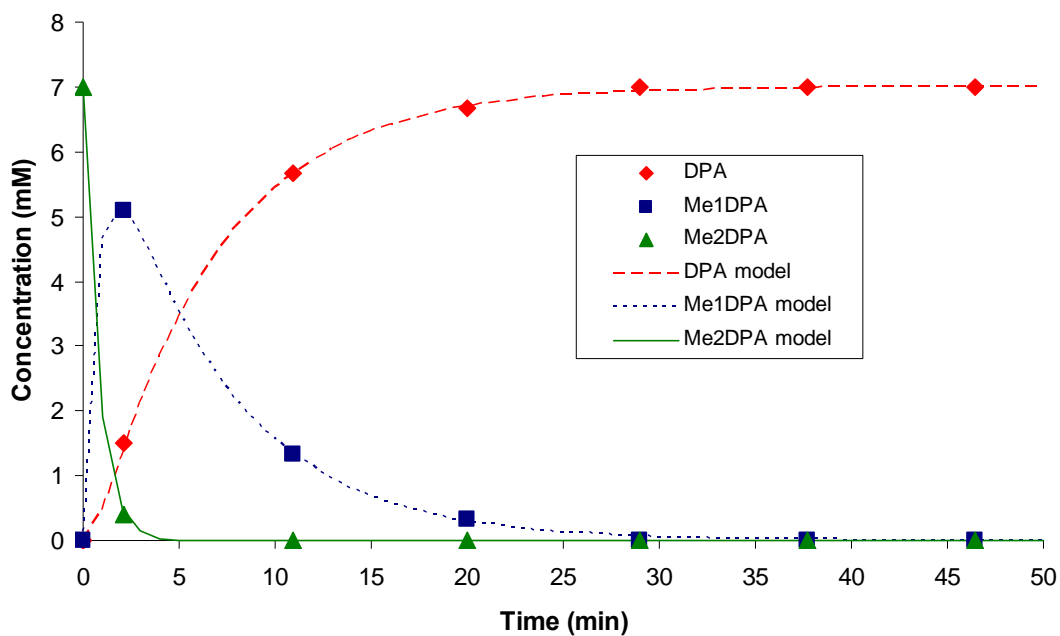
Figure 5-5. Concentration of Me$_2$DPA, Me$_1$DPA, and DPA as a function of time in basic MeOH (data points) and fit of a first-order, irreversible kinetics model (lines).

Kinetics parameters to model the hydrolysis were determined from the data presented in Figure 5-5 in the same manner reported above for acid catalysis. The equations are written below for the hydrolysis reactions in differential [Eqns. (5-16)-(5-18)] and integral [Eqns. (5-19)-(5-21)] forms. (Again, zeroes subscripts indicate initial concentrations; $C_{Me_1DPA_0}$ and C_{DPA_0} were both zero.)

$$-\frac{dC_{Me_2DPA}}{dt} = k_3 C_{Me_2DPA} \tag{5-16}$$

$$-\frac{dC_{Me_1DPA}}{dt} = -k_3 C_{Me_2DPA} + k_4 C_{Me_1DPA} \tag{5-17}$$

$$-\frac{dC_{DPA}}{dt} = -k_4 C_{Me_1DPA} \tag{5-18}$$

$$C_{Me_2DPA}(t) = C_{Me_2DPA_0} e^{-k_3 t} \tag{5-19}$$

$$C_{Me_1DPA}(t) = C_{Me_2DPA_0} \frac{k_3}{k_4 - k_3} \left(e^{-k_3 t} - e^{-k_4 t} \right) - C_{Me_1DPA_0} e^{-k_4 t} \tag{5-20}$$

$$C_{DPA}(t) = C_{Me_2DPA_0} \left[1 + \frac{k_3}{k_4 - k_3} \left(e^{-k_4 t} - e^{-k_3 t} \right) - e^{-k_3 t} \right] \\ + C_{Me_1DPA_0} \left(1 - e^{-k_4 t} \right) + C_{DPA_0} \tag{5-21}$$

The best-fit values for the rate constants k_3 and k_4 were found to be 1.31 min^{-1} and 0.164 min^{-1}, respectively. Using these rate constants plus initial Me$_2$DPA concentration of 7 mM, the model [Eqns. (5-19)-(5-21)] appears to fit well (Figure 5-5). However, these constants may be in significant error. Because all the Me$_2$DPA and Me$_1$DPA were completely hydrolyzed within the first 5 and 25 min, respectively, only one data point (at 2.1 min) was available for fitting k_3 and only 3 data points (at 2.1, 10.9, and 20.0 min)

were available for fitting k_4. More frequent sampling of the solution (or use of another analytical technique) would improve this accuracy, although it was unnecessary given that the key purpose of the present study was to assess how quickly the hydrolysis reactions operate from a practical point of view.

5.4 *Base hydrolysis of DPA-discussion*

The OH⁻ concentration requires special attention because it is the species active for Me₂DPA hydrolysis as well as overall spore biomarker chemolysis, yet it depends on factors including the prior degree of H_2SO_4 methylation and the relative amounts of MeOH and H_2O in the solvent. The implication is that significant variations may occur in the chromatograms depending on the state of the reagents! Although all species present influence ionic strength and overall solution properties, here the total concentration of base and H_2O (in MeOH) are assumed to be the only variables influential on the total amount of hydrolytically active OH⁻. Bender and Glasson's data [251] were used to estimate the quantity of hydroxide in the solution by Eq. (5-22), where C_{base} , C_{OH^-} , and C_{H_2O} are the total base (MeO⁻ + OH⁻), OH⁻, and H_2O concentrations, respectively. The function $f_{B\&G}(C_{H_2O})$ is the fraction of base that is hydroxide and was obtained by fitting a cubic spline to Bender and Glasson's data.

$$C_{OH^-} = C_{base} \; f_{B\&G}(C_{H_2O})$$ (5-22)

Since the basic strength decreases from 334 to 320 mM in 5.6 M nominal H_2O as the reaction proceeds (14 mM OH⁻ are consumed in the hydrolysis of 7 mM Me₂DPA), the OH⁻ concentration, as computed by Eq. (5-22), decreases from 14.4 to 13.8 mM.

Because this variation is small (–4%), C_{OH^-} may be assumed constant (mean value = 14.1 mM) and, like the acid-catalyzed study in which H^+ was constant, a first-order reaction model is justified. Note that a lower concentration of base and/or the presence of other groups susceptible to hydrolysis by OH⁻ reduce further C_{base} (and thus C_{OH^-}), although groups where transmethylation by MeO⁻ may occur will not.

The concentration of hydrolytically active OH⁻ is around 14.1 mM during the course of the reaction, while catalytically active H^+ is ~360 mM and the attacking methanol is 24.6 M. A more direct comparison of the methylation and hydrolysis rates would be possible if the concentration of H^+-activated DPA species were known. Were the methylation conducted in anhydrous methanol and the hydrolysis in a solution of higher water content, this disparity in relative reaction rates would be even greater (although solubility of DPA species in high H_2O solutions is low). These results are consistent with what is known about the relative rates of acid-catalyzed formation and base-driven hydrolysis of esters, as discussed in Section 2.2.3.1.

The first methyl group is hydrolyzed from Me_2DPA nearly 10 times more quickly than the second group (from Me_1DPA), which is understood to result because Me_2DPA is neutral in basic solution, while Me_1DPA^- is not, so the former is much more easily attacked by the negatively-charged OH⁻. Similar ratios were observed for the hydrolysis of di-methyl esters of straight-chain di-acids, the rate constant ratio (k_1/k_2) decreasing in the order 9.7, 6.5, 5.0, 4.3, 3.9, and 3.6 for succinic (C4), glutaric (C5), adipic (C6), pimelic (C7), suberic (C8), and azalaic (C9) acids, respectively [406].

It is possible that the negative charge on Me_1DPA^- allows this biomarker to resist hydrolysis during solvent evaporation, especially if Me_1DPA^- precipitates out of solution

(e.g., as a Na^+ salt). If so, Me_1DPA^- is more reactive for methylation by TMA^+ than is Me_2DPA^{2-} since (1) it only possesses 1 free acid site with (2) a pK_a value that is relatively high so it is presumably a more highly active nucleophile (see Sections 2.2.3.2 and 2.2.5, and 10.1 as well as Appendix E). Consequently, the surviving Me_1DPA may be responsible for some of the observed increase in Me_2DPA yields following the initial addition of methanolic H_2SO_4 to spores.

5.5 *A process model of acid- and base-driven reactions*

The foregoing can all be assembled together into an overall model describing the degree of methylation of spore DPA as first the acidic and second basic solutions are added to the suspension. Whenever concentrations of H^+/MeOH and/or OH^- are different than those of the studies reported in this dissertation, the rate constants k_1, k_2, k_3, and k_4 are easily converted to other conditions per Eqns. (5-23)-(5-26) (the prime symbol denotes an adjusted value).

$$k'_1 = 0.0472 \frac{C_{H^+}}{360\,\text{mM}} \frac{C_{MeOH}}{24.6\,\text{M}}\,\text{min}^{-1} \tag{5-23}$$

$$k'_2 = 0.0294 \frac{C_{H^+}}{360\,\text{mM}} \frac{C_{MeOH}}{24.6\,\text{M}}\,\text{min}^{-1} \tag{5-24}$$

$$k'_3 = 1.31 \frac{C_{OH^-}}{14.1\,\text{mM}}\,\text{min}^{-1} \tag{5-25}$$

$$k'_4 = 0.164 \frac{C_{OH^-}}{14.1\,\text{mM}}\,\text{min}^{-1} \tag{5-26}$$

The conversions of Eqns. (5-23)-(5-26) are valid as long as the reactions are conducted between 20-22°C and the acid, MeOH, and base are in large excess relative to DPA, although even if these stipulations are met, large deviations from the conditions employed to obtain k_1, k_2, k_3, and k_4 probably challenge the reliability of the conversion equations.

Beginning with the assumptions that the spores are dry, that they readily release their DPA to the external solution, that matrix effects are insignificant, that conditions during Step 1 (column IV of Table 5-1) and Step 3 (column IV of Table 5-2) prevail (these are reproduced in Table 5-3), at the beginning of the second step there will be ~ 2.9 M H_2O, 0.266 M $MeO^- + OH^-$, and thus an estimated 6.1 mM concentration of OH^-.

Table 5-3. Summary of events during the 5-step standard spore biomarker derivatization protocol. All species are dissolved in MeOH.

Step ID	Solvent composition	Active H^+ or OH^- concentration	Total time	Total volume	Rate constants (min^{-1})
Steps 1-2	24.6 M MeOH 450 mM H_2O	**360 mM H^+** (from HMeSO$_4$)	1 min	500 μL	$k'_1 = 0.0472$ $k'_2 = 0.0294$
Step 3	23.5 M MeOH 2.8 M H_2O	275 mM (total OH^- + MeO^-); **6.1 mM OH^-**	9 min	800 μL	$k'_3 = 0.565$ $k'_4 = 0.0708$

In Figure 5-6A, the computed concentrations of all three species as a function of time is displayed, with Me$_2$DPA replotted as ppm m/v in Figure 5-6B. Liquid-phase Brønsted acid catalysis does not rapidly produce high Me$_2$DPA yields under the conditions employed.
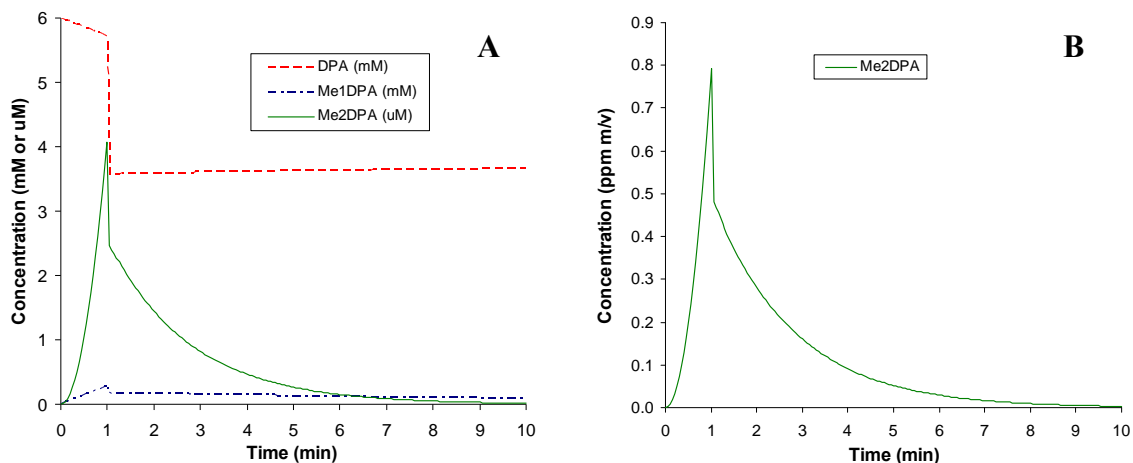
Figure 5-6. Predicted concentration vs. time profiles for DPA, Me₁DPA, and Me₂DPA in mM (A) and concentration of only Me₂DPA in ppm m/v (B) at room temperature.

Although the kinetics will be different, similar reactions will occur at *free* carboxylate functionalities (e.g., fatty acids and free amino acids). However, the process is more complicated when the fatty acids and amino acids must be freed from their respective glyceryl ester or peptide linkages, which is slow at room temperature (particularly for acid-catalyzed reactions).

It is worth recalling that the GC sampling protocol of interest does not analyze the contents of the basic reagent mixture from the liquid phase as does LC. Rather, a small volume of solvent + reagent + analytes is collected onto the coiled wire filament (CWF) and the solvent evaporated away prior to introduction into the heated GC inlet. This process greatly concentrates the OH⁻ both because the total solvent volume decreases and because the proportion of H_2O relative to MeOH increases (due to the $OH^- \leftrightarrows MeO^-$ equilibrium) since MeOH is more volatile.[39] The net result is that hydrolysis of pre-

---

[39] Unlike ethanol-water mixtures, MeOH-H_2O does <u>not</u> possess an azeotrope [395].

formed methyl esters is greatly accelerated and (presumably) driven to (near) completion as evaporation proceeds.

Modeling the processes and reactions that occur during drying under ambient conditions would require consideration of heat transfer to and mass transfer from the wire, temperature (the wire cools as evaporation proceeds), solubilities of salts and biological compounds in a complex matrix (e.g., see [32, 407]), and special correlations for rates of hydrolysis in concentrated, non-ideal, mixed-solvent solutions. Instead, since the high-temperature reaction processes are more influential than the low-temperature drying ones, the focus for experimental work emphasized statistically-based design of experiments for mixtures of ionic compounds that are present on the CWF as it goes into the GC inlet and is heated rapidly. These experiments are discussed in Chapter 8 following an analysis of the coiled wire filament (Chapter 6) and some exploratory experiments involving $HMeSO_4$ and its salts (Chapter 7).

6 COILED WIRE FILAMENT CHARACTERIZATION

6.1 *Reproducibility of sample volume using machine-coiled wires*

Two individual machine-coiled wires were dipped into each of two solutions (CH_2Cl_2 or MeOH) spiked with chrysene, air-dried, and injected into the GC. A total of 9 injections were made for each wire with each solvent, with flaming of the wire carried out between each 3 consecutive samples. A peak area vs. sample volume calibration curve was produced by transferring between 0.3 and 0.9 µL of the same CH_2Cl_2 or MeOH solutions via microsyringe to a coiled wire filament.

Using the calibration data, the average volumes taken up were 0.66 (±0.03) µL and 0.64 (±0.02 µL), respectively, for the above solvents (numbers in parentheses are 95% confidence intervals on the mean). Overall 95% confidence intervals (indicative of errors of the method) were ±0.13 µL and ±0.09 µL, respectively, giving ±19% and ±14% as expected deviations from the means reported above. Thus, 19 out of 20 liquid samples taken up by the wire will likely be between 0.53-0.79 µL or 0.55-0.73 µL depending on whether the solvent is CH_2Cl_2 or MeOH, respectively.

6.2 *Geometric considerations for sample volume uptake*

The regular, reproducible geometry of machine-coiled Pt-Ir wires allows for a variety of computations to be performed that relate to its use in sampling (see schematics

in Figure 2-4 for dimensions). At 1.2 cm long (l_{coil}), the manufactured coils contain

approximately 68 coils (n_{coil}) at a diameter of 89 μm (d_{wire}) and a mean coil diameter

267 μm ($d_{mean} = 3\,d_{wire}$). This translates into a total uncoiled length, l_{wire}, of 5.70 cm

($\pi \cdot d_{mean} \cdot n_{coil}$) and a total external surface area of 15.9 mm^2 ($\pi \cdot l_{wire} \cdot d_{wire}$). The open

area of the gap formed by two adjacent coil wraps is approximately 5.0 mm^2 [area =

$\pi \cdot d_{mean} \cdot l_{gap} \cdot (n_{coil} - 1)$; $l_{gap} = d_{wire} = 0.89$ μm].

To validate the experimentally-observed volumetric uptake, the available internal

volume of the CWF may be estimated from its geometry. The 1.2 cm-long coil can be

apportioned into "virtual" concentric hollow cylinders with diameters of $2\,d_{wire}$ (the coil

inner diameter), $3\,d_{wire}$ (the coil mean diameter), or $4\,d_{wire}$ (the coil outer diameter; see

Figure 2-4), which contain volumes of 0.30, 0.67, and 1.19 μL, respectively. However, in

the latter two cases, a portion of the volume enclosed by the virtual cylinder is occupied

by the solid wire itself (v_{wire}), which has a total volume of 0.35 μL [$l_{wire} \cdot \pi \cdot \left(\dfrac{d_{wire}}{4}\right)^2$].

Some of this volume is within the intermediate (0.67 μL) virtual cylinder (for the present

purposes, approximately half of it, or 0.17 μL, is assumed[40]) and all of it is in the largest

(1.19 μL) virtual cylinder. Therefore, the empty volumes within the aforementioned

virtual cavities available for housing liquid are 0.30, 0.50, and 0.84 μL, respectively. The

experimentally-observed collection volume of 0.65 ±0.15 μL as well as physical

observations of the morphology of entrained liquids indicate that the solid-liquid-air

---

[40] In reality, somewhat less than half the coiled wire volume is in this virtual cylinder of intermediate size
and the curvature of the coil would need to be taken into account for better estimates.

boundary of freshly entrapped liquid is located at a point on the wire lying somewhere between the coil mean and outer diameter, as illustrated in Figure 2-4. Better predictions of the volume taken up would require more complex considerations than those given here and would involve solvent surface tension, the wire's surface wettability, and the resultant liquid-solid contact angle (functions of its chemical composition and surface roughness) [408-410]. Since the wire's physical and chemical properties vary as the wire is used (particularly with flame treatments), the entrained volume will vary accordingly. Therefore, a complex analysis was not conducted.

6.3 *Influence of geometry on heat and mass transfer*

The evaporation rate of solvent in or on the coil is enhanced relative to that of a solitary spherical liquid droplet evaporating from a wire surface for multiple reasons. The coiled wire promotes drying by spreading the liquid over a larger area. As the solvent evaporates, excess liquid (e.g., volume beyond its dipping capacity, or approximately >1 µL) is continuously wicked away from any large adhering droplet(s) into the internal cavity via capillarity, where improved heat and mass transfer results from liquid spreading. During evaporation, the liquid volume decreases and sometimes breaks apart into smaller bodies with higher surface area to volume ratios than would be the case for a single evaporating spherical droplet (see Figure 8-15C later in this dissertation). The spreading over a larger area thus increases heat and mass transfer rates due to the larger liquid-air interfacial area and overall total area.

Once the coiled wire filament is installed inside the heated injection port, rapid heating of the wire, sample, and reagents are required for obtaining the best quantitative

results and chromatographic behavior since ideally, the sample moves as a narrow plug into the column (see Figure 2-3C). Insights regarding these phenomena may be gained from considering the processes involved. The geometry of the coiled wire alters the flow patterns and reduces boundary layer thickness at the external portion of the coil, which increases the rates of heat and mass transfer. This effect has been exploited for improved SPME sampling: Ciucanu reported better results with small coiled wires coated with PDMS sorbent polymers compared to straight SPME fibers [211-213, 411]. Similarly, incorporation of spiral inserts into GC inlets has been utilized as a means for improving mixing between sample/carrier solvent vapors and carrier gas in GC injection systems [412, 413]. Admittedly, the rate of flow over the wire is so slow that heat/mass transfer effects due to the coiled geometry may be of little significance, although more investigations in this area are needed for definitive conclusions.

6.4 *A simple heating model*

The thermal behavior of the coiled wire upon insertion into the GC inlet is complicated since many heat transfer mechanisms operate (see Figure 6-1): The sheathed wire begins to be warmed by thermal conduction as soon as the needle contacts and penetrates the septum (I). Convection to the needle and wire occurs as warmed He gas passes from the pressurized GC inlet (~12-75 psig, as described above) into the needle, compressing the gas contained therein since the back end of the needle is gas-tight (II; leaking of this back seal would result in faster heating and loss of sample). Furthermore, the retracted coiled wire is heated when/if the needle contacts the inside of the liner (III), and after extension, the coiled wire is heated by direct conduction of heat where it

touches the liner (IV). He carrier gas flowing over the needle and wire also convects heat to these bodies (V). A minor amount of radiative heat transfer occurs from the heated injection liner to the wire and needle (VI). The heating phenomena will further be influenced by the physical condition of the needle and coil such as presence of bends, the angle of insertion, the condition of the septum, liner dimensions, the quantity and location(s) of the sample plus reagents and/or residual solvent within the coil, operator skill and consistency, etc.
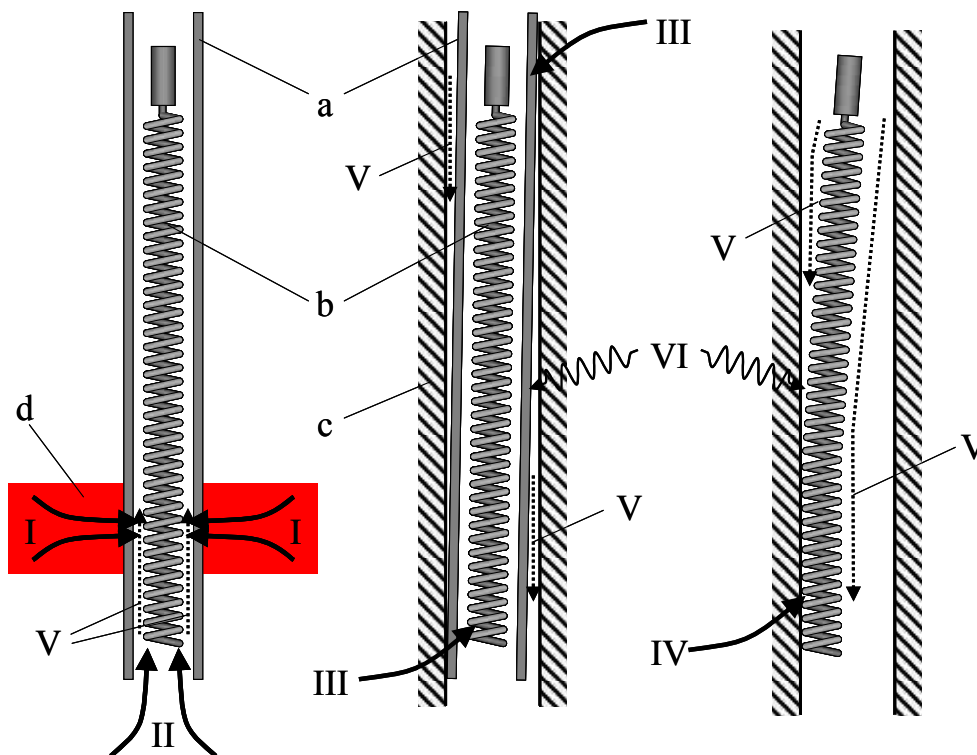
Figure 6-1. Heating mechanisms of CWF as it is introduced into the GC. (a) Needle, (b) coiled wire filament, (c) heated GC inlet liner, (d) inlet septum. Solid arrows indicate heating by conduction, small dashed arrows heating by He convection, and wavy arrows heating via radiation.

To provide a understanding of the wire heating process, one very simplified case is considered in which a metal body possessing the same volume as the coiled wire

filament (0.35 mm^3), initially at 25°C, is inserted into a fluid of constant temperature (290°C). The wire temperature vs. time in this case is readily modeled according to the lumped capacitance method (see [414] and Section 4.1) since the wire has sufficient thermal conductivity and is small enough that thermal gradients within it are negligible.[41] The flow in this case is decidedly laminar since the Reynolds number (based on the coil OD of 360 μm and 0.6 cm^3/min He flow at 290°C and 30 psig) is 0.07.

The temperature-time profiles of a variety of materials[42,43] were estimated (Figure 6-2) with assumptions that the carrier gas remains isothermal at 290°C (probably only a fair assumption—see below) as it passes on the outside along the length of a clean, dry coil having an initial temperature of 25°C; that heat transfer occurs only via convection from the hot carrier gas with $h = 0.1$ mW/mm^2/K (i.e., 100 W/m^2/K, which is a typical median value for heat transfer of this nature[44] [414]); and that the external portion of the coiled wire ($A_s = 8$ mm^2) is the principal surface where the heat exchange occurs (since flow through the inside portion of the coil is impeded by the coiled wire walls). The model predicts that all metallic wire materials reach maximum temperature within 5-10 s, and the quartz material heats to a final temperature in just over 3 s. Of course, these values are absolutely subject to the assumptions for the values of h and A_s, and again depend on the assumed external fluid temperature.

---

[41] The Biot number is $\ll 0.1$ for all solid metal and ceramic materials having the dimensions of the coiled wire filament (computations not shown).

[42] Values for the specific heat and density of these materials, obtained from a variety of sources, were assumed to be constant over the temperature range of interest.

[43] The specific heat of 90-10 Pt-Ir alloys was not readily available, but is probably close to that of 100% Pt.

[44] Correlations for convective heat transfer from co-axial flow of a fluid on the outside of a short helical coil were not immediately available.
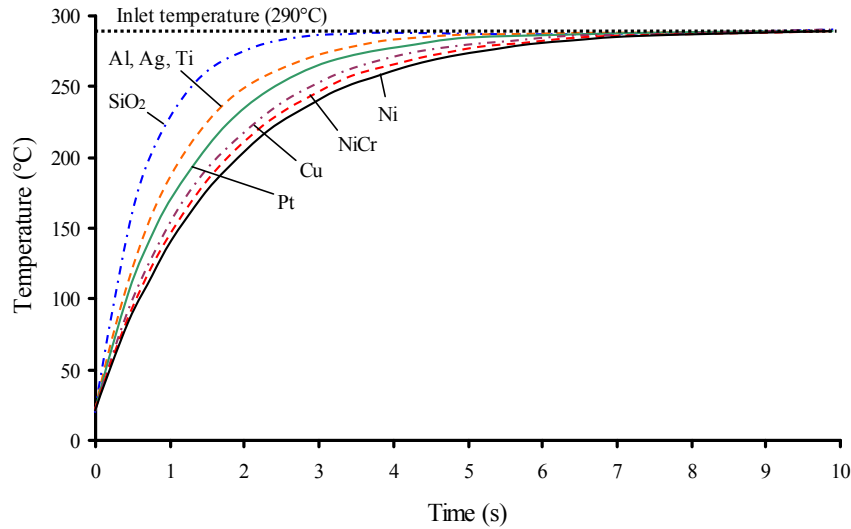
Figure 6-2. Results of model of coiled wire heating.

The actual rate of heat transfer to the wire relative to that which would occur at constant external carrier gas temperature may be much lower than predicted by Eq. (6-1) since a temperature differential drives heat transfer of this nature, as manifest by examination of the general form of the equation for forced convection heat transfer in a fluid [Eq. (6-1)]. Here, $\dot{q}$ is the rate of convective heat transfer (in energy/time units such as W or mW) and T_w represents the wire temperature (in K; all other variables the same as above).

$$\dot{q} = h\,A_s\,(T_\infty - T_w) \tag{6-1}$$

The above cooling effects challenge the assumption that T_∞ is constant; instead, it is a function of time and position along the wire. Nevertheless, despite the complex heating phenomena, for a given filament geometry the relative heating rates will be the same regardless of the heat transfer mechanisms.

Given that the model is correct, it predicts that the wire reaches its final temperature by at most 10 s, reflecting thermal behavior that is much different compared to most analytical pyrolyzers, which typically heat samples to above 350°C in less than 1-2 s, frequently between 100-200 milliseconds [14]. The slower heating rate of the coiled wire filament may give it advantages in that (1) it does not "flash" volatilize solvent and/or sample material as do actively energized pyrolysis devices, reducing the rate of liner contamination, and (2) it maintains reactants in the condensed phase for longer times, potentially enhancing the extents of some reactions (more research on both of these possibilities is recommended).

6.5 *Disadvantages of the CWF*

In the embodiments reported here, the sub-microliter-sized sampling volume may be too low for some applications (although concentration may be accomplished by continued application with a syringe pump or repeated dippings and drying). With the reproducibility being about ±20% of its nominal volume, it is not as reliable as a syringe for measuring liquid volumes. Thus, an internal standard is recommended for quantitation, although this author's experience is that the overall injection process may induce so much variability that an internal standard does not offer much help (see Section 8.3.3 for further discussion). During pre-injection solvent evaporation (and even upon insertion into the GC injection port), volatile compounds are lost more readily than less volatile species, leading to discrimination that affects quantitative analysis even with an internal standard. Sample carry-over may occur if the wire is improperly cleaned or if particularly dirty, viscous, or "sticky" samples are used. Samples can leave deposits

122

inside the needle housing, on the liner, and even on the coil itself. Nonvolatile materials can be converted to difficult-to-remove carbonaceous deposits during flame cleaning. The wire's metal construction may induce undesirable catalytic reactions, although its very small surface area ensures such reactions are small. Of course, it is limited by its final temperature and heatup rate, where pyrolyzers are not.

Although the coiled wire filament is easy to use and consistently retains approximately 0.5- to 0.8-μL of sample with minimal user intervention, for some applications this level of reproducibility may not be satisfactory. Furthermore, extended use leads to coil deformations and irreversible deposition of solids such that volumes taken up change even more.

7   SOME CHARACTERIZATIONS OF HMeSO$_4$ AND ITS SALTS

7.1   *Kinetics of H$_2$SO$_4$ methylation to HMeSO$_4$*

A methanolic H$_2$SO$_4$ solution was produced volumetrically to be 1 M (2 N, or 5.5 vol%). Titrations were conducted on it with 1 N NaOH, and points of inflection computed according to the method described in Section 4.3. Figure 7-1 displays the titration data and illustrates the acid's weakening over time, eventually decreasing to around half the initial value (1 mol/L). The rate of decrease in acid strength slowed as the reaction progressed, leveling off after about 1 week (168 h) of reaction time.

A least-squares fit of the data in Figure 7-1 to the first-order model indicated by Eq. (7-1), where $C_{H_2SO_{40}}$ indicates initial H$_2$SO$_4$ concentration, gives $k_1 = 3.6 \times 10^{-2}$ h^{-1} (9.9×10^{-6} s^{-1}), which, although in error (see Figure 7-2), compares well with literature reports for the same reaction (e.g., at 25°C k_1 values in ≤ 5 wt% (2.2 vol%) H$_2$SO$_4$ solutions were approximately 5×10^{-6} s^{-1} [356], while in ~21 vol% H$_2$SO$_4$ k_1 ranged from 21 to 25×10^{-6} s^{-1} [377]). This rate constant may be converted to other temperatures by applying an activation energy from the literature (e.g., 32.4 ±0.4 kcal/mol [356]).

$$C_{HMeSO_4} = C_{H_2SO_{40}}\left[1 - \exp\left(-k_1 t\right)\right] \qquad (7\text{-}1)$$

One source of error in the data used for this fit was that isothermal conditions were not maintained during H$_2$SO$_4$ addition—an exothermic event—although it probably did not influence the final product formed.
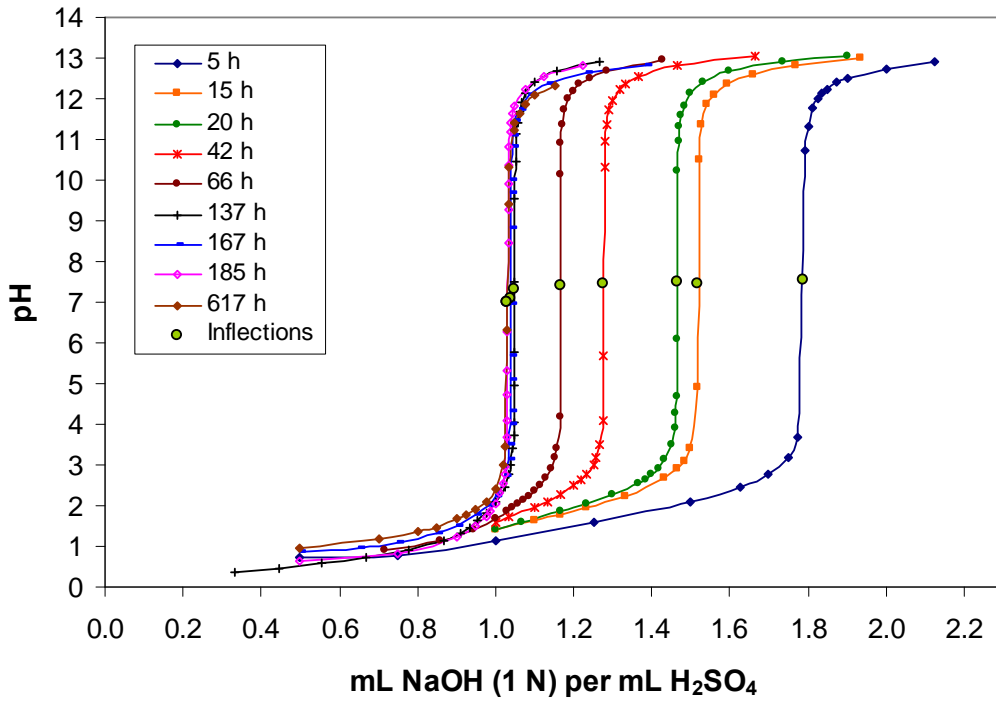
Figure 7-1. Titration of a single batch of methanolic H$_2$SO$_4$ over time.
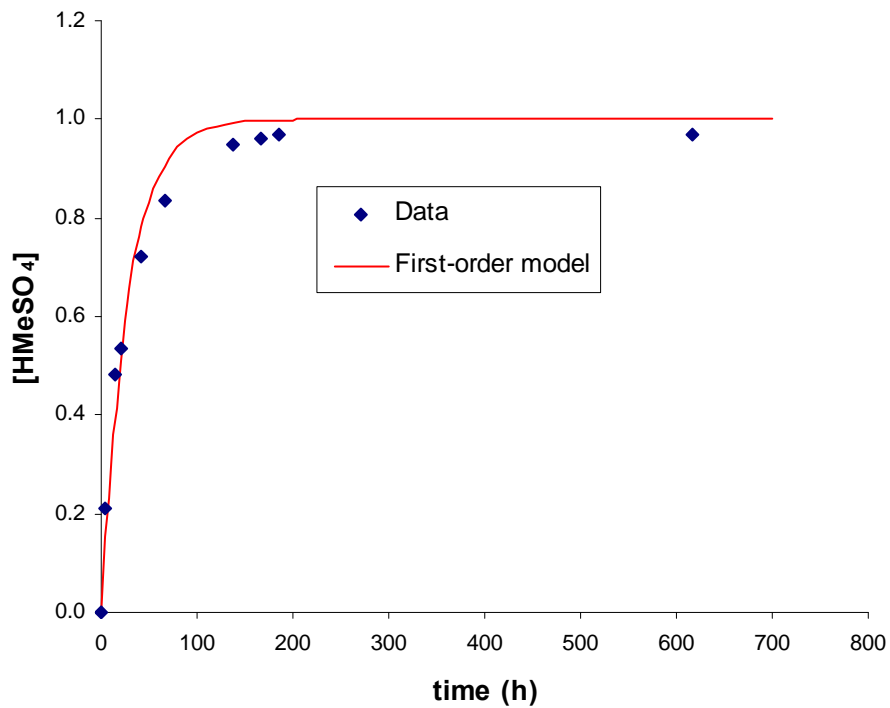
Figure 7-2. Data and model for rate of methylation of sulfuric acid in a 5.5 % v/v (1 M) methanol solution.

7.2 *MeSO₄⁻ salts and Me₂DPA yield from CaDPA and Na₂DPA*

Once methyl sulfate was discovered to be active for the methylation of DPA, the effect of the $MeSO_4^-$ cation on Me_2DPA yield was determined with CaDPA and Na_2DPA. Li^+, Na^+, K^+, Cs^+, and TMA^+ salts of $MeSO_4^-$ were prepared (along with TMA-OH) and combined with CaDPA or Na_2DPA such that the final DPA concentration was 500 μM and the methyl donor:DPA ratio ranged from 1-50. The CWF was dipped in these solutions (or in a calibration solution consisting of 1-500 μM Me_2DPA in MeOH) and the injections were carried out at the standard 290°C injector setpoint. The calibration curve was used to convert peak areas to % conversion of DPA (data not shown).

Figure 7-3 and Figure 7-4 display the results for CaDPA and Na_2DPA, respectively (conducted in 50/50 water/MeOH to improve solubility of DPA salts). More data was not obtained using $NaMeSO_4$ and $KMeSO_4$ salts in the Na_2DPA study because of time constraints on the instrument and because the GC column (or inlet liner) had begun to exhibit signs of decomposition as manifest by siloxanes, particularly at methyl donor:DPA ratios above 10:1. In general, above this 10:1 ratio, further increases in the percent conversion of DPA to Me_2DPA were not apparent save in the case of TMA-$MeSO_4$, which appeared to effect the same degree of DPA conversion as the alkali metal salts did at a 10:1 ratio.

In neither figure does TMA-OH exhibit as high activity as do $MeSO_4^-$ salts. Another key observation is that the Na_2DPA data (Figure 7-4) exhibited much greater scatter than the CaDPA (Figure 7-3), and in both figures, there are some extreme outliers for Me_2DPA yield from TMA-$MeSO_4$. Although the reason was not determined, it is thought to result from the significant differences in the stability constants of DPA with

Ca^{2+} and the alkali cations or TMA^+. Divalent Ca^{2+} remains bound by chelation to DPA even in the presence of Li^+, Na^+, K^+, Cs^+, and TMA^+ cations, but Na^+ is more easily displaced/exchanged. Conditions in the solution or on the wire are apparently different enough between runs (due to different degrees of hydration, random features in ion associations and precipitations, etc.) that different complexes between DPA^{2-}, $MeSO_4^-$, Na^+, the $MeSO_4^-$ countercation, and any solvent are formed.
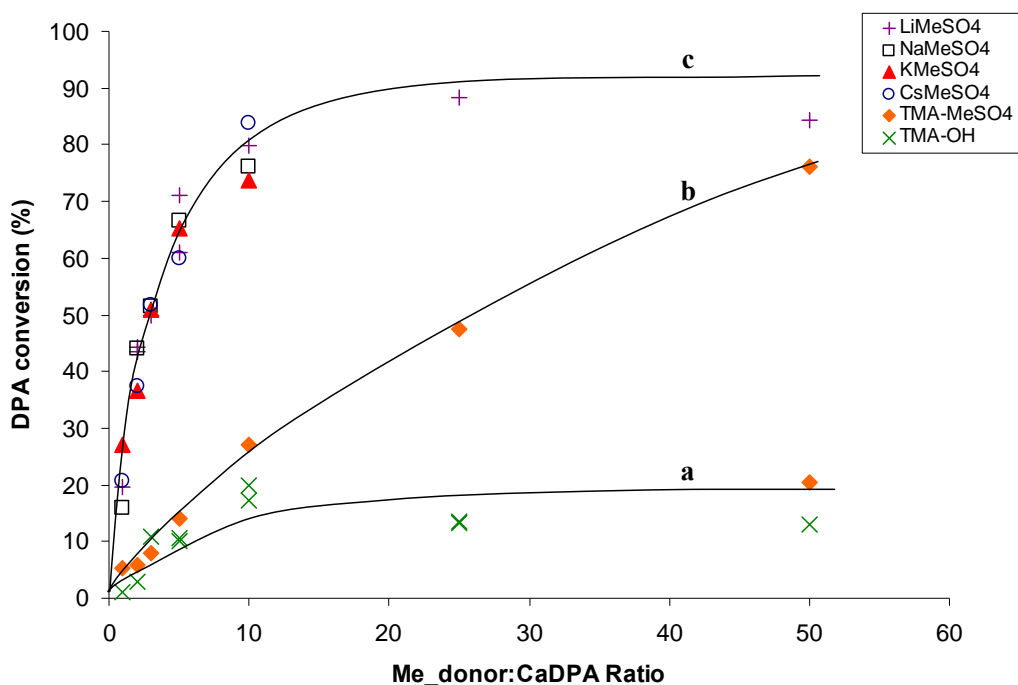
Figure 7-3. Percent conversion DPA to Me₂DPA vs. methyl donor:CaDPA ratio. Curves labeled a, b, and c indicate apparent trends in the data, not a regression. The TMA-MeSO₄ molecule was considered to be a single methyl donor.

Substantiating this conclusion are the results of a study that found HCl-neutralized TMA-OH solutions of fatty acids gave higher standard deviations than with basic solutions, which was attributed to the TMA^+ soaps' becoming partially dissociated: "As ion-pair stability [between phenols and cationic reagent] decreases, more

128

derivatization reagent is needed to secure complete methylation" [415]. TMS$^+$ salts

formed fewer methylated products with phenols, apparently due to weaker ion pairing.

This problem (difference in methylation efficiency) was not observed with stronger

aliphatic acids [330].
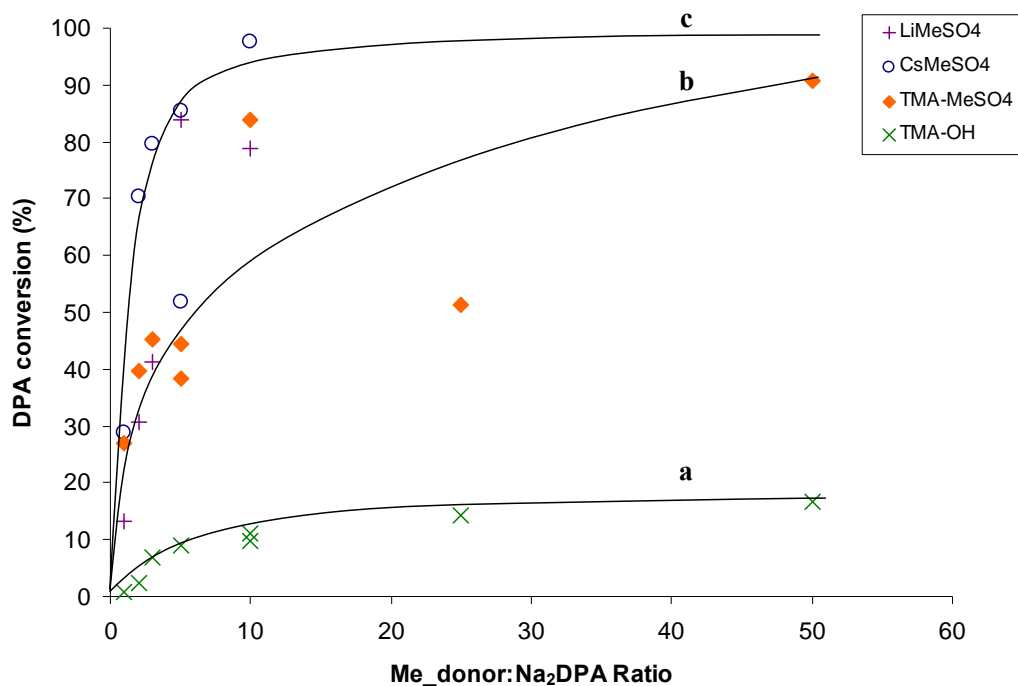
Figure 7-4. Percent conversion DPA to Me$_2$DPA vs. methyl donor:Na$_2$DPA ratio. Curves labeled a, b, and c indicate apparent trends in the data, not regression. The TMA-MeSO$_4$ molecule was considered to be a single methyl donor.

Although the data of Figure 7-4 are scattered (and, unfortunately, data for

NaMeSO$_4$ and KMeSO$_4$ are absent), CsMeSO$_4$ appears to be more active in methylating

Na$_2$DPA than LiMeSO$_4$ (the "outlier" points at methyl donor:Na$_2$DPA ratio of 5

challenge this claim). Also, comparing the results with TMA-MeSO$_4$ from Figure 7-4

with those of Figure 7-3 indicates that Na$_2$DPA is less "poisoned" than CaDPA for

methylation by TMA-MeSO$_4$, probably because the large TMA$^+$ cation exchanges much

more easily with Na-DPA complexes than with the multidentate CaDPA chelate, and/or because Na^+ polarizes the DPA's carboxylate oxygen to a lower degree (i.e., withdraws electrons more weakly) than Ca^{2+}, and/or the doubly-charged Ca^{2+} repels TMA^+ more strongly than singly-charged Na^+. Since Na^+ and Ca^{2+} are approximately the same size (0.95 and 0.99 Å, respectively [416]) and since there are two Na^+ cations—but only one Ca^{2+}—per DPA molecule, steric hindrance does not appear to explain the differences in reactivity.

7.3 *Thermogravimetric analysis (TGA) of MeSO$_4$ salts*

Thermogravimetric analysis (TGA) was used to explore the temperature dependence on the rate of decomposition of three $MeSO_4^-$ salts either synthesized in the present study or purchased commercially. Percent weight loss of an original sample weighing on the order of 5-10 mg (Figure 7-5) was recorded as the sample was heated at 5°C/min in an inert atmosphere (He or N_2).

Similar reactions as those identified for heating $KMeSO_4$ in air [417], shown by Eqns. (7-2) and (7-3), are apparent for $NaMeSO_4$ (theoretical wt% values indicated in Figure 7-5), and more closely match their theoretical values.

$$KMeSO_4 \ (s) \rightarrow K_2S_2O_7 \ (s) + Me_2O \ (g) \tag{7-2}$$

$$K_2S_2O_7 \ (g) \rightarrow SO_3 \ (g) + K_2SO_4 \ (s) \tag{7-3}$$

As it is heated, $TMA\text{-}MeSO_4$ behaves much differently than do $KMeSO_4$ and $NaMeSO_4$. An initial mass loss at about 250°C is followed by a precipitous loss at around 300°C. Although not shown in Figure 7-5, by 360°C, both $TMA\text{-}MeSO_4$ samples level off at ~4% of their original weight values, indicating that near-complete loss of all

material occurs during heating. Though presently only a conjecture, one possible reaction explaining the thermal behavior of TMA-MeSO$_4$ is that shown by Eq. (7-4).

$$TMA\text{-}MeSO_4 \text{ (s)} \rightarrow (CH_3)_3N \text{ (g)} + Me_2O \text{ (g)} + SO_3 \text{ (g)} \qquad (7\text{-}4)$$
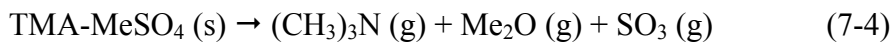
If Eq. (7-4) is correct, TMA-MeSO$_4$ may be a useful *in-situ* methylation reagent for GC since it does not leave a non-volatile, active alkali metal sulfate salt. However, the inlet to the instrument apparently must be heated at or above 350°C for this reaction to work. Furthermore, additional chemical components (e.g., from the sample) give the possibility for other reactions not described by Eqns. (7-2), (7-3), and (7-4) to occur, which may still produce non-volatile sulfate residues. For example, CaSO$_4$ would be expected from bacterial spores.
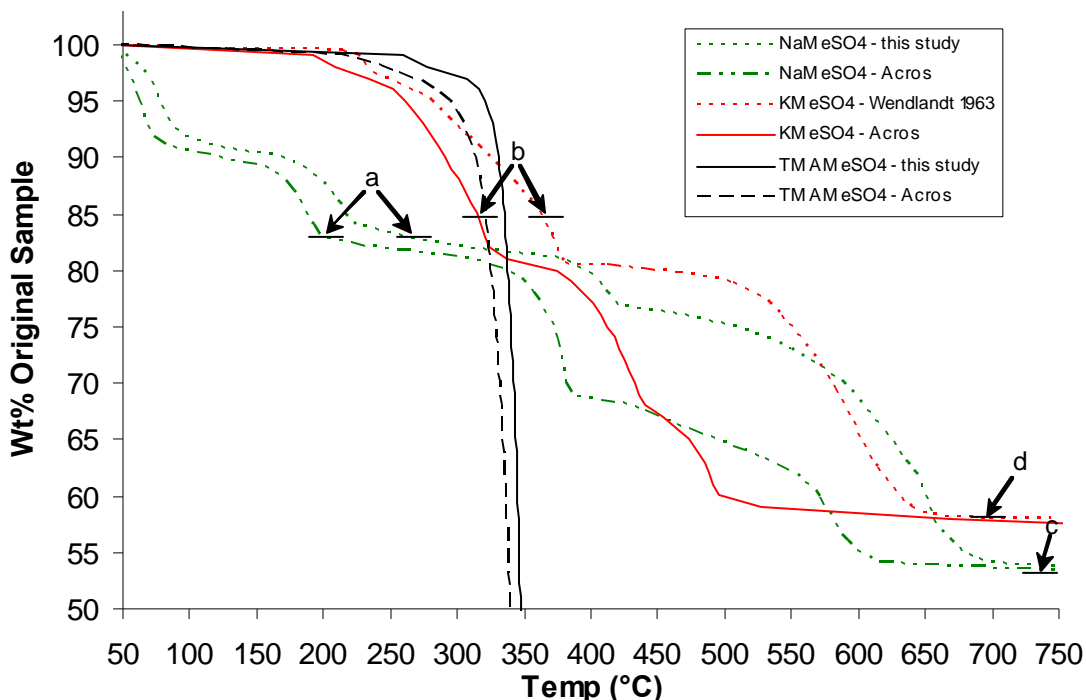
Figure 7-5. Sample weight percent versus temperature for TGA analysis of NaMeSO$_4$, KMeSO$_4$, and TMA-MeSO$_4$ (this study) and KMeSO$_4$ (from [417]). Horizontal line segments indicate theoretical wt% values for Na$_2$S$_2$O$_7$ (82.3%; a), K$_2$S$_2$O$_7$ (84.7%; b), Na$_2$SO$_4$ (53.0%; c), and K$_2$SO$_4$ (58.0%; d).

The thermograms of MeSO$_4^-$ salts of a given cation, although not identical, are close at temperatures below 300°C. The differences are probably due to the methods of preparation of the reagent, which resulted in differences in purity and perhaps crystalline structures. Differences in the molecular morphology or macroscale packing of the crystals in the TGA pan may have influenced rates of mass transfer as well. For all samples, discrepancies may occur due to irregular boiling or splashing of the samples at very high temperatures.

There are obvious differences in the thermal behavior among the three salts in the temperature regime of interest to GC (<300°C). First, NaMeSO$_4$ loses weight between about 50-100°C and again between 175-225°C, while the other two salts are more thermally stable, not losing significant mass until about 250°C. Although the reasons for this behavior are unknown, they may be due either to the increased polarizability or due to the steric hindrance that the cation presents to methyl transfer reactions, both of which depend on cation size (the crystalline radii of Na$^+$, K$^+$, and TMA$^+$ are 0.95 [416], 1.33 [416], and ~2.4–3.2Å [418, 419], respectively).

8 MIXTURES STUDIES WITH IONIC METHYLATING REAGENTS

8.1 *Na₂DPA methylation in TMA⁺, Na⁺, OH⁻, and MeSO₄⁻ mixtures*

8.1.1 Design details

It was of interest to explore whether some ternary or quaternary ionic blend was more effective than binary ionic reagents in producing Me₂DPA. An experiment was carried out in which the total concentration of the two FCs (fundamental constituents) active for methylation (TMA⁺ and MeSO₄⁻) was kept at a constant 50:1 ratio relative to DPA [Eq. (8-1)]. Also, DPA concentration was kept constant at 1 mM [Eq. (8-2)]. Thus, all experiments were conducted in a 25-fold stoichiometric excess relative to DPA, and the other ions were varied with respect to this relationship.

$$\frac{\left(C_{TMA^+} + C_{MeSO_4^-} \right)}{C_{DPA^{2-}}} = 50 \tag{8-1}$$

$$C_{DPA^{2-}} = 1 \text{ mM} \tag{8-2}$$

Figure 8-1 displays the mixture space for these experiments, which is the plane **qrsuv** residing inside of a tetrahedron whose vertices correspond with each ion in the system. Points **q** and **r** are not on the edges of the tetrahedron because some Na⁺ is introduced from the source of DPA, Na₂DPA. Also, although a point **t** is indicated in the

figure, such a mixture is not physically attainable because Eq. (8-1) requires that there always be some TMA^+ and/or $MeSO_4^-$, while point **t** represents a mixture that consists *only* of NaOH. Only an infinite amount of NaOH would satisfy the constraints imposed by point **t**—obviously an impossible scenario. This feature of the chemical mixture is clarified by the discussion in Section 8.3.8.
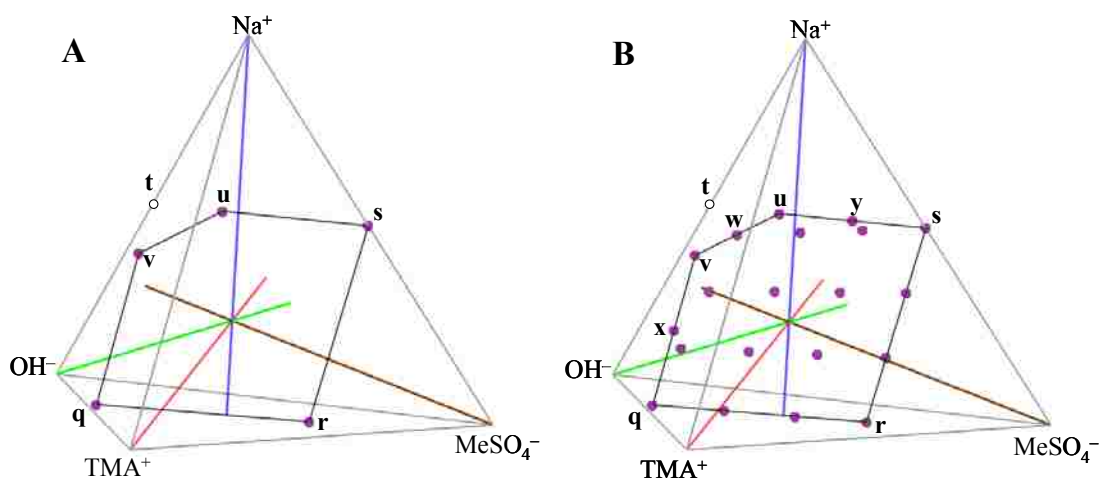
Figure 8-1. Experimental design points for model compound study. (A) indicates the convex hull of the entire design, and (B) displays all mixture points investigated. See text for details.

Eqns. (8-3) through (8-7) are the matrices underlying the experimental design. In Eq. (8-3), Ξ_0 is the convex hull of the entire design space obtained by considering single and binary combinations of reagents (e.g., NaOH alone or stoichiometric NaOH + $HMeSO_4$; the non-integer values in Ξ_0 result because the Na^+ from Na_2DPA, which was always constant at 2 mM, was considered as part of the ionic mixture). H_0 [Eq. (8-4)] is a set of convex multipliers (discussed further in Section 4.4.5 and Appendix A) that were used to obtain some points on the *perimeter* of **qrst** in Figure 8-1B (including points **u**, **v**, **w**, **x**, and **y**). Another convex set contained within the first, Ξ_1 [Eq. (8-5)], was generated

by using points **q**, **r**, **s**, and **w** (**w** is an interpolation between points **u** and **v**) and another

convex multiplier, **H₁** [Eq. (8-6)], was employed to interpolate within **qrsw**. The points

within **qrsw** were added in order to sample the experimental field uniformly. All

experimental points were assembled into a single matrix via Eq. (8-7).

$$
\Xi_0 =
\begin{bmatrix}
 & TMA^+ & Na^+ & OH^- & MeSO_4^- \\
\hline
q & 0.4902 & 0.0196 & 0.4902 & 0 \\
r & 0.4808 & 0.0385 & 0 & 0.4808 \\
s & 0 & 0.5098 & 0 & 0.4902 \\
u & 0 & 0.5032 & 0.3380 & 0.1588 \\
v & 0.1205 & 0.3819 & 0.4976 & 0
\end{bmatrix}
\tag{8-3}
$$

$$
H_0 =
\begin{bmatrix}
 & q & r & s & u & v & w & x & y \\
\hline
q & 1 & 0 & 0 & 0 & 0 & 0 & 0.5 & 0 \\
r & 0 & 1 & 0 & 0 & 0 & 0 & 0 & 0 \\
s & 0 & 0 & 1 & 0 & 0 & 0 & 0 & 0.5 \\
u & 0 & 0 & 0 & 1 & 0 & 0.5 & 0 & 0.5 \\
v & 0 & 0 & 0 & 0 & 1 & 0.5 & 0.5 & 0
\end{bmatrix}
\tag{8-4}
$$

$$
\Xi_1 =
\begin{bmatrix}
 & TMA^+ & Na^+ & OH^- & MeSO_4^- \\
\hline
q & 0.4902 & 0.0196 & 0.4902 & 0 \\
r & 0.4808 & 0.0385 & 0 & 0.4808 \\
s & 0 & 0.5098 & 0 & 0.4902 \\
w & 0.0603 & 0.4425 & 0.4178 & 0.0794
\end{bmatrix}
\tag{8-5}
$$

$$
H_1 = \frac{1}{3}
\begin{bmatrix}
q & 0 & 1 & 1 & 1 & 1 & 2 & 0 & 0 & 2 & 1 & 0 & 0 \\
r & 1 & 0 & 1 & 1 & 0 & 1 & 2 & 0 & 0 & 2 & 1 & 0 \\
s & 1 & 1 & 0 & 1 & 0 & 0 & 1 & 2 & 0 & 0 & 2 & 1 \\
w & 1 & 1 & 1 & 0 & 2 & 0 & 0 & 1 & 1 & 0 & 0 & 2
\end{bmatrix}
\tag{8-6}
$$

$$
X_{des} =
\begin{bmatrix}
H_0{}^T \Xi_0 \\
H_1{}^T \Xi_1
\end{bmatrix}
\tag{8-7}
$$

The volumes of TMA-OH, HMeSO$_4$, and NaOH required to satisfy Eqns. (8-1) and (8-2) were computed by material balances on each component using $\mathbf{X}_{\mathbf{des}}$ and the known stock solution concentrations. Immediately after mixing the appropriate volumes of stock solutions into the aggregate solution and diluting, the coiled wire was dipped in the solution, air-dried, and injected as described in Section 3.4.1. An example chromatogram is shown in Figure 8-2. Some tailing of the Me$_2$DPA peak is typical.
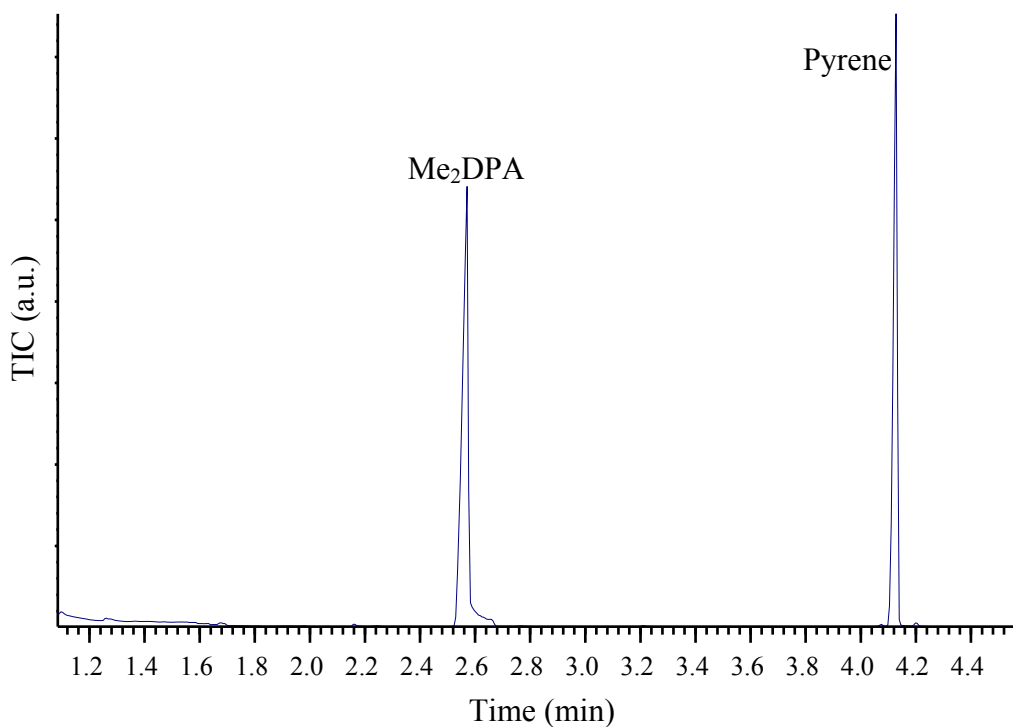
Figure 8-2. Example chromatogram from Na$_2$DPA model compound study.

8.1.2 Results

The net quantity of Me$_2$DPA produced by each experiment was computed by integrating its peak using the characteristic mass spectral ion of Me$_2$DPA, m/z 137, and comparing the area to a known concentration of Me$_2$DPA introduced into the GC using

the CWF. A fourth-order polynomial [Eq. (8-8); referred to as "**lm**" for "linear model"] was fit to the Me$_2$DPA percent yield data using TMA$^+$ and MeSO$_4^-$ as the two independent ions (χ_1 and χ_2, respectively). The fit is displayed as a contour plot in Figure 8-3.

$$
\begin{aligned}
f_{lm}(\chi,\beta) = \ & \beta_0 + \beta_1\chi_1 + \beta_2\chi_2 + \beta_3\chi_1^{\ 2} + \beta_4\chi_2^{\ 2} + \beta_5\chi_1\chi_2 + \\
& \beta_6\chi_1^{\ 3} + \beta_7\chi_2^{\ 3} + \beta_8\chi_1^{\ 2}\chi_2 + \beta_9\chi_1\chi_2^{\ 2} + \\
& \beta_{10}\chi_1^{\ 4} + \beta_{11}\chi_2^{\ 4} + \beta_{12}\chi_1^{\ 3}\chi_2 + \beta_{13}\chi_1^{\ 2}\chi_2^{\ 2} + \beta_{14}\chi_1\chi_2^{\ 3}
\end{aligned}
\tag{8-8}
$$
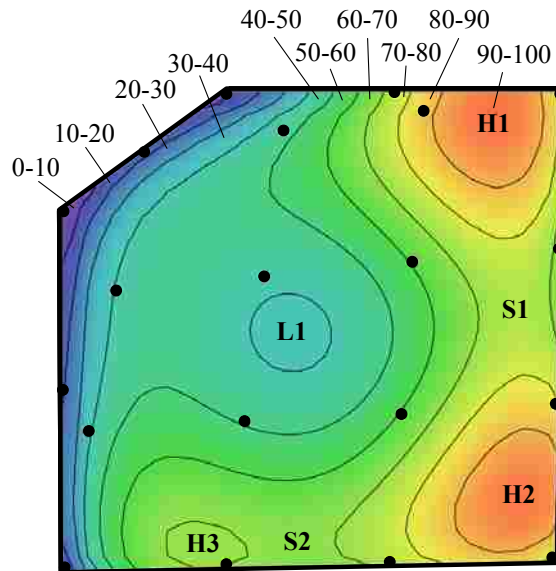
Figure 8-3. Contour plot of percent Me$_2$DPA yields from pure DPA (as Na$_2$DPA). Two saddle points (S1 and S2), one local minimum (L1), and two local maxima (H1 and H2) are indicated.

Although the model predicts regions of maximum response at the points labeled **H1** and **H2** in Figure 8-3, no data were available in those regions to verify that the model's near-100%-conversion predictions are valid. Additionally, the results of this Na$_2$DPA study are only partially useful since spores possess the Ca^{2+} form of DPA, which is shielded from chemicals by the spore's protective structural features. CaDPA

was not utilized in this study because of its very low solubility in 100% MeOH

(worsened by addition of ionic reagents since increasing the ionic concentration of a

solution decreases the degree to which ions exist in dissociated form [32]), while

Na_2DPA is sufficiently soluble.[45] Thus, these results are limited in their applicability to

spores, although the experiment did establish a useful method. Given that Me_2DPA yield

from spore CaDPA is more important than that from Na_2DPA model compound, a more

detailed discussion on the model is reserved for spore DPA conversion below.

8.2 *Spore DPA behavior in TMA^+, $MeSO_4^-$ mixtures*

8.2.1 Experimental design

A similar experiment as that with Na_2DPA was done with BA and BT spores, but

with the constraint that the total concentration of methyl-donating reagents be 750 mM

[Eq. (8-9)] in 500 µL total aggregate solution volume, which was consistent with the

standard, previously adopted protocol (cf. Table 5-2).

$$\left(C_{TMA^+} + C_{MeSO_4^-} \right) = 750 \text{ mM} \tag{8-9}$$

Spores were delivered as wet pellets in Eppendorf tubes obtained by centrifuging

500 µL aliquots from stock suspensions that were approximately 10^{10} spores/mL. The

mean DPA concentration of 500 µL samples of each spore type was determined by

autoclaving in 1.5 M H_2SO_4 followed by LC analysis. DPA did not decompose under the

acidic autoclave conditions since the DPA LC peak areas did not change before and after

---

[45] See Footnote 34.

the autoclave treatment (data not shown). BA and BG spores possessed 7.09 ±0.56 and

5.56 ±0.15 mM total DPA, respectively (errors are 95% confidence intervals on the

mean). These concentration values served as the basis for computing the percent

conversion of spore DPA to Me_2DPA. At the conditions employed, the Me donor (TMA^+

+ $MeSO_4^-$) to DPA ratio was 106 and 135 times the DPA content of the BA and BG

spores, respectively.

Exploration of the reagent mixture's effect on Me_2DPA yield were obtained in a

similar manner as described for the Na_2DPA study above via Eqns. (8-9)-(8-11).

$$
\Xi_0 = \begin{array}{c|cccc}
 & TMA^+ & Na^+ & OH^- & MeSO_4^- \\
\hline
q & 0.5 & 0 & 0.5 & 0 \\
r & 0.5 & 0 & 0 & 0.5 \\
s & 0 & 0.5 & 0 & 0.5 \\
t & 0 & 0.5 & 0.5 & 0
\end{array}
\qquad (8\text{-}10)
$$

$$
H_0 = \begin{array}{c|cccccccccccc}
 & q & r & s & u & v & w & x & y & z & a & b & c \\
\hline
q & 1 & 0 & 0 & 0 & 0.5 & 0.25 & 0.25 & 0 & 0.5 & 0 & 0.25 & 0.5 \\
r & 0 & 1 & 0 & 0 & 0 & 0 & 0.25 & 0.5 & 0.5 & 0.25 & 0.5 & 0.25 \\
s & 0 & 0 & 1 & 0.5 & 0 & 0.25 & 0.25 & 0.5 & 0 & 0.5 & 0.25 & 0 \\
t & 0 & 0 & 0 & 0.5 & 0.5 & 0.5 & 0.25 & 0 & 0 & 0.25 & 0 & 0.25
\end{array}
\qquad (8\text{-}11)
$$

The spore experiments were conducted in two blocks, however. Initially, the mixture

points indicated by Figure 8-4A were studied ("block 1"). The observation that the

Me_2DPA yields were highest within **rsuz** led to additional experiments ("block 2"),

indicated by red X's in Figure 8-4B, which were computed by convex multiplications of

points **ryxz** and **suxy** to interpolate between them (**H** matrices not shown). Since spores

were in limited supply, only some of the 11 additional block 2 "red X" design points (7

for BA and 6 for BG) were studied for each spore type (Figure 8-5).
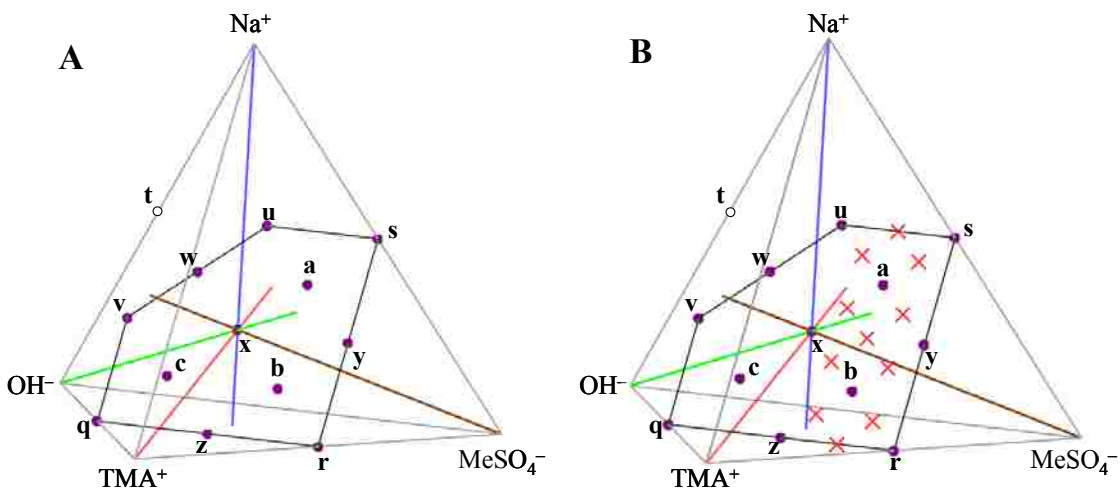
Figure 8-4. Experimental design points for spore study showing (A) the initial experimental design and (B) the expanded design with added points indicated by "red X's".
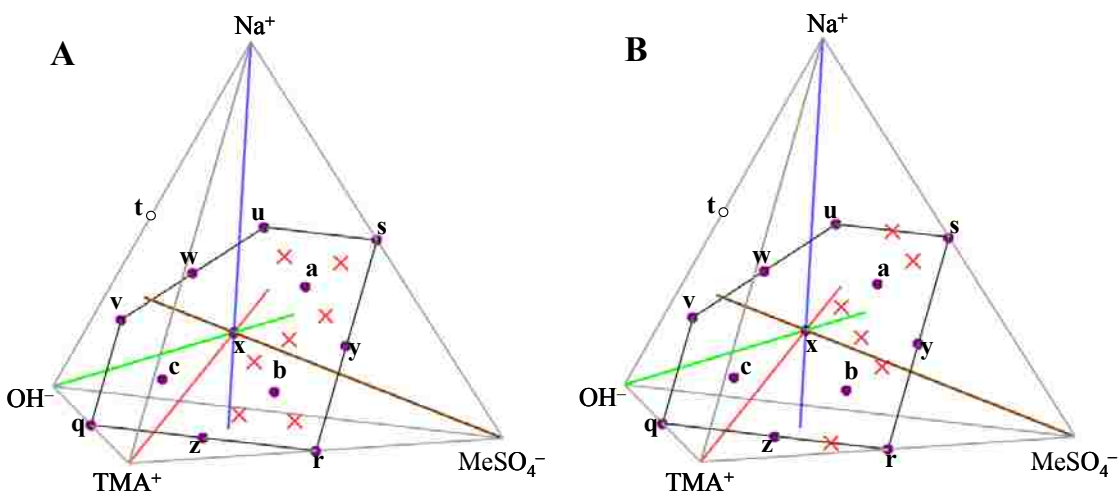
Figure 8-5. Experimental points for (A) BA and (B) BG spores. "Red X's" indicate the block 2 points that were sampled for each spore type.

The mixtures of reagents, diluent solvent, and internal standard intended for spore biomarker derivatizations were computed by material balances. Each aggregate solution was prepared separately from the spores in a 0.5 dram glass vial immediately before analysis and transferred into the spore-pellet-containing Eppendorf tube using a Pasteur

pipette. In cases where Na^+ and $MeSO_4^-$ were both present, a white precipitate was always observed, which prompted adding 100 μL H_2O to the solution for all samples to abet salt solubility. This increased volume (600 μL vs. 500 μL) was factored into the computations on Me_2DPA yields. (Although the effect of water on solubility was marginal, the precipitate did <u>not</u> negatively affect DPA yields; in fact, the highest Me_2DPA conversion was obtained in mixtures where a precipitate was present.)

Spores were mixed well with the reagents by dislodging/mashing/resuspending the dense spore pellet residing at the bottom of the Eppendorf tube (a result of centrifugation) with the round, sealed end of a glass capillary melting point tube after which the Eppendorf tube was vortexed for at least 20-30 s to homogenize the spore + reagent solution/mixture. The protocol was conducted in this way in order to (1) avoid exposure of spores to temporarily highly acidic or basic conditions (which might confound results with process variables) and (2) mimic the most ideal, simplest-case where a *single* solution is added to spores prior to sample introduction into the GC.

8.2.2   Spore Me₂DPA yields results

Three example chromatograms from BA spores analyzed in this study are displayed in Figure 8-6 to illustrate some of the effects that the reagent composition has on spore biomarker yields. Two key spore biomarker types visible in the chromatogram are (1) DPA, as Me_2DPA and MeMPA (the methyl ester of DPA's singly decarboxylated form, monopicolinic acid or MPA; see Figure 2-12), and (2) fatty acids (FAs), as their methyl esters (FAMEs). Pyrene was added separately as an internal standard. In Figure 8-6, point **q** represents an aggregate solution that contained TMA-OH alone, point **s** is

pure NaMeSO$_4$ (no OH$^-$ present), and point **a** is a mixture of all four ions, where

$x_{\text{TMA}^+} = 0.125$, $x_{\text{Na}^+} = 0.375$, $x_{\text{OH}^-} = 0.125$, and $x_{\text{MeSO}_4^-} = 0.375$ (a 1:3:1:3 ratio).
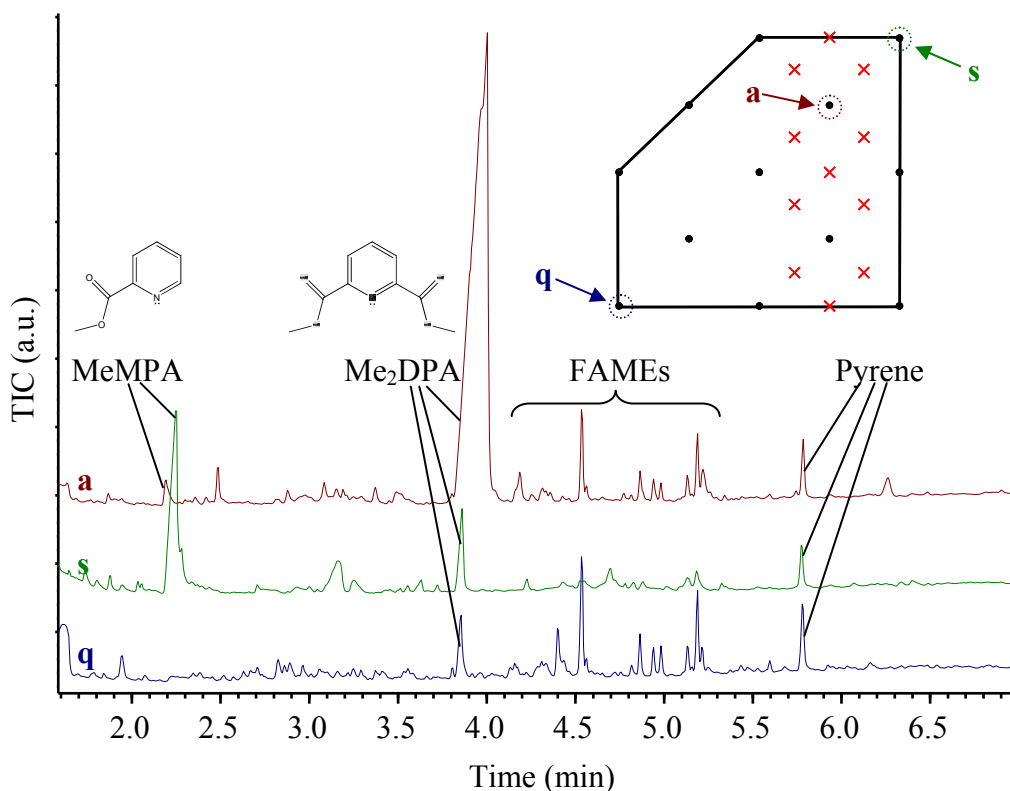
Figure 8-6. Example chromatograms for BA spore study produced at different points in the experimental design space.

At point **a**, Me$_2$DPA is produced in yields so high (approximately 95% overall conversion!) that the column was overloaded, as manifest by the sawtooth-shaped peak. Points **q** and **s** both reflect about 1-10% Me$_2$DPA conversion, although at point **s**, the MeMPA peak area exceeds that of Me$_2$DPA. MeMPA is not obvious at point **q**, but some is seen in **a**. Points **a** and **q** exhibit similar FAME profiles, while the conversion to FAMEs is very low at point **s**.

8.2.3 Discussion of spore mixtures experiments

Figure 8-6 provides an opportunity for some commentary about the chemistry of this single-step reaction that produces Me$_2$DPA. In Figure 8-6**s**, FAMEs yields are lower, presumably because OH$^-$ is not present to hydrolyze the ester bonds of the bound fatty acids—a prerequisite for methylation of the same via the S$_N$2 mechanism.

Also, the DPA decarboxylation observed in Figure 8-6**s** (with pure NaMeSO$_4$) probably results from the presence of H$^+$ if HMeSO$_4$ was in slight excess relative to NaOH. Mechanisms are known for decarboxylation of aromatic acids in both protonated and de-protonated forms [236]. Loss of the first carboxylate group of DPA by both mechanisms is shown in Figure 8-7.
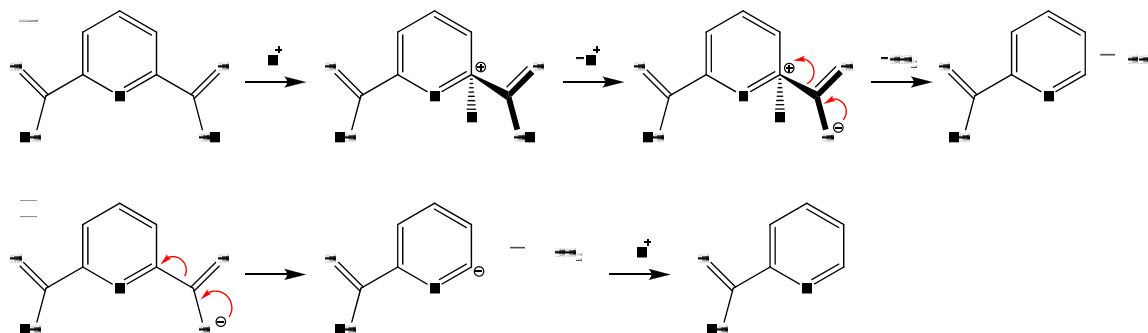
Figure 8-7. Known decarboxylation mechanisms for aromatic carboxylic acids, applied to DPA, for (A) acid-catalyzed and (B) base driven mechanisms (refer to Figure 2-12).

This author's experience is that in the heated GC inlet (290°C), DPA decarboxylates to a much greater extent in the presence of acid compared to base, although H$_2$DPA is known to decarboxylate between about 230-240°C [181, 303], possibly because this temperature is high enough to activate proton transfers indicated by Figure 8-7A between DPA molecules. The apparent higher thermal stability of CaDPA

[302] may result from the attraction of electrons on the carboxylate groups by Ca^{2+}, which may reduce their activity towards $-COO^-$ cleavage.

The results of the mixture experiments that focused on Me_2DPA yields from spores have very practical implications. Our research group has considered the *relative* yields of biomarkers important for differentiation of spores, for example, using the relative ratios of FAMEs to Me_2DPA to normalize results for improved differentiation success [420]. However, the experiments conducted with spores in this reagent mixture study indicate that altering the methylation reagent mixture changes the relative yields of methylated biomarkers with different chemical functionalities (Figure 8-6). Since this dissertation has focused only on spore Me_2DPA yields, a study of the reagent mixture's effects on both absolute yields and relative ratios between biomarkers is advisable. Data for this investigation on FAMEs and MeMPA are available in the chromatograms obtained for the Me_2DPA studies and may be analyzed by a successor student.

8.2.4 Fitting spore Me$_2$DPA data to models

The spore Me_2DPA percent yield data were fitted to the linear and nonlinear models shown by Eqns. (8-8) (rewritten below), (8-12), and (8-13) [referred to as "**lm**", "**nlm_1**", and "**nlm_2**," respectively; note that Eqns. (8-12), and (8-13) are based on the standard gamma distribution, Eq. (8-14)]. χ_1 and χ_2 are mole fractions of TMA^+ and $MeSO_4^-$, respectively. The best-fit parameters ($\boldsymbol{\beta}$) for the linear model, Eq. (8-8), were obtained by standard linear regression methodology, while Eqns. (8-12) and (8-13) required iterative nonlinear methods.

144

Unfortunately, most of the best-fitting **β** parameters for the nonlinear equations did not converge as the fitting algorithm progressed. As the **β**'s grew, numerical errors forced premature termination of the solver [note that the high values for the **β**'s occur in exponential terms in Eqns. (8-12) and (8-13)].[46]

$$f_{lm}(\boldsymbol{\chi}, \boldsymbol{\beta}) = \beta_0 + \beta_1\chi_1 + \beta_2\chi_2 + \beta_3\chi_1^2 + \beta_4\chi_2^2 + \beta_5\chi_1\chi_2 +$$
$$\beta_6\chi_1^3 + \beta_7\chi_2^3 + \beta_8\chi_1^2\chi_2 + \beta_9\chi_1\chi_2^2 + \tag{8-8}$$
$$\beta_{10}\chi_1^4 + \beta_{11}\chi_2^4 + \beta_{12}\chi_1^3\chi_2 + \beta_{13}\chi_1^2\chi_2^2 + \beta_{14}\chi_1\chi_2^3$$

$$f_{nlm\_1}(\boldsymbol{\chi}, \boldsymbol{\beta}) = \left[\exp(\beta_0)(\beta_3 - \chi_1)^{\beta_1 - 1}\exp(-(\beta_3 - \chi_1)\beta_2) + \right.$$
$$\left. \exp(\beta_4)(\chi_1 - \beta_7)^{\beta_5 - 1}\exp(-(\chi_1 - \beta_7)\beta_6)\right] \tag{8-12}$$
$$(\beta_{10} - \chi_2)^{\beta_8 - 1}\exp(-(\beta_{10} - \chi_2)\beta_9)$$

$$f_{nlm\_2}(\boldsymbol{\chi}, \boldsymbol{\beta}) = \exp(\beta_0)(\beta_3 - \chi_1)^{\beta_1 - 1}\exp(-(\beta_3 - \chi_1)\beta_2)$$
$$(\beta_{10} - \chi_2)^{\beta_8 - 1}\exp(-(\beta_{10} - \chi_2)\beta_9) +$$
$$\exp(\beta_4)(\chi_1 - \beta_7)^{\beta_5 - 1}\exp(-(\chi_1 - \beta_7)\beta_6) \tag{8-13}$$
$$(\beta_{13} - \chi_2)^{\beta_{11} - 1}\exp(-(\beta_{13} - \chi_2)\beta_{12})$$

$$d_{gamma}(x, a, b) = \frac{b^a}{\Gamma(a)}(x)^{a-1}\exp(-bx) \tag{8-14}$$

Although model convergence was not attained in the conventional manner (i.e., the **β**'s converge to consistent values as the solver runs), a special criterion was determined to specify convergence: When 10 consecutive residual sum of squared (RSS) error values changed less than 0.01% after each iteration, the model was considered

---

[46] Other forms of the gamma distribution were explored that either were not stable in the nonlinear solver or gave essentially identical fits as judged by the RSS values. A modified beta distribution was also attempted, although the nonlinear solver would not even commence toward a solution even with apparently good, reasonable guess values.

converged and $\boldsymbol{\beta}$ at that tenth sequential iteration was used for the model (see Figure 8-8

and Table 8-1). Little reduction of the RSS occurred upon further iterations, which is seen

in Figure 8-8 as the "leveling off" of the RSS values as the solver ran further.
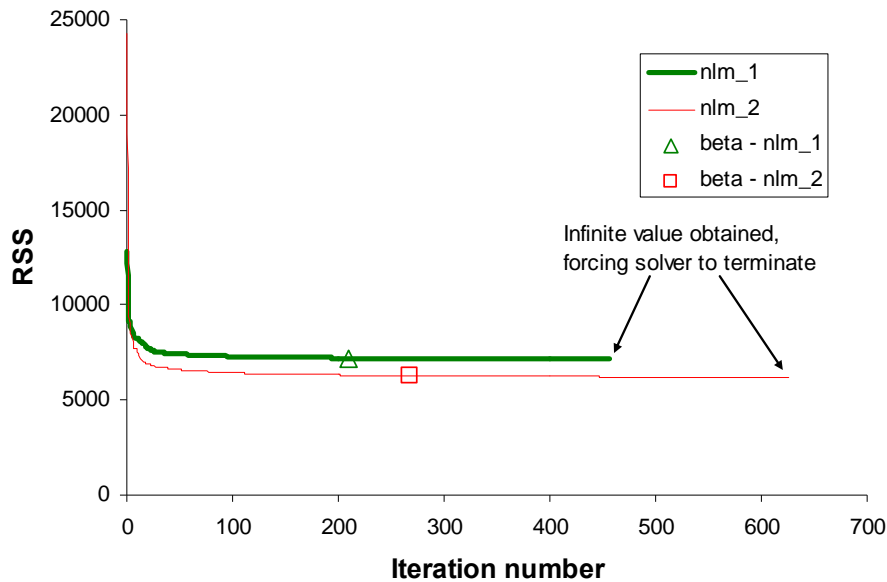
Figure 8-8. Residual sums of squared errors for nlm_1 and nlm_2 [Eqns. (8-12) and (8-13), respectively] vs. iteration number of the nonlinear solver. Triangle and square symbols indicate the iteration from which the $\boldsymbol{\beta}$ values were obtained for the models (Table 8-1).

Table 8-1 lists, for each model, the residual sum of squares (RSS) values, the

Akaike Information Criterion (AIC), the Pearson r, r^2, and r_{adj}^2 values, and the best-fit $\boldsymbol{\beta}_*$

parameter values. The standard F-test cannot be used to compare models that are not

nested, so other means were employed as a means for model comparison. First of all,

nlm_1 and **nlm_2** have lower RSS values, higher r, r^2, and r_{adj}^2 values,[47] and employ

fewer parameters compared **lm**, indicating that **lm** is less effective in describing the

---

[47] Recall r^2 values indicate the proportion of the variability in the data that is explained by the model.

variability in the data. Also, **nlm_1** and **nlm_2** visibly appear to match the data better.

The AIC values of **nlm_1** and **nlm_2** are lower than that of **lm**, indicating that the

nonlinear fits are better than the linear one.[48] Although **nlm_2** has a much lower RSS

value than **nlm_1**, both models' AIC and $r_{adj}{}^2$ values are close, indicating the difficulty in

judging which fits the data better. For the sake of parsimony, **nlm_1** is recommended

until further experimentation and analysis are conducted to conclude otherwise.

Table 8-1. Best-fit parameters, β_*, for Eqns. (8-8), (8-12), and (8-13). Although many digits in the β_* values are reported so that the model may be exactly reproduced, only 2-3 are generally significant.

Parameter or statistic	Linear fit [Eq. (8-8)]	Nonlinear fit 1 [Eq. (8-12)]	Nonlinear fit 2 [Eq. (8-13)]
$RSS^{\diamond}$	8120	7210	6260
$AIC^{\dagger}$	238	226	226
$r, r^2, r_{adj}{}^2$	0.88, 0.77, 0.62	0.89, 0.79, 0.71	0.91, 0.82, 0.72
β_0	183.0	282.452	275.205
β_1	-720.3	189.192	63.37
β_2	-2796.8	223.938	136.572
β_3	-3068.1	1.23625	0.847482
β_4	13226.7	191.068	147.719
β_5	11945.6	177.006	275.745
β_6	16707.9	134.937	161.899
β_7	-21622	-1.17131	-1.56571
β_8	-15577.2	38.6648	213.869
β_9	-30382	63.4954	165.635
β_{10}	-18242.7	0.946597	1.58446
β_{11}	9894.3	*N/A*	6.30737
β_{12}	3422.4	*N/A*	26.3127
β_{13}	20622.4	*N/A*	0.579785
β_{14}	23053.9	*N/A*	*N/A*

$^{\diamond}$ Residual sum of squared errors.
† Akaike's information criterion; see text for details.

---

[48] Note that AIC comparisons are also rigorous only with nested models.
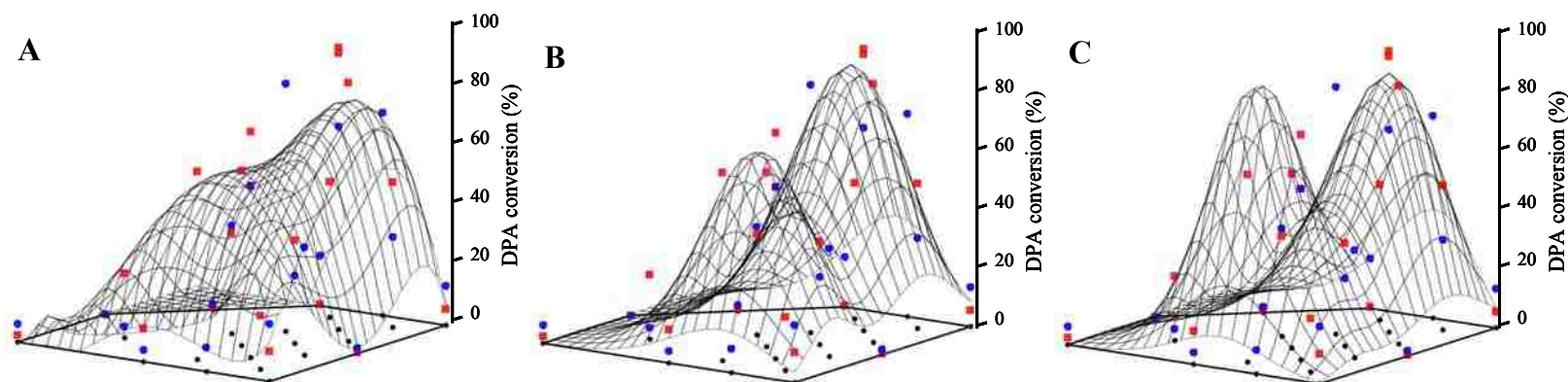
Figure 8-9. Me₂DPA percent conversion data plus wireframe representations of the models. Red squares are BA spores and blue circles are BG spores. (A) Eq. (8-8) [lm], (B) Eq. (8-12) [nlm_1], and (C) Eq. (8-13) [nlm_2].
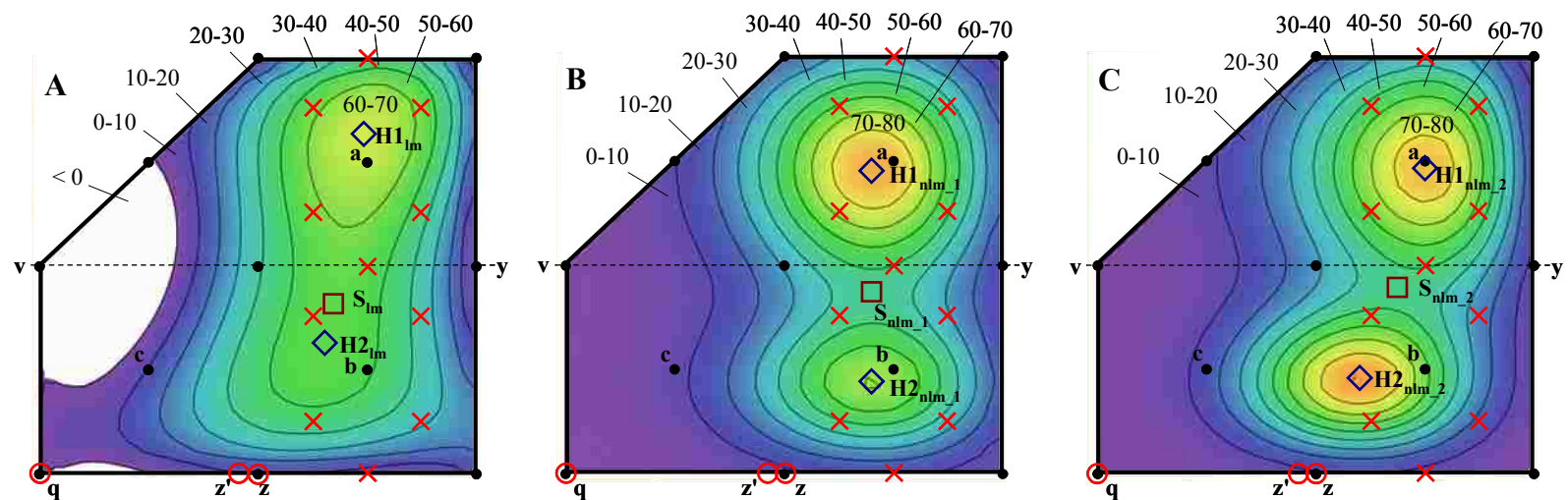
Figure 8-10. Contour plots of best fit models to the conversion of spore DPA to Me₂DPA using (A) Eq. (8-8) [lm], (B) Eq. (8-12) [nlm_1], and (C) Eq. (8-13) [nlm_2]. On the perimeter of the plots are indicated approximate percent conversions of DPA to Me₂DPA predicted by the models. Lowercase letters indicate reagent combinations discussed in the text. Local maxima for each model are indicated by H1 and H2, and a saddle point by S. A special discussion on the response at the circled points q, z, and z' is included in Appendix C.

The fits to the data for each of these models are shown in Figure 8-9 and Figure 8-10 (both are included on the same page). Due to the large degree of scatter in the response data, there are no obvious differences in percent Me$_2$DPA yields between BA and BG spores, so both were used in fitting single models rather than 2 separate models for each species. Although differences in *total* DPA amounts between spore species and even batches are expected, there is no reason to suspect any difference in *percent* DPA methylation of spores since the GC injector setpoint of 290°C is greater than 250°C, the reported temperature where DPA begins to escape the spores [300-302].

All three models exhibit reasonably close agreement for the location of the two observed maxima, **H1** and **H2**, and the saddle point, **S**. (The points **H1**, **S**, and **H2** from Figure 8-10 are overlaid together in Figure 8-12C as part of a later discussion on OH$^-$ effects.) Although the linear model identifies where regions of maximum response occur (discussed further below), it underestimates the magnitude of those points, it largely misses the significant decrease seen in the Me$_2$DPA response along **vy**, and it erroneously predicts *negative* Me$_2$DPA yields in some regions (see Figure 8-9A and Figure 8-10A).

In contrast, the nonlinear models are very descriptive of the dip seen near line **vy** and at the points of highest response in the interior of the design space. Also, the nonlinear models are always positive. Although this last feature is advantageous since data cannot be negative, the drawback is that the nonlinear models may under predict Me$_2$DPA response as χ moves far away from the optimal mixture, χ_* (that is, as the mixture is changed drastically relative to that where the local maxima of Me$_2$DPA percent conversion are found). Such is the case at points **q** and **r** in Figure 8-10, where the nonlinear models consistently under predict the response.

149

Using these models, the "best" recipes for TCM are reported in Table 8-2, where total methyl donor concentration is constant at 750 mM, total volume is 500 μL, and stock reagents are 2.0 M each. Appropriate volumes of stock reagents are readily computed from the data in Table 8-2 by appropriate material balances. Also in Table 8-2 are the predictions for the percent conversion of DPA to Me_2DPA based on the models of Eqns. (8-8), (8-12), and (8-13) and the best-fit $\boldsymbol{\beta}_*$ in Table 8-1.

Table 8-2. Volumes of reagents corresponding to critical points labeled in Figure 8-10 assuming stock solutions are all 2.0 M.

Model	ID in Figure 8-10	TMA-OH (2.0 M)	HMeSO$_4$ (2.0 M)	NaOH (2.0 M)	Solvent	Internal standard	Predicted Me$_2$DPA yield
lm	**H1$_{lm}$**	37 μL	150 μL	165 μL	98 μL	50 μL	76.1%
[Eq.	**S$_{lm}$**	87	100	61	202	50	60.6
(8-8)]	**H2$_{lm}$**	96	92	43	219	50	60.9
nlm_1	**H1$_{nlm\_1}$**	51	136	142	121	50	89.5
[Eq.	**S$_{nlm\_1}$**	84	103	62	200	50	44.2
(8-12)]	**H2$_{nlm\_1}$**	98	89	28	235	50	70.6
nlm_2	**H1$_{nlm\_2}$**	49	139	135	127	50	87.8
[Eq.	**S$_{nlm\_2}$**	83	104	66	197	50	46.3
(8-13)]	**H2$_{nlm\_2}$**	105	82	30	232	50	92.6

8.2.5 Quantitation of ions on the coiled wire filament

Since the sum of moles of TMA^+ + $MeSO_4^-$ was held constant at 750 mM for all experiments, the *net* quantity of ions collected by the coiled wire filament (CWF) varied with the mixture fractions. For example, a 100% TMA-MeSO₄ solution (**r** in Figure 8-5) had 375 mM each of TMA^+ and $MeSO_4^-$ and no Na^+ or OH^-. For a mixture with equal quantities of TMA^+, Na^+, OH^-, and $MeSO_4^-$ (**x** in Figure 8-5), the concentration of each

species was 375 mM, and so the total concentration was 1500 mM. Figure 8-11 indicates, with blue dashed lines, the mixtures where the total molar amount of ions collected by the wire was constant (note 750 mM total methyl donor concentration contributes 490 nmol in 0.65 µL). Further exposition on this topic of non-constant ions is given in Appendix A.
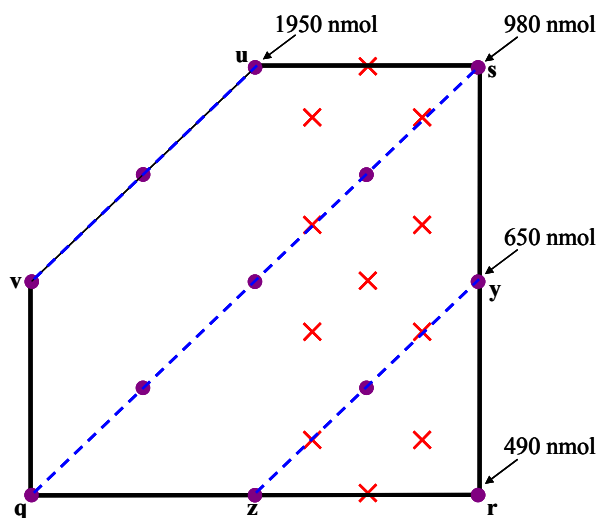
Figure 8-11. Mixture design space for spores. Blue dashed lines indicate the *total* quantity (in nmol) of ions that are transferred to the coiled wire filament assuming a volumetric uptake of 0.65 µL.

Figure 8-12 displays both the total abundances of each FC on the CWF in the mixtures design space as well as lines of constant mixture fraction for each ionic FC. The solid contour lines (constant moles) would coincide with the dashed lines (constant mole/mixture fractions) if a constant total molar basis (rather than constant TMA^+ + $MeSO_4^-$ basis) had been chosen for the experimental design. The local maxima and saddle points predicted by the models (originally presented in Figure 8-10) are re-plotted in Figure 8-12C because there appears to be a correlation between total amount of OH^- and these critical points from the models.
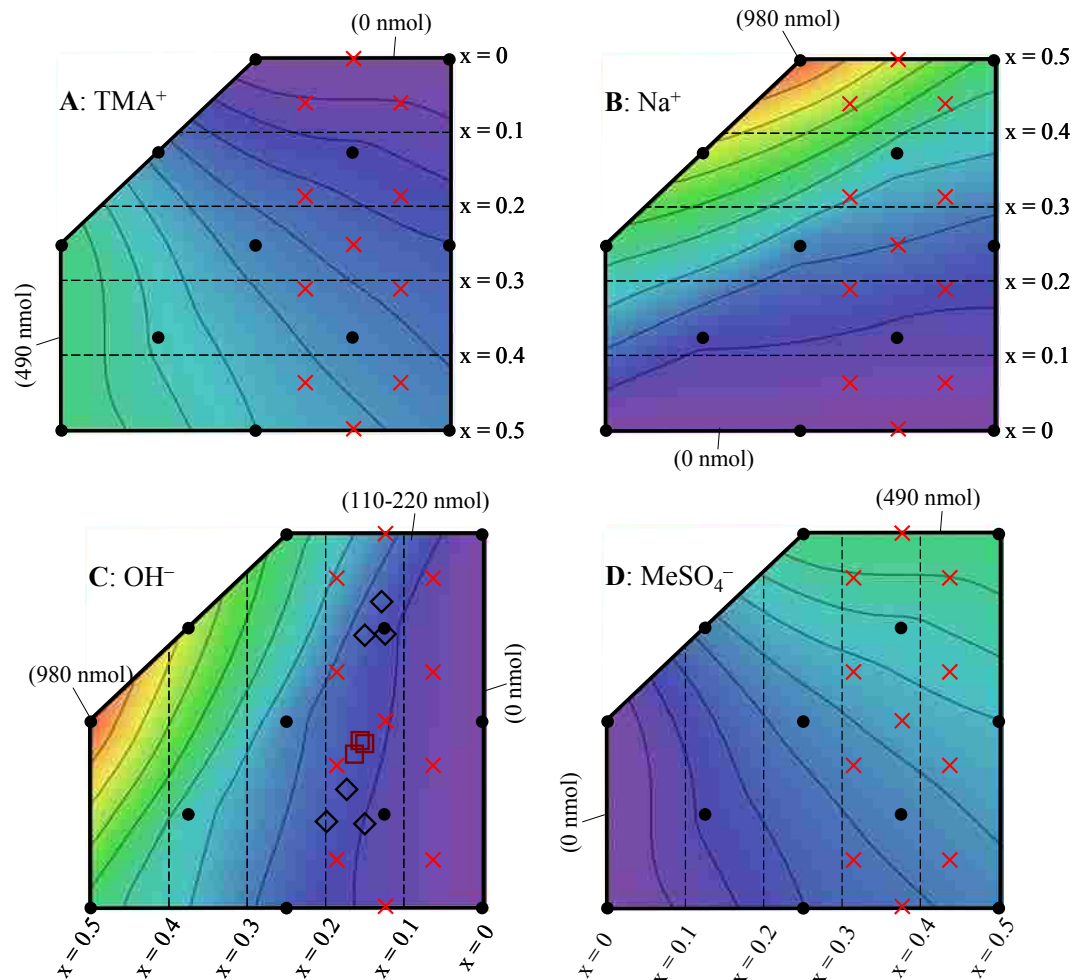
Figure 8-12. Contour plots representing the reagent quantities taken up by the coiled wire (solid lines) and mole fractions (dashed lines) for (A) TMA$^+$, (B) Na$^+$, (C) OH$^-$, and (D) MeSO$_4^-$. The numbers in parentheses indicate the minimum and maximum quantities of the given ion, in nmol, assuming 0.65 µL uptake by the CWF. Waviness in contours is an artifact of interpolating between the main design points.

If the apparent correlation between OH$^-$ amount and the models' critical points implicates total amount of OH$^-$ (rather than just its mixture fraction), then the hydrolysis process probably depends on the OH$^-$:spore ratio plus process conditions such as gas flow rate or liner and coil dimensions because these variables influence CWF heat-up rate, mass transport of volatilized materials away from the CWF, and residence times of reactive/reacting vapors in the system. If, on the other hand, these local maxima and

saddle points identify *absolute* optimal mixtures that are independent of total OH$^-$ (at least above some threshold amount of total methyl donor plus hydrolytic reagents) then the net quantity of reagents is less important than their relative mixture amounts. Thus, on a constant methyl donor basis, the maximum percent conversion of DPA to Me$_2$DPA would indicate a result that is more globally applicable. The relative importance of total reagent vs. mixture amount remains to be established.

8.3   *Sources of experimental errors for spore Me$_2$DPA yields data*

Many different physical sources of error were present that would have contributed to the scatter seen in percent yield of Me$_2$DPA. These sources are categorized roughly into problems related to spore homogeneity, GC calibration curves, activity and thermal gradients within the injection port liner, and instability of reagents (probably MeSO$_4^-$) during solvent evaporation. Additionally, LC calibration may have been slightly biased compared to actual spore DPA measurements.

8.3.1   Difficulty in obtaining homogeneous spores samples

One possible source of error in assessing the quantitative yield of spore Me$_2$DPA was due to the difficulty of resuspending spores in a homogeneous manner after they had been densely packed in a pellet at the bottom of an Eppendorf tube. Even with strongly acidic or basic reagents plus and mechanical breakup using the melting point capillary tube, residual small spore "clumps" remained that would not disintegrate. Although these were small and the majority of spores appeared homogenized, bias of the CWF towards capture of smaller particles produced errors that correlated with sample inhomogeneity.

One solution to this problem is to apply ultrasound. However, this was not employed here because ultrasound involved an additional process step that may have ruptured spores and/or released their DPA prematurely [421]. More importantly, sonication can promote undesirable reactions between the reagents such as premature $MeSO_4^-$ hydrolysis.

8.3.2 Solvent evaporation and sample effects on mixture composition

General experience established that dilute (< 1 M) $MeSO_4^-$ solutions in MeOH with only a few percent water are stable against acid or base hydrolysis (as judged by titration reproducibility), which is consistent with the literature. This feature is useful because a stock solution may be prepared in advance and used weeks later as long as it is kept neutral and/or in methanol of low water content. However, with increasing base concentration and water concentration, which prevail during evaporation of solvent on the coiled wire filament, the $MeSO_4^-$ reagent may be appreciably hydrolyzed, which may become a source of error in the *independent* variable, $\boldsymbol{\chi}$, rather than in the *dependent* variable, $\mathbf{y}$ [e.g., see Eq. (4-9)].

This phenomenon was briefly investigated with the reference protocol in mind (i.e., no $NaMeSO_4$ was present) using two $MeSO_4^-$ solutions—one acidic ("Solution A"), and the other basic ("Solution B"). Solution A was prepared to be 235 mM by dilution of a $HMeSO_4$ stock solution (final water concentration was also about 235 M H_2O). Solution B was prepared by adding TMA-OH to $HMeSO_4$, and was intended to have final concentrations similar to the reference spore derivatization mixture—235 mM $MeSO_4^-$, 500 mM TMA^+, and 265 mM OH^- (note the added TMA-OH contributed about 2.5 M

H$_2$O). To each solution, about 5 vol% or ~2.8 M water was added (the remainder being MeOH) to simulate the water content expected in actual spore samples (note Solution B had ~5.3 M total water).

Two 200 μL-sized aliquots of each of these solutions were transferred to glass vials and the solvent evaporated under N$_2$. Once dry, the solutions were re-constituted in 1 mL of either MeOH or H$_2$O (to see if the reconstituting solvent had any influence) and stored until titrated, at which point several mL more water was added in order to cover the pH electrode and to provide an aqueous environment for the same. Titrations were conducted on Solutions A and B once before drying ("fresh"), once after being reconstituted in H$_2$O or MeOH ("dry H$_2$O" or "dry MeOH"), and once again, without drying, about 10 h later after all other titrations were complete ("old") to verify that time was not responsible for changes in titration endpoints.

The titration data are shown for Solution A in Figure 8-13 and Solution B in Figure 8-14. Each data set in Figure 8-14 had two inflection points. Points of inflection, reported in Table 8-3, were found numerically according to the method described in Section 4.3 and used to make inferences about the extents of hydrolysis of MeSO$_4^-$.

The points of inflection (Table 8-3) were understood to reflect the neutralization points of the acid or base, which changes with the degree of MeSO$_4^-$ hydrolysis. No observable change in the acid strength of Solution A (fresh vs. old) was observed. However, the evaporation process did alter solution acidity, increasing it by 22% for the water-reconstituted sample and by 26% for that re-dissolved in MeOH. The sample reconstituted in water showed a slightly lower acidity gain when, theoretically, it should have been higher since water, not MeOH, is hydrolytically active against MeSO$_4^-$. This

difference is thought to lie within experimental error and it is concluded the reconstitution solvent did not truly influence the observed degree of hydrolysis with acidic mixtures.

Although the belief that reconstituting solvent has no effect, but that differences are due to experimental irreproducibilities is also held for Solution B, the solution reconstituted in water was higher in acidity than that in MeOH (lower 1st inflection points in Table 8-3), giving evidence that the solvent of reconstitution had an effect. Again, the solvent evaporation procedure was not carefully controlled and is probably the source of error (e.g., two different streams of N_2 were used for each vial; faster drying by one stream would have resulted in lower temperatures, lower times for reaction, and hence reduced hydrolysis compared to slow drying).
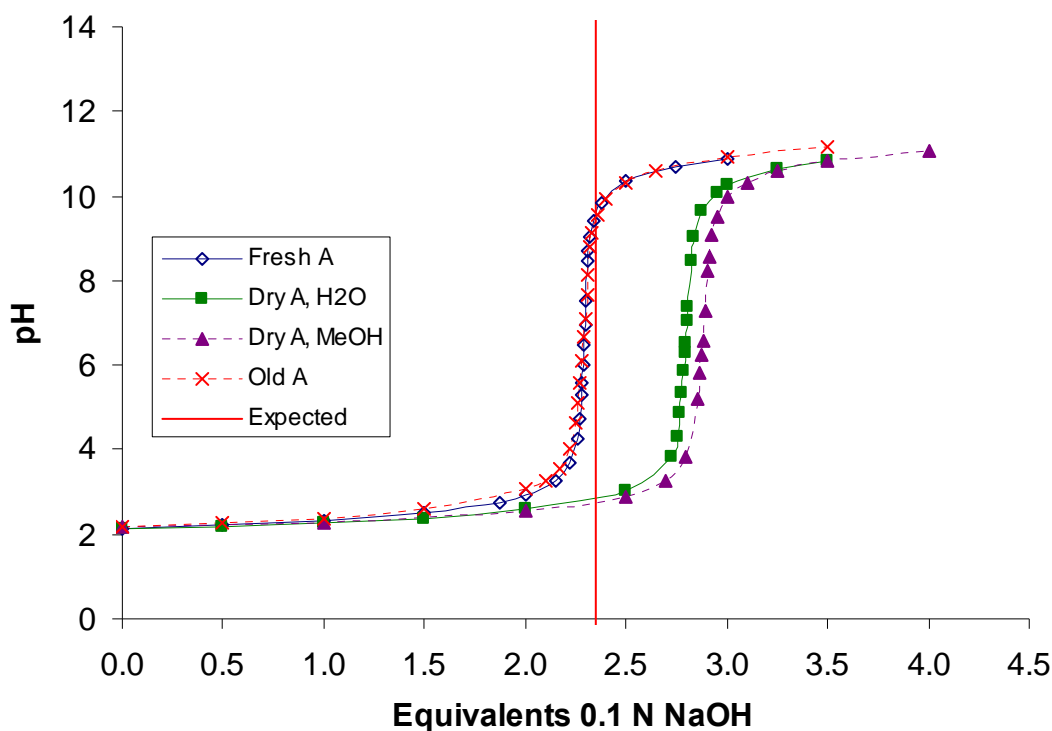
Figure 8-13. Titration data for acidic Solution A before and after drying. Expected value (2.35) indicated by vertical red line.
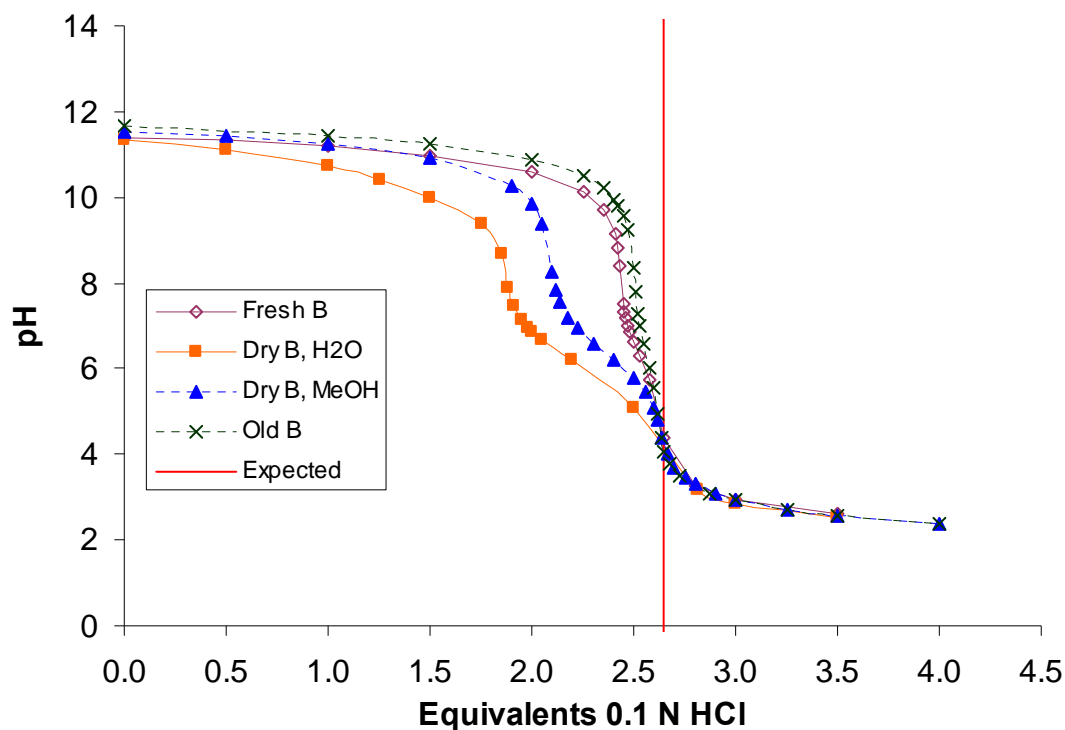
Figure 8-14. Titration data for basic Solution B before and after drying. Expected value (2.65) indicated by vertical red line.

Table 8-3. Inflection points from titration data from Figure 8-13 and Figure 8-14.

Condition of titrand	Solution A (mM)	Solution B (mM)
Fresh	229	1st 245 2nd 261
Dry, reconstituted in H_2O	280	1st 189 2nd 253
Dry, reconstituted in MeOH	289	1st 210 2nd 263
Old (~10 h)	229	1st 251 2nd 262

The titrations of Solution B in Figure 8-14 show two inflections, the first due to neutralization of OH^- and the second to protonation of SO_4^{2-} (probably involving displacement of TMA^+ in $[TMA^+SO_4^-]^-$ by H^+). That two inflection points were observed

in the titrations of "fresh" and "old" Solution B indicated the presence of free (nonmethylated) sulfate at respective amounts of 6.1% and 4.2% (computed by comparing the first to the second inflection point values; see Table 8-3). If experimental error is ruled out as a cause, the remaining possibilities for explaining the presence of initial SO_4^{2-} are that (1) conversion of H_2SO_4 to $HMeSO_4$ in the stock solution was incomplete, (2) additional hydrolysis occurred upon addition of water immediately prior to titration, and/or (3) some hydrolysis of $MeSO_4^-$ occurred upon preparation of Solution B. The fact that the SO_4^{2-} is apparently lower in "old" Solution B compared to the "fresh" solution supports the second possibility.

The percent of $MeSO_4^-$ in Solution B that was hydrolyzed during the drying step was computed for both dried solutions by comparing the 1st inflections of the same against the average of the 1st inflections of the "fresh" and "old" solutions (248 mM; see Table 8-3). The solution reconstituted in H_2O exhibited 24% hydrolysis, and that redissolved in MeOH was only hydrolyzed by 15%. Again, it is thought that the discrepancy is actually due to differences occurring during drying rather than the solvent identity, although this was not confirmed.

It is surprising that drying the $MeSO_4^-$ salts under alkaline conditions effected an extent of hydrolysis on par with drying in acidic solutions because the literature reports that hydrolysis is much faster in acid than in alkali [390]. The discrepancy could be due to the extra water in the alkaline solutions compared to the acidic ones, or to other differences in drying rates. Also, the literature suggests that hydrolysis of $MeSO_4^-$ in solution may occur even more rapidly with alkali metals in place of TMA^+. For example, although $HMeSO_4$ was stable for weeks in dilute aqueous solutions, it was over 90%

hydrolyzed overnight in the presence of coal fly ash [422], which perhaps was a result of the ash's mineral content. The same apparent enhanced reactivity of $MeSO_4^-$ salts to methylation in the presence of alkaline cations was manifest by the DPA conversion data discussed previously.

The net conclusion from this study is that what is believed to be on the wire based on the stoichiometry of the added reagents is probably incorrect due to the side reaction summarized by Eq. (8-15). This is one potential source of error.

$$MeSO_4^- + OH^- \rightarrow SO_4^{2-} + MeOH \qquad (8\text{-}15)$$

This reaction is undesirable because it reduces/depletes *both* the concentration of methyl donor *and* the thermochemolytically-active OH^-. The implication is that despite efforts to accurately control the final concentrations/ratios of $MeSO_4^-$, OH^-, and other cations, the final composition may be significantly different than the one intended. In the terminology of the mixture experiments, a significant uncertainty would result in $\mathbf{x_{des}}$ (and thus $\mathbf{\chi_{des}}$), as well as the net ratio of methylation reagent present. The high degree of scatter in the response variable was very likely strongly influenced by the uncertainty in $\mathbf{x_{des}}$.

Another possible error source is that samples susceptible to hydrolysis consume OH^-, which ultimately reduces the basicity of the solution and mixture fraction of OH^-. Hydrolysis of alkyl esters, illustrated in Figure 2-9 parts A and D, serve as example reactions of how hydrolysis depletes OH^-.

Nevertheless, even with a significant random component, given that the precursor mixture compositions were systematically manipulated, the deviations in $\mathbf{x_{des}}$ must possess a systematic component as well. Therefore, conclusions about the "best" mixture

for spore DPA release and methylation remain valid, even if a precise knowledge of the mixture that resides on the wire is unknown.

8.3.3 Inconsistencies in sample deposition on the wire

Experience has shown that the rather crude nature of drying the sample following collection on the wire can affect the gas chromatograms since not only do varying amounts of solvent remain from one injection to the next, but the resultant salt mixtures can vary compositionally (e.g., due to different degrees of hydrolysis of $MeSO_4^-$), likely morphologically (drying rate and temperature affects the size and structure of salt crystals), and probably physically [depending on the particular wire used, the age of the wire, and random effects, liquid droplets migrate to different locations on the wire (see Figure 8-15), and physical separations between liquid and solid materials have been observed].
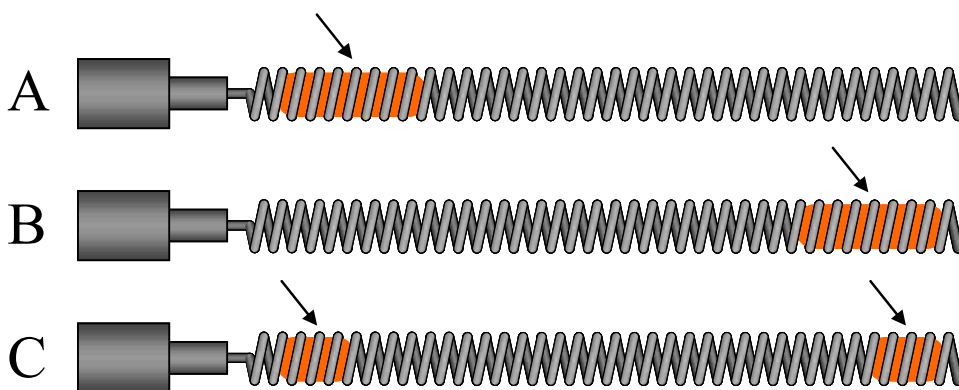
Figure 8-15. Illustration of possible locations of sample on the CWF after evaporation. Sample may remain (A) at back or upper end, (B) at the tip or front end, (C) split into two locations, etc.

8.3.4 GC calibration curve problems

A challenge to rigorous statistical analytical methods was the variability in the calibration curves that were produced for each study. The purpose of the calibration curve was to convert measured peak areas to absolute Me_2DPA amounts and ultimately to percent DPA conversions by comparing the observed Me_2DPA against the known amount of DPA in the sample (e.g., as determined by LC-UV analysis of spore hydrolyzates).

A different calibration curve was produced for each study since over time, the detector response may drift, etc. Figure 8-16 presents portions of a *series* of calibration curves generated for several studies pursued during this work (only one of which—the spores data—actually employed one of those curves). Figure 8-16A and B were generated by carefully transferring known *volumes* of standardized concentrations of Me_2DPA + internal standard with a microliter syringe to the CWF and using, respectively, a GC equipped with a quadrupole mass spectrometer (MS) and flame ionization detector (FID) for detection.[49] Figure 8-16C was obtained by repeated dipping of the coiled wire (nominal 0.65 μL sampling volume assumed from previous CWF volumetric uptake study). Figure 8-16D displays the Me_2DPA peak area vs. the internal standard peak area. Data in Figure 8-16C and D were obtained with the MS detector.

The reason that a relatively information-poor calibration curve, Figure 8-16C, was generated and used for quantifying the spore studies resulted primarily from (1) the limited time on the GC instrument during that particular series of experiments, but also

---

[49] All GC parameters were comparable for the MS and FID studies except that GC column outlet pressure was higher with the FID because this detector operates at atmospheric pressure, unlike the MS, which operates under vacuum.

because (2) foreknowledge about the variability present in the data gave little motivation to proceed with many more injections of standard Me$_2$DPA solutions (i.e., further data acquisition of different quantities of Me$_2$DPA would produce marginal refinement in the certainty of the calibration curve; see below). The mean integrated m/z 137 peak areas for five injections of 3.0 nmol Me$_2$DPA was 9.63×10^7, with 95% confidence intervals on this mean being $\pm 1.63 \times 10^7$ ($\pm 16.9\%$ of the mean response at 3.0 nmol, which is entirely consistent with the reproducibility reported in Section 6.1).
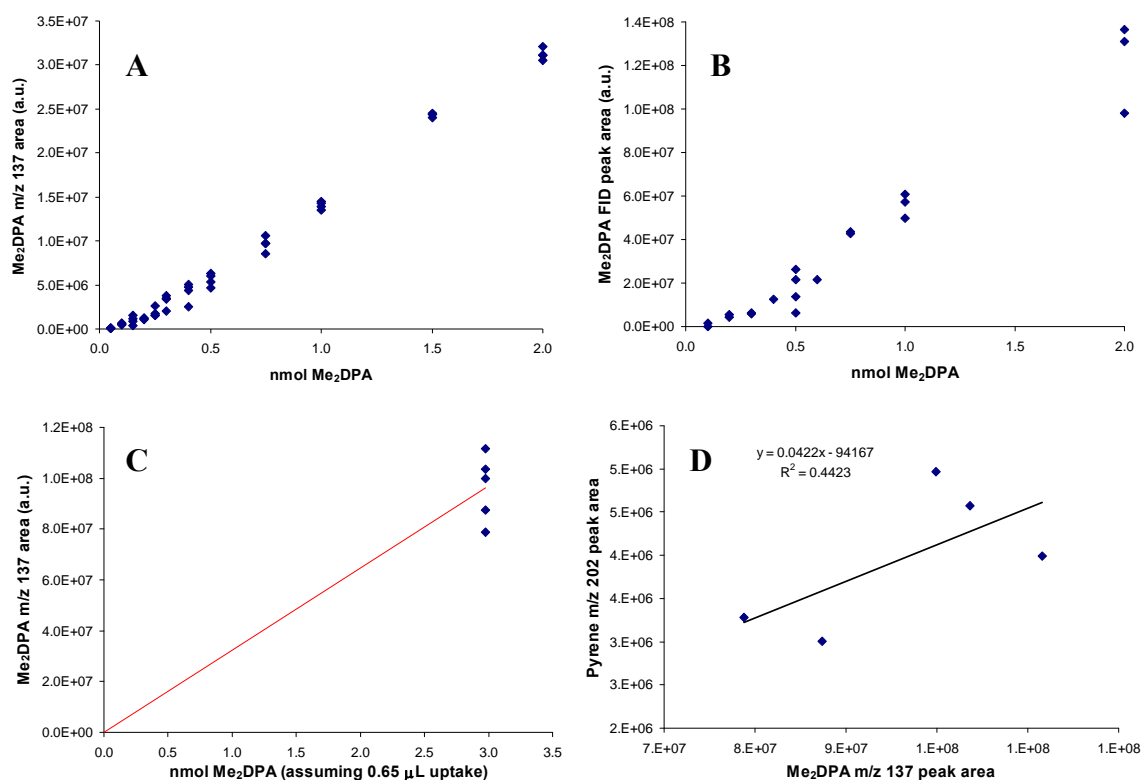
Figure 8-16. Example calibration curves for Me$_2$DPA. Curves (A) and (B) are from experiments where Me$_2$DPA was carefully applied to the CWF using a microliter syringe, while (C) was obtained by *dipping* the CWF in a calibration solution of known Me$_2$DPA concentration. (D) displays the integrated peak area of pyrene internal standard vs. that of Me$_2$DPA.

To convert Me_2DPA peak areas to absolute Me_2DPA amounts for comparison with LC data, it was assumed that the Me_2DPA response was linear from the origin to the mean response data (hence the red line in Figure 8-16C) and that this line could be extrapolated beyond the data (previous studies, not displayed, had established that the curve was linear at quantities in excess of 4 nmol). Assuming 0.65 μL nominal uptake of well-suspended spores, the total maximum amount of DPA collected by the wire was 3.6 and 4.6 nmol for BG and BA spores, respectively, so the extrapolation was not far. Due to the non-linear, upward concavity in the calibration curves seen in Figure 8-16A and B (and assumed to exist in Figure 8-16C), interpolation between the origin and the single mean response at 3 nmol in Figure 8-16C probably biased the low Me_2DPA yields towards underestimates for the actual amount of Me_2DPA produced. Thus, overall error in the estimated quantity of Me_2DPA for lower response values was probably ±20%.

Furthermore, the application of a standard compound-based calibration curve to spores encounters additional errors for reasons that are discussed in Section 8.3.6 regarding liner deactivation during sample injection.

Many key pieces of information are contained within Figure 8-16A-D. First, the data are considerably scattered for both MS and FID detector types. The primary reason is believed to result from the premature loss of Me_2DPA during needle insertion through the heated GC septum (e.g., Me_2DPA passes through the septum purge instead of into the column, remains adhered to the inside walls of the needle where contact with the coil is made, or the He gas leaks backwards through the seal in the coiled wire filament's assembly; see Figure 1-4d). It is also possible that the active Pt-Ir metal catalyzes premature decomposition of the Me_2DPA, although this is probably insignificant given

the relatively low surface area and low residence times of the wire, plus the absence of decomposition products such as pyridine in the chromatograms. Residual liquid solvent carried into the GC inlet, which can vary significantly from one injection to the next, can influence the amount of analyte that reaches the column. The backflashing that occurs in the inlet (manifest by an inlet pressure spike for most samples) carries the sample backwards, although the solvent may have positive effects by temporarily passivating surfaces. The preferred remedy to the above problems is to use an autosampler device in place of manual injection, which improve all aspects pertaining to reproducible CWF handling and would speed up needle insertion, possibly minimizing the problems of premature CWF heating inside the needle and the presumed resultant reproducibility problems. However, such a device would need to include a means for cleaning or replacing the CWF between samples.

A second key revelation of Figure 8-16A and B is that in the low Me_2DPA range (i.e., up to about 0.5 nmol) the curves for both detector types are concave upwards, becoming linear at higher Me_2DPA quantities, so a best-fit calibration is not a straight line.[50] Because similar curvature is observed with both detector types, it probably does not result from detector nonlinearity, but rather may be from differences in Me_2DPA desorption behavior from the wire. Such problems may result from monolayer vs. multilayer wire coverage due to the active wire surface that adsorbs Me_2DPA more strongly than bulk Me_2DPA. The liner surface may play a similar role.

---

[50] No equation linear in its parameters could be found that would sufficiently fit this data, making either a nonlinear fit or a transformation a necessity.

Third, in Figure 8-16A and B (and possibly C), the vertical scatter in the calibration data do not appear to be normally and uniformly scattered around a mean regression line, but rather seem to be skewed downward. If true, this observation supports what is believed about the variability of this process, which depends on two key random variables that *cannot* be controlled by the operator, i.e., (1) a variable quantity of Me$_2$DPA, Q, is collected by the coil and (2) only a *fraction*, F, of the total collected amount of Q is ultimately eluted and detected. The observed Me$_2$DPA peak area, Y, for the entire process may be modeled as Eq. (8-16) [or (8-17) if F is the fraction of Q that is *not* detected], where α is the response factor of the instrument.

$$Y = \alpha\, QF \qquad\qquad (8\text{-}16)$$

$$Y = \alpha\, Q\left(1 - F\right) \qquad\qquad (8\text{-}17)$$

Given what is known about the dipping/dropping process for transferring material to the CWF, Q is likely normally distributed, while the fraction F follows a distribution whose domain is the interval [0,1], e.g., a beta distribution [Eq. (8-18)].

$$d_{\text{beta}}\left(x, a, b\right) = \frac{\Gamma\left(a + b\right)}{\Gamma\left(a\right)\Gamma\left(b\right)} x^{a-1}\left(1 - x\right)^{b-1} \qquad\qquad (8\text{-}18)$$

The facts that the calibration data are curved upward and that the variance seems to depend on the net quantity of Me$_2$DPA sampled (a fourth piece of information presented by Figure 8-16) probably result from some type of dependence of F on Q, the possible reasons for which were discussed previously.

Fifth, the addition of the chemically inert pyrene (or chrysene) internal standard does <u>not</u> serve its intended purpose of improving the precision of estimating Me$_2$DPA

quantities. If it did, the Me$_2$DPA and pyrene peak areas observed after repeated sampling of the same solution would exhibit a correlation statistic near 1. However, Figure 8-16D shows that there was little correlation between Me$_2$DPA and pyrene peak areas in the dataset corresponding to Figure 8-16C (pyrene data not shown); i.e., the Pearson's *r* correlation value is 0.665. In fact, because the Me$_2$DPA and pyrene area have strong random, independent components [each can be modeled by Eqns. (8-16) or (8-17) as discussed above], the relative variance of Me$_2$DPA/pyrene is actually *higher* than the relative variance of either compound's area alone, which was definitely observed both with the calibration and the experimental spore derivatization data. Thus, Me$_2$DPA peak areas were used for analyses rather than Me$_2$DPA/pyrene area ratios. Unfortunately, much of the observed Me$_2$DPA peak area data obtained from spore and model DPA derivatization studies were in the highly scattered, nonlinear region where uncertainty in Me$_2$DPA amount is high. Fortunately, the variability is thought to be attenuated by the apparent liner passivation induced by the methylation reagents (discussed below in Section 8.3.6).

8.3.5   Thermal gradient in the liner

Once inserted and fully extended, the wire resides ~3.2 to ~4.4 cm from the top of the inlet liner. The GC inlet is not isothermal in this region. At a setpoint of 290°C, the temperature varies about 15°C along the length of the wire (Figure 8-17). The key implication of this temperature gradient is that a volatile or reactive sample may exhibit different products in the chromatogram depending on its physical location on the wire (cf. Section 8.3.3, especially Figure 8-15). If the thermal history and residence times of

different samples vary, qualitative and quantitative differences in chromatographic results would not be surprising.
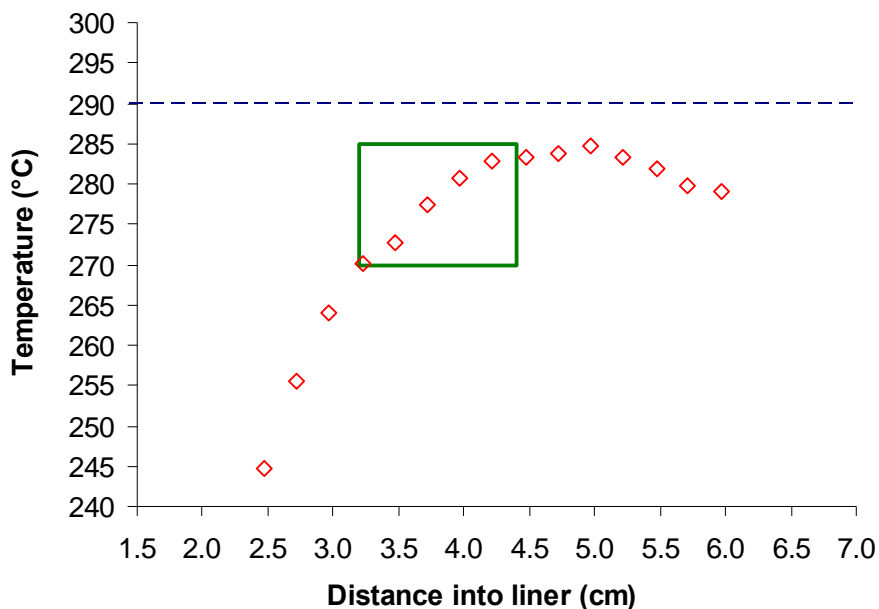
Figure 8-17. Measured liner temperature profile at 290°C setpoint (indicated by a dashed horizontal line). Solid rectangle delineates the physical location of the CWF (vertical border lines) and ~15°C temperature gradient along the wire (horizontal border lines) based on the temperature data. Total liner length is ~7.9 cm.

High thermal gradients along a liner caused descrimination in analysis by injection of a series of *n*-alkanes in hexane, the higher boiling compounds' peak areas diminishing as the temperature gradient increased [423]. The chromatographic significance of different temporal- and positional-thermal profiles along the CWF has not yet been explored in depth by us, but has been addressed elsewhere for a passively heated sample probe using very non-polar and polar model compounds [424]. The nonpolar analyte was readily and rapidly volatilized from all materials studied, but the polar compound exhibited slow volatilization when the heating rates were slow (due to higher thermal masses of different probe materials) and when the sample carrier had a

chemically active surface. From the pyrolysis literature, a general consensus about whether fast heating is better for avoiding undesirable decompositions during thermochemical methylation is mixed and appears to depend on a variety of factors including sample identity and final temperature [287, 315, 365, 425]. Apparently, only through trial and error can the best conditions for thermal analysis be determined.

8.3.6 Liner activation and contamination from sample injection

Nonvolatile chemicals (Na^+ and SO_4^{2-}) are major components of the best-performing mixture, point **a** in Figure 8-10. Although ideally these chemicals remain on the coiled wire during the whole process, in reality each injection probably deposits Na_2SO_4 (perhaps initially as $NaMeSO_4$ or $TMA-MeSO_4$), $CaSO_4$, and other polar nonvolatile chemicals on the surfaces of the liner. This process is conceivably worse if residual solvent evaporation facilitates deposition of these chemicals onto the liner. The deposition of polar species in a liner (especially Na^+) causes tailing problems in chromatograms, reducing sensitivity for detection.

Experimental evidence is that deposition of Na_2SO_4 inside the liner does occur. First, when a clean CWF was inserted without any chemicals inside the GC inlet after the spore experiments involving TMA-OH, NaOH, and $HMeSO_4$, then removed from the inlet and placed in a Bunsen flame, the flame yellowed substantially. The wire was cleaned by rinsing and flame-drying and the process was repeated with the same results. Second, when Me_2DPA and pyrene model compounds were introduced without any reagents via the CWF into the GC, peak tailing was obvious. The chromatograms in Figure 8-18 and Figure 8-19 display peaks from two chromatograms obtained from the

spore Me$_2$DPA optimization study described above (with varying amounts of TMA$^+$, Na$^+$, OH$^-$, and MeSO$_4^-$ in the presence of spores). Also included are the peaks of two chromatograms obtained just after the spore studies using pure Me$_2$DPA + pyrene applied to the CWF. The tailing of these model compounds was much more pronounced than tailing of the same chemicals released and derivatized *during* the spore studies. Fortunately, moderate peak tailing does not significantly influence the quantitative analysis since peak areas are the same so long as the peak is not overwhelmed in the chromatogram's baseline noise and any surface activity does not permanently adsorb analytes or induce their decomposition.
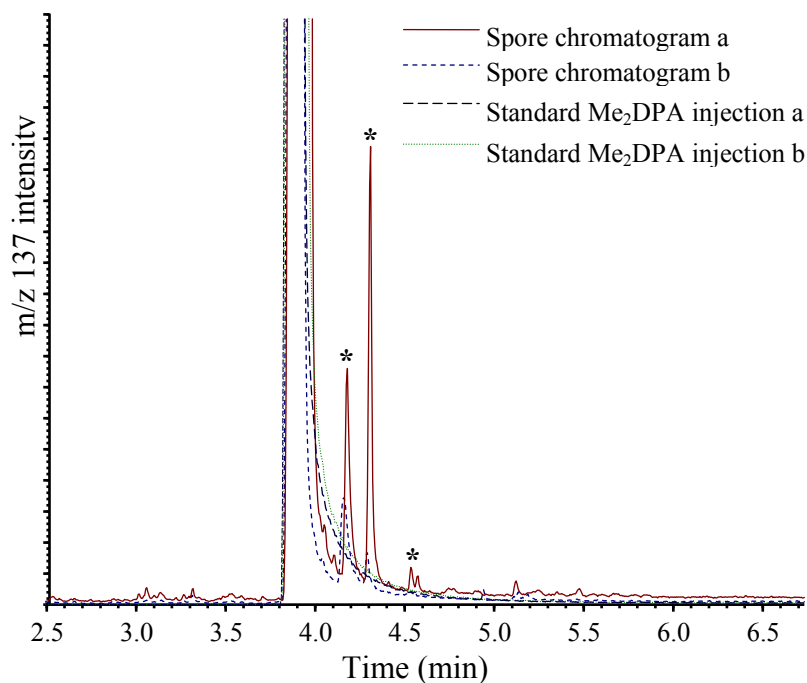
Figure 8-18. Overlaid m/z 137 chromatograms of Me$_2$DPA peaks from spore derivatizations and from pure Me$_2$DPA. The chemical identity of the compounds corresponding to peaks indicated by *'s, which appear only in chromatograms of spores, is unknown.

MeSO$_4^-$ and/or TMA$^+$ may temporarily passivate the liner's (and perhaps the CWF's) surface during sample introduction. The sample matrix may also assist in passivation [426]. Liner passivation helps to produce good peak shapes despite the ultimate deposition of Na$_2$SO$_4$, improves peak area reproducibility, and even increases quantitative yields due to avoidance of irreversible sample adsorption or decomposition [427]. These factors may help explain the large degree of scatter seen in the calibration curves, which did not co-introduce any TMA$^+$ or MeSO$_4^-$ salts. If this passivation occurs, it is also conceivable that methylation of volatilized biomarkers happens on the liner's surface and not just on or near the wire alone. Where GC inlet liner activation or contamination is pronounced, the liner may be cleaned by H$_2$O/MeOH rinsings and re-deactivated (see Section 3.4.1).
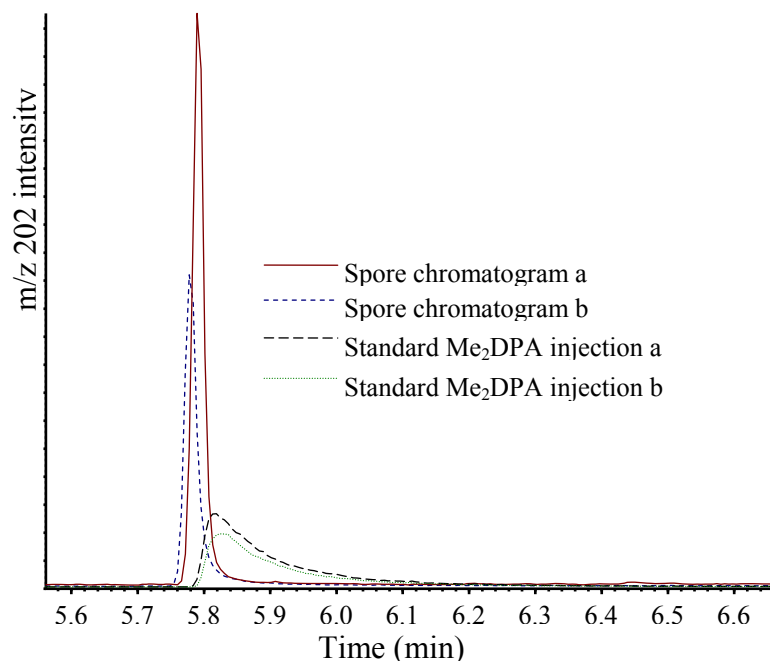
Figure 8-19. Overlaid m/z 202 chromatograms of the pyrene internal standard peaks from spores and pyrene.

8.3.7 Errors in DPA quantitation by LC

Uncertainties in LC are much lower than in GC in part since it is relatively easy to transfer nearly 100% of an already-liquid sample into the LC separation column. The uncertainty in spore DPA amount came mostly from the different quantities of spores contained within the Eppendorf tube used for each study and errors in breaking up the spore pellet. However, one potential issue with LC is that the countercation bound to DPA influences the UV absorbance spectrum [181, 428-430]. To examine this possibility, simple comparisons of Na_2DPA to CaDPA and Na_2DPA to H_2DPA LC peak areas were made.[51] The Na_2DPA and CaDPA samples exhibited identical peak areas (although the CaDPA peak was slightly broader). However, H_2DPA gave 8.8% higher peak area in the 250-350 nm UV absorbance range compared to Na_2DPA, suggesting that applying calibration curves created from H_2DPA to CaDPA may result in ~9% underestimates of actual DPA content (and thus *over*estimates in total percent conversion to Me_2DPA in the GC). This was probably not a huge problem with the spore CaDPA, since the excess H_2SO_4 probably removed Ca^{2+} from DPA, replacing it with H^+ while forming $CaSO_4$.

8.3.8 Commentary on analysis and modeling of spore Me₂DPA yields

Performing statistical tests of the models was problematic for several reasons. First, the number of parameters fit was quite large compared to the size of the data set; i.e., parameters for Eqns. (8-8), (8-12), and (8-13) totaled 15, 11, and 14, respectively,

---

[51] 3.51 mM is the approximate aqueous solubility of CaDPA observed for these studies. It was prepared by diluting 351 μL of 10 mM Na_2DPA in 351 μL of 10 mM $CaCl_2$ plus 298 μL H_2O.

while the number of experimental data points was 39. Second, there was large variation in the data, both experimental and from the calibration curve (Figure 8-16C). Although the fits were done using least squares and the residuals appeared to be evenly scattered about zero, a few exceptions to this even scatter caused a third problem: In order to fit the high response data well, the nonlinear models ended up slightly underestimating the response at points **q** and **r** and overestimating it at points **u** and **v**. However, these errors are small since the size of the residual scales with the magnitude of the response, which actually was a fourth problem: non-constant variance in the errors. This can be addressed by weighting the least-squares regression or via transformations of the response and model.

Given all the above uncertainties, if anything, the major statistical violation in this analysis is that the data were overfit so that some terms or parameters are not truly statistically significant. However, it is difficult to test parameter significance in nonlinear models, so all terms in all models were retained. Since the purpose of modeling was to estimate the optimal ionic reagent mixture composition and <u>not</u> to test for significance of factors or to estimate physically meaningful parameters, the marginal benefits of finding better models or pursuing statistically rigorous fits to the data were greatly outweighed by the effort that would have been required. The large uncertainties discussed above make a study of the propagation of errors difficult. Fortunately, least squares is an efficient, unbiased estimator for the *mean* values of parameters, in spite of the sources of uncertainty.

8.3.9 Analysis of variance as a robust model validation

An analysis of variance (ANOVA) on Me$_2$DPA yields at several mixture points in Figure 8-10 is a very informative and statistically conclusive test that is unaffected by the above problems. The data at point **a** (near **H1**), point **b** (near **H2**), and the point midway between points **a** and **b**, called **ab$_{mid}$** (near **S**) were compared pair-wise by single factor ANOVA with the assumptions that the variance could be pooled and that the data for each factor (point) were normally distributed (reasonable assumptions for these three data points given that their mean responses ranged from 30-86% and their individual standard deviations were 8-15%). The probabilities that the pairwise differences in mean response (**a** vs. **ab$_{mid}$**, **b** vs. **ab$_{mid}$**, and **a** vs. **b**) are <u>not</u> zero are very small (p-values were 0.004, 0.025, and 0.080, respectively).[52] Therefore, it may be concluded with a high degree of certainty that there truly is a minimum between points **a** and **b**, and thus at least two local maxima since Me$_2$DPA response around the perimeter of the design space (**qrsuv**) was, relative to the areas near **H1**, **H2**, and **S**, quite close to zero. There is also evidence that the mean Me$_2$DPA response differs at points **a** and **b**, although it is not as strong since 0.080 is very close to the cutoff value of 0.05 for statistical significance. In conclusion, there are at least two different blends of TMA-OH, NaOH, and HMeSO$_4$ in MeOH/H$_2$O that are most effective in converting spore DPA to Me$_2$DPA at the conditions employed.

Regarding the reduced methylation activity along the line **vy** in Figure 8-10, it is noteworthy that the quantities of Na$^+$ and TMA$^+$ are equal here ($x_{Na^+} = x_{TMA^+} = 0.25$). Three possibilities for this 1:1 molar ratio of Na$^+$ and TMA$^+$ exhibiting a decrease in

---

[52] The uncertainty in the calibration curve would not affect this interpretation since converting observed peak areas to Me$_2$DPA quantities involved multiplication of the former by a single constant.

methylating capacity are (1) that the methylating power of $MeSO_4^-$ is reduced in some manner (e.g., by steric hindrances or special arrangements in the crystal structure of whatever salts are formed) and/or (2) that premature decomposition of $MeSO_4^-$ occurs more rapidly at this salt mixture, e.g., as the reagents are dried on the wire, and/or (3) spore DPA release or diffusion is somehow reduced, or decomposition increased, by this combination of ions compared to other mixtures.

Finally, the models definitely capture the essence of the chemical reactivity of the TMA^+, Na^+, OH^-, and $MeSO_4^-$ system with the constraints imposed. They also lay the groundwork for subsequent studies where the statistical problems can be addressed.

8.4 *Comparing IMDOE, traditional mixture DOE, and factorial designs*

One final point of discussion pertains to the question: How does the IMDOE approach employed here compare with more "traditional" approaches involving either factorial designs or mixture experiments centered on ion-paired reagents that are much simpler to design, conduct, and analyze? In Figure 8-20A the IMDOE experimental design for the spore studies is reproduced along with the equivalent information displayed in a more traditional mixtures perspective using a ternary diagram for TMA-OH, NaOH, and HMeSO₄ (Figure 8-20B) plus a rectangular Cartesian plot (Figure 8-20C) that represents the total quantities of each reagent added as x, y, and z coordinates (typical for a factorial design). Each of these figures is a 5-sided plane with vertices **qrsuv**, although the shape of each is stretched relative to the other two. The general pattern of the sample points remains the same, although as Figure 8-20A, B, and C are considered in turn, the points bunch together near the line **rs**, but separate as the distance

174

from this line increases. (Note that the equations for producing the above-mentioned information are found in Appendix A and Appendix B.)

For comparison to Figure 8-20C, Figure 8-20D and Figure 8-20E are included to illustrate how the design would have appeared had different bases been chosen. Figure 8-20D is for the case where all ions sum to 750 mM (not just TMA^+ and $MeSO_4^-$), and Figure 8-20E is a design where all binary salts sum to 750 mM (note the similarity between Figure 8-20B and Figure 8-20E). All of these designs correspond to Figure 8-20A and Figure 8-20B if the absolute molar quantities are converted to ionic or ion-pair salt mixture fractions, respectively.

In all three approaches to DOE (factorial designs, mixture experiments, and mixture experiments with ions), given the constraint indicated by Eq. (8-9) with a three-component chemical system, only two degrees of freedom are available. How these degrees of freedom are partitioned—and thus how the experimental points are distributed relative to one another—depends on the perspective taken for the design. If *absolute* amounts of TMA-OH, NaOH, and $HMeSO_4$ (arguably the simplest method for DOE) are specified, then the factorial design may be preferred, although the constraint imposed by Eq. (8-9) requires careful modifications to the usual "high-low" approach to manipulation of factors (discussed below). If it is relative amounts of TMA-OH, NaOH, and $HMeSO_4$ blended together, then the traditional *mixture* DOE with a chosen basis (i.e., constant moles, constant mass, constant amount of one component) is recommended. Finally, if a fundamental picture of what ions are playing which role and if the experimenter wants to ensure efficient and complete sampling of the ionic mixture design space, or if there are several means to obtain the same mixture of ions, then IMDOE is most useful.
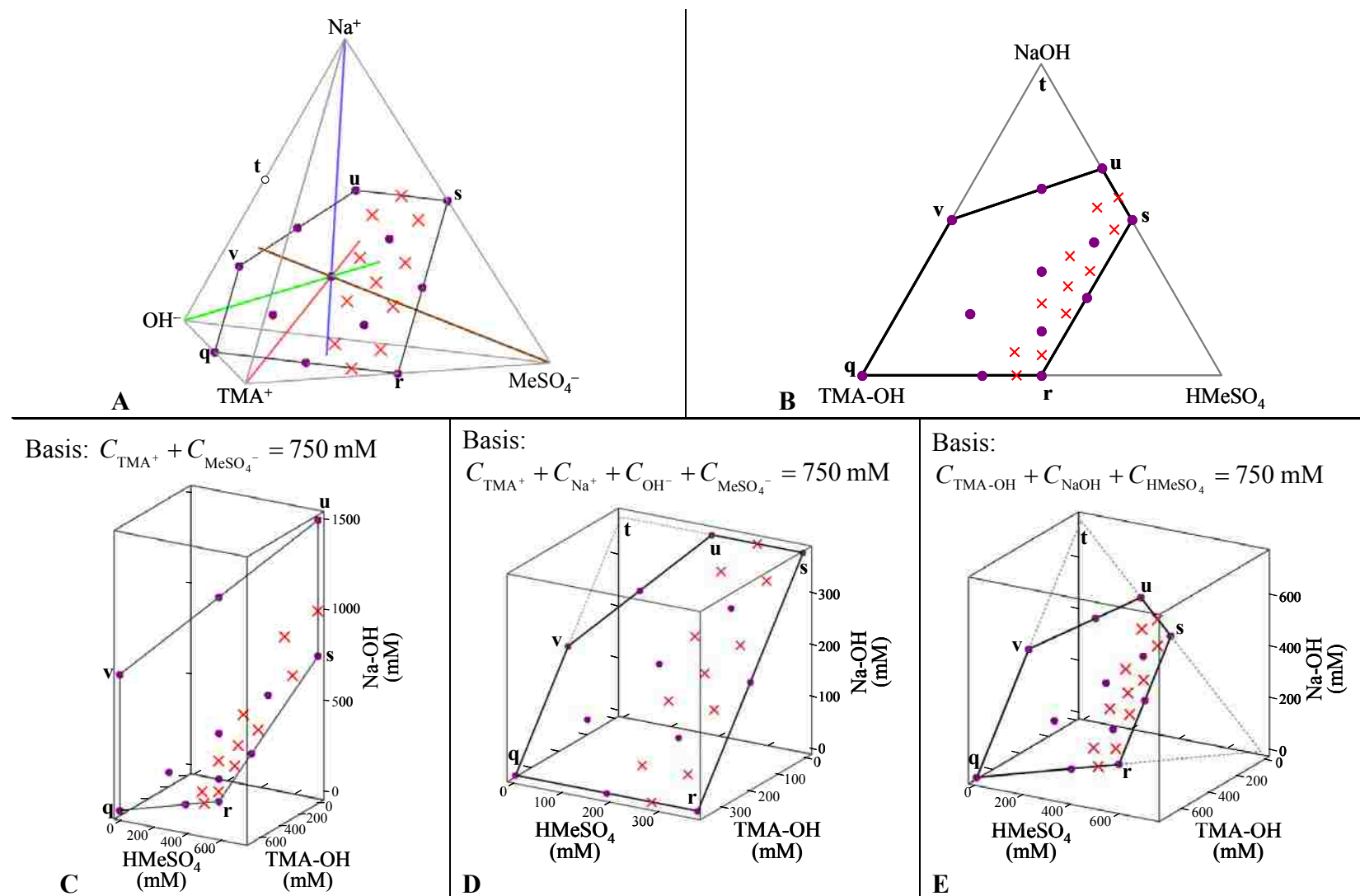
Figure 8-20. Experimental design for the spore study as represented by (A) the IMDOE approach, (B) a traditional mixture experimental design, and (C)-(E) designs employing the same mixtures as in (A) and (B) but with different bases (indicated in the figure).

All three approaches are valid means for finding optimal conditions for a process, and all could have been used for the present investigation. However, one advantage that the IMDOE approach has over the others is that the transformation from total amount to mixture fractions of ions distributes the experimental conditions in a different way— arguably more effectively—than do either factorial designs or traditional mixtures. With the IMDOE studies on the spores indicated here, a knowledge of the ion chemistry helped to specify clear constraints (e.g., avoiding acidic conditions or too much OH^-) and allowed 12 lattice points to be spaced uniformly within these constraints (points indicated by purple dots in Figure 8-20A), which allowed for immediate identification of regions of maximum reaction performance given the key research question: *How does the body of ions surrounding methyl donating reagents affect their reactivity with nucleophilic spore biomarkers?* Once these general regions had been identified additional experiments were added (points indicated by red X's in Figure 8-20) to further refine the model using the few remaining spores samples.

As an ultimate illustration of the effectiveness of this DOE using mixtures of ions, Figure 8-21 is given to illustrate how the mixtures perspective would appear if the experiments had been designed from a factorial approach using two levels of reagent concentrations, 100 and 250 mM, with points in between these extreme values (Figure 8-21A). The resultant ion-pair mixtures are shown in Figure 8-21B (because point **d** is acidic it is not a good candidate for study) and Figure 8-21C, where the convex hull from the spores experiments is included for reference.

The results of the factorial design, while definitely arriving at an optimal reagent mixture, may be confusing to interpret chemically because the basis for comparison is not

fundamentally-rooted. To illustrate, Table 8-4 presents the concentration of each ionic

species in the mixtures according to the design presented by Figure 8-21. The total

methyl donor concentration is not constant, varying from 200-500 mM (importantly, this

is not shown by Figure 8-21 B and C). Hence, a question that is not easily answered by

this design is, *"Given that an observed maximum is found, to what extent is it a result of*

the intrinsic mixture vs. the total *amount of methylating reagent?"* Indeed, interpretation

of the *reasons* for increased Me$_2$DPA yields may be difficult with a factorial design.

Either way, understanding the chemical behavior of the ions—the most fundamental parts

of the reacting mixture—would need to be addressed. Incorporating those effects into the

design at the outset is thus frequently preferable, although there are instances where it

may not be so. For example, an experimenter does not always know—or care about—the

chemical mechanisms involved in a process and is more interested in finding an optimal

way to combine reagents within constraints (e.g., solubility limits, stock solution

constraints). In such cases, it may be preferable to employ a more traditional,

straightforward approach, in which instance a factorial design may be perfectly

satisfactory.

However, even where a mechanism is unknown, taking a more fundamental

perspective for DOE may appropriately (re)direct the work, as was the case in this

author's investigations. Many variations of ionic mixtures experiments were conducted

prior to those discussed in Sections 8.1 and 8.2. It was actually via an experiment

involving a mixture of MeSO$_4^-$, SO$_4^{2-}$, OH$^-$, and Cl$^-$ plus TMA$^+$ that the true chemical

reason for enhanced DPA methylation (via MeSO$_4^-$) was identified. Hence, design of

experiments around a constant concentration of methyl-donor ions [Eq. (8-9)] was

justifiably a good choice.
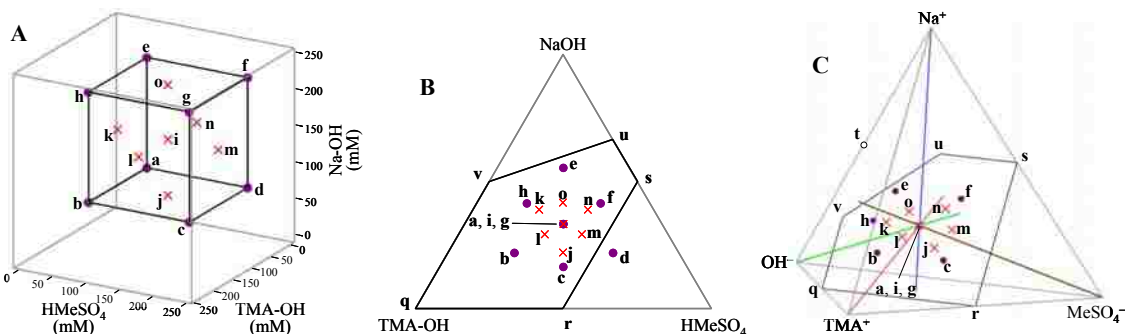
Figure 8-21. Factorial design (A) converted to (B) mixture plots of binary salts and (C) mixture plots of ions. See text for details.

Table 8-4. Concentration of each ion and total methyl donors (in mM) in a solution produced according to the design in Figure 8-21A.

Point ID	TMA$^+$	Na$^+$	OH$^-$	MeSO$_4^-$	Total Me
a	100	100	100	100	**200**
b	250	100	250	100	**350**
c	250	100	100	250	**500**
d*	100	100	-50*	250	**350**
e	100	250	250	100	**200**
f	100	250	100	250	**350**
g	250	250	250	250	**500**
h	250	250	400	100	**350**
i	175	175	175	175	**350**
j	175	100	100	175	**350**
k	175	175	250	100	**275**
l	250	175	250	175	**425**
m	175	175	100	250	**425**
n	100	175	100	175	**275**
o	175	250	250	175	**350**

* The negative value of this design point indicates that it is acidic and cannot be displayed in Figure 8-21C.

179

9   SEM OF SPORES BEFORE AND AFTER REACTION

Early in the investigation, it was of interest to visualize what happens to the spores as they are chemically and thermally treated. Suspensions of *B. thuringiensis* spores were mixed with the appropriate chemical mixture and applied as a 2-µL droplet (via a micropipette) directly to a twisted pair of ~90 µm Pt wires.[53] After solvent evaporation, the twisted wire was inserted for one min into a GC inlet with flowing He set to 290°C. Chemical treatments of interest involved (1) addition of MeOH alone (Figure 9-1), (2) addition of 333 mM methanolic TMA-OH (Figure 9-2), (3) exposure to 375 mM methanolic H_2SO_4 followed by addition of 667 mM methanolic TMA-OH (Figure 9-3),[54] and (4) addition of only H_2SO_4 in MeOH (Figure 9-4).

9.1   *Heating spores in the absence of chemicals*

Figure 9-1 shows spores before and after heating without any chemicals. There is little physical change apparent, save the cracking that occurs through some material[55] that covers them and the wire surface. This cracking suggests that the spores had shrunk,

---

[53] Twisted wire pairs were used with disposability in mind because they required little time and effort to produce compared to coiled wire filaments. As a result, the liquid had to be applied by a micropipette rather than dipping.

[54] The addition of TMA-OH reduced the H_2SO_4 concentration to 313 mM. Because the degree of $HMeSO_4$ formation from H_2SO_4 was unknown, the final OH^- concentration could have ranged from 42-355 mM.

[55] The material covering the spores was thought to be residual growth media or vegetative cell remnants that were not completely rinsed away during the cleaning process. Investigations not summarized here established that it did not affect the chemical analysis by GC-MS.

which was probably due to a loss of water and other volatile components. It seems that temperature alone did not "break open" the spores, at least not on a macro-scale. These results differ from another publication where temperatures above 250°C degraded spore structures to the degree that individual spores appeared to "melt together" [300].

9.2 *Heating spores with TMA-OH*

Figure 9-2 shows the spores before and after heating in the presence of TMA-OH. In Figure 9-2A it appears that TMA-OH may have provided an additional coating to the spores (the textural features on the spores appear obscured compared to Figure 9-1A), which completely disappears after heating along with a large portion of the spores themselves. In fact, the spores appear to have lost their exosporia and most possess protrusions after heating (Figure 9-2B). Close examination also reveals that the surfaces are roughened. That significant quantities of Me_2DPA are detected following such treatments indicates that the spores are physically compromised.
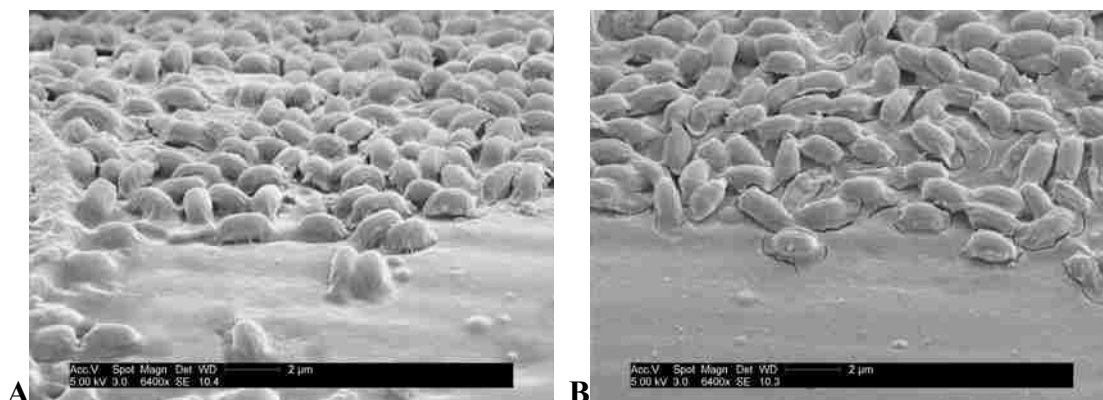
Figure 9-1. Spores of *B. thuringiensis*, originally suspended in MeOH, (A) before and (B) after heating to 290°C for 1 min in the absence of chemicals.
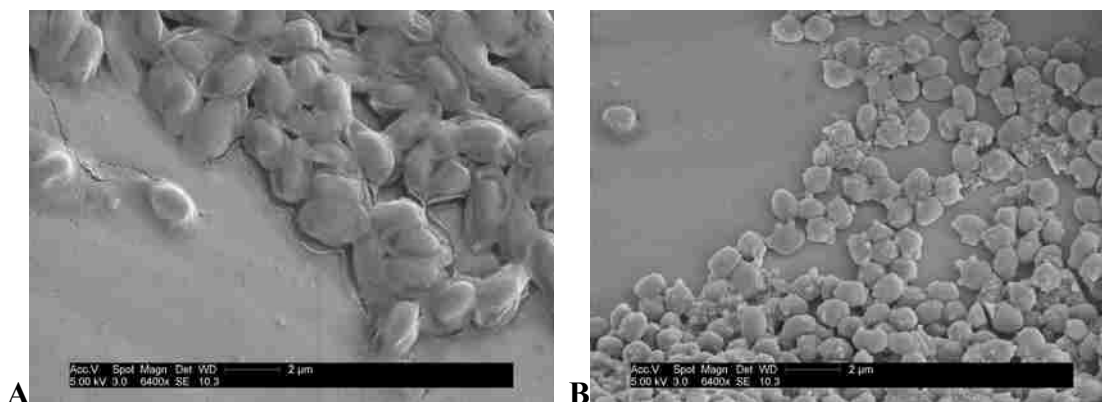
Figure 9-2. Spores of *B. thuringiensis* in the presence of 333 mM TMA-OH (A) before and (B) after heating for 1 min at 290°C.

9.3 *Heating spores with H_2SO_4 + TMA-OH*

Figure 9-3 shows the results before and after heating the spores that had first been acid-treated prior to addition of TMA-OH. After heating, this residue exhibits various surface patterns (e.g., stretch marks, rough spots, cracks, and protrusions), probably due to losses of water, spore volatiles, and at least some of the excess TMA^+.

In neither image are distinct, recognizable spores apparent because they are buried by the thick, nonvolatile coating, although close examination reveals individual bumps that *may* be spores (but these features are hardly conclusive). Initially, it was suspected that the acid had completely dissolved the spores. However, careful examination of other SEM images involving acid addition revealed the presence of intact spores.

9.4 *Addition of methanolic H_2SO_4 only to spores*

One example showing intact spores following H_2SO_4 treatment is Figure 9-4, which was obtained after simply adding 375 mM methanolic H_2SO_4 (no TMA-OH) to

spores and evaporating the solvent away, which left behind a viscous liquid probably comprised of a combination of H_2SO_4 and $HMeSO_4$. Distinct spores are clearly visible under a thin portion of the acid residue.
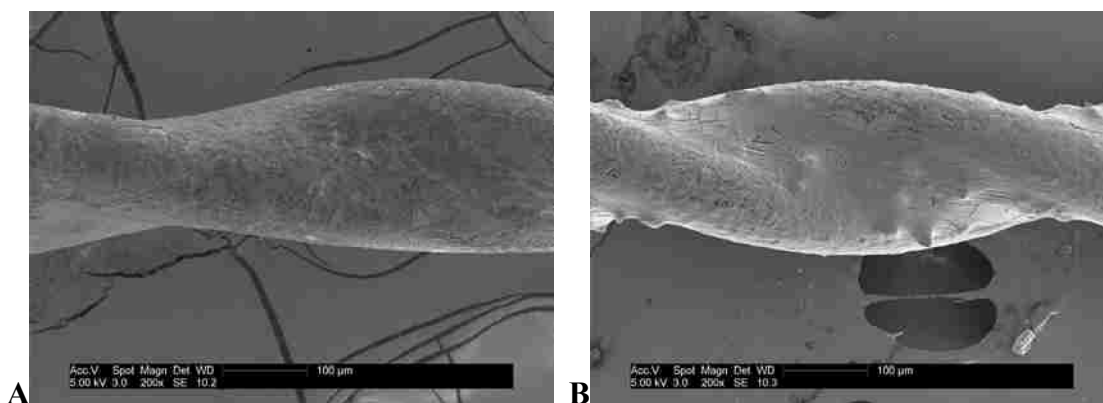
Figure 9-3. Spores of *B. thuringiensis* combined with 375 mM H_2SO_4 + 667 mM TMA-OH in MeOH (A) before and (B) after heating at 290°C for 1 min (see footnote 54).

The residue was very sensitive to the electron beam. In Figure 9-4, the cracking (e.g., bottom right corner) and roughening seen above various spores as well as the rectangles just left of top center of the figure (produced while adjusting the electron beam for taking the image) were a result of some type of localized heating or offgassing that was fast enough to be visible in the time during which the image was being captured. Such effects were not observed in samples that did not possess H_2SO_4, and the influence was less important when TMA-OH had been added.

Although the acid becomes more concentrated as the solvent evaporates, the conditions seem hardly sufficient to dissolve the spores. Not only does Figure 9-4 support this claim, but so do published protocols for conditions required to completely hydrolyze bacterial endospore components including peptidoglycan polymers (recall that

184

peptidoglycan is one of the most robust components of the spore) and proteins. For example, a quantitative yield of spore hexosamine monomers from peptidoglycan was obtained after hydrolysis at 100°C in 6 N HCl for 5 [431] or even 16 [432] h. Even longer times were employed to hydrolyze other cortex components (e.g., diaminopimelic acid was freed by hydrolysis in 6 N HCl for 20 h at 110°C, and muramic acid lactams from peptidoglycan required hydrolysis in 6N HCl at 108°C for 44 h [432]).[56] A protocol for hydrolyzing all spore proteins to amino acids also involved refluxing spores in 6 N HCl for 24 h [303].
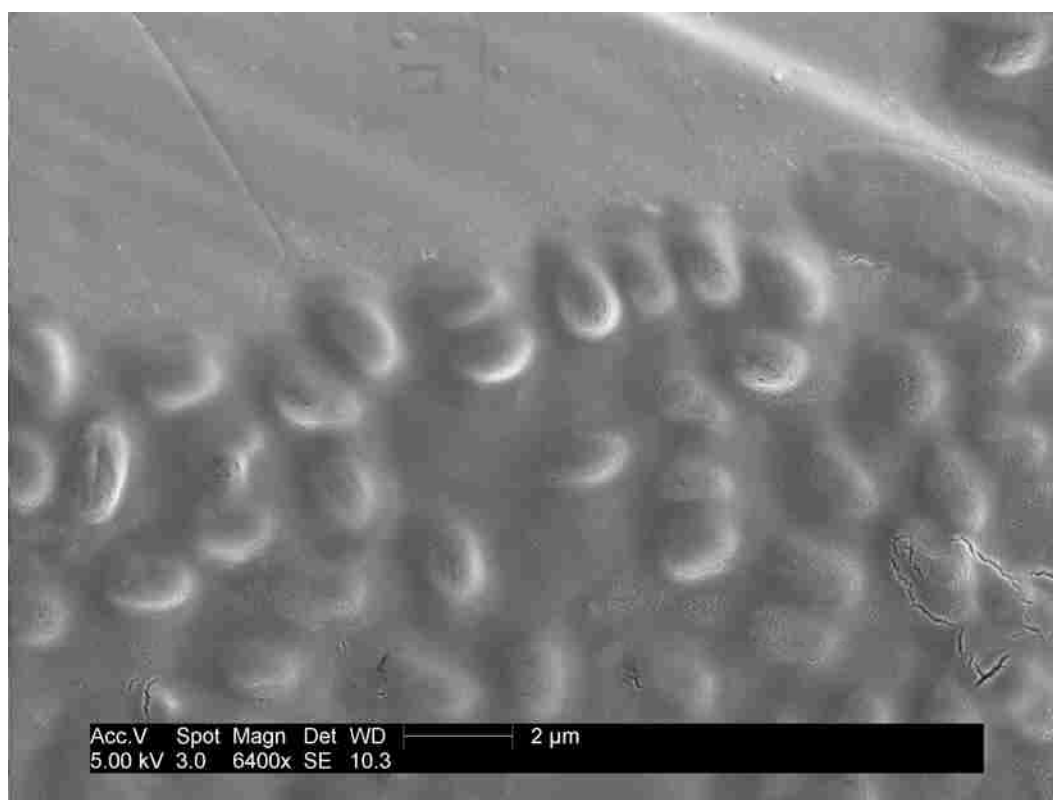
Figure 9-4. *B. thuringiensis* spore contours are clearly visible on wire after evaporating away MeOH from 375 mM H$_2$SO$_4$.

---

[56] Less severe conditions (2 N HCl at unspecified times and temperature—probably reflux at 100°C for several h) were required to obtain non-amino sugars from the spores [431].

Since the spores of the present study were suspended in acidified methanol (not water), the rate of methanolysis is important to consider. A recent study comparing methanolysis to hydrolysis of plant polysaccharides revealed that, although both hydrolysis and methanolysis function well with many sugars, acidic methanol is much less effective at cleaving highly ordered polysaccharides than is aqueous acid (although the comparison was not necessarily "fair" since the concentrations, acid identities, and temperatures employed were not identical) [433]. Protocols for acid-catalyzed methanolysis of plant polysaccharides in 2 N HCl require heating to 100°C for 3-5 h [433], which is similar to the standard protocols for hydrolysis of spore sugar polymers.

These literature protocols strongly support the claim that the spore structure remains mostly intact (although perhaps permeabilized and maybe even "popped") as it resides in 375 mM methanolic H_2SO_4 for 1 min at room temperature. Although the solution is made basic by TMA-OH addition prior to solvent evaporation, from Figure 9-2A, the spores are obviously intact after exposure to and drying in the presence of TMA-OH. In conclusion, at the conditions employed, neither acid nor base rapidly "dissolve" spores. Rather, the processes that occur upon heating the spores in the presence of these chemicals are responsible for bulk spore destruction.

10 PROPOSED SPORE DPA METHYLATION MODEL

10.1 *Discussion of reaction paradigms*

In Chapter 1 (Section 1.4), three paradigms reflecting the progression in understanding methanolic H_2SO_4 and its effects on spore DPA yields were presented, and Chapters 5, 7, 8, and 9 present important experimental results on these paradigms (Appendix C addresses the paradigms with even more experimental results). The experimental results on acid catalysis and base hydrolysis established that **Paradigm A** (acid catalysis) is not responsible for the increased Me_2DPA yields in the chromatograms observed by adding methanolic H_2SO_4 before adding TMA-OH. Both aspects of **Paradigm B**, though they may contribute to Me_2DPA yields, were ruled out as major contributors, as discussed in Appendix C for Ca^{2+} sequestration by SO_4^{2-} and Appendix D for acid breakup of the spore. In addition to the evidence presented in these Appendix chapters, there is little reason to believe the presence of SO_4^{2-} significantly promotes DPA methylation by TMA^+ alone. First, TMA^+ is known to be a weak methyl donor, and second, DPA (free or bound) is a poor nucleophile given its very low first pK_a value (see Sections 2.2.3.2 and 2.2.5 as well as Appendix E) and hence is a weak methyl group acceptor. These features combine to give the data presented by Figure 7-3 and Figure 7-4, where Me_2DPA yields from CaDPA and Na_2DPA (chelated and non-chelated, respectively) are comparable for the different sulfate-containing methylating reagents. It

is thus concluded that **Paradigm C** (methyl transfer by $MeSO_4^-$) is the primary route to the much improved Me_2DPA yields with this reagent system.

Paradigms B and **C** may actually both operate together. Addition of $HMeSO_4$ to spores prior to TMA-OH and/or NaOH weaken their structure by acid-driven mechanisms that have yet to be elucidated. At this point, it seems that the acid assists in penetrating a spore permeability barrier (probably the inner membrane) that base cannot [107]. Indeed, addition of acid before TMA-OH improves spore Me_2DPA yields compared to the case where the same combination of acid and TMA-OH are mixed together before addition to spores (see Appendix C). However, in light of the one-step procedure that gives near-quantitative conversion to Me_2DPA (using a mixture of TMA^+, Na^+, OH^-, and $MeSO_4^-$), the improvement seen by adding acid first is no longer relevant.

Regardless of the possible effect of acid treatment of spores, methylation of CaDPA by $MeSO_4^-$ is probably assisted by Ca^{2+} sequestration, as now explained. Figure 10-1 displays a possible reaction mechanism between CaDPA and $NaMeSO_4$. It is proposed that (1) Ca^{2+} remains bound to DPA during the approach of $NaMeSO_4$. (2) Ca^{2+}, a center of positive charge, attracts electrons of the negatively charged $MeSO_4^-$. (3) Although Ca^{2+} withdraws electrons from the DPA carboxyl group, inactivating its nucleophilic character and slowing methyl transfer in the process, it simultaneously attracts the electrons from the $MeSO_4^-$ moiety, promoting the methyl exchange by weakening the $Me-SO_4^-$ bond. (4) Two separate reaction steps follow. The first one involves the net exchange of the methyl sulfate's Me^+ group and Na^+ to DPA^{2-}, with dipicolinic acid's Ca^{2+} being accepted by SO_4^{2-}, forming the stable $CaSO_4$ salt (Figure 10-1A). The second step is illustrated in Figure 10-1B, where, $NaMeSO_4$ loses its Me^+

group to Me_1DPA and gains a second Na^+ in the process (from the $NaMe_1DPA$ molecule), forming Na_2SO_4.
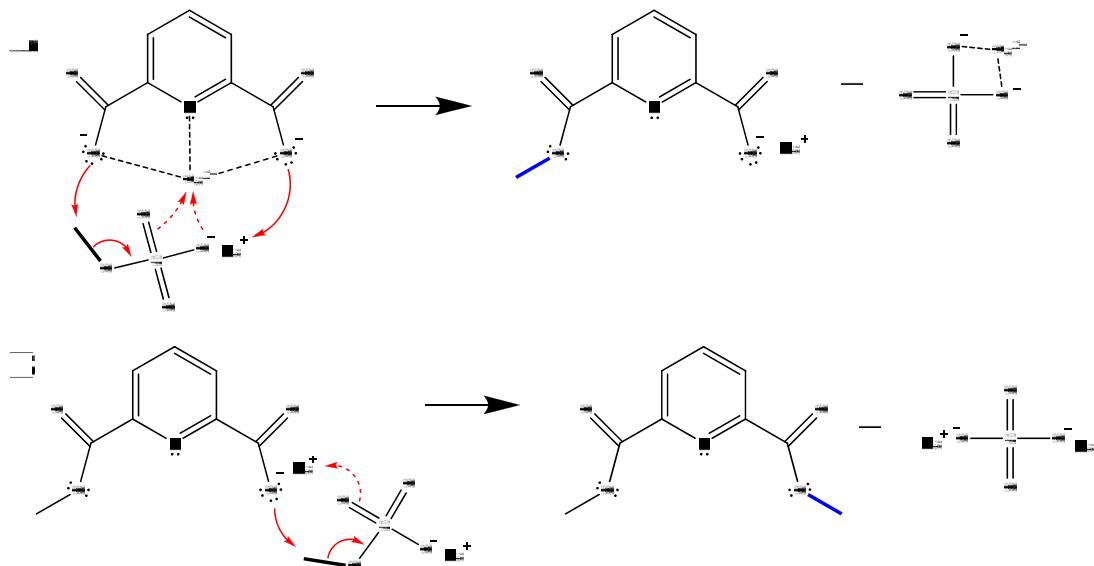
Figure 10-1. Proposed mechanism of CaDPA methylation by NaMeSO$_4$ for the first (A) and second (B) carboxylate groups of DPA.

In aqueous solution, the relative association equilibrium increases in the order $CaMeSO_4^+ \ll CaSO_4 \ll CaDPA$. The logs of these compounds' association constants [$\log(K_{ass})$] are about <0.5 [434, 435], 2.3-2.7 [436, 437], and 4.0-4.4, respectively [307, 438, 439] (the extent of each association differs from the next by approximately two orders of magnitude). By analogy to the weaker association of $CaMeSO_4^+$ compared to $CaSO_4$, the binding between Ca^+ and DPA^{2-} is greatly diminished by the first methylation of DPA, which forms Me_1DPA^-. At the same time, ion pair formation between the resultant SO_4^{2-} and Ca^{2+} becomes more favorable.

According to the data in Figure 7-3 and Figure 7-4, approximately 5-10 times as much TMA-MeSO$_4$ as NaMeSO$_4$ is required to achieve an equivalent Me$_2$DPA yield per

mole of CaDPA (Figure 7-3) or Na$_2$DPA (Figure 7-4). Three possible reasons for this difference are considered here. Figure 10-2 illustrates the first possibility. The smaller cation, Na$^+$, polarizes (draws electrons from) MeSO$_4^-$ more strongly than the larger TMA$^+$ cation because its charge density is much higher (ionic radii are 0.95 Å [416] and about 3.0 Å [440], respectively). Consequently, the Me–SO$_4^-$ bond of the Na$^+$ salt is weaker than that of the TMA$^+$ salt and therefore more reactive towards nucleophilic displacement.
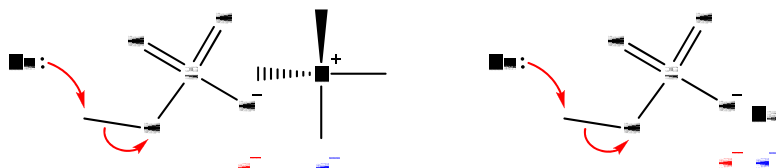
Figure 10-2. Replacement of TMA$^+$ with Na$^+$ moves the positive charge closer to the sulfate moiety, which attracts electrons more strongly, and increases the overall activity of the methyl group towards attack by a nucleophile, Nu: (e.g., the carboxylate oxygen of DPA in Figure 10-1).

Another possible reason for decreased TMA$^+$ salt reactivity relative to Na$^+$ is that the former forms complexes with (Ca)DPA and MeSO$_4^-$ in conformations that are less active for methylation. In addition to being large, TMA$^+$ is not spherical, and its positive charge is located in "patches" between its methyl groups, where anions tend to associate (i.e., in between three of its methyl groups [441-443]). Special, yet unknown conformational preferences may exist for TMA$^+$ salts that inhibit methylations.

Finally, the proposed mechanism for methylation of the first carboxylated group of DPA with NaMeSO$_4$ involves transfer of Me$^+$ and Na$^+$ to Me$_2$DPA in exchange for Ca^{2+} Figure 10-1A). If Na$^+$ is replaced by TMA$^+$ in that reaction, the products would be TMA-Me$_1$DPA and CaSO$_4$ (Figure 10-3A). The TMA-Me$_1$DPA salt may then react to

form Me_2DPA + trimethylamine (Figure 10-3B). How reactive the TMA-Me_1DPA salt is for thermal S_N2 methylation is not known, although from reaction principles pertaining to relative pK_a values presented in Sections 2.2.3.2 and 2.2.5, its reactivity is probably low. An alternative mechanism for the second methylation is given in Figure 10-3C. Here, the Me_1DPA^- (as a TMA^+ salt) is methylated by the $MeSO_4^-$ anion complexed with a second TMA^+ cation, and the product is TMA_2SO_4.

The possibility that Me_2SO_4 is the active methyl donor and forms upon heating $NaMeSO_4$ and/or TMA-$MeSO_4$ must be addressed. In Section 2.2.5.5, the decomposition of *acidic* $HMeSO_4$ to form Me_2SO_4 and H_2SO_4 at high temperature was discussed, the process yields being improved by addition of NaCl salt, which prevents hydrolysis of Me_2SO_4. The mixtures studied here contained Na^+ as well, although most experiments included OH^- rather than H^+ and all of them included water (water sources were discussed in Chapter 5 and listed in Table 5-1 and Table 5-2). Since water and especially OH^- rapidly hydrolyze Me_2DPA [444], the formation of Me_2SO_4 at these conditions is unlikely. The possibility that TMA^+-$MeSO_4^-$ converts into Me_2SO_4 + trimethylamine is unlikely because the pK_a of trimethylamine is much higher than both $HMeSO_4$ and HSO_4^- (cf. Table 2-2), making it the least reactive of the three in releasing a methyl group.

10.2 *Effects of ionic mixtures on spores*

Speculations may be made regarding the reasons for the overall reactivity of the best-performing ionic mixtures, which seem to occur near specific ratios of the ions involved. The "point **a**" mixture of 1:3:1:3 TMA^+:Na^+:OH^-:$MeSO_4^-$ (Figure 8-6a, Figure

8-10) included *stoichiometric* $Na^+ + MeSO_4^-$, as does the overall mechanism presented in Figure 10-1. The reasons for the effectiveness of the apparent second optimum at the "point **b**" mixture of 3:1:1:3 are not clear at this point.
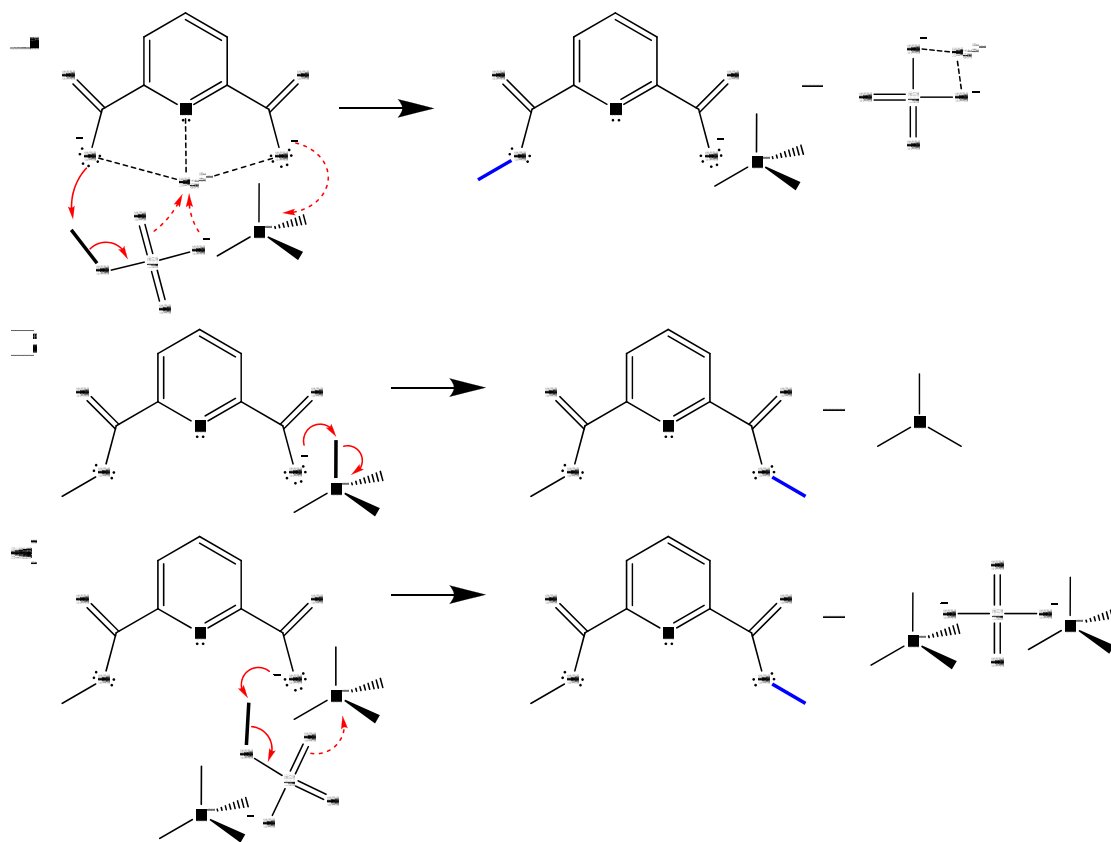
Figure 10-3. Possible routes to methylation of CaDPA with TMA-MeSO₄.

As discussed previously, the total amount of OH^- seems important for spore structure hydrolysis to release DPA, enabling rapid methylation. Both the point **a** and the point **b** mixtures appear to fall within a region of constant OH^- amount (see Figure 8-12C and related discussion). If the methylation mechanism proposed by Figure 10-1 is correct, then Na^+ is tied up by $MeSO_4^-$ and so the OH^- is paired with the residual cation, TMA^+ (both compounds are almost certainly hydrated). Although the size of TMA^+ cation is

relative large compared to Na$^+$, its (TMA$^+$'s) low polarizability and relative hydrophobic nature may actually assist its penetration into the spore, especially in MeOH where TMA-OH solubility is higher than NaOH. That penetration of TMA-OH into the spore occurs is reflected by the excellent yields of FAMEs at 100% TMA-OH (cf. Figure 8-6q), although the relatively high pK$_a$ value of carboxylic acids (~5 [310]) renders them much more susceptible to methylation by TMA$^+$ than is DPA (pK$_{a1}$ and pK$_{a2}$ for the carboxylates of DPA are 0.5 and 2.2, respectively [74, 173, 307-309]). Furthermore, the bond strength of the TMA$^+$-OH$^-$ ion pair is lower than that of the Na$^+$-OH$^-$ pair in MeOH, making dissociation less energy-costly.

Methyl transfer requires that MeSO$_4^-$ and DPA^{2-} have physical contact with one another, which is brought about by any process or phenomenon that assists the escape of DPA (presumably as CaDPA) from the spores and prevents the premature decomposition or loss of the TMA$^+$ and MeSO$_4^-$ methylating reagents.

There are other possible ways that ions can influence spores. For example, at 510°C, the presence of inorganic compounds (Na$_2$CO$_3$, NaOH, HCl, ZnCl$_2$, NaH$_2$PO$_4$, Na$_2$HPO$_4$, NaCl, MgSO$_4$, and sea salt) gives rise to very significantly different ratios of pyrolysis products obtained from amylose, a polymer of glucose, which was attributed to the Lewis and Brönsted acid-base activity of the matrix component additive [445].

High concentrations of so-called chaotropic salts in solution are known to disrupt the fine structure of microbial cells and spores. For example, treatment of *B. subtilis* cells with 4 M guanidine thiocyanate at 37°C for 5 h degrades their membranes and nucleus, causing relocation of DNA. Moreover, heating to 100°C for 20 min brings about complete degradation of the cells, even converting the cell wall into separate "clumps."

After 20 min at 100°C, spores of *B. subtilis* lose stain resistance and refractility, with partial degradation of coats and no apparent degradation of the cortex. These processes enhance the release of their DNA by denaturing proteins and loosening/permeabilizing the cell wall [446]. Specific ion effects on macromolecules are well-known, with some ions being more effective at denaturing proteins and penetrating lipid layers than others [447].

Although the cortex has insignificant capacity to bind DPA *in vitro* [61], it acts as an "almost infinite ionic reservoir" for cations [448] with ion exchange potential at levels of billions of protons per spore [448, 449]. Thus, the cortex and coats might accumulate TMA^+ and OH^- ions. The expansion/contraction of spore cortex [448] and bacterial cell wall peptidoglycan [450-458] with metal cations and pH occurs since repulsive charges of anionic groups are neutralized by cations [459]. The mechanical properties of cell-free peptidoglycan are notably altered by salts, e.g., the presence of NaCl and $(NH_4)_2SO_4$ render cell walls of *B. subtilis* more ductile and decreases their tensile strength and modulus of elasticity [460, 461]. All of these phenomena may be relevant to the enhancement of spore Me_2DPA yields observed with the mixtures of TMA^+, Na^+, OH^-, and $MeSO_4^-$.[57]

Ions may also stabilize interactions between the negatively charged DPA^{2-} and $MeSO_4^-$ during this reaction. It is known that reactions between like-charged species in solution (e.g., hydrolysis of $NaMeSO_4$ by OH^- [462]) follow the so-called "positive salt effect," which increases charge separation [463].

---

[57] Addition of ethanol, a dehydrating reagent, was stated to condense the lattice constant of bacterial peptidoglycan [455], and methanol might be expected to do the same. If this occurs, the ease diffusion into or out of the spore may be inhibited.

Accordingly, as the spore structure takes up Na^+ or TMA^+, spore biomarker release may be assisted by altering the spore's mechanical properties, accelerating spore decomposition by hydrolysis, promoting methylation reactions and diffusion of methylating agents, DPA, and methylated products, etc.

It is interesting that the highest methylation activity was seen in precipitate-containing solutions. (Even if a precipitate is not obtained in the solution, one will materialize on the coiled wire filament as the solvent evaporates away, which was observed by SEM analysis, e.g., Figure 9-2 and Figure 9-3.) Although not characterized, it seems reasonable to consider the precipitate to be primarily $NaMeSO_4$, which is quite insoluble in MeOH (as are other Na^+ salts), while $TMA-MeSO_4$ is soluble. Although a precipitated salt complex probably does not penetrate the spores, it will surround the spore and may promote spore decomposition as thermally promoted interactions and reactions occur. Since DPA exits the spore at temperatures above 250°C [300-302], thermally-released (Ca)DPA may pass through this salt, react, and exit as Me_2DPA.

10.3 *Proposed model of new, single-step process*

Figure 10-4 displays schematically what are thought to be, based on the foregoing discussion, the key mechanisms operating as spores are heated with the optimal "point **a**" mixture in the GC inlet to temperatures in excess of 250°C. First, CaDPA is released from the spores as they are thermochemolytically degraded. It may directly exit the spore in an unaltered condition (Figure 10-4g) to possibly be methylated at another location (e.g., on the liner or in the gas phase near Figure 10-4i). It also may pass through the salt coating surrounding the spore where it reacts to methylated product. Some DPA

decomposes to MPA (either before or after the first methylation) and pyridine (Figure 10-4f).

Although not indicated in Figure 10-4, evaporated solvent and many other compounds form part of this complex mixture, which possesses solid, liquid, and gaseous components. Modeling the reactions between these species is a difficult undertaking once all aspects of the transient nature of the problem are identified. Fortunately, statistical methods provide a powerful means for doing so in a much more convenient manner.
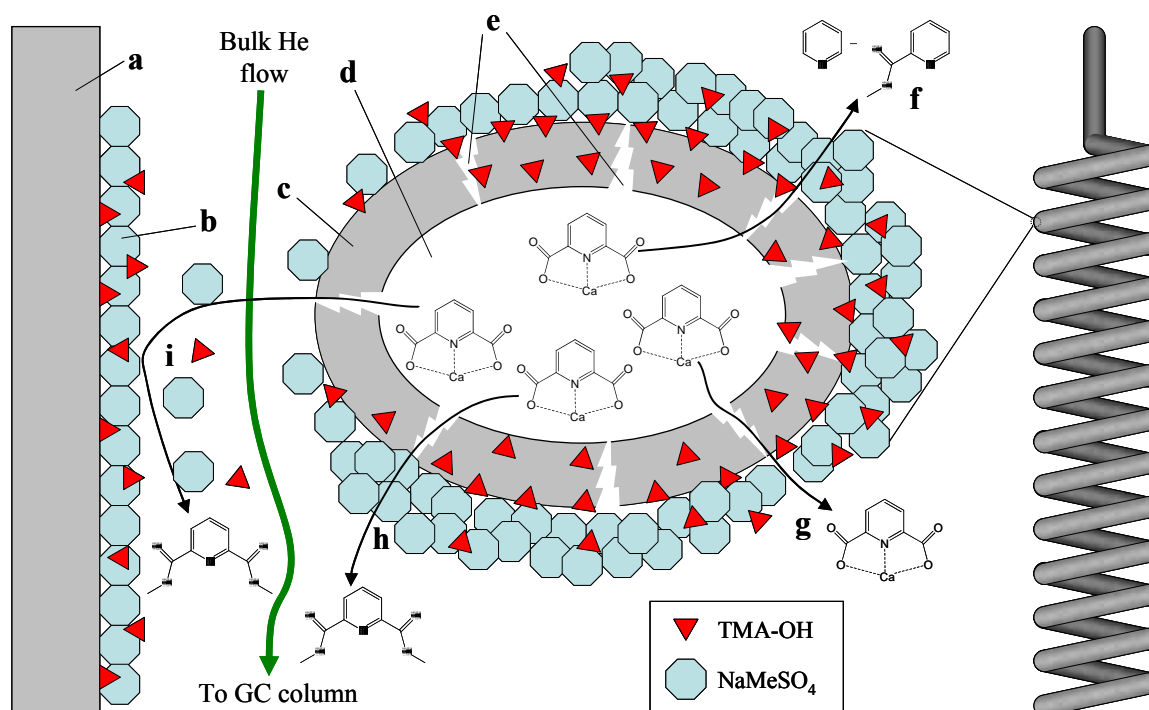
Figure 10-4. Conceptual model of spore CaDPA methylation in theGC inlet with the salt mixtures explored here. (a) GC liner, (b) coating of salts on liner surface, (c) spore outer layers (coat, cortex), (d) spore core containing CaDPA, (e) spore structure degraded by thermochemolysis, (f) DPA decomposition products, pyridine and monopicolinic acid methyl ester, (g) escape of non-methylated CaDPA from spore, (h) DPA methylated during passage through reactive coating on spores, (i) methylation of DPA occurs on liner surface.

11 CONCLUSIONS AND RECOMMENDATIONS

11.1 *Overall conclusions from these studies*

1. The coiled wire filament (CWF) is a very simple and useful means for introducing "dirty" samples containing large amounts of nonvolatiles, including bacterial endospores plus derivatization reagents such as tetramethylammonium hydroxide (TMA-OH), into a GC inlet with minimal contamination.

2. The perspective that the bacterial endospore's robust structure is primarily responsible for the difficulty of obtaining methylated DPA by heating spores with TMA-OH is incorrect. Rather, TMA-OH is simply not chemically well-suited for DPA methylation, at least at the temperatures employed in these investigations (290°C). Although DPA's complexing with Ca^{2+} plays some role in attenuating this reaction, the major reason for sub-quantitative Me_2DPA yields is that at least one of the carboxylate oxygens of DPA are weak nucleophiles that do not aggressively attack methyl groups on the TMA^+ cation.

3. The enhanced yield of Me_2DPA seen by the sequential addition of acidic $HMeSO_4$ (originally assumed to be H_2SO_4) followed by TMA-OH cannot be attributed to acid catalysis, nor is the spore rapidly degraded by hydrolysis/methanolysis under such conditions at ambient temperature. However, acid addition before base probably permeabilizes the spore to an extent that

Me$_2$DPA yields are increased either by reagent penetration inward and/or DPA escape outwards before heating in the GC.

4. The small quantity of Me$_2$DPA formed in acidic MeOH is rapidly hydrolyzed upon addition of methanolic TMA-OH. This reaction is accelerated by evaporation of MeOH as OH$^-$ is concentrated. Accordingly, levels of Me$_2$DPA formed by acid catalysis are below the detection limit of the GC-MS instrument.

5. Using TMA-OH alone, a nominal 10% of total spore DPA was converted to Me$_2$DPA, while MeSO$_4^-$ was about 10 times more active in the presence of TMA$^+$, Na$^+$, and OH$^-$ at a stoichiometric blend of approximately 3:1:3:1, respectively. Fatty acid methyl ester (FAME) profiles of the spores, although dwarfed by the peak area from total spore Me$_2$DPA, were unaltered by this reagent mixture.

6. A method for optimizing a gas chromatographic response that depends on mixtures of ions (here, TMA$^+$, Na$^+$, OH$^-$, and MeSO$_4^-$) was employed for the first time. The abbreviation *IMDOE* for *ionic mixtures design of experiments* is proposed as nomenclature for the method. IMDOE is a means for finding optimal conditions by systematically organizing combinations of ions and analyzing the mixture by the same, rather than by their (usually) binary salt precursors. This method allows for an efficient sampling of possible combinations of ions given constraints and a basis that is meaningful in the context of the experiments. The IMDOE approach is broadly applicable to many different applications.

7. Use of the CWF for sample introduction, while generally convenient and clean, is not recommended as a quantitative tool. A thorough errors analysis on this

process revealed that peak area reproducibility using the CWF was nominally ±20% average values. For quantitation, more traditional methods of careful chemical extraction, derivatization, and liquid injection are recommended. DPA quantitation by LC is much more accurate and reproducible than by GC.

11.2 *Recommendations for further work*

1. The very active reaction mixture of TMA^+, Na^+, OH^-, and $MeSO_4^-$ found for producing high yields of Me_2DPA comes with a catch: it incorporates components that leave Na_2SO_4 and other nonvolatile residues in the GC inlet. Na_2SO_4 is an "active" compound that causes peak tailing and may induce sample decomposition. It also degrades surface deactivation treatments and damages the GC column's stationary phase (e.g., alkali metal hydroxides (K, Rb, Cs) catalytically rearrange and depolymerize siloxane polymers [464]). Although a dirtied, activated liner in a laboratory GC is easily cleaned or exchanged, this is not a luxury with field-portable instrumentation. Therefore, the most important recommendation for future work is to either develop a more "chromatographically friendly" methylation mixture or to find a way to protect the liner and column from damage (perhaps through use of removable liner cartridges). Fortunately, the damage to the liner experienced in these studies, even after 50 or more injections, was only manifest if fresh derivatization reagent mixture was not co-introduced with the sample.

2. Pursuant to the basis used for the design summarized in this dissertation where mixtures of Na^+ and OH^- varied around a constant sum quantity of TMA^+ +

$MeSO_4^-$, several additional experiments are recommended for understanding

better the chemical behavior of the TCM mixtures in producing Me_2DPA.

a. Mixture points not investigated here may be studied in order to continue
the model development process reviewed in Section 4.4.2. For example,
points midway between **xz**, **ux**, **sy**, and **ry** in Figure 8-4 are of particular
interest since they are nearby the apparent regions of maximum response
and should provide key information for model validation or refinement.

b. The influence of the ratio of methyl donor reagent to spores should be
studied (probably at mixtures close to those found to be optimal in this
study, although this remains to be verified), which would allow for
assessment of the variability in biomarker responses when very large or
small quantities of spores are analyzed (something not easily controlled in
the field). This may be done either by changing the total quantity of spores
in the Eppendorf tube and introducing constant reagent concentrations to
suspend them prior to sampling by the wire, and/or by keeping the amount
of spores constant and diluting the reagents. The optimal ionic mixtures
identified here may shift to different reagent mixtures if the reagent:spore
ratios are changed. Determining whether this is the case will further refine
understanding of the chemical mechanisms at hand. This type of study has
been called a "mixture-amount" experiment [27].

c. Since the best Me_2DPA responses are seen at a small range of total OH^-
amounts (Figure 8-12C), a refinement of the design space to cover only
this range (e.g., 0-300 nmol) is recommended. One uncertainty is whether

the *total* amount of OH$^-$ that resides on the wire, the OH$^-$:spore ratios, or OH$^-$ mole fraction has the greatest influence on Me$_2$DPA yields.

3. In addition to studying DPA, investigating how other biomarkers (and biomarker ratios) behave as a function of mixtures is recommended.

4. It is not understood *why* the gamma-function-based model fits the data well. Currently, the proposed explanation is that there must be a careful balance between the quantity of OH$^-$ and the amounts of chemicals possessing a methyl group, be they methyl donor reagents or methylated biomarkers. Too much OH$^-$ and these methyl groups are irreversibly hydrolyzed to form MeOH and deprotonated product; too little OH$^-$ and spore thermochemolysis is diminished. Consideration of the chemical features and performing derivations from first principles may establish the reasons for the best-fitting functions' belonging to the exponential family of statistical distributions.

5. Addressing the issues related to flow patterns over the wire and wire heat-up rates was beyond the scope of this work, but may be addressed experimentally and/or computationally by a successor. Experiments could include changing wire material, geometry, or size; varying gas flow rate; altering liner dimensions; and changing solvent type and amount remaining on the wire. Computational fluid dynamics modeling of the gas flow patterns around and through the CWF would provide insights into the flow patterns around the coil and therewith residence times of the gas in the liner plus mass and heat transfer effects. Advanced models and experimentation could consider the highly endothermic process of solvent evaporation, including gas expansion that is known to induce back-flow. It may

also be helpful to study the effects of GC inlet temperature since that used in these studies, 290°C, was chosen after optimizing Me_2DPA yields with TMA-OH addition only. Once the flow, heat transfer, and mass transport features are understood, kinetics of the release and derivatization reactions might be incorporated. Although modeling takes time to implement, a successful model can ultimately save time and permit virtual experimentation, accelerating the development of new applications.

6. In addition to a computational fluid dynamics modeling, possibilities for stochastic modeling and designed experimentation consistent with Eqns. (8-16) or (8-17) in Section 8.3.2 are possible. Such work is important for quantitative analysis by solvent-less sampling in general.

7. Relevant to all the above proposals is a consideration of other methylation reagents or ions. For example, K^+ may be used instead of or in addition to Na^+. Also, items **2**, **5**, and **6** in Table 2-2 might be explored.

8. Additional characterizations of the most active methylation mixtures by SEM (such as Figure 9-1 through Figure 9-4), titrations (see Figure 8-13, Figure 8-14, and Table 8-3), and other experiments to further understand spore/biomarker chemistry could not be conducted due to time constraints. Physical and chemical characterization of the four-component TMA^+, Na^+, OH^-, and $MeSO_4^-$ mixture is recommended to understand its reactivity and stability. In addition to SEM and titrations, possible investigations could include light absorbance or Raman spectroscopy and X-ray diffraction [465] to understand the sizes, structures, and reactivities of the precipitates obtained by mixing TMA-OH, NaOH, and

HMeSO$_4$ (or other reagents) in MeOH and drying them on the CWF. Approaches based on mixtures experiments have been reported elsewhere [32, 407].

9. Although a chemical mechanism for the methylation of CaDPA was proposed here and discussed in the context of the experimental results, it is not proven. The mechanism may be validated or refined by a variety of means, such as crystallography of the CaDPA-NaMeSO$_4$ complexes. Isotopically-labeled TMA$^+$ may be employed to understand the relative importance of TMA$^+$ in methylating DPA and other biomarkers.

10. The author has attempted to summarize his means for design and analysis of data obtained with mixtures of ionic systems (Appendix A). The design and analysis of experiments involving mixtures of ions (IMDOE) appears to be a powerful approach to conducting effective experiments and understanding the chemistry of the interactions involving more than two ions. In this author's perspective, further opportunities are available in the following areas.

   a. Further review is recommended to evaluate computer codes that have been developed for determining the extreme points and convex hull of constrained mixture spaces, with focus on the constraints imposed by ionic systems. Several codes referenced in the literature include the CONVRT, XVERT, XVERT1, and CONSIM algorithms as well as a software package for design and analysis of mixture experiments entitled MIXSOFT [27, 28].

   b. Similarly, a more effective, rapid, and general means for choosing convex multipliers of the extreme points (or another method for interpolating

within them) may be useful for IMDOE experiments that are bounded by radical "shapes" that are very different from simplexes (a simplex is an *n*-dimensional analogue of a triangle, e.g., a tetrahedron). Experimental points chosen for 5-sided planes (Figure 8-3 and Figure 8-4) were assigned manually and somewhat subjectively by noticing that the design space was rectangular in shape with one of its corners cut off. Thus, the author was able to select points for study, essentially by interpolating within square convex hulls. This approach was possible because the dimensionality of the problem allowed for it to be visualized in a tetrahedral mixture plot. Admittedly, the author's subjectivity became part of the design. Mixtures experiments involving 5 or more components cannot be visualized directly and so must be selected by other means.

c. Following scoping experiments that are broadly distributed across the design space, one may wish to add additional experiments to further refine the model either by informing the selection of an appropriate model form [e.g., selection of, $f(\chi, \beta)$, the function of Eq. (4-9), as discussed in Sections 4.4.1 and 4.4.2] or for refinement of parameters in the model. For mixtures of 4 or fewer components, experiments may be added based on visual interpretation of the data (as was done in the spore DPA studies presented in this dissertation; see Figure 8-4 and Figure 8-5), but the process is biased by the operator's judgment and might not be the most efficient means to achieve the desired information. An algorithm or heuristic may be employed to determine a (next) point or set of points for

experimentation based on what the experimenter wants to learn. Methods

for such purposes have already been developed. For example, Cornell [27]

explains their use with linear response models for mixtures and Critchfield

[466] provides an example plus references for optimal experimental

design using models that are nonlinear in their parameters.

d. In the experiments on spore Me_2DPA yields, nonlinear functions fit the

response data better than did a high-order polynomial with linear

parameters. However, the nonlinear models required considerable effort

on the part of the author to find good guess values. It would be useful to

have an automated means for identifying regions of maximum response

within a mixture space, perhaps providing other information about their

shape (i.e., variance, skewness, etc.) so that effective models and guess

values for model parameters might be automatically selected for a

nonlinear solver. This might be implemented, for example, by fitting a

linear polynomial first and using it to obtain appropriate guesses for non-

linear functions and their parameters.

12 REFERENCES

(1)   Hawley, R. J.; Eitzen, E. M., Jr. *Annu Rev Microbiol* **2001**, *55*, 235-253.

(2)   Beeching, N. J.; Dance, D. A. B.; Miller, A. R. O.; Spencer, R. C. *Br Med J* **2002**, *324*, 336-339.

(3)   Oyston, P. C. F. In *Nato Science Series, Series I: Life and Behavioural Sciences*; DelVecchio, V. G., Krcmery, V., Eds., **2003**; Vol. 352, pp 1-5.

(4)   Bhalla, D. K.; Warheit, D. B. *Toxicol Appl Pharmacol* **2004**, *199*, 71-84.

(5)   Jernigan, D. B.; Raghunathan, P. L.; Bell, B. P.; Brechner, R.; Bresnitz, E. A.; Butler, J. C.; Cetron, M.; Cohen, M.; Doyle, T.; Fischer, M.; Greene, C.; Griffith, K. S.; Guarner, J.; Hadler, J. L.; Hayslett, J., A.; Meyer, R.; Petersen, L. R.; Phillips, M.; Pinner, R.; Popovic, T.; Quinn, C. P.; Reefhuis, J.; Reissman, D.; Rosenstein, N.; Schuchat, A.; Shieh, W.-J.; Siegal, L.; Swerdlow, D. L.; Tenover, F. C.; Traeger, M.; Ward, J. W.; Weisfuse, I.; Wiersma, S.; Yeskey, K.; Zaki, S.; Ashford, D. A.; Perkins, B. A.; Ostroff, S.; Hughes, J.; Fleming, D.; Koplan, J. P.; Gerberding, J. L. *Emerg Infect Dis* **2002**, *8*, 1019-1028.

(6)   Meselson, M.; Guillemin, J.; Hughjones, M.; Langmuir, A.; Popova, I.; Shelokov, A.; Yampolskaya, O. *Science* **1994**, *266*, 1202-1208.

(7)   Seidel, H. J.; Cotta, G. A. *Unweltmed Forsch Prax* **2002**, *7*, 117-124.

(8)   Turner, M. *Cent Afr J Med* **1980**, *26*, 160-161.

(9)   Van Ness, G. B. *Science* **1971**, *172*, 1303-1307.

(10)   Alberty, E. In *The Salt Lake Tribune (www.sltrib.com)*: Salt Lake City, **2008**.

(11)   Gehrke, S. In *The Salt Lake Tribune (www.sltrib.com)*: Salt Lake City, **2008**.

(12)   Anonymous In *The Daily Herald (www.heraldextra.com)*: Provo, UT, **2009**.

(13)   Alberty, E. In *The Salt Lake Tribune (www.sltrib.com)*: Salt Lake City, **2009**.

(14)   Smith, P. R. MS Thesis, Brigham Young University, Provo, **2005**.

(15)   Krebs, M. D.; Mansfield, B.; Yip, P.; Cohen, S. J.; Sonenshein, A. L.; Hitt, B. A.; Davis, C. E. *Biomol Eng* **2006**, *23*, 119-127.

(16)   Gooding, J. J. *Anal Chim Acta* **2006**, *559*, 137-151.

(17)   Edwards, K. A.; Clancy, H. A.; Baeumner, A. J. *Anal Bioanal Chem* **2006**, *384*, 73-84.

(18)   Cottingham, K. *Anal Chem* **2006**, *78*, 18-23.

(19)   Zhang, X.; Young, M. A.; Lyandres, O.; Van Duyne, R. P. *J Am Chem Soc* **2005**, *127*, 4484-4489.

(20)   Gluodenis, T.; Kunitsky, C. *Modern Drug Discovery* **2004**, *7*, 47-50.

(21)   Stachowiak, J. C.; Shugard, E. E.; Mosier, B. P.; Renzi, R. F.; Caton, P. F.; Ferko, S. M.; Van de Vreugde, J. L.; Yee, D. D.; Haroldsen, B. L.; VanderNoot, V. A. *Anal Chem* **2007**, *79*, 5763-5770.

(22)   Wang, D.-B.; Bi, L.-J.; Zhang, Z.-P.; Chen, Y.-Y.; Yang, R.-F.; Wei, H.-P.; Zhou, Y.-F.; Zhang, X.-E. *Analyst* **2009**, *134*, 738-742.

(23)   Farquharson, S.; Inscore, F.; Sperry, J. F. *Proc SPIE-Int Soc Opt Eng* **2006**, *6378*, 63780R/63781-63780R/63787.

(24)   Snyder, A. P. *Field Anal Chem Technol* **1999**, *3*, 219-220.

(25)   Chada, V. G. R.; Sanstad, E. A.; Wang, R.; Driks, A. *J Bacteriol* **2003**, *185*, 6255-6261.

(26)   Truong, T. V.; Nackos, A. N.; Murray, J. A.; Kimball, J. A.; Hawkes, J. E.; Harvey, D. J.; Tolley, H. D.; Robison, R. A.; Bartholomew, C. H.; Lee, M. L. *J Chromatogr A* **2009**, *1216*, 6852–6857.

(27)   Cornell, J. A. *Experiments with Mixtures: Designs, Models, and the Analysis of Mixture Data*, 3rd ed.; Wiley: New York, **2002**.

(28)   Schrevens, E.; Cornell, J. *Plant Soil* **1993**, *154*, 45-52.

(29)   Schrevens, E.; De Rijck, G. In *Proceedings of the Section on Physical and Engineering Statistics*; American Statistical Association, **2008**.

(30)   De Rijck, G.; Schrevens, E. *Sci Hortic* **1998**, *76*, 149-159.

(31)   De Rijck, G.; Schrevens, E.; Leuven, K. U. *Acta Hortic* **1999**, *481*, 205-212.

(32)   De Rijck, G.; Schrevens, E. *J Plant Nutr* **1999**, *22*, 259-268.

(33)   De Rijck, G.; Schrevens, E. *J Agric Eng Res* **1999**, *72*, 355-362.

(34)   Schrevens, E.; Cornell, J. *Dev Plant Soil Sci* **1993**, *53*, 179-186.

(35) Morgan, S. L.; Fox, A.; Gilbart, J. *J Microbiol Methods* **1989**, *9*, 57-69.

(36) MIDI, **2009**. *Sherlock® Microbial Identification Systems*. <u>www.midi-inc.com</u> (accessed June 2009).

(37) Brondz, I. *Anal Chim Acta* **2002**, *465*, 1-37.

(38) Mallidis, C. G.; Scholefield, J. *J Appl Bacteriol* **1987**, *62*, 65-69.

(39) Mowry, C.; Morgan, C.; Grye-Mason, G.; Theisen, L.; Trudell, D.; Baca, Q.; Chambers, W.; Martinez, J.; Sandia National Laboratories: Albuquerque, **2003**.

(40) Murrell, W. G.; Warth, A. D. In *Spores III*; Campbell, L. L., Halvorson, H. O., Eds.; American Society for Microbiology: Ann Arbor, Michigan, **1965**, pp 1-24.

(41) Beaman, T. C.; Greenamyre, J. T.; Corner, T. R.; Pankratz, H. S.; Gerhardt, P. *J Bacteriol* **1982**, *150*, 870-877.

(42) Popham, D. L.; Illades-Aguiar, B.; Setlow, P. *J Bacteriol* **1995**, *177*, 4721-4729.

(43) Vinter, V. In *The Bacterial Spore*; Gould, G. W., Hurst, A., Eds.; Academic Press: London, **1969**, pp 73-123.

(44) Doi, R. H. In *Bacillus*; Harwood, C. R., Ed.; Plenum Press: New York, **1989**, pp 169-215.

(45) Foster, J. W.; Perry, J. J. *J Bacteriol* **1954**, *67*, 295-302.

(46) Foerster, H. F.; Foster, J. W. *J Bacteriol* **1966**, *91*, 1333-1345.

(47) Hardwick, W. A.; Foster, J. W. *J Bacteriol* **1953**, *65*, 355-360.

(48) Pelcher, E. A.; Fleming, H. P.; Ordal, Z. J. *Can J Microbiol* **1963**, *9*, 251-258.

(49) Liu, H.; Bergman, N. H.; Thomason, B.; Shallom, S.; Hazen, A.; Crossno, J.; Rasko, D. A.; Ravel, J.; Read, T. D.; Peterson, S. N.; Yates, J., III; Hanna, P. C. *J Bacteriol* **2004**, *186*, 164-178.

(50) Setlow, P. *J Appl Microbiol* **2006**, *101*, 514-525.

(51) Neidhardt, F. C.; Ingraham, J. L.; Schaechter, M. *Physiology of the Bacterial Cell: A Molecular Approach*; Sinauer Associates: Sunderland, Mass., **1990**.

(52) Driks, A. *Cell Mol Life Sci* **2002**, *59*, 389-391.

(53) Waites, W. M. In *Fundamental and Applied Aspects of Bacterial Spores*; Dring, G. J., Ellar, D. J., Gould, G. W., Eds.; Academic Press: London, **1985**, pp 383-396.

(54)   Phillips, Z. E. V.; Strauch, M. A. *Cell Mol Life Sci* **2002**, *59*, 392-402.

(55)   Marquis, R. E. In *Metal Ions and Bacteria*; Beveridge, T. J., Doyle, R. J., Eds.; Wiley: New York, **1989**, pp 247-274.

(56)   Errington, J. *Trends Genet* **1996**, *12*, 31-34.

(57)   Popham, D. L. *Cell Mol Life Sci* **2002**, *59*, 426-433.

(58)   Lewis, J. C. In *The Bacterial Spore*; Gould, G. W., Hurst, A., Eds.; Academic Press: London, **1969**, pp 301-358.

(59)   Setlow, P. In *Annual Review of Microbiology*; Ornston, L. N., Balows, A., Greenberg, E. P., Eds., **1995**; Vol. 49, pp 29-54.

(60)   Palacios, P.; Burgos, J.; Hoz, L.; Sanz, B.; Ordonez, J. A. *J Appl Bacteriol* **1991**, *71*, 445-451.

(61)   Warth, A. D. *Adv Microb Physiol* **1978**, *17*, 1-45.

(62)   Warth, A. D. In *Sporulation and Germination (Spores VIII)*; Levinson, H. S., Sonenshein, A. L., Tipper, D. J., Eds.; American Society for Microbiology: Washington, D.C., **1981**, pp 249-252.

(63)   Pendukar, S. H.; Kulkarni, P. R. *Nahr-Food* **1988**, *32*, 1003-1004.

(64)   Lindsay, J. A.; Murrell, W. G. *Curr Microbiol* **1985**, *12*, 329-333.

(65)   Lindsay, J. A.; Murrell, W. G. *Curr Microbiol* **1986**, *13*, 255-259.

(66)   Pogliano, K.; Harry, E.; Losick, R. *Mol Microbiol* **1995**, *18*, 459-470.

(67)   Sharp, M. D.; Pogliano, K. In *Bacillus Subtilis and Its Closest Relatives*; Sonenshein, A. L., Hoch, J. A., Losick, R., Eds.; ASM Press: Washington, D.C., **2002**, pp 15-20.

(68)   Driks, A. In *Bacillus Subtilis and Its Closest Relatives*; Sonenshein, A. L., Hoch, J. A., Losick, R., Eds.; ASM Press: Washington, D.C., **2002**, pp 527-535.

(69)   Sabli, M. Z. H.; Setlow, P.; Waites, W. M. *Lett Appl Microbiol* **1996**, *22*, 405-407.

(70)   Tipper, D. J.; Gauthier, J. J. In *Spores V*; Halvorson, H. O., Hanson, R., Campbell, L. L., Eds.; American Society for Microbiology: Washington, D.C., **1972**, pp 3-12.

(71)   Levine, B. A. In *Fundamental and Applied Aspects of Bacterial Spores*; Dring, G. J., Ellar, D. J., Gould, G. W., Eds.; Academic Press: London, **1985**, pp 47-58.

(72)   Setlow, P. *J Appl Bacteriol* **1994**, *76*, S49-S60.

(73)   Nelson, D. L.; Spudich, J. A.; Bonsen, P. P. M.; Bertsch, L. L.; Kornberg, A. In *Spores IV*; Cambell, L. L., Ed.; American Society for Microbiology: Bethesda, **1969**, pp 59-71.

(74)   Rajan, K. S.; Grecz, N. In *Spore Research 1976*; Barker, A. N., Wolf, J., Ellar, D. J., Dring, G. J., Gould, G. W., Eds.; Academic Press: London, **1977**; Vol. 2, pp 527-543.

(75)   Marshall, B. J.; Murrell, W. G. *J Appl Bacteriol* **1970**, *33*, 103-129.

(76)   Setlow, B.; Atluri, S.; Kitchel, R.; Koziol-Dube, K.; Setlow, P. *J Bacteriol* **2006**, *188*, 3740-3747.

(77)   Stewart, G. S. A. B.; Eaton, M. W.; Johnstone, K.; Barrett, M. D.; Ellar, D. J. *Biochim Biophys Acta, Biomembr* **1980**, *600*, 270-290.

(78)   Murrell, W. G. In *Sporulation and Germination (Spores VIII)*; Levinson, H. S., Sonenshein, A. L., Tipper, D. J., Eds.; American Society for Microbiology: Washington, D. C., **1981**, pp 64-77.

(79)   Franks, F. In *Fundamental and Applied Aspects of Bacterial Spores*; Dring, G. J., Ellar, D. J., Gould, G. W., Eds.; Academic Press: London, **1985**, pp 3-19.

(80)   Bloomfield, S. F.; Arthur, M. *J Appl Bacteriol* **1994**, *76*, 91S-104S.

(81)   Oyama, J. *Kenkyu Hokoku - Kogyo Gijutsuin Hakko Kenkyusho* **1961**, *20*, 105-112.

(82)   Oyama, J. *Kenkyu Hokoku - Kogyo Gijutsuin Hakko Kenkyusho* **1961**, *20*, 95-103.

(83)   Oyama, J. *Kenkyu Hokoku - Kogyo Gijutsuin Hakko Kenkyusho* **1961**, *20*, 83-93.

(84)   Oyama, J. *Kenkyu Hokoku - Kogyo Gijutsuin Hakko Kenkyusho* **1962**, *21*, 103-108.

(85)   Oyama, J.; Nakamura, N.; Tanabe, O. *Bull Agric Chem Soc Jpn* **1960**, *24*, 743-744.

(86)   Oyama, J.; Nakamura, N.; Tanabe, O. *Kenkyu Hokoku - Kogyo Gijutsuin Hakko Kenkyusho* **1961**, *19*, 75-81.

(87)   Hodson, P. H.; Darlington, W. A. ((Monsanto Co.).). US Patent 3,334,021, **1967**.

(88)   Kalle, G. P.; Khandekar, P. S. *J Biosci* **1983**, *5*, 43-52.

(89)   Huang, S.; Chen, D.; Pelczar, P. L.; Vepachedu, V. R.; Setlow, P.; Li, Y. *J Bacteriol* **2007**, *189*, 4681-4687.

(90) Levinson, H. S.; Hyatt, M. T.; Moore, F. E. *Biochem Biophys Res Commun* **1961**, *5*, 417-421.

(91) Riemann, H. In *Spores II*; Halvorson, H. O., Ed.; Burgess Publishing Company: Minneapolis, **1961**, pp 24-48.

(92) Lewis, J. C. *J Biol Chem* **1972**, *247*, 1861-1868.

(93) Riemann, H.; Ordal, J. Z. *Science (Washington, DC, United States)* **1961**, *133*, 1703-1704.

(94) Sarasanandarajah, S.; Kunnil, J.; Bronk, B. V.; Reinisch, L. *Appl Opt* **2005**, *44*, 1182-1187.

(95) Shafaat, H. S.; Ponce, A. *Abstracts of Papers, 231st ACS National Meeting, Atlanta, GA, United States, March 26-30, 2006* **2006**, INOR-783.

(96) Hindle, A. A.; Hall, E. A. H. *Analyst* **1999**, *124*, 1599-1604.

(97) Crafts-Lighty, A.; Ellar, D. J. *J Appl Bacteriol* **1980**, *48*, 135-145.

(98) Gerhardt, P.; Beaman, T. C.; Corner, T. R.; Greenamyre, J. T.; Tisa, L. S. *J Bacteriol* **1982**, *150*, 643-648.

(99) Alberto, F.; Botella, L.; Carlin, F.; Nguyen-the, C.; Broussolle, V. *FEMS Microbiol Lett* **2005**, *253*, 231-235.

(100) Fujita, Y.; Yasuda, Y.; Kozuka, S.; Tochikubo, K. *Microbiol Immunol* **1989**, *33*, 391-401.

(101) Koshikawa, T.; Beaman, T. C.; Pankratz, H. S.; Nakashio, S.; Corner, T. R.; Gerhardt, P. *J Bacteriol* **1984**, *159*, 624-632.

(102) Nakashio, S.; Gerhardt, P. *J Bacteriol* **1985**, *162*, 571-578.

(103) Cowan, A. E.; Koppel, D. E.; Setlow, B.; Setlow, P. *Proc Natl Acad Sci USA* **2003**, *100*, 4209-4214.

(104) Cowan, A. E.; Olivastro, E. M.; Koppel, D. E.; Loshon, C. A.; Setlow, B.; Setlow, P. *Proc Natl Acad Sci USA* **2004**, *101*, 7733-7738.

(105) Swerdlow, B. M.; Setlow, B.; Setlow, P. *J Bacteriol* **1981**, *148*, 20-29.

(106) Gerhardt, P.; Black, S. H. *J Bacteriol* **1961**, *82*, 750-760.

(107) Setlow, B.; Loshon, C. A.; Genest, P. C.; Cowan, A. E.; Setlow, C.; Setlow, P. *J Appl Microbiol* **2002**, *92*, 362-375.

(108) Cortezzo, D. E.; Koziol-Dube, K.; Setlow, B.; Setlow, P. *J Appl Microbiol* **2004**, *97*, 838-852.

(109) Cortezzo, D. E.; Setlow, P. *J Appl Microbiol* **2005**, *98*, 606-617.

(110) Blankenship, L. C.; Pallansch, M. J. *J Bacteriol* **1966**, *92*, 1615-1617.

(111) Foster, S. J. *J Appl Bacteriol Symp Suppl* **1994**, *76*, 25S-39S.

(112) Fox, A.; Morgan, S. L. In *Instrumental Methods for Rapid Microbiological Analysis*; Nelson, W. H., Ed.; VCH, **1985**.

(113) Fox, A.; Black, G. E. In *Mass Spectrometry for the Characterization of Microorganisms*; Fenselau, C., Ed.; American Chemical Society: Washington, D.C., **1994**; Vol. 541, pp 107-131.

(114) Atrih, A.; Bacher, G.; Korner, R.; Allmaier, G.; Foster, S. J. *Microbiology (Reading, United Kingdom)* **1999**, *145*, 1033-1041.

(115) Atrih, A.; Zöllner, P.; Allmaier, G.; Foster, S. J. *J Bacteriol* **1996**, *178*, 6173-6183.

(116) Popham, D. L.; Helin, J.; Costello, C. E.; Setlow, P. *J Bacteriol* **1996**, *178*, 6451-6458.

(117) Atrih, A.; Foster, S. J. *Antonie van Leeuwenhoek* **1999**, *75*, 299-307.

(118) Marquis, R. E.; Bender, G. R.; Carstensen, E. L.; Child, S. Z. In *The Target of Penicillin*; Hakenbeck, R., Höltje, J.-V., Labischinski, H., Eds.; Walter de Gruyter: Berlin, **1983**, pp 43-48.

(119) Sousa, J. C.; Silva, M. T.; Balassa, G. *Ann Microbiol* **1978**, *129 B*, 377-390.

(120) Imae, Y.; Strominger, J. L. *J Bacteriol* **1976**, *126*, 907-913.

(121) Imae, Y.; Strominger, M. B.; Strominger, J. L. *Spores* **1978**, *7*, 62-66.

(122) Lewis, J. C.; Snell, N. S.; Burr, H. K. *Science* **1960**, *132*, 544-545.

(123) Alderton, G.; Snell, N. *Biochem Biophys Res Commun* **1963**, *10*, 139-143.

(124) Alderton, G.; Thompson, P. A.; Snell, N. *Science* **1964**, *143*, 141-143.

(125) Gould, G. W.; Dring, G. J. In *Advances in Microbial Physiology Volume 11*; Rose, A. H., Tempest, D. W., Eds.; Academic Press: London, New York, **1974**; Vol. 11, pp 137-164.

(126) Gould, G. W.; Dring, G. J. *Nature* **1975**, *258*, 402-405.

(127)   Gould, G. W.; Dring, G. J. In *Spores VI*; Gerhardt, P., Costilow, R. N., Sadoff, H. L., Eds.; American Society for Microbiology: Washington, D.C., **1975**, pp 541-546.

(128)   Gould, G. W. *J Appl Bacteriol* **1977**, *42*, 297-309.

(129)   Popham, D. L.; Gilmore, M. E.; Setlow, P. *J Bacteriol* **1999**, *181*, 126-132.

(130)   Meador-Parton, J.; Popham, D. L. *J Bacteriol* **2000**, *182*, 4491-4499.

(131)   Warth, A. D. In *Fundamental and Applied Aspects of Bacterial Spores*; Dring, G. J., Ellar, D. J., Gould, G. W., Eds.; Academic Press: London, **1985**, pp 209-225.

(132)   Gould, G. W.; Dring, G. J. In *Spore Research 1976*; Barker, A. N., Wolf, J., Ellar, D. J., Dring, G. J., Gould, G. W., Eds.; Academic Press: London, **1977**; Vol. 2, pp 421-429.

(133)   Algie, J. E. *Curr Microbiol* **1980**, *3*, 287-290.

(134)   Aronson, A. I.; Fitz-James, P. *Bacteriol Rev* **1976**, *40*, 360-402.

(135)   Driks, A. *Microbiol Mol Biol Rev* **1999**, *63*, 1-20.

(136)   Hunnell, J. W.; Ordall, Z. J. In *Spores II*; Halvorson, H. O., Ed.; Burgess Publishing Company: Minneapolis, **1961**, pp 101-112.

(137)   Gorman, S. P.; Scott, E. M.; Hutchinson, E. P. *J Appl Bacteriol* **1984**, *57*, 153-163.

(138)   Laaberki, M.-H.; Dworkin, J. *J Bacteriol* **2008**, *190*, 6197-6203.

(139)   Laaberki, M. H.; Dworkin, J. E. *Symbiosis* **2008**, *46*, 95-100.

(140)   Henriques, A. O.; Moran, C. P., Jr. *Annu Rev Microbiol* **2007**, *61*, 555-588.

(141)   Klobutcher, L. A.; Ragkousi, K.; Setlow, P. *Proc Natl Acad Sci USA* **2006**, *103*, 165-170.

(142)   Driks, A. *Phytopathology* **2004**, *94*, 1249-1251.

(143)   Ragkousi, K.; Eichenberger, P.; van Ooij, C.; Setlow, P. *J Bacteriol* **2003**, *185*, 2315-2329.

(144)   Bagyan, I.; Setlow, P. *J Bacteriol* **2002**, *184*, 1219-1224.

(145)   Chirakkal, H.; O'Rourke, M.; Atrih, A.; Foster, S. J.; Moir, A. *Microbiology (Reading, United Kingdom)* **2002**, *148*, 2383-2392.

(146) Gerhardt, P.; Scherrer, R.; Black, S. H. In *Spores V*; Halvorson, H. O., Hanson, R., Campbell, L. L., Eds.; American Society for Microbiology: Washington, D.C., **1972**, pp 68-74.

(147) Nishihara, T.; Takubo, Y.; Kawamata, E.; Koshikawa, T.; Ogaki, J.; Kondo, M. *J Biochem, Tokyo* **1989**, *106*, 270-273.

(148) Watt In *Sporulation and Germination (Spores VIII)*; Levinson, H. S., Sonenshein, A. L., Tipper, D. J., Eds.; American Society for Microbiology: Washington, D.C., **1981**, pp 253-255.

(149) Bayliss, C. E.; Waites, W. M. *J Appl Bacteriol* **1979**, *47*, 263-269.

(150) Vary, J. C. *J Bacteriol* **1973**, *116*, 797-802.

(151) Beaman, T. C.; Pankratz, H. S.; Gerhardt, P. *Appl Environ Microbiol* **1988**, *54*, 2515-2520.

(152) Rowley, D. B.; Levinson, H. S. *J Bacteriol* **1967**, *93*, 1017-1022.

(153) Fitz-James, P. C.; Young, I. E. *J Bacteriol* **1959**, *78*, 743-754.

(154) Beaman, T. C.; Pankratz, H. S.; Gerhardt, P. *J Bacteriol* **1972**, *109*, 1198-1209.

(155) Takumi, K.; Kinouchi, T.; Kawata, T. *Microbiol Immunol* **1979**, *23*, 443-454.

(156) Sousa, J. C.; Silva, M. T.; Balassa, G. *Nature* **1976**, *263*, 53-54.

(157) Sousa, J. C.; Silva, M. T.; Balassa, G. *Ann Microbiol* **1978**, *129 B*, 339-362.

(158) Ghebrehiwet, B.; Tantral, L.; Titmus Mathew, A.; Panessa-Warren Barbara, J.; Tortora George, T.; Wong Stanislaus, S.; Warren John, B. *Adv Exp Med Biol* **2007**, *598*, 181-197.

(159) Matz, L. L.; Beaman, T. C.; Gerhardt, P. *J Bacteriol* **1970**, *101*, 196-201.

(160) Matz, L.; Gerhardt, P. In *Bacteriological Proceedings*; American Society for Microbiology, **1964**.

(161) Berger, J. A.; Marr, A. G. *J Gen Microbiol* **1960**, *22*, 147-157.

(162) Charlton, S.; Moir, A. J. G.; Baillie, L.; Moir, A. *J Appl Microbiol* **1999**, *87*, 241-245.

(163) Steichen, C.; Chen, P.; Kearney, J. F.; Turnbough, C. L., Jr. *J Bacteriol* **2003**, *185*, 1903-1910.

(164) Daubenspeck, J. M.; Zeng, H. D.; Chen, P.; Dong, S. L.; Steichen, C. T.; Krishna, N. R.; Pritchard, D. G.; Turnbough, C. L. *J Biol Chem* **2004**, *279*, 30945-30953.

(165) Borman, S. *Chem Eng News* **2005**, *83*, 10.

(166) Dong, S.; McPherson, S. A.; Tan, L.; Chesnokova, O. N.; Turnbough, C. L., Jr.; Pritchard, D. G. *J Bacteriol* **2008**, *190*, 2350-2359.

(167) Curran, H. R.; Brunstetter, B. C.; Myers, A. T. *J Bacteriol* **1943**, *45*, 485-494.

(168) Slepecky, R. A.; Foster, J. W. *J Bacteriol* **1959**, *78*, 117-123.

(169) Thomas, R. S. *J Cell Biol* **1964**, *23*, 113-133.

(170) Knaysi, G. *J Bacteriol* **1961**, *82*, 556-563.

(171) Knaysi, G. *J Bacteriol* **1965**, *90*, 453-455.

(172) Bernhard, K.; Utz, R. In *Bacillus Thuringiensis, an Environmental Pesticide: Theory and Practice*; Entwistle, P. F., Cory, J. S., Bailey, M. J., Higgs, S., Eds.; John Wiley & Sons: Chichester, **1993**, pp 255-267.

(173) Rajan, K. S.; Jaw, R.; Grecz, N. *Bioinorg Chem* **1978**, *8*, 477-491.

(174) Aoki, H.; Slepecky, R. *Spore Res 1973, [Proc Br Spore Group Meet]* **1974**, 93-102.

(175) Aoki, H.; Slepecky, R. A. *J Bacteriol* **1973**, *114*, 137-143.

(176) Walker, H. W.; Matches, J. R.; Ayres, J. C. *J Bacteriol* **1961**, *82*, 960-966.

(177) Murrell, W. G. In *Advances in Microbial Physiology Volume 1*; Rose, A. H., Wilkinson, J. F., Eds.; Academic Press: London, **1967**, pp 133-251.

(178) Gould, G. W. In *Bacterial Spore Vol. 2*; Hurst, A., Gould, G. W., Eds.; Academic Press: London, **1983**, pp 173-209.

(179) Cliff, J. B.; Jarman, K. H.; Valentine, N. B.; Golledge, S. L.; Gaspar, D. J.; Wunschel, D. S.; Wahl, K. L. *Appl Environ Microbiol* **2005**, *71*, 6524-6530.

(180) Kamei, T.; Kamikado, H.; Kaneko, K.; Nakai, Y.; Sato, J. *Nihon Bokin Bobai Gakkaishi* **1991**, *19*, 445-450.

(181) Powell, J. F. *Biochem J* **1953**, *54*, 210-211.

(182) Stewart, M.; Somlyo, A. P.; Somlyo, A. V.; Shuman, H.; Lindsay, J. A.; Murrell, W. G. *J Bacteriol* **1980**, *143*, 481-491.

(183) Han, C. S.; Xie, G.; Challacombe, J. F.; Altherr, M. R.; Bhotika, S. S.; Bruce, D.; Campbell, C. S.; Campbell, M. L.; Chen, J.; Chertkov, O.; Cleland, C.; Dimitrijevic, M.; Doggett, N. A.; Fawcett, J. J.; Glavina, T.; Goodwin, L. A.; Hill, K. K.; Hitchcock, P.; Jackson, P. J.; Keim, P.; Kewalramani, A. R.; Longmire, J.;

Lucas, S.; Malfatti, S.; McMurry, K.; Meincke, L. J.; Misra, M.; Moseman, B. L.; Mundt, M.; Munk, A. C.; Okinaka, R. T.; Parson-Quintana, B.; Reilly, L. P.; Richardson, P.; Robinson, D. L.; Rubin, E.; Saunders, E.; Tapia, R.; Tesmer, J. G.; Thayer, N.; Thompson, L. S.; Tice, H.; Ticknor, L. O.; Wills, P. L.; Brettin, T. S.; Gilna, P. *J Bacteriol* **2006**, *188*, 3382-3390.

(184) Brar, S. K.; Verma, M.; Tyagi, R. D.; Surampalli, R. Y.; Barnabe, S.; Valero, J. R. *Process Biochem* **2007**, *42*, 773-790.

(185) Glare, T. R.; O'Callaghan, M. *Bacillus Thuringiensis: Biology, Ecology and Safety*; John Wiley & Sons: Chichester, **2000**.

(186) Song, Y. J.; Yang, R. F.; Guo, Z. B.; Zhang, M. L.; Wang, X. H.; Zhou, F. *J Microbiol Methods* **2000**, *39*, 225-241.

(187) Wunschel, D.; Fox, K. F.; Black, G. E.; Fox, A. *Syst Appl Microbiol* **1994**, *17*, 625-635.

(188) Stratis-Cullum, D. N.; Griffin, G. D.; Mobley, J.; Vass, A. A.; Vo-Dinh, T. *Anal Chem* **2003**, *75*, 275-280.

(189) Carrera, M.; Zandomeni, R. O.; Fitzgibbon, J.; Sagripanti, J. L. *J Appl Microbiol* **2007**, *102*, 303-312.

(190) Marriott, P. J. *J Chromatogr Libr* **2004**, *69A*, 319-368.

(191) Grob, K. *Split and Splitless Injection for Quantitative Gas Chromatography: Concepts, Processes, Practical Guidelines, Sources of Error*, 4th ed.; Wiley-VCH: New York, **2001**.

(192) Bailey, R. *J Environ Monit* **2005**, *7*, 1054-1058.

(193) Hinshaw, J. V. *J Chromatogr Sci* **1988**, *26*, 142-145.

(194) Condon, R. D.; Ettre, L. S. In *Instrumentation in Gas Chromatography*; Krugers, J., Ed.; Centrex Publishing Company: Eindhoven, **1968**, pp 87-105.

(195) de Zeeuw, J. *Am Lab* **2005**, *37*, 18,20.

(196) Harris, R. J.; Harris, R. J., Jr. (Precision Sampling Corporation). US Patent 3474674, **1969**.

(197) Golovistikov, J. N. (Bolshoi Kondratievsky). US Patent 3733909, **1973**.

(198) Parker, K. D.; Fontan, C. R.; Kirk, P. L. *Anal Chem* **1963**, *35*, 356-359.

(199) McComas, D. B.; Goldflen, A. *Anal Chem* **1963**, *35*, 263-264.

(200) Yannone, M. E. *J Gas Chromatogr* **1968**, *6*, 465-468.

(201)   Shadkami, F.; Helleur, R. *J Chromatogr A* **2009**, *1216*, 5903-5910.

(202)   Dettner, K.; Schwinger, G.; Wunderle, P. *J Chem Ecol* **1985**, *11*, 859-883.

(203)   Hamilton, C. H. In *Instrumentation in Gas Chromatography*; Krugers, J., Ed.; Centrex Publishing Company: Eindhoven, **1968**, pp 33-52.

(204)   The Hamilton Company *Anal Chem* **1963**, *35*, 124A.

(205)   Carson, L. M.; Uglum, K. L. *J Gas Chromatogr* **1965**, *3*, 208-209.

(206)   da Silva, U. F.; L. Borba, E.; Semir, J.; Marsaioli, A. J. *Phytochemistry* **1999**, *50*, 31-34.

(207)   Pragst, F. *Anal Bioanal Chem* **2007**, *388*, 1393-1414.

(208)   Arthur, C. L.; Pawliszyn, J. *Anal Chem* **1990**, *62*, 2145-2148.

(209)   Pawliszyn, J. US Patent 5691206, **1997**.

(210)   Ciucanu, I. *Rev Chim* **2006**, *57*, 923-926.

(211)   Ciucanu, I.; Caprita, A.; Chiriac, A.; Barna, R. *Anal Chem* **2003**, *75*, 736-741.

(212)   Ciucanu, I. *Anal Chem* **2002**, *74*, 5501-5506.

(213)   Ciucanu, I.; Swallow, K. C.; Caprita, R. *Anal Chim Acta* **2004**, *519*, 93-101.

(214)   Cagnazzo, G.; Ros, A.; Bignardi, G. *J Chromatogr* **1965**, *19*, 185-189.

(215)   Cagnazzo, G.; Ros, A.; Bignardi, G. *Monit Ostet-Ginecol* **1964**, *35*, 374-393.

(216)   Ros, A. *J Gas Chromatogr* **1965**, *3*, 252.

(217)   Ros, A. *Boll - Soc Ital Biol Sper* **1964**, *40*, 1669-1671.

(218)   Tinti, P. *J Gas Chromatogr* **1966**, *4*, 140-141.

(219)   Blomstrand, R.; Gürtler, J. *Acta Chem Scand* **1964**, *18*, 276-278.

(220)   Biermann, C. J.; McGinnis, G. D. *Analysis of Carbohydrates by GLC and MS*; CRC Press: Boca Raton, Fla., **1989**.

(221)   Drucker, D. B. *Microbiological Applications of Gas Chromatography*; Cambridge University Press: Cambridge [Eng.] ; New York, **1981**.

(222)   Odham, G.; Larsson, L.; Mårdh, P.-A. *Gas Chromatography/Mass Spectrometry Applications in Microbiology*; Plenum Press: New York, **1984**.

(223) Fox, A.; Morgan, S. L.; Larsson, L.; Odham, G. *Analytical Microbiology Methods: Chromatography and Mass Spectrometry*; Plenum Press: New York, **1990**.

(224) Kuksis, A. In *Handbook of Lipid Research: Fatty Acids and Glycerides*; Kuksis, A., Ed.; Plenum: New York, **1978**; Vol. 1, pp 1-76.

(225) Sigma-Aldrich *Derivatization Reagents for Selective Response and Detection in Complex Matrices*; Sigma-Aldrich Co.: St. Louis, **2007**.

(226) Halket, J. M.; Zaikin, V. G. *Eur J Mass Spectrom* **2004**, *10*, 1-19.

(227) Molnár-Perl, I. *Journal of Chromatography, A* **2000**, *891*, 1-32.

(228) Rompa, M.; Kremer, E.; Zygmunt, B. *Anal Bioanal Chem* **2003**, *377*, 590-599.

(229) Christie, W. W. In *Advances in Lipid Methodology-Two*; Christie, W. W., Ed.; The Oily Press: Dundee, **1993**, pp 69-111.

(230) Shantha, N. C.; Napolitano, G. E. *J Chromatogr* **1992**, *624*, 37-51.

(231) Nimz, E. L.; Morgan, S. L. *J Chromatogr Sci* **1993**, *31*, 145-149.

(232) Liu, K. S. *J Am Oil Chem Soc* **1994**, *71*, 1179-1187.

(233) Carrapiso, A. I.; Garcia, C. *Lipids* **2000**, *35*, 1167-1177.

(234) Rosenfeld, J. M. *Anal Chim Acta* **2002**, *465*, 93-100.

(235) Bondioli, P. *Top Catal* **2004**, *27*, 77-82.

(236) Smith, M.; March, J. *March's Advanced Organic Chemistry : Reactions, Mechanisms, and Structure*, 6th ed.; Wiley-Interscience: Hoboken, N.J., **2007**.

(237) Adler, M.; Adler, S.; Boche, G. *J Phys Org Chem* **2005**, *18*, 193-209.

(238) Jencks, W. P.; Gilbert, H. F. *Pure Appl Chem* **1977**, *49*, 1021-1027.

(239) Bruice, P. Y. *Organic Chemistry*, 3rd ed.; Prentice Hall: Upper Saddle River, N.J., **2001**.

(240) Stoffel, W.; Chu, F.; Ahrens, E. H. *Anal Chem* **1959**, *31*, 307-308.

(241) Liu, Y.; Lotero, E.; Goodwin Jr, J. G. *J Mol Catal A: Chem* **2006**, *245*, 132-140.

(242) Glass, R. L. *Lipids* **1971**, *6*, 919-925.

(243) Carreau, J. P.; Dubacq, J. P. *J Chromatogr* **1978**, *151*, 384-390.

(244) Christie, W. W. *J Lipid Res* **1982**, *23*, 1072-1076.

(245) Pardee, A. M.; Reid, E. E. *J Ind Eng Chem* **1920**, *12*, 129-133.

(246) Suter, B.; Grob, K.; Pacciarelli, B.; Novoselac, A. *Mitt Geb Lebensm Hyg* **1997**, *88*, 259-276.

(247) Suter, B.; Grob, K.; Pacciarelli, B. *Z Lebensm-Unters Forsch A: Food Res Technol* **1997**, *204*, 252-258.

(248) Schuchardt, U.; Lopes, O. *J Am Oil Chem Soc* **1988**, *65*, 1940-1941.

(249) Caldin, E. F.; Long, G. *Nature* **1953**, *172*, 583-584.

(250) Caldin, E. F.; Long, G. *Journal of the Chemical Society (Resumed)* **1954**, 3737-3742.

(251) Bender, M. L.; Glasson, W. A. *J Am Chem Soc* **1959**, *81*, 1590-1597.

(252) Abrash, H. I. *J Chem Educ* **2001**, *78*, 1496-1498.

(253) Kossa, W. C.; MacGee, J.; Ramachandran, S.; Webber, A. J. *J Chromatogr Sci* **1979**, *17*, 177-187.

(254) Hammett, L. P.; Pfluger, H. L. *J Am Chem Soc* **1933**, *55*, 4079-4089.

(255) Serjeant, E. P.; Dempsey, B. *Ionisation Constants of Organic Acids in Aqueous Solution*; Pergamon Press: Oxford, **1979**.

(256) Bonvicini, P.; Levi, A.; Lucchini, V.; Scorrano, G. *J Chem Soc, Perkin Trans 2* **1972**, 2267-2269.

(257) Guthrie, J. P. *Can J Chem* **1978**, *56*, 2342-2354.

(258) Högfeldt, E. *Stability Constants of Metal-Ion Complexes, Part A: Inorganic Ligands*, 1st ed.; Pergamon: Oxford, **1979**.

(259) Perrin, D. D.; International Union of Pure and Applied Chemistry. Commission on Equilibrium Data. *Ionisation Constants of Inorganic Acids and Bases in Aqueous Solution*, 2nd ed.; Pergamon Press: Oxford [Oxfordshire] ; New York, **1982**.

(260) Roberts, J. D.; Webb, R. L.; McElhill, E. A. *J Am Chem Soc* **1950**, *72*, 408-411.

(261) Marshall, H. P.; Grunwald, E. *J Am Chem Soc* **1954**, *76*, 2000-2004.

(262) Rived, F.; Roses, M.; Bosch, E. *Anal Chim Acta* **1998**, *374*, 309-324.

(263) Rived, F.; Canals, I.; Bosch, E.; Roses, M. *Anal Chim Acta* **2001**, *439*, 315-333.

(264) Bacarella, A. L.; Grunwald, E.; Marshall, H. P.; Purlee, E. L. *J Org Chem* **1955**, *20*, 747-762.

(265) Arnett, E. M. *Acc Chem Res* **1973**, *6*, 404-409.

(266) Kirkland, J. J. *Anal Chem* **1961**, *33*, 1520-1524.

(267) Hetman, N. E.; Arlt, H. G.; Paylor, R.; Feinland, R. *J Am Oil Chem Soc* **1965**, *42*, 255-256.

(268) Prelog, V.; Piantanida, M. *Hoppe-Seylers Z Physiol Chem* **1936**, *244*, 56-58.

(269) Fuson, R. C.; Corse, J.; Horning, E. C. *J Am Chem Soc* **1939**, *61*, 1290.

(270) Carr, F. H.; Pyman, F. L. *J Chem Soc, Trans* **1914**, *105*, 1591-1638.

(271) Green, G. H.; Kenyon, J. *J Chem Soc* **1950**, 1589-1596.

(272) Ishikawa, K.; Kanazawa, S.; Fukushima, Y.; Morishita, S. (Nisso Petrochemical Industries Co., Ltd.). JP Patent 61246145, **1986**.

(273) Wolfenden, R.; Yuan, Y. *Proc Natl Acad Sci USA* **2007**, *104*, 83-86.

(274) Takashima, K.; Riveros, J. M. *Mass Spectrom Rev* **1999**, *17*, 409-430.

(275) Takashima, K.; Riveros, J. M. *J Am Chem Soc* **1978**, *100*, 6128-6132.

(276) Amijee, M.; Wells, R. J. *J Chromatogr A* **1994**, *662*, 123-137.

(277) Brondz, I.; Olsen, I. *J Chromatogr* **1992**, *576*, 328-333.

(278) Brondz, I.; Olsen, I. *J Chromatogr* **1992**, *598*, 309-312.

(279) Blokker, P.; Pel, R.; Akoto, L.; Brinkman, U. A. T.; Vreuls, R. J. J. *J Chromatogr A* **2002**, *959*, 191-201.

(280) McKinney, D. E.; Carson, D. M.; Clifford, D. J.; Minard, R. D.; Hatcher, P. G. *J Anal Appl Pyrolysis* **1995**, *34*, 41-46.

(281) Bailey, J. J. *Anal Chem* **1967**, *39*, 1485-1489.

(282) Lloyd, J. B. F.; Roberts, B. R. G. *J Chromatogr* **1973**, *77*, 228-232.

(283) Venema, A.; Geest, R. C. A. B. *J Microcolumn Sep* **1995**, *7*, 337-343.

(284) Downing, D. T. *Anal Chem* **1967**, *39*, 218-221.

(285) Challinor, J. M. *J Anal Appl Pyrolysis* **2001**, *61*, 3-34.

(286) de Leeuw, J. W.; Baas, M. *J Anal Appl Pyrolysis* **1993**, *26*, 175-184.

(287) Holzer, G.; Bourne, T. F.; Bertsch, W. *J Chromatogr* **1989**, *468*, 181-190.

(288) Dworzanski, J. P.; Berwald, L.; Meuzelaar, H. L. C. *Appl Environ Microbiol* **1990**, *56*, 1717-1724.

(289) Dworzanski, J. P.; Berwald, L.; McClennen, W. H.; Meuzelaar, H. L. C. *J Anal Appl Pyrolysis* **1991**, *21*, 221-232.

(290) Kralert, P. G.; Alexander, R.; Kagi, R. I. *Org Geochem* **1995**, *23*, 627-639.

(291) West, J. C. *Anal Chem* **1975**, *47*, 1708-1709.

(292) Woo, K. L.; Kim, J. I. *J Chromatogr A* **1999**, *862*, 199-208.

(293) Metcalfe, L. D.; Wang, C. N. *J Chromatogr Sci* **1981**, *19*, 530-535.

(294) Ito, Y.; Ogasawara, H.; Ishida, Y.; Ohtani, H.; Tsuge, S. *Polym J* **1996**, *28*, 1090-1095.

(295) Tanczos, I.; Pokol, G.; Borsa, J.; Toth, T.; Schmidt, H. *J Anal Appl Pyrolysis* **2003**, *68-9*, 173-185.

(296) Challinor, J. M. *J Anal Appl Pyrolysis* **1994**, *29*, 223-224.

(297) Kaal, E.; Janssen, H.-G. *Journal of Chromatography, A* **2008**, *1184*, 43-60.

(298) Pitthard, V.; Finch, P.; Bayerova, T. *J Sep Sci* **2004**, *27*, 200-208.

(299) Hendricker, A. D.; Abbas-Hawks, C.; Basile, F.; Voorhees, K. J.; Hadfield, T. L. *Int J Mass spectrom* **1999**, *191*, 331-342.

(300) Beverly, M. B.; Voorhees, K. J.; Hadfield, T. L. *Rapid Commun Mass Spectrom* **1999**, *13*, 2320-2326.

(301) Snyder, A. P.; Maswadeh, W. M.; Wick, C. H.; Dworzanski, J. P.; Tripathi, A. *Thermochim Acta* **2005**, *437*, 87-99.

(302) Snyder, A. P.; Tripathi, A.; Dworzanski, J. P.; Maswadeh, W. M.; Wick, C. H. *Anal Chim Acta* **2005**, *536*, 283-293.

(303) Perry, J. J.; Foster, J. W. *J Bacteriol* **1955**, *69*, 337-346.

(304) Lee, W. H.; Ordal, Z. J. *J Bacteriol* **1963**, *85*, 207-217.

(305) Kuske, C. R.; Banton, K. L.; Adorada, D. L.; Stark, P. C.; Hill, K. K.; Jackson, P. J. *Appl Environ Microbiol* **1998**, *64*, 2463-2472.

(306) Belgrader, P.; Okuzumi, M.; Pourahmadi, F.; Borkholder, D. A.; Northrup, M. A. *Biosensors & Bioelectronics* **2000**, *14*, 849-852.

(307) Tang, T.; Rajan, K. S.; Grecz, N. *Biophys J* **1968**, *8*, 1458-1474.

(308) Perrin, D. D. *Stability Constants of Metal-Ion Complexes, Part B: Organic Ligands*, 1st ed.; Pergamon: Oxford, **1979**.

(309) Funahashi, S.; Haraguchi, K.; Tanaka, M. *Inorg Chem* **1977**, *16*, 1349-1353.

(310) Kanicky, J. R.; Shah, D. O. *J Colloid Interface Sci* **2002**, *256*, 201-207.

(311) Hendricker, A. D.; Voorhees, K. J. *J Anal Appl Pyrolysis* **1998**, *48*, 17-33.

(312) Voorhees, K. J.; Basile, F.; Beverly, M. B.; Abbas-Hawks, C.; Hendricker, A.; Cody, R. B.; Hadfield, T. L. *J Anal Appl Pyrolysis* **1997**, *40-1*, 111-134.

(313) Abbas-Hawks, C.; Voorhees, K. J.; Hadfield, T. L. *Rapid Commun Mass Spectrom* **1996**, *10*, 1802-1806.

(314) Snyder, A. P.; Dworzanski, J. P.; Tripathi, A.; Maswadeh, W. M.; Wick, C. H. *Anal Chem* **2004**, *76*, 6492-6499.

(315) Anderson, K. B.; Winans, R. E. *Anal Chem* **1991**, *63*, 2901-2908.

(316) Goodacre, R.; Shann, B.; Gilbert, R. J.; Timmins, E. M.; McGovern, A. C.; Alsberg, B. K.; Kell, D. B.; Logan, N. A. *Anal Chem* **2000**, *72*, 119-127.

(317) Snyder, A. P.; Thornton, S. N.; Dworzanski, J. P.; Meuzelaar, H. L. C. *Field Anal Chem Technol* **1996**, *1*, 49-59.

(318) Morgan, S. L.; Fox, A.; Rogers, J. C.; Watt, B. E. In *Modern Techniques for Rapid Microbiological Analysis*; Nelson, W. H., Ed.; VCH: New York, **1991**.

(319) Basile, F.; Beverly, M. B.; Voorhees, K. J.; Hadfield, T. L. *Trends Anal Chem* **1998**, *17*, 95-109.

(320) Hermosin, B.; Saiz-Jimenez, C. *J Anal Appl Pyrolysis* **1999**, *49*, 417-424.

(321) Asperger, A.; Engewald, W.; Fabian, G. *J Anal Appl Pyrolysis* **1999**, *52*, 51-63.

(322) Lewis, J. C. *Anal Biochem* **1967**, *19*, 327-337.

(323) Ishida, Y.; Ohtani, H.; Tsuge, S. *J Anal Appl Pyrolysis* **1995**, *33*, 167-180.

(324) van den Berg, J. D. J.; Boon, J. J. *J Anal Appl Pyrolysis* **2001**, *61*, 45-63.

(325) Marshall, B. J.; Murrell, W. G.; Scott, W. J. *J Gen Microbiol* **1963**, *31*, 451-460.

(326) Oguri, N.; Onishi, A.; Uchino, S.; Nakahashi, K.; Yamasaki, N.; Jin, X. G. *J High Resolut Chromatogr* **1993**, *16*, 597-600.

(327) Tabor, M. W.; MacGee, J.; Holland, J. W. *Appl Environ Microbiol* **1976**, *31*, 25-28.

(328) Pan, L.; Pawliszyn, J. *Anal Chem* **1997**, *69*, 196-205.

(329) Hardell, H. L.; Nilvebrant, N. O. *J Anal Appl Pyrolysis* **1999**, *52*, 1-14.

(330) Amijee, M.; Cheung, J.; Wells, R. J. *J Chromatogr A* **1996**, *738*, 43-55.

(331) Downing, D. T.; Greene, R. S. *Anal Chem* **1968**, *40*, 827-828.

(332) MacGee, J.; Allen, K. G. *J Chromatogr* **1974**, *100*, 35-42.

(333) Gerhardt, K. O.; Gehrke, C. W. *J Chromatogr* **1977**, *143*, 335-344.

(334) Williams, M. *J Chromatogr* **1982**, *234*, 468-471.

(335) Butte, W.; Eilers, J.; Kirsch, M. *Anal Lett* **1982**, *15*, 841-850.

(336) Ralls, J. W. *Anal Chem* **1960**, *32*, 332-336.

(337) Titherley, A. W. *J Chem Soc, Trans* **1901**, *79*, 391-411.

(338) Simon, L. J. *Comptes Rendus* **1923**, *176*, 583-586; 900-902.

(339) Sizov, S. Y.; Utrobin, N. P.; Semenova, L. V.; Darmanyan, A. P.; Tyabin, N. V. *Prikladnaya Biokhimiya i Mikrobiologiya* **1980**, *16*, 618-620.

(340) Rusev, I.; Chochkova, D. *Khimiya Ind* **1986**, *58*, 445-447.

(341) Boesten, W. H. J.; Quaedflieg, P. J. L. M. (DSM NV, Heerlen, NL). US Patent 6222013, **2001**.

(342) Wolski, A.; Magielka, S. (Polfa). PL Patent 159729, **1993**.

(343) Callahan, B. P.; Wolfenden, R. *J Am Chem Soc* **2003**, *125*, 310-311.

(344) Forrester, J.; Jones, R. V. H.; Preston, P. N.; Simpson, E. S. C. *J Chem Soc, Perkin Trans 1: Org Bio-Org Chem* **1999**, 3333-3335.

(345) Anonymous; U.S. Department of Health and Human Services, **2005**.

(346) Tan, E. L.; Brimer, P. A.; Schenley, R. L.; Hsie, A. W. *J Toxicol Environ Health* **1983**, *11*, 373-380.

(347) Fisher Scientific, **2009**. *Potassium Methyl Sulfate Msds*. http://fscimage.fishersci.com/msds/95639.htm.

(348) Hansen, L. D.; White, V. F.; Eatough, D. J. *Environ Sci Technol* **1986**, *20*, 872-878.

(349) Claesson, P. *J Prakt Chem* **1879**, *19*, 231-265.

(350) Kuh, E. GB Patent 149688, **1921**.

(351) Roberts, E. ((Minister of Supply).). GB Patent 774384, **1957**.

(352) Tian, A. *Bull Soc Chim Fr* **1950**, 1223-1232.

(353) Tian, A. *Bull Soc Chim Fr* **1951**, *18*, 531-534.

(354) Suter, C. M.; Oberg, E. *J Am Chem Soc* **1934**, *56*, 677-679.

(355) Almstead, N.; Christ, W.; Miller, G.; Reilly-Packard, S.; Vargas, K.; Zuman, P. *Tetrahedron Lett* **1987**, *28*, 1627-1628.

(356) Wittmann, Z.; Marko-Monostory, B. *Chim Acad Sci Hung* **1979**, *99*, 375-380.

(357) Kane, S. M.; Leu, M.-T. *J Phys Chem A* **2001**, *105*, 1411-1415.

(358) Kazansky, V. B. *React Kinet Catal Lett* **1999**, *68*, 35-43.

(359) Van Loon, L. L.; Allen, H. C. *J Phys Chem B* **2004**, *108*, 17666-17674.

(360) Eatough, D. J.; Lee, M. L.; Later, D. W.; Richter, B. E.; Eatough, N. L.; Hansen, L. D. *Environ Sci Technol* **1981**, *15*, 1502-1506.

(361) Kaal, E.; de Koning, S.; Brudin, S.; Janssen, H.-G. *Journal of Chromatography, A* **2008**, *1201*, 169-175.

(362) Mowry, C.; Morgan, C. H.; Baca, Q.; Manginell, R. P.; Kottenstette, R. J.; Lewis, P.; Frye-Mason, G. C. *Proc SPIE-Int Soc Opt Eng* **2002**, *4575*, 83-90.

(363) Akoto, L.; Pel, R.; Irth, H.; Brinkman, U. A. T.; Vreuls, R. J. J. *J Anal Appl Pyrolysis* **2005**, *73*, 69-75.

(364) Mlejnek, O.; Cvečková *J Chromatogr* **1974**, *94*, 135-142.

(365) Poerschmann, J.; Parsi, Z.; Gorecki, T.; Augustin, J. *J Chromatogr A* **2005**, *1071*, 99-109.

(366) Joll, C. A.; Huynh, T.; Heitz, A. *J Anal Appl Pyrolysis* **2003**, *70*, 151-167.

(367) Ding, W. H.; Chen, C. T. *Journal of Chromatography, A* **1999**, *857*, 359-364.

(368) Ding, W. H.; Liu, C. H.; Yeh, S. P. *Journal of Chromatography, A* **2000**, *896*, 111-116.

(369) Havey, C. D.; Basile, F.; Mowry, C.; Voorhees, K. J. *J Anal Appl Pyrolysis* **2004**, *72*, 55-61.

(370) Beverly, M. B.; Basile, F.; Voorhees, K. J.; Hadfield, T. L. *Rapid Commun Mass Spectrom* **1996**, *10*, 455-458.

(371) Griest, W. H.; Wise, M. B.; Hart, K. J.; Lammert, S. A.; Thompson, C. V.; Vass, A. A. *Field Anal Chem Technol* **2001**, *5*, 177-184.

(372) Luo, S.; Mohr, J.; Sickenberger, D.; Hryncewich, A. *Field Anal Chem Technol* **1999**, *3*, 357-374.

(373) Ishida, Y.; Katagiri, M.; Ohtani, H. *J Chromatogr A* **2009**, *1216*, 3296-3299.

(374) Hüschens, R.; Funke, S.; Stuehmer, W. (Kali-Chemie A.G.). DE Patent 2,222,597, **1973**.

(375) Timofeeva, M. N.; Maksimovskaya, R. I.; Paukshtis, E. A.; Kozhevnikov, I. V. *J Mol Catal A: Chem* **1995**, *102*, 73-77.

(376) Bailey, G. F.; Karp, S.; Sacks, L. E. *J Bacteriol* **1965**, *89*, 984-987.

(377) Deno, N. C.; Newman, M. S. *J Am Chem Soc* **1950**, *72*, 3852 - 3856.

(378) Torn, R. D.; Nathanson, G. M. *J Phys Chem B* **2002**, *106*, 8064-8069.

(379) Zhao, J.; Krishna, V.; Moudgil, B.; Koopman, B. *Sep Purif Technol* **2008**, *61*, 341-347.

(380) Westcott, C. C. *pH Measurements*; Academic Press: New York, **1978**.

(381) Hall, W. G.; Power, D. C. (Johnson Mathey Public Limited Company). US Patent 5853904, **1998**.

(382) El-Bisi, H. M.; Lechowich, R. V.; Amaha, M.; Ordal, Z. J. *J Food Sci* **1962**, *27*, 219-231.

(383) Janssen, F. W.; Lund, A. J.; Anderson, L. E. *Science* **1958**, *127*, 26-27.

(384) Montgomery, D. C.; Runger, G. C.; Hubele, N. F. *Engineering Statistics*, 2nd ed.; John Wiley: New York, **2001**.

(385) Berkovitz, L. D. *Convexity and Optimization in R^n* J. Wiley: New York, **2002**.

(386) Levitin, G.; Myneni, S.; Hess, D. W. *Electrochem Solid-State Lett* **2003**, *6*, G101-G104.

(387) Harlow, G. A.; Noble, C. M.; Wyld, G. E. A. *Anal Chem* **1956**, *28*, 787-791.

(388) Cundiff, R. H.; Markunas, P. C. *Anal Chem* **1962**, *34*, 584-585.

(389) Berthelot *Bull Soc Chim Fr* **1873**, *2*, 295-300.

(390) Burwell, R. L., Jr. *J Am Chem Soc* **1952**, *74*, 1462-1466.

(391) Wells, A. F. *Structural Inorganic Chemistry*, 5th ed.; Oxford University Press: Oxford, **1984**.

(392) Musker, W. K.; Stevens, R. R. *J Am Chem Soc* **1968**, *90*, 3515-3521.

(393) Ablett, S.; Darke, A. H.; Lillford, P. J.; Martin, D. R. *Int J Food Sci Technol* **1999**, *34*, 59-69.

(394) Strahs, G.; Dickerson, R. E. *Acta Crystallogr* **1968**, *B24*, 571-578.

(395) Bruce, M. L.; Lee, R. P.; Stephens, M. W. *Environ Sci Technol* **1992**, *26*, 160-163.

(396) Sandler, S. I. *Chemical and Engineering Thermodynamics*, 3rd ed.; Wiley: New York, **1999**.

(397) Dennis, J. E., Jr.; Gay, D., M.; Welsch, R., E. *ACM Trans Math Softw* **1981**, *7*, 369-383.

(398) Dennis, J. E., Jr.; Gay, D., M.; Welsch, R., E. *ACM Trans Math Softw* **1981**, *7*, 348-368.

(399) Banerjee, D. K.; Fuller, M. J.; Chen, H. Y. *Anal Chem* **1964**, *36*, 2016-2020.

(400) Banick, W. M., Jr.; Francis, E. C. *Talanta* **1966**, *13*, 979-983.

(401) Kanning, E. W.; Bobalek, E. G.; Byrne, J. B. *J Am Chem Soc* **1943**, *65*, 1111-1116.

(402) Comer, J. E. A. In *Comprehensive Medicinal Chemistry II, Vol. 5*; Triggle, D. J., Taylor, J. B., Eds.; Elsevier Science: Boston, MA, **2007**, pp 357-397.

(403) Wright, M. R. *J Chem Soc [Sect] B: Phys Org* **1967**, 1265-1267.

(404) Wright, M. R. *J Chem Soc [Sect] B: Phys Org* **1969**, 707-710.

(405) Bender, M. L. *Adv Chem Ser* **1963**, *37*, 19-36.

(406) Ingold, C. K. *J Chem Soc* **1931**, 2170-2179.

(407) Pitzer, K. S., Ed. *Activity Coefficients in Electrolyte Solutions*, 2 ed.; CRC Press: Boca Raton, **1991**.

(408) Hitchcock, S. J.; Carroll, N. T.; Nicholas, M. G. *Journal of Materials Science* **1981**, *16*, 714-732.

(409) Kumar, G.; Prabhu, K. N. *Adv Colloid Interface Sci* **2007**, *133*, 61-89.

(410) Zhang, X.; Yu, S.; He, Z.; Miao, Y. *Surf Rev Lett* **2004**, *11*, 7-13.

(411) Ciucanu, I. *Rev Chim Bucharest* **2006**, *57*, 923-926.

(412) Silvis, P. H.; Walsh, J. W.; Shelow, D. M. (Restek Corporation). US Patent 5119669, **1992**.

(413) Grob, K.; Wagner, C. *J High Resolut Chromatogr* **1993**, *16*, 429-432.

(414) Incropera, F. P.; DeWitt, D. P. *Fundamentals of Heat and Mass Transfer*, 4th ed.; Wiley: New York, **1996**.

(415) Martínez-Castro, I.; Alonso, L.; Juárez, M. *Chromatographia* **1986**, *21*, 37-40.

(416) Cotton, F. A.; Wilkinson, G. *Advanced Inorganic Chemistry : A Comprehensive Text*, 4th ed.; Wiley: New York, **1980**.

(417) Wendlandt, W. W.; Sturm, E. *J Inorg Nucl Chem* **1963**, *25*, 535-544.

(418) Sutra, G. *J Chim Phys Phys-Chim Biol* **1946**, *43*, 279-289.

(419) Gill, D. S. *Electrochim Acta* **1979**, *24*, 701-703.

(420) Kimball, J. A.; Truong, T. V.; Nackos, A. N.; Bartholomew, C. H.; Lee, M. L.; Tolley, H. D.; Robison, R. A. In *59th Pittsburgh Conference on Analytical Chemistry and Applied Spectroscopy*: New Orleans, LA, **2008**.

(421) Belgrader, P.; Hansford, D.; Kovaks, G.; Venkateswaran, K.; Mariella, R.; Milanovice, F.; Nasarabadi, S.; Okuzumi, M.; Pourahmadi, F.; Northrup, M. *Anal Chem* **1999**, *71*, 4232-4236.

(422) Lee, M. L.; Later, D. W.; Rollins, D. K.; Eatough, D. J.; Hansen, L. D. *Science (Washington, DC, United States)* **1980**, *207*, 186-188.

(423) Grob, K., Jr.; Neukom, H. P. *J Chromatogr* **1980**, *198*, 64-69.

(424) Rasmussen, K. E.; Karlsen, J. *J Chromatogr* **1974**, *90*, 285-289.

(425) del Río, J. C.; McKinney, D. E.; Knicker, H.; Nanny, M. A.; Minard, R. D.; Hatcher, P. G. *J Chromatogr A* **1998**, *823*, 433-448.

(426) Grob, K.; Biedermann, M. *Anal Chem* **2002**, *74*, 10-16.

(427) Grob, K. *J High Resolut Chromatogr Chromatogr Comm* **1980**, *3*, 585-586.

(428) Halvorson, H.; Howitt, C. In *Spores II*; Halvorson, H. O., Ed.; Burgess Publishing Company: Minneapolis, **1961**, pp 149-179.

(429) Nudelman, R.; Bronk, B. V.; Efrima, S. *Appl Spectrosc* **2000**, *54*, 445-449.

(430) Xie, J. R. H.; Smith, V. H.; Allen, R. E. *Chem Phys* **2006**, *322*, 254-268.

(431) Warth, A. D.; Ohye, D. F.; Murrell, W. G. *J Cell Biol* **1963**, *16*, 579-592.

(432) Mallidis, C. G.; Scholefield, J. *J Appl Bacteriol* **1987**, *63*, 207-215.

(433) Willför, S.; Pranovich, A.; Tamminen, T.; Puls, J.; Laine, C.; Suurnäkki, A.; Saake, B.; Uotila, K.; Simolin, H.; Hemming, J.; Holmbom, B. *Ind Crop Prod* **2009**, *29*, 571-580.

(434) Pollard, H. B.; Creutz, C. E.; Pazoles, C. J.; Hansen, J. *Anal Biochem* **1977**, *83*, 311-314.

(435) Christoffersen, G. R. J.; Skibsted, L. H. *Comp Biochem Physiol A: Physiol* **1975**, *52*, 317-322.

(436) Nakayama, F. S.; Rasnick, B. A. *Anal Chem* **1967**, *39*, 1022-1023.

(437) Kumar, A.; Sanghavi, R.; Mohandas, V. P. *J Chem Eng Data* **2007**, *52*, 902-905.

(438) Tang, T. Dissertation, Illinois Institute of Technology, Chicago, IL, **1969**.

(439) Grecz, N.; Tang, T.; Rajan, K. S. In *Spores V*; Halvorson, H. O., Hanson, R., Campbell, L. L., Eds.; American Society for Microbiology: Washington, D.C., **1972**, pp 53-60.

(440) Arzik, S.; Yildiran, H. *J Fac Sci, Ege Univ, Ser A-B* **1996**, *19*, 74-80.

(441) Harmon, K. M. *J Mol Struct* **2009**, *919*, 117-121.

(442) Meot-Ner, M.; Deakyne, C. A. *J Am Chem Soc* **1985**, *107*, 469-474.

(443) Rosenfield, R. E., Jr.; Murray-Rust, P. *J Am Chem Soc* **1982**, *104*, 5427-5430.

(444) Kremann, R. *Monatsh Chem* **1907**, *28*, 13-32.

(445) van Der Kaaden, A.; Haverkamp, J.; Boon, J. J.; De Leeuw, J. W. *J Anal Appl Pyrolysis* **1983**, *5*, 199-220.

(446) Duda, V. I.; Danilevich, V. N.; Suzina, N. E.; Shorokhova, A. P.; Dmitriev, V. V.; Mokhova, O. N.; Akimov, V. N. *Microbiology* **2004**, *73*, 341-349.

(447) Zhang, Y.; Cremer, P. S. *Curr Opin Chem Biol* **2006**, *10*, 658-663.

(448) Bonvouloir, E. M.; Kazakov, S. V., New Brunswick, NJ, May 22-25, 2005 **2005**.

(449) Kazakov, S.; Bonvouloir, E.; Gazaryan, I. *J Phys Chem B* **2008**, *112*, 2233-2244.

(450) Beveridge, T. J.; Williams, F. M. R.; Koval, J. J. *Can J Microbiol* **1978**, *24*, 1439-1451.

(451) Beveridge, T. J.; Murray, R. G. E. *Curr Microbiol* **1979**, *2*, 1-4.

(452) Beveridge, T. J. *Environ Biogeochem Geomicrobiol, Proc Int Symp, 3rd* **1978**, *3*, 975-987.

(453) Beveridge, T. J.; Fyfe, W. S. *Can J Earth Sci* **1985**, *22*, 1893-1898.

(454) Beveridge, T. J.; Murray, R. G. E. *J Bacteriol* **1976**, *127*, 1502-1518.

(455) Beveridge, T. J. In *The Target of Penicillin: The Murein Sacculus of Bacterial Cell Walls: Architecture and Growth*; Hakenbeck, R., Höltje, J.-V., Labischinski, H., Eds.; Walter de Gruyter: Berlin, **1983**, pp 35-41.

(456) Marquis, R. E. *J Bacteriol* **1968**, *95*, 775-781.

(457) Ou, L.-T.; Marquis, R. E. *J Bacteriol* **1970**, *101*, 92-101.

(458) Ou, L.-T.; Marquis, R. E. *Can J Microbiol* **1972**, *18*, 623-629.

(459) Doyle, R. J. In *Metal Ions and Bacteria*; Beveridge, T. J., Doyle, R. J., Eds.; Wiley: New York, **1989**, pp 275-293.

(460) Thwaites, J. J.; Surana, U. C. *J Bacteriol* **1991**, *173*, 197-203.

(461) Thwaites, J. J.; Surana, U. C.; Jones, A. M. *J Bacteriol* **1991**, *173*, 204-210.

(462) Green, G. H.; Kenyon, J. *J Chem Soc* **1950**, 1389-1391.

(463) Calhoun, G. M.; Burwell, R. L., Jr. *J Am Chem Soc* **1955**, *77*, 6441-6447.

(464) Gilbert, A. R.; Kantor, S. W. *J Polym Sci* **1959**, *40*, 35-58.

(465) Kantiranis, N. *Constr Build Mater* **2003**, *17*, 91-96.

(466) Critchfield, B. L., Brigham Young University, Provo, **2006**.

(467) Hadi, A. S. *Matrix Algebra as a Tool*; Duxbury Press: Belmont, Calif., **1996**.

(468) Callan, D. *Coll Math J* **1998**, *29*, 145-147.

(469) Barvinok, A. *A Course in Convexity*; American Mathematical Society: Providence, RI, **2002**.

(470) Klee, V. *Mathematika* **1964**, *11*, 59-63.

(471) Prenowitz, W.; Jantosciak, J. *Join Geometries : A Theory of Convex Sets and Linear Geometry*; Springer-Verlag: New York, **1979**.

(472) Robinow, C. F. *Addendum. 2. Structure of Resting Bacterial Spores*; Harvard University Press: Cambridge, **1949**.

(473) Robinow, C. F. In *The Bacteria: A Treatise on Structure and Formation (Vol. 1)*; Gunsalus, I. C., Stanier, R. Y., Eds.; Academic Press: New York, **1960**, pp 207-248.

(474) Robinow, C. F. *J Bacteriol* **1953**, *66*, 300-311.

(475) Robinow, C. F. *J Bacteriol* **1953**, *65*, 378-382.

(476) Young, E.; Fitz-James, P. C. *J Cell Biol* **1962**, *12*, 115-133.

(477) Robinow, C. F. *J Gen Microbiol* **1951**, *5*, 439-457.

(478) Fitz-James, P. C.; Young, I. E. *J Bacteriol* **1959**, *78*, 755-764.

(479) Bisset, K. A.; Hale, C. M. F. *J Hyg* **1951**, *49*, 201-204.

(480) Handley, P. S. In *Spore Research 1976*; Barker, A. N., Wolf, J., Ellar, D. J., Dring, G. J., Gould, G. W., Eds.; Academic Press: London, **1977**; Vol. 2, pp 735-751.

(481) Tipper, D. J.; Johnson, W. C.; Chambliss, G. H.; Mahler, I.; Arnaud, M.; Halvorson, H. O. In *Sporulation and Germination (Spores VIII)*; Levinson, H. S., Sonenshein, A. L., Tipper, D. J., Eds.; American Society for Microbiology: Washington, D.C., **1981**, pp 178-183.

(482) Warth, A. D. *Appl Environ Microbiol* **1979**, *38*, 1029-1033.

(483) Mayall, B. H.; Robinow, C. F. *J Appl Bacteriol* **1957**, *20*, 333-341.

(484) Young, I. E., University of Western Ontario, London (Ontario, Canada), **1958**.

(485) Lechtman, M. D.; Bartholomew, J. W.; Phillips, A.; Russo, M. *J Bacteriol* **1965**, *89*, 848-854.

(486) Setlow, P. *J Bacteriol* **1978**, *136*, 331-340.

(487)   Hathout, Y.; Setlow, B.; Cabrera-Martinez, R.; Fenselau, C.; Setlow, P. *Appl Environ Microbiol* **2003**, *69*, 1100-1107.

(488)   Fonrodona, G.; Rafols, C.; Bosch, E.; Roses, M. *Anal Chim Acta* **1996**, *335*, 291-302.

(489)   Burstein, S.; Lieberman, S. *J Am Chem Soc* **1958**, *80*, 5235-5239.

(490)   Atkins, P. W. *Physical Chemistry*, 6th ed.; Freeman: New York, **1998**.

(491)   Rosés, M.; Bosch, E. *Journal of Chromatography, A* **2002**, *982*, 1-30.

(492)   Bates, R. G. *Determination of pH: Theory and Practice*, 2 ed.; Wiley: New York, **1973**.

(493)   Popovych, O.; Tomkins, R. P. T. *Nonaqueous Solution Chemistry*; John Wiley & Sons: New York, **1981**.

(494)   Buckenmaier, S. M. C.; McCalley, D. V.; Euerby, M. R. *Journal of Chromatography, A* **2004**, *1026*, 251-259.

(495)   Rosés, M.; Subirats, X.; Bosch, E. *Journal of Chromatography, A* **2009**, *1216*, 1756-1775.

(496)   Subirats, X.; Rosés, M.; Bosch, E. *Separation and Purification Reviews* **2007**, *36*, 231-255.

(497)   Shibata, F. L. E.; Oda, S. *Nippon Kagaku Kaishi (1921-47)* **1931**, *52*, 590-600.

(498)   Modro, T. A.; Yates, K.; Janata, J. *J Am Chem Soc* **1975**, *97*, 1492-1499.

(499)   Campbell, M. L.; Waite, B. A. *J Chem Educ* **1990**, *67*, 386-388.

(500)   Hussain, F.; Haque, S. S. *Pak J Sci Ind Res* **1963**, *6*, 251-255.

(501)   Kanning, E. W.; Byrne, J. B.; Bobalek, E. G. *J Am Chem Soc* **1944**, *66*, 1700-1703.

(502)   Guthrie, R. D.; Govindan, M. *J Am Chem Soc* **1979**, *101*, 5769-5773.

(503)   Lubes, V. *J Solut Chem* **2005**, *34*, 899-915.

(504)   Costa, F. L.; Lugo, M. L.; Lubes, V. R. *J Solut Chem* **2007**, *36*, 1287-1299.

(505)   Janjic, T. J.; Pfendt, L. B.; Pasulj, M. B. *Monatsh Chem* **1984**, *115*, 125-133.

(506)   Lide, D. R., Ed. *Crc Handbook of Chemistry and Physics, 89th Edition (Internet Version 2009)*; CRC Press/Taylor and Francis: Boca Raton, FL, **2009**.

(507)   Vandenbelt, J. M.; Henrich, C.; Vanden Berg, S. G. *Anal Chem* **1954**, *26*, 726-727.

(508)   Ludwig, M.; Baron, V.; Kalfus, K.; Pytela, O.; Vecera, M. *Collect Czech Chem Commun* **1986**, *51*, 2135-2142.

(509)   Thamer, B. J.; Voigt, A. F. *J Phys Chem* **1952**, *56*, 225-232.

(510)   Maxwell, W. R.; Partington, J. R. *Trans Faraday Soc* **1935**, *31*, 922-935.

(511)   Venimadhavan, S.; Shelly, K. P.; Stewart, R. *The Journal of Organic Chemistry* **1989**, *54*, 2483-2485.

(512)   Perrin, D. D. *Dissociation Constants of Organic Bases in Aqueous Solution*; Butterworths: London, **1965**.

(513)   Lugo, M. L.; Lubes, V. R. *J Chem Eng Data* **2007**, *52*, 1217-1222.

(514)   Rosés, M.; Canals, I.; Allemann, H.; Siigur, K.; Bosch, E. *Anal Chem* **1996**, *68*, 4094-4100.

(515)   Bosch, E.; Bou, P.; Allemann, H.; Rosés, M. *Anal Chem* **1996**, *68*, 3651-3657.

(516)   Macey, M. G. *Flow Cytometry : Principles and Applications*; Humana Press: Totowa, N.J., **2007**.

(517)   Church, B. D.; Halvorson, H. *Nature (London, United Kingdom)* **1959**, *183*, 124-125.

(518)   Schumacher, W. C.; Storozuk, C. A.; Dutta, P. K.; Phipps, A. J. *Appl Environ Microbiol* **2008**, *74*, 5220-5223.

Appendix A   MIXTURE EXPERIMENTS DERIVATIONS

A.1 Introduction to the "solution mixture problem"

The work reported in this dissertation entails studying Me$_2$DPA yield (the response), which depends on the composition of dissolved salts in an "aggregate solution" containing a source of non-methylated DPA (usually bacterial endospores). Essentially, the aggregate solution is prepared by (1) making m different "stock solutions," each with known salt concentration, $c_{0,i}$, and (2) transferring a specific volume, $v_{0,i}$, from each stock solution into a separate container to produce an "aggregate solution" (see Figure A-1). (Note the 0 subscript indicates initial or original stock solution, and the subscript i is an integer ranging from 1 to m.) Small aliquots are taken from the aggregate solution by dipping the CWF in it, the solvent is dried from the CWF, and GC injection follows. The thermochemolysis and methylation reactivity of the residual material on the CWF is evaluated via the Me$_2$DPA chromatographic peak area [and/or some other response variable(s)] plus assurance of satisfactory GC inlet and column performance/longevity.

The above situation is an example of an optimization problem whose organization can be approached in many ways with varying degrees of complexity and systematicity. For example, volumes of reagents from stock solutions may be combined with a sample, the GC analysis performed, and the reagents adjusted by the operator to ensure the chromatogram is satisfactory (e.g., the Me$_2$DPA yield is sufficiently high based on prior

experience). Alternatively, the reagent volumes may be carefully varied according to a pre-determined plan or design, and a statistically-significant correlation between the organization behind the experimental design and some response variable identified and explored.
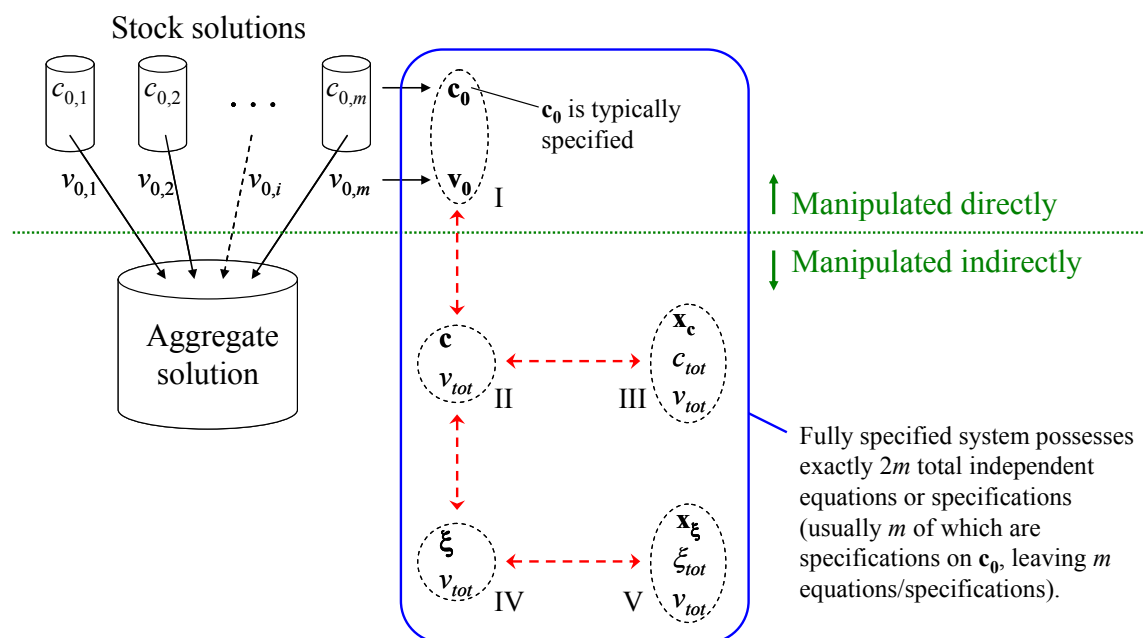
Figure A-1. Visual summary of process for preparing a mixture of dissolved salts plus illustration several means to quantitatively specify the mixture system. See text for details.

Regardless of the means employed to find an optimal reagent mixture, fundamental to any approach is that there are exactly zero degrees of freedom (*df*) in the chemical system prepared for each test. In other words, once the aggregate solution has been prepared, the total number of independently controlled quantities (e.g., volumes and concentrations of the stock solutions employed in sample preparation) always equals the total number of independent specifications made on the system, whatever the form those specifications may take. Figure A-1 summarizes this visually.

Preparation of thermochemolysis reagent mixtures from m different stock solutions involves $2m$ degrees of freedom since m different stock solution concentrations are prepared and m different volumes are transferred to the aggregate solution ($m + m = 2m$).[58] However, since the m stock solutions are usually prepared in advance in bulk and at specific concentrations that remain constant, typically only m decisions or specifications are made. Accordingly, the resultant optimization problem is m-dimensional, so m independent equality constraints must be assigned to the system. Such are the problems and experiments in this dissertation.

In most instances, there will be some specifications that the operator wishes to impose on the system, such as specific total sample solution volume, volume of an internal standard added to the sample solution, concentrations of one or more reagents, specific pH, etc. Say s total specifications are made, where $s < m$. Then there are $m - s$ residual degrees of freedom that provide flexibility and thus the opportunity for optimization. This gap in complete specification of the system is a common feature in the practical implementation of all conceivable forms of experimental designs, be they based on factors or mixtures.

The purpose of this appendix chapter is to introduce relationships and methods by which the degrees of freedom involved in blending salt-containing solutions may be dispersed into mixture variables rather than volumetric solution amounts or absolute concentrations of undissociated salts from those solutions. Initially, some chemistry background is given along with assumptions upon which the experimental designs rely.

---

[58] Temperature (T) and pressure (P) are two additional degrees of freedom that are neglected here since the mixing process occurs at ambient conditions where T and P have no influence on reagent mixture composition.

A.2 Definition of fundamental constituents

The IMDOE (ionic mixture design of experiments) focuses on what are considered *fundamental constituents* (FCs) of the system. For the present purposes, FCs are defined as entities that retain their chemical identity both as dissolved species in solution and, following solution removal, as constituents of a solid matrix at room temperature and pressure. The reactive behavior of this mixture of FCs at the elevated temperature and pressure of the GC injection port becomes the key response against which a model is compared.

With respect to GC thermochemolysis methylation reagent mixtures, FCs are typically charged molecular and atomic cations and anions ("ions") that comprise salts, which can separate from one another in solution. In salts, ions are found in numerical combinations such that the net electrical charge is zero. The neutrality feature results from the physics and chemistry of matter: under "normal" conditions (e.g., non-plasma, absence of high-strength electric fields) no ionic species will exist without one or more nearby counter-ions to balance its charge. In fact, an ion is charged in the first place because it gains one or more electron that another has lost (or vice-versa). Thus, ions always come in combinations of two or more, and there is always at least one species of opposite charge present.

Placed in a liquid-phase environment, salts not only may dissolve, their solid-phase components disappearing into the solution (described mathematically by a specific *solubility product*), but the dissolved portions have the potential to dissociate to some degree into their charged constituents due to special stabilizing interactions between the ions and the dispersing/solvating medium (indicated mathematically by *dissociation* or

238

stability constants). The term *fundamental constituents* (again, FCs) refers to the most elementary form of an ion that will not dissociate any further in a solution. Monatomic ions (e.g., H^+, Na^+, Cl^-) fall into this category, as do polyatomic (molecular) ions that act as discrete charged units in forming acid, base, and salt complexes, at least at room temperature (e.g., TMA^+, SO_4^{2-}, OH^-, $MeSO_4^-$). Any species found in an ionic compound with a potential to dissociate in solution (including Brønsted-Lowry acids or bases, which are proton donors and acceptors), regardless of the extent of its dissociation or even whether it is in solution or present as a solid material, is considered to be an ion.

Ions dissociated from some original salt may re-combine with themselves and/or with other ions from other salts present in the mixture to produce salts that differ compositionally—and thus possibly in their physical and chemical properties—from the original set of salts introduced. Depending on the intrinsic properties of the solution (including the solvent or solvent mixture, set of salts introduced, net concentrations, and temperature), the solubility of particular salt complexes may be very high, intermediate, or quite low, and the separations and recombinations among ions will range in their degree of completeness.

A.3 Ions and TCM

The sample derivatization protocol is summarized by the following three stages:

1. Various reagents and the sample are combined in a liquid medium (MeOH).
2. A small volume of the liquid mixture is collected by the coiled wire filament and the liquid is evaporated.
3. The "dry" TCM salts/sample mixture is heated in the GC inlet, where biomarker chemicals are released, react with the TCM reagents, and pass into the GC separation column.

A number of variables influence what occurs during each of these three general steps. During Step 1, the salt solubilities, ion-ion interactions, kinetics of dissociation and association, temperature, elapsed time, amount of water present, degree of mixing (sample homogeneity), reagent purity, sample matrix properties, and some degree of randomness determine the chemical properties of the mixture such as the composition of any precipitates formed. During the evaporation occurring at Step 2, additional heat and mass transport mechanisms operate, affecting the solvent evaporation behavior and thus the solvent composition and overall temperature. The degree of drying may vary as samples of different water/solvent affinity are tested or if the drying step is not reproduced exactly. There are many variables influencing the form of the mixture that goes into Step 3 where the important TCM reactions occur.

A careful study of each step would doubtless reveal information useful for optimization purposes, but understanding such phenomena requires an advanced approach to a problem that may be effectively addressed through simpler means. Since the reagent-analyte agglomerate deposited on the coiled wire filament that goes into the heated GC inlet and reacts to make biomarkers, the key question of interest for optimizing the thermal chemolysis/methylation reactions is, *Which combination of stock reagents performs best for derivatizing spore biomarkers when all are simply mixed together and air-dried prior to GC-MS analysis?* In other words, *What is the best reagent mixture for releasing and derivatizing spore biomarkers?* The IMDOE is therefore focused on studying the effects of this mixture on a response (Me_2DPA yield).

A.4 Describing blended solutions as mixtures

IMDOE for the TCM methodology focuses on the details entailed in blending a set of dissolved ionic compounds. Figure A-1 illustrates relationships between (I) the volumes, $\mathbf{v_0}$, and concentrations, $\mathbf{c_0}$, of m reagent "stock solutions"[59] and (II, III, IV, and V) the several means for expressing the composition of the "aggregate solution" with total volume v_{tot}. In (II), $\mathbf{c}$ represents the diluted concentrations of the original species (neglecting their dissociations and reassociations), and in (IV), ξ indicates the concentration of the (usually ionic) n fundamental components (FCs) having the potential to exist in dissociated form. In (III) and (V), mixture fractions of the undissociated salts and dissociated ions are indicated, respectively, by $\mathbf{x_c}$ and $\mathbf{x_\xi}$ (equivalent to mole fractions with the solvent ignored).

Two approaches may be taken towards formulating the important relationships shown in Figure A-1, here called "top-down" or "bottom-up." The "top-down" approach is more straightforward and will be explained initially. Since "bottom-up" calculations are necessary for experimental design, they will be covered in detail as well.

A.4.1 The "top-down" derivations

For all computations, volume changes due to mixing are assumed negligible (the solutions are assumed to be ideal), so the total volume in the mixture, v_{tot}, is equal to the

---

[59] Although contrary to the engineering convention of using uppercase for concentration and volume (i.e., C_0 and V_0), bolded lowercase letters are employed to be in line with vector notation because they represent 1-dimensional vectors that represent a *collection* of concentrations or volumes. Likewise, bolded uppercase letters designate two-dimensional matrices.

sum of the m individual reagent stock volumes, $\mathbf{v_0}$ [Eq. (A-1)]. $\mathbf{c}$, the concentration of the undissociated m molecular species in that solution, is given by Eq. (A-2), where $\mathbf{c_0}$ is a vector representing the stock solution concentrations.

$$v_{tot} = \sum_{i=1}^{m} v_{0_i} \tag{A-1}$$

$$\mathbf{c} = v_{tot}^{-1}(\mathbf{c_0} \cdot \mathbf{v_0}) \tag{A-2}$$

In Eq. (A-2), the · (dot) in $(\mathbf{c_0} \cdot \mathbf{v_0})$ indicates that this is an *element-wise* or *Hadamard product*, which yields an vector of the same size as its arguments. In contrast, an *inner* or *dot product* is the type of multiplication implied when vectors or matrices are simply written side-by-side [467]. Any dot/inner products between vectors will be indicated as $\mathbf{a}^{\mathsf{T}}\mathbf{b}$ (note: elsewhere, the dot/inner product is frequently written as $\langle \mathbf{a}, \mathbf{b} \rangle$).

A.4.1.1 Mixtures of undissociated salts

The mixture fraction of the undissociated salts, $\mathbf{x_c}$, is computed from Eq. (A-2) by summing all concentrations to obtain the total concentration, c_{tot} [Eq. (A-3)], and dividing each concentration, c_i, by c_{tot} [Eq. (A-4)].

$$c_{tot} = \sum_{i=1}^{m} c_{0_i} \tag{A-3}$$

$$\mathbf{x_c} = \left(c_{tot}^{-1}\right)\mathbf{c} \tag{A-4}$$

However, because not all individual solutions in the blend are intended to be studied as a mixture variable (some may be solvents, others may contain materials that

are inert such as internal standards or species removed from the design), only those

solutions possessing components that may become part of the mixture should be included

in $\mathbf{x}_c$. This is achieved by producing an m dimensioned vector, $\boldsymbol{\kappa}_c$, that possesses only

1's and 0's. $\boldsymbol{\kappa}_c$ is used to generate the $d \times m$ and $r \times m$ ($r = m - d$) incidence matrices, $\mathbf{D}_c$

and $\mathbf{R}_c$, respectively, according to Scheme 1 and Scheme 2.

Scheme 1. Pseudocode for computing the design matrix, $\mathbf{D}_c$, from the design vector, $\boldsymbol{\kappa}_c$ (note: c subscripts removed in code).

```
1       Function D(κ(m))
2           dim D(sum(κ(m)),m)=0
3           i=1
4           for j from 1 to m
5               if κ(j)=1 then
6                   D(i,j)=1
7                   i=i+1
8               end if
9           next j
10      Output D
11      End
```

Scheme 2. Pseudocode for computing the removed matrix, $\mathbf{R}_c$, from the design vector, $\boldsymbol{\kappa}_c$ (note: c subscripts removed in code).

```
1       Function R(κ(m))
2           dim R(m-sum(κ(m)),m)=0
3           i=1
4           for j from 1 to m
5               if κ(j)=0 then
6                   R(i,j)=1
7                   i=i+1
8               end if
9           next j
10      Output R
11      End
```

$\mathbf{D}_c$ and $\mathbf{R}_c$ possess only 1's and 0's, the 1's going into the columns

corresponding to the particular FC that is to be included (in $\mathbf{D}_c$) or removed (in $\mathbf{R}_c$).

Each row of $\mathbf{D_c}$ and $\mathbf{R_c}$ will possess exactly one 1. Each column of $\mathbf{D_c}$ and $\mathbf{R_c}$ will

possess *at most* one 1 <u>between the two matrices</u> (that is, if a given column in $\mathbf{D_c}$

possesses a 1, then the same column in $\mathbf{R_c}$ must possess only 0's, and vice-versa). Thus,

between $\mathbf{D_c}$ and $\mathbf{R_c}$, there will be m total 1's and $m^2 - m$ total 0's.

$\mathbf{D_c}$ and $\mathbf{R_c}$ form an orthogonal matrix,[60] as shown by Eqns. (A-5) and (A-6).

$$\begin{bmatrix} \mathbf{D_c} \\ \mathbf{R_c} \end{bmatrix}^{\mathrm{T}} \begin{bmatrix} \mathbf{D_c} \\ \mathbf{R_c} \end{bmatrix} = \begin{bmatrix} \mathbf{D_c}^{\mathrm{T}} & \mathbf{R_c}^{\mathrm{T}} \end{bmatrix} \begin{bmatrix} \mathbf{D_c} \\ \mathbf{R_c} \end{bmatrix} = \mathbf{I}_m \tag{A-5}$$

$$\begin{bmatrix} \mathbf{D_c} \\ \mathbf{R_c} \end{bmatrix} \begin{bmatrix} \mathbf{D_c} \\ \mathbf{R_c} \end{bmatrix}^{\mathrm{T}} = \begin{bmatrix} \mathbf{D_c} \\ \mathbf{R_c} \end{bmatrix} \begin{bmatrix} \mathbf{D_c}^{\mathrm{T}} & \mathbf{R_c}^{\mathrm{T}} \end{bmatrix} = \mathbf{I}_m \tag{A-6}$$

Any matrix with at least one of its dimensions being m (i.e., m rows and/or m

columns) may be multiplied by Eq. (A-5) or (A-6) to partition it into components that

may be more useful for subsequent manipulations. For example, Eq. (A-7) partitions $\mathbf{c}$

[from Eq. (A-2)] into its "design" and "removed" components, $\mathbf{c_{des}}$ and $\mathbf{c_{rem}}$.

$$\begin{aligned} c_{tot} &= \mathbf{1}_m^{\mathrm{T}} \mathbf{c} \\ &= \mathbf{1}_m^{\mathrm{T}} \mathbf{I}_m \mathbf{c} \\ &= \mathbf{1}_m^{\mathrm{T}} \begin{bmatrix} \mathbf{D_c}^{\mathrm{T}} & \mathbf{R_c}^{\mathrm{T}} \end{bmatrix} \begin{bmatrix} \mathbf{D_c} \\ \mathbf{R_c} \end{bmatrix} \mathbf{c} \\ &= \begin{bmatrix} \mathbf{1}_m^{\mathrm{T}} \mathbf{D_c}^{\mathrm{T}} & \mathbf{1}_m^{\mathrm{T}} \mathbf{R_c}^{\mathrm{T}} \end{bmatrix} \begin{bmatrix} \mathbf{D_c} \mathbf{c} \\ \mathbf{R_c} \mathbf{c} \end{bmatrix} \\ &= \begin{bmatrix} \mathbf{1}_d^{\mathrm{T}} & \mathbf{1}_r^{\mathrm{T}} \end{bmatrix} \begin{bmatrix} \mathbf{c_{des}} \\ \mathbf{c_{rem}} \end{bmatrix} \\ &= \mathbf{1}_d^{\mathrm{T}} \mathbf{c_{des}} + \mathbf{1}_r^{\mathrm{T}} \mathbf{c_{rem}} \\ &= c_{tot,des} + c_{tot,rem} = c_{tot} \end{aligned} \tag{A-7}$$

---

[60] An orthogonal matrix, $\mathbf{A}$, satisfied the relationship $\mathbf{A}^{\mathrm{T}}\mathbf{A} = \mathbf{I} = \mathbf{A}\mathbf{A}^{\mathrm{T}}$.

$\mathbf{c}_{\text{des}}$ and $\mathbf{c}_{\text{rem}}$ are respectively rewritten as Eqns. (A-8) and (A-9)

$$\mathbf{c}_{\text{des}} = \mathbf{D}_{\text{c}}\mathbf{c} \qquad\qquad \text{(A-8)}$$

$$\mathbf{c}_{\text{rem}} = \mathbf{R}_{\text{c}}\mathbf{c} \qquad\qquad \text{(A-9)}$$

Using $\mathbf{c}_{\text{des}}$, Eqns. (A-3) and (A-4) are rewritten as Eqns. (A-10) and (A-11), respectively, which are suitable for design of experiments using only mixtures of a desired set of stock solutions.

$$c_{tot,des} = \sum_{i=1}^{d} c_{des_i} \qquad\qquad \text{(A-10)}$$

$$\mathbf{x}_{\text{c,des}} = \left(c_{tot,des}^{-1}\right)\mathbf{c}_{\text{des}} \qquad\qquad \text{(A-11)}$$

A.4.1.2 *Mixtures of ionic fundamental constituents*

It is desirable to consider mixtures of the dissociated forms of each salt contained within $\mathbf{c}$; that is, mixtures of the fundamental *ionic* constituents, $\boldsymbol{\xi}$. Eq. (A-12) displays the conversion from $\mathbf{c}$ to $\boldsymbol{\xi}$. Here, the *n* x *m stoichiometry matrix*, $\boldsymbol{\Phi}$, linearly transforms the *molecular* concentrations of the mixture (placed in the columns of $\boldsymbol{\Phi}$) to the *fundamental* constituent concentrations using the stoichiometry of the dissociations (indicated by the rows of $\boldsymbol{\Phi}$) that may occur within the salt, acid, and/or base complexes present in the stock solutions. Table A-1 and Eq. (A-16), which are discussed again and in greater depth below, provide an example of $\boldsymbol{\Phi}$ that may be referenced for clarification.

$$\boldsymbol{\xi} = \boldsymbol{\Phi}\mathbf{c} \qquad\qquad \text{(A-12)}$$

In $\boldsymbol{\Phi}$, -1 (negative 1) is used to represent H^+, while $+1$ is used for OH^- (this convention may be reversed if desired). This sign convention accounts for the rapid neutralization reaction that forms water (or possibly methanol), as discussed in Section 4.4.4, when acidic and basic chemicals are mixed. Although the OH^- is negatively charged, its presence is assigned a value of $+1$ in $\boldsymbol{\Phi}$ because the final aggregate solution mixture is known or desired in advance to be basic so the total amount of OH^- added to the system will exceed the quantity of H^+. This sign convention should be reversed if an acidic aggregate solution mixture solution is desired.

Any potentially chemically active species that do not dissociate may also be included as a single row item with a single numeric entry in $\boldsymbol{\Phi}$. Each column where a dissociation between ions occurs will have at least two entries, it will have only one entry if no dissociations occur, and will have no entries if the column corresponds to an inert liquid that possesses no FCs (e.g., an internal standard or diluent solvent).

One important feature of Eq. (A-12) is that the degrees of freedom of ξ, or $df(\xi)$ (that is, the number of $\xi_i \in \xi$ that are independent), is <u>at most</u> $n-1$ [Eq. (A-13)] for systems consisting of charged FCs.[61] Therefore, $\boldsymbol{\Phi}$ is always rank-deficient.[62]

$$df(\xi) = \text{rank}(\boldsymbol{\Phi}) \le n-1 \qquad (A\text{-}13)$$

This characteristic exists because each column of $\boldsymbol{\Phi}$ represents a neutral molecular species, so the sum of its constituent row elements will be zero; hence, there is

---

[61] If the mixture consists entirely of neutral, non-dissociating species, then the charge balance in all subsequent computations is irrelevant.

[62] The *rank* of a matrix is is the number of linearly independent rows or columns it possesses, which is also the size of its largest invertible submatrix [468], which must be square. With charged species $\boldsymbol{\Phi}$ is rank-deficient because rank($\boldsymbol{\Phi}$) < min(m,n).

a linear combination among the rows of $\mathbf{\Phi}$ that produces a row of zeroes. The loss in degrees of freedom due to the intrinsic physical requirement of *charge balance* is given mathematically by Eq. (A-14) [and in vector notation by Eq. (A-15)]. The n elements of $\mathbf{q}$ are the charge of each corresponding ionic species in the mixture. They are usually from the set $\{0, \pm 1, \pm 2, \pm 3\}$. Eq. (A-14) is built into Eq. (A-12) via $\mathbf{\Phi}$ and need not be supplied for the "top-down" derivations; however, the "bottom-up" approach must take it into account in one form or another, as will be demonstrated later.

$$\sum_{i=1}^{n} q_i \xi_i = 0 \qquad\qquad \text{(A-14)}$$

$$\mathbf{q}^{\mathrm{T}} \xi = 0 \qquad\qquad \text{(A-15)}$$

A second feature of Eq. (A-12) is that negative values within ξ are physically absurd with one possible exception: Like with $\mathbf{\Phi}$, if the value of the element of ξ corresponding to OH^- (i.e., ξ_{OH^-}) is positive, then the system will be basic; if it is negative, it will be acidic. The two cases (overall acidity and basicity) are mutually exclusive states of the system and must be treated accordingly. Whenever acidic and basic stock solutions are blended and thus the aggregate solution may be acidic or basic, then the $+/-$ convention for the OH^- row in $\mathbf{\Phi}$ is still employed, but special handling is required (1) to convert any negative values of ξ_{OH^-} to positive ones in order to represent ξ_{H^+} (e.g., by using an absolute value function), (2) to recognize that the quantity now indicates H^+ and not OH^-, (3) to assign the appropriate charge to the element of the charge vector, $\mathbf{q}$, that corresponds to H^+/OH^- (i.e., $q_{OH^-} = -1$ and $q_{H^+} = +1$), and (4) to map any values of ξ or $\mathbf{x}_\xi$ to separate plot regions or vector spaces that correspond

specifically to a basic or an acidic mixture for appropriate visualization and analysis purposes.

An example stoichiometry matrix is given by Table A-1 and Eq. (A-16). The rows and columns of the latter correspond, respectively, to elements of $\boldsymbol{\varphi}_\xi$ and $\boldsymbol{\varphi}_c$. The matrix is populated with integers corresponding to the dissociation stoichiometry. Although 4 separate stock solutions ($\boldsymbol{\varphi}_c$) are blended to produce 4 FCs ($\boldsymbol{\varphi}_\xi$), rank($\boldsymbol{\Phi}$) $= 4 - 1 = 3$.

Table A-1. Example stoichiometric matrix.

	TMA-OH	NaOH	HMeSO$_4$	MeOH
TMA$^+$	1	0	0	0
Na$^+$	0	1	0	0
OH$^-$	1	1	−1	0
MeSO$_4^-$	0	0	1	0

$\boldsymbol{\Phi}$:

$$\boldsymbol{\varphi}_\xi = \begin{bmatrix} \text{TMA}^+ \\ \text{Na}^+ \\ \text{OH}^- \\ \text{MeSO}_4^- \end{bmatrix}, \; \boldsymbol{\varphi}_c = \begin{bmatrix} \text{TMA-OH} \\ \text{HMeSO}_4 \\ \text{NaOH} \\ \text{MeOH} \end{bmatrix}, \; \boldsymbol{\Phi} = \begin{bmatrix} 1 & 0 & 0 & 0 \\ 0 & 1 & 0 & 0 \\ 1 & 1 & -1 & 0 \\ 0 & 0 & 1 & 0 \end{bmatrix} \qquad \text{(A-16)}$$

With ξ, it is possible to compute $\mathbf{x}_\xi$, the mixture fractions of all fundamental constituents in the mixture. As was done for $\mathbf{x}_c$ [Eqns. (A-3) and (A-4)], Eqns. (A-17) and (A-18) are employed to compute $\mathbf{x}_\xi$, the mixture fractions.

$$\xi_{tot} = \sum_{i=1}^{n} \xi_i \qquad \text{(A-17)}$$

$$\mathbf{x}_\xi = \left(\xi_{tot} \right)^{-1} \xi \qquad \text{(A-18)}$$

Combination of Eqns. (A-1), (A-2), (A-12), (A-17), and (A-18) gives Eq. (A-19), which establishes the relationship between the mixture fractions of all fundamental constituents, $\mathbf{x}_\xi$, and all directly manipulated concentrations, $\mathbf{c_0}$, and volumes, $\mathbf{v_0}$, associated with the stock solutions that are combined together.

$$\mathbf{x}_\xi = \left(\mathbf{1}_n^{\mathrm{T}}\left[\boldsymbol{\Phi}(\mathbf{c_0}\cdot\mathbf{v_0})\right]\right)^{-1}\boldsymbol{\Phi}(\mathbf{c_0}\cdot\mathbf{v_0}) \tag{A-19}$$

A scenario that is more general and possesses greater experimental versatility is derived by selecting a *d*-element subset of the *n* fundamental constituents to form the basis of the mixture design since there may be instances where one or more FCs are left out of the mixture design specifications, perhaps because they are always kept constant, they are inert to the dependent variable(s) of interest, or because a double mixture design is pursued (see [33]). *Note: The removed components must be maintained at constant concentrations for the ensuing equations and derivations to be valid*.

Those elements of ξ that are part of the design may be identified by using the vector $\boldsymbol{\kappa}_\xi$. $\boldsymbol{\kappa}_\xi$ possesses only 1's and 0's as did $\boldsymbol{\kappa}_c$. Again, 1's indicate which FCs are kept for the design, and 0's designate removed FCs. From $\boldsymbol{\kappa}_\xi$, the incidence matrices $\mathbf{D}_\xi$ and $\mathbf{R}_\xi$ are computed as described previously for the non-dissociated case, only this time they are *d* x *n* and *r* x *n* ($r = n - d$) dimensioned, respectively (see Scheme 3 and Scheme 4). The variables *d* and *r* are not necessarily numerically equivalent between $\mathbf{D}_c/\mathbf{R}_c$ and $\mathbf{D}_\xi/\mathbf{R}_\xi$, but they are written identically for simplicity.

Scheme 3. Pseudocode for computing the design matrix, $\mathbf{D}_\xi$, from the design vector, κ_ξ (note: ξ subscripts removed in code).

```
1       Function D(κ(n))
2          dim D(sum(κ(n)),n)=0
3          i=1
4          for j from 1 to n
5             if κ(j)=1 then
6                D(i,j)=1
7                i=i+1
8             end if
9          next j
10      Output D
11      End
```

Scheme 4. Pseudocode for computing the removed matrix, $\mathbf{R}_\xi$, from the design vector, κ_ξ (note: ξ subscripts removed in code).

```
1       Function R(κ(n))
2          dim R(n-sum(κ(n)),n)=0
3          i=1
4          for j from 1 to n
5             if κ(j)=0 then
6                R(i,j)=1
7                i=i+1
8             end if
9          next j
10      Output R
11      End
```

$\mathbf{D}_\xi$ and $\mathbf{R}_\xi$ have the same utility as $\mathbf{D}_c$ and $\mathbf{R}_c$. For example, they can be arranged to form an orthogonal matrix, i.e., in the same manner illustrated by Eqns. (A-5) and (A-6). Therefore, Eqns. (A-20) and (A-21) respectively partition Eqns. (A-17) and (A-15) into their design and removed components. In Eq. (A-21), since the quantity ξ_{rem} is constant, as is $\mathbf{q}_{rem}$, the quantity $\mathbf{q}_{des}{}^T\xi_{des}$ is also constant. Thus, ξ_{des} possesses degrees of freedom only within the charge balance constraint.

$$\xi_{tot} = \mathbf{1}_n{}^{\mathrm{T}}\boldsymbol{\xi}$$
$$= \mathbf{1}_n{}^{\mathrm{T}}\mathbf{I}_n\boldsymbol{\xi}$$
$$= \mathbf{1}_n{}^{\mathrm{T}}\begin{bmatrix} \mathbf{D}_\xi{}^{\mathrm{T}} & \mathbf{R}_\xi{}^{\mathrm{T}} \end{bmatrix}\begin{bmatrix} \mathbf{D}_\xi \\ \mathbf{R}_\xi \end{bmatrix}\boldsymbol{\xi}$$
$$= \begin{bmatrix} \mathbf{1}_n{}^{\mathrm{T}}\mathbf{D}_\xi{}^{\mathrm{T}} & \mathbf{1}_n{}^{\mathrm{T}}\mathbf{R}_\xi{}^{\mathrm{T}} \end{bmatrix}\begin{bmatrix} \mathbf{D}_\xi\boldsymbol{\xi} \\ \mathbf{R}_\xi\boldsymbol{\xi} \end{bmatrix} \qquad \text{(A-20)}$$
$$= \begin{bmatrix} \mathbf{1}_d{}^{\mathrm{T}} & \mathbf{1}_r{}^{\mathrm{T}} \end{bmatrix}\begin{bmatrix} \boldsymbol{\xi}_{\mathbf{des}} \\ \boldsymbol{\xi}_{\mathbf{rem}} \end{bmatrix}$$
$$= \mathbf{1}_d{}^{\mathrm{T}}\boldsymbol{\xi}_{\mathbf{des}} + \mathbf{1}_r{}^{\mathrm{T}}\boldsymbol{\xi}_{\mathbf{rem}}$$
$$= \xi_{tot,des} + \xi_{tot,rem} = \xi_{tot}$$

$$0 = \mathbf{q}^{\mathrm{T}}\boldsymbol{\xi}$$
$$= \mathbf{q}^{\mathrm{T}}\mathbf{I}_n\boldsymbol{\xi}$$
$$= \mathbf{q}^{\mathrm{T}}\begin{bmatrix} \mathbf{D}_\xi{}^{\mathrm{T}} & \mathbf{R}_\xi{}^{\mathrm{T}} \end{bmatrix}\begin{bmatrix} \mathbf{D}_\xi \\ \mathbf{R}_\xi \end{bmatrix}\boldsymbol{\xi}$$
$$= \begin{bmatrix} \mathbf{q}^{\mathrm{T}}\mathbf{D}_\xi{}^{\mathrm{T}} & \mathbf{q}^{\mathrm{T}}\mathbf{R}_\xi{}^{\mathrm{T}} \end{bmatrix}\begin{bmatrix} \mathbf{D}_\xi\boldsymbol{\xi} \\ \mathbf{R}_\xi\boldsymbol{\xi} \end{bmatrix} \qquad \text{(A-21)}$$
$$= \begin{bmatrix} \mathbf{q}_{\mathbf{des}}{}^{\mathrm{T}} & \mathbf{q}_{\mathbf{rem}}{}^{\mathrm{T}} \end{bmatrix}\begin{bmatrix} \boldsymbol{\xi}_{\mathbf{des}} \\ \boldsymbol{\xi}_{\mathbf{rem}} \end{bmatrix}$$
$$= \mathbf{q}_{\mathbf{des}}{}^{\mathrm{T}}\boldsymbol{\xi}_{\mathbf{des}} + \mathbf{q}_{\mathbf{rem}}{}^{\mathrm{T}}\boldsymbol{\xi}_{\mathbf{rem}} = 0$$

Any equality having n rows may be partitioned by multiplying both sides by $\begin{bmatrix} \mathbf{D}_\xi \\ \mathbf{R}_\xi \end{bmatrix}$, as shown by the example of Eq. (A-22).

$$\boldsymbol{\xi} = \boldsymbol{\Phi}\mathbf{c}$$
$$\begin{bmatrix} \mathbf{D}_\xi \\ \mathbf{R}_\xi \end{bmatrix}\boldsymbol{\xi} = \begin{bmatrix} \mathbf{D}_\xi \\ \mathbf{R}_\xi \end{bmatrix}\boldsymbol{\Phi}\mathbf{c}$$
$$\begin{bmatrix} \mathbf{D}_\xi\boldsymbol{\xi} \\ \mathbf{R}_\xi\boldsymbol{\xi} \end{bmatrix} = \begin{bmatrix} \mathbf{D}_\xi\boldsymbol{\Phi}\mathbf{c} \\ \mathbf{R}_\xi\boldsymbol{\Phi}\mathbf{c} \end{bmatrix} \qquad \text{(A-22)}$$
$$\begin{bmatrix} \boldsymbol{\xi}_{\mathbf{des}} \\ \boldsymbol{\xi}_{\mathbf{rem}} \end{bmatrix} = \begin{bmatrix} \mathbf{D}_\xi\boldsymbol{\Phi}\mathbf{c} \\ \mathbf{R}_\xi\boldsymbol{\Phi}\mathbf{c} \end{bmatrix}$$

In this manner, Eqns. (A-23) and (A-24) are obtained from Eq. (A-12).

$$\boldsymbol{\xi_{des}} = (\mathbf{D_\xi \Phi}) \mathbf{c} \tag{A-23}$$

$$\boldsymbol{\xi_{rem}} = (\mathbf{R_\xi \Phi}) \mathbf{c} \tag{A-24}$$

Eq. (A-23) is treated to obtain a mixture fraction of design components, $\mathbf{x_{\xi,des}}$, via Eqns. (A-25) and (A-26).

$$\xi_{tot,des} = \sum_{i=1}^{d} \xi_{des\, i} \tag{A-25}$$

$$\boxed{\mathbf{x_{\xi,des}} = \left(\xi_{tot,des}\right)^{-1} \boldsymbol{\xi_{des}}} \tag{A-26}$$

Combination of Eqns. (A-1), (A-2), (A-23), (A-25), and (A-26) gives Eq. (A-27). Eq. (A-27) is preferred over Eq. (A-19) for computing the mixture fraction of the design from the volumes and concentrations of the stock solutions because Eq. (A-27) includes only the FCs the user intends to vary. (Note: $\mathbf{x_{\xi,des}} = \mathbf{x_\xi}$ when $\boldsymbol{\kappa} = \mathbf{1}_n$, $d = n$, and $\mathbf{D_\xi} = \mathbf{I}_n$.) Again, Eq. (A-27) is only exact if $\boldsymbol{\xi_{rem}}$ is constant.

$$\boxed{\mathbf{x_{\xi,des}} = \left(\mathbf{1}_d^{\mathrm{T}} \left[\mathbf{D_\xi \Phi}(\mathbf{c_0 \cdot v_0})\right]\right)^{-1} \mathbf{D_\xi \Phi}(\mathbf{c_0 \cdot v_0})} \tag{A-27}$$

From here onward, $\mathbf{x_{\xi,des}}$ is always written whether or not components of $\boldsymbol{\xi}$ have been removed from the experimental design since $\mathbf{x_\xi}$ is simply a specific case where $\boldsymbol{\xi_{rem}} = \{\ \}$ (i.e., no components are removed from the experimental design).

Although Eqns. (A-19) and (A-27) require $\mathbf{c_0}$ and $\mathbf{v_0}$ for their computations (and consequently information about $\boldsymbol{\xi}$ and v_{tot}), mixture fraction values alone (i.e., $\mathbf{x_{\xi,des}}$) provide no concentration or volume information for converting these specifications into

actual measurements of the stock solutions. Some information in the form of volume(s) and concentration(s) must be provided to translate $\mathbf{x}_{\xi,des}$ into $\mathbf{v}_0$.

A.4.2 "Bottom-up" computations

Although calculating $\mathbf{x}_{c,des}$ and $\mathbf{x}_{\xi,des}$ (together referred to as $\mathbf{x}$) from known stock solution volumes and concentrations is important and useful, the design of mixture experiments involves the reverse, "bottom-up" calculations; that is, computing the correct combination of reagents and solvents required to produce the specified $\mathbf{x}$ and achieve other desired physical constraints of the system (total volume, stock solution concentrations, pH requirements, etc.). Usually, the specific problem that is addressed is, *what combination of volumes, $\mathbf{v}_0$, of each stock solution of known concentrations, $\mathbf{c}_0$, generates* (1) *a mixture composition, $\mathbf{x}$,* (2) *a desired concentration basis for experimental design (e.g., at least one specific element of either $\mathbf{c}$ or ξ is met), and* (3) *a total final volume, v_{tot}?* Although other scenarios are conceivable, they are not considered here.

In Section 4.4.1, the definitions and key concepts of mixtures were given, and their specific advantages expounded in Section 4.4.6. Mixtures experiments are rooted in the idea that the mixture fraction, $\mathbf{x}$, can be specified directly and then the physical mixture of chemicals are prepared accordingly for further study. Unfortunately, one of the challenges of mixtures experiments with solutes in solutions is that a mixture fraction alone (i.e., $\mathbf{x}_{c,des}$ or $\mathbf{x}_{\xi,des}$) provides no information about the concentration of the species in the solution or the solution's volume. (Although the intrinsic properties under

253

investigation are independent of the solution volume, it is required for actual physical preparation of sample solution for study.) When values of $\mathbf{x}_{c,des}$ or $\mathbf{x}_{\xi,des}$ are translated into concentrations, all stock solution volumes must be positive (although removal of liquid volumes or salts may be possible mathematically, it is impossible physically!) and the aggregate solution concentrations must be positive [with the possible exception of ξ_{H^+/OH^-}, as described in the discussion of Eq. (A-12) in Section A.4.1]. Additionally, when the mixture experiment is designed around ions, values of $\mathbf{x}_{\xi,des}$ are only physically meaningful if the charge balance [intrinsic to Eq. (A-12) and indicated separately by Eq. (A-14)] of the ions is satisfied for a given $\mathbf{x}_{\xi,rem}$. This is expounded below.

A.4.2.1 Constraints on mixture of undissociated salts

Up to $d-1$ constraints can be made on values of $\mathbf{x}_{c,des}$, which is already constrained by the requirement that its elements sum to 1 per its definition [Eq. (A-11)]. The specifications can be made through Eq. (A-28), where $\mathbf{G}_c$ contains up to $d-1$ rows and $\mathbf{x}_{c,spec}$ has up to $d-1$ elements (here $d \le m$). $\mathbf{x}_{c,spec}$ must be chosen so that all $\mathbf{x}_{c,des}$ are non-negative since negative values have no meaning. This may be done by trial-and-error or by the convex multiplier method discussed later in further detail (Section A.5).

$$\begin{bmatrix} \mathbf{1}_d^{\mathrm{T}} \\ \mathbf{G}_c \end{bmatrix} \mathbf{x}_{c,des} = \begin{bmatrix} 1 \\ \mathbf{x}_{c,spec} \end{bmatrix} \tag{A-28}$$

From $\mathbf{x}_{c,des}$, the known $\mathbf{c}_{rem}$, and (possibly) some other relationships or specifications on values of $\mathbf{c}_{des}$ allow $\mathbf{c}$ to be computed. Finally, the desired stock

solution reagents, $\mathbf{v_0}$, are found from providing at least one specification on volumes (usually v_{tot} plus internal standard volume) and using Eq. (A-2). In the end, the number of direct specifications made on the system must equal m.

A.4.2.2 Constraints on mixtures of ionic FCs

The requirements imposed on selecting proper values of $\mathbf{x_{\xi,des}}$ make arbitrary selection of mixture fractions difficult. Three total constraints exist on $\mathbf{x_{\xi,des}}$: First, the *mixture fraction constraint* of Eq. (A-29) must be satisfied. Second, the charge balance must be met [Eq. (A-30)]. Third, an inequality requirement on the values of $\mathbf{x_{\xi,des}}$ exists: Under no circumstances can any of their elements be less than zero [see Eq. (A-31)].

Any specifications made on $\mathbf{x_{\xi,des}}$ may be expressed by Eq. (A-32), where $\mathbf{G_\xi}$ contains up to $d-2$ rows and $\mathbf{x_{\xi,spec}}$ has up to $d-2$ elements (recall $d \le n$).

$$\sum_{i=1}^{d} x_{\xi,des_i} = 1 \tag{A-29}$$

$$\sum_{i=1}^{d} q_{des_i} x_{\xi,des_i} = -\left(\sum_{i=1}^{d} \xi_{des_i}\right)^{-1} \sum_{j=1}^{r} q_{rem_j} \xi_{rem_j}$$
$$= -\left(\xi_{tot,des}\right)^{-1} \sum_{j=1}^{r} q_{rem_j} \xi_{rem_j} \tag{A-30}$$

$$x_{\xi,des_i} \ge 0 \quad \forall x_{\xi,des_i} \in \mathbf{x_{\xi,des}} \tag{A-31}$$

$$\begin{bmatrix} \mathbf{1}_d^{\mathrm{T}} \\ \mathbf{q_{des}}^{\mathrm{T}} \\ \mathbf{G_\xi} \end{bmatrix} \mathbf{x_{\xi,des}} = \begin{bmatrix} 1 \\ -\left(\mathbf{1}_d^{\mathrm{T}} \boldsymbol{\xi_{des}}\right)^{-1} \mathbf{q_{rem}}^{\mathrm{T}} \boldsymbol{\xi_{rem}} \\ \mathbf{x_{\xi,spec}} \end{bmatrix} \tag{A-32}$$

Eq. (A-32) reveals that at most $d - 2$ values of $\mathbf{x}_{\xi,\mathbf{des}}$ may be independently

selected via $\mathbf{x}_{\xi,\mathbf{spec}}$. In such cases, $\mathbf{G}_{\xi}$ becomes a $d - 2$ x d incident matrix, $\mathbf{G}_{\xi}^{*}$, having

exactly 2 columns that contain *only* zeroes, a single one appearing in each of the

remaining columns. The two "zeroes columns" cannot be chosen arbitrarily, however, as

now explained. By assigning $\mathbf{\Gamma} = \begin{bmatrix} \mathbf{1}_d^{\mathrm{T}} \\ \mathbf{q}_{\mathbf{des}}^{\mathrm{T}} \\ \mathbf{G}_{\xi}^{*} \end{bmatrix}$ and $\mathbf{\gamma} = \begin{bmatrix} 1 \\ -\left(\mathbf{1}_d^{\mathrm{T}}\mathbf{\xi}_{\mathbf{des}}\right)^{-1}\mathbf{q}_{\mathbf{rem}}^{\mathrm{T}}\mathbf{\xi}_{\mathbf{rem}} \\ \mathbf{x}_{\xi,\mathbf{spec}} \end{bmatrix}$, Eq. (A-33) is

obtained.

$$\mathbf{\Gamma}\mathbf{x}_{\xi,\mathbf{des}} = \mathbf{\gamma} \tag{A-33}$$

In order to solve for $\mathbf{x}_{\xi,\mathbf{des}}$, $\mathbf{\Gamma}$ must be invertible; that is, $\mathrm{rank}(\mathbf{\Gamma}) = d$. Within $\mathbf{\Gamma}$,

$\mathbf{G}_{\xi}^{*}$ has exactly 2 columns that contain only zeroes, so no information is provided about

the two corresponding $\mathbf{x}_{\mathbf{des}}$ (say, $x_{des\,i}$ and $x_{des\,j}$). Their determination depends on the

rank of the 2 x 2 submatrix consisting of elements from the first two rows of $\mathbf{\Gamma}$ and same

two "zeroes columns" in $\mathbf{G}_{\xi}^{*}$. This submatrix is referred to as $\mathbf{\Gamma}^{*}$ and is shown as Eq.

(A-34). For inversion of Eq. (A-33), $\mathbf{\Gamma}^{*}$ must also be invertible, which is only possible if

$\mathrm{rank}(\mathbf{\Gamma}^{*})$ is 2 and thus if and only if $q_k \neq q_l$.

$$\mathbf{\Gamma}^{*} = \begin{bmatrix} 1 & 1 \\ q_k & q_l \end{bmatrix} \tag{A-34}$$

Thus, the general rule for selecting which x_{ξ,des_i} may be specified independently

is simply stated as follows: The charges on the two FCs that will <u>not</u> be independently

(i.e., which $d - 2$ columns of $\mathbf{G}_{\xi}^{*}$ are <u>not</u> populated with zeroes) specified must be

unequal in order for $\mathbf{\Gamma}$ in Eq. (A-33) to be full-rank. q_k and q_l may both be positive or negative, but may not have the exact same value. This same rule holds where $\mathbf{x}_{\xi,\mathbf{des}}$ is the independent variable for a statistical model [see Eq. (4-9)].

For clarity, hereafter the $d-2$ element set of $\mathbf{x}_{\xi,\mathbf{des}}$ that is specified will be referred to as $\boldsymbol{\chi}_{\xi,\mathbf{des}}$, as shown by Eq. (A-35).

$$
\begin{bmatrix} \mathbf{1}_d^{\mathrm{T}} \\ \mathbf{q}_{\mathbf{des}}^{\mathrm{T}} \\ \mathbf{G}_\xi^* \end{bmatrix} \mathbf{x}_{\xi,\mathbf{des}} = \begin{bmatrix} -\left(\mathbf{1}_d^{\mathrm{T}}\boldsymbol{\xi}_{\mathbf{des}}\right)^{-1}\mathbf{q}_{\mathbf{rem}}^{\mathrm{T}}\boldsymbol{\xi}_{\mathbf{rem}} \\ \boldsymbol{\chi}_{\xi,\mathbf{des}} \end{bmatrix} \tag{A-35}
$$

Although the <u>equality</u> constraints of Eqns. (A-29) and (A-30) are included in Eq. (A-35) and a means has been described for determining a proper $\mathbf{G}_\xi^*$, one problem yet remains: How to select values of $\mathbf{x}_{\xi,\mathbf{des}}$ (e.g., via $\boldsymbol{\chi}_{\xi,\mathbf{des}}$) so that the <u>inequality</u> of Eq. (A-31) is always satisfied. One means for selecting realistic values of $\mathbf{x}_{\xi,\mathbf{des}}$ is to generate a set of $\boldsymbol{\chi}_{\xi,\mathbf{des}}$, solve Eq. (A-35) for the two remaining values, x_{ξ,des_k} and x_{ξ,des_l}, and then accept or reject the proposed selection of $\boldsymbol{\chi}_{\xi,\mathbf{des}}$ depending on whether or not x_{ξ,des_k} and x_{ξ,des_l} are both ≥ 0. A computationally more efficient approach for selecting valid $\boldsymbol{\chi}_{\xi,\mathbf{des}}$ that provides a more reliable and systematic means for determining possible values of all $\mathbf{x}_{\xi,\mathbf{des}}$ is preferred and is made possible by convex set theory, discussed in the following section.

As with the $\mathbf{x}_{\mathbf{c},\mathbf{des}}$ above, determining the stock solution reagents, $\mathbf{v}_0$, to produce the desired value of $\mathbf{x}_{\xi,\mathbf{des}}$ require $\boldsymbol{\xi}_{\mathbf{rem}}$ and (possibly) other relationships or specifications on values of $\boldsymbol{\xi}_{\mathbf{des}}$ [for example, Eqns. (A-42) and (A-43), which are discussed below,

could be employed]. Once ξ is known, $\mathbf{c}$ is determined by a modified form of Eq. (A-12) in which mathematically redundant rows in $\mathbf{\Phi}$ (and corresponding elements of ξ) are removed and new mathematically independent rows are added to $\mathbf{\Phi}$ (and their corresponding constant terms appended to ξ) to make this modified version of Eq. (A-12) invertible. Finally, the desired stock solution reagents, $\mathbf{v_0}$, are found by making at least one specification on volumes (usually v_{tot} plus internal standard volume) and then solving Eq. (A-2). Again, the number of direct specifications made on the system equals m. For example, the spores studies involved 5 solutions ($m = 5$): TMA-OH, Na-OH, HMeSO$_4$, MeOH, and an inert internal standard. For the experiments conducted on this system, three specifications constant for all experiments were made. First, total volume was fixed at 500 μL. Second, internal standard volume addition was constant at 100 μL for each sample. Third, the total methyl donor concentration ($c_{\mathrm{TMA^+}} + c_{\mathrm{MeSO_4^-}}$) was kept constant at 750 mM [Eq. (8-9)]. These three requirements left two independent specifications to be made, which were systematically assigned via the mixture fractions, $\mathbf{x}_{\xi,\mathbf{des}}$.

A.5 *Mixtures and convexity*

What will be shown in this section is that all realistic (physically achievable) values of $\mathbf{x}_{\xi,\mathbf{des}}$ belong to a set of numbers that is convex in nature. A convex set possesses useful properties that greatly facilitate realistic and efficient assignments of values to $\mathbf{x}_{\xi,\mathbf{des}}$ for design purposes.

A.5.1 Convexity defined

A set of numeric elements, say S, is convex if for every two points in the set, any point lying on the straight line interval between them is also in the set [469]. Any member of a convex set may be determined by some special linear combination, called a *convex combination*, of a set of points containing S (further discussion on this containing set will be given). A convex combination is defined as follows: Given a set of w points $\{\mathbf{x}_1,\ldots,\mathbf{x}_w\}$ from $\Re^d$ (the real number system of dimension d), a point, $\mathbf{x}_{\mathbf{conv}}$, computed per Eq. (A-36) is a convex combination of $\{\mathbf{x}_1,\ldots,\mathbf{x}_w\}$. $\mathbf{x}_{\mathbf{conv}}$ is thus essentially a linear weighted average of $\{\mathbf{x}_1,\ldots,\mathbf{x}_w\}$.

$$\mathbf{x}_{\mathbf{conv}} = \sum_{i=1}^{w}\eta_i\mathbf{x}_i \,, \;\; \sum_{i=1}^{w}\eta_i = 1, \; \eta_i \geq 0 \text{ for } i=1,\ldots,w \tag{A-36}$$

Convexity may be easily visualized in lower dimensions, as illustrated by Figure A-2. A line drawn between any two points belonging to a given convex set is always entirely within the set. Non-convex sets cannot guarantee this result.
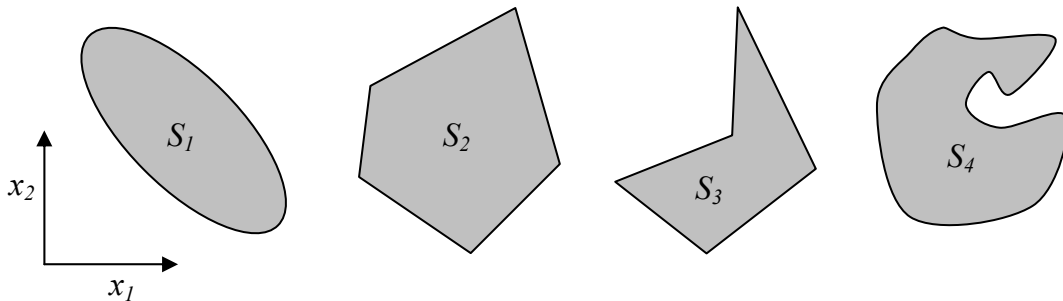
Figure A-2. Illustrations of two convex sets (S_1 and S_2) and two non-convex sets (S_3 and S_4) in $\Re^2$ (i.e., in two dimensions, x_1 and x_2).

That S is convex can be established mathematically—a necessity for sets of high dimensionality. Any two points, $\mathbf{x}'$ and $\mathbf{x}''$, are chosen such that $\{\mathbf{x}', \mathbf{x}''\} \in S$, and a third point, $\mathbf{x}'''$, is defined to be located on the interval $[\mathbf{x}', \mathbf{x}'']$ by using a simple convex combination of $\mathbf{x}'$ and $\mathbf{x}''$ [see Eqns. (A-37) and (A-38), noting that $\eta + (1-\eta) = 1$]. To belong to S, $\mathbf{x}'''$ must satisfy the same criteria as do $\mathbf{x}'$ and $\mathbf{x}''$.

$$[\mathbf{x}', \mathbf{x}''] = \{\eta\mathbf{x}' + (1-\eta)\mathbf{x}'' : 0 \le \eta \le 1\} \tag{A-37}$$

$$\mathbf{x}''' = \eta\mathbf{x}' + (1-\eta)\mathbf{x}'', \ 0 \le \eta \le 1 \tag{A-38}$$

A.5.2 Establishing convexity of mixture components

In the case of mixture components, elements of the set S_{des} containing all possible values of $\mathbf{x}_{\xi,\mathbf{des}}$ must satisfy Eqns. (A-29), (A-30), and (A-31) [see Eq. (A-39)].

$$S_{des} = \left\{ \begin{array}{l} \mathbf{x}_{\xi,\mathbf{des}} \in \mathfrak{R}^n : \quad \forall x_{\xi,des_i} \in \mathbf{x}_{\xi,\mathbf{des}} \quad x_{\xi,des_i} \ge 0, \ \sum_{i=1}^{n} x_{\xi,des_i} = 1, \\[3mm] \sum_{i=1}^{n} q_{des_i} x_{\xi,des_i} = -\left(\sum_{i=1}^{n} \xi_{des_i}\right)^{-1} \sum_{i=1}^{r} q_{rem_i} \xi_{rem_i} \end{array} \right\} \tag{A-39}$$

Thus, the validity of Eq. (A-40) must be established for each of the constraints on $\mathbf{x}_{\xi,\mathbf{des}}$: the mixture constraint [Eq. (A-29)], the charge balance constraint [Eq. (A-30)], and the realistic x constraint [Eq. (A-31)].

$$\mathbf{x}'''_{\xi,\mathbf{des}} = \eta\mathbf{x}'_{\xi,\mathbf{des}} + (1-\eta)\mathbf{x}''_{\xi,\mathbf{des}}, \ 0 \le \eta \le 1 \tag{A-40}$$

Eq. (A-41) demonstrates that the *mixture constraint* holds. Because $0 \le \eta \le 1$ and $0 \le (1-\eta) \le 1 \ \forall \eta$, and since $x'_{\xi,des_i} \ge 0 \ \forall x'_{\xi,des_i} \in \mathbf{x}'_{\xi,\mathbf{des}}$ and $x''_{\xi,des_i} \ge 0 \ \forall x''_{\xi,des_i} \in \mathbf{x}''_{\xi,\mathbf{des}}$, any

product of $\mathbf{x}'_{\xi,\mathbf{des}}$ with η or $\mathbf{x}''_{\xi,\mathbf{des}}$ with $(1-\eta)$ is ≥ 0. Thus, the *realistic x constraint* is met.

$$
\begin{aligned}
\sum_{i=1}^{n} x'''_{\xi,des_i} &= \sum_{i=1}^{n}\left(\eta x'_{\xi,des_i} + (1-\eta)x''_{\xi,des_i}\right) \\
&= \eta \sum_{i=1}^{n} x'_{\xi,des_i} + (1-\eta)\sum_{i=1}^{n} x''_{\xi,des_i} \\
&= \eta(1) + (1-\eta)(1) \\
&= 1
\end{aligned}
\tag{A-41}
$$

However, establishing convexity is more complicated for the charge balance constraint of Eq. (A-30) because $\mathbf{x}_{\xi,\mathbf{des}}$ by itself only possesses information about the *relative* concentrations within $\xi_{\mathbf{des}}$, while information about relative values of all charged elements of the system (i.e., elements within ξ) is required for charge balance. To continue, relationships between $\xi_{\mathbf{des}}$ and $\xi_{\mathbf{rem}}$ must be provided, beginning with the charge balance and adding, as necessary, other *constant* relationships between $\xi_{\mathbf{des}}$ and $\xi_{\mathbf{rem}}$ that are true for some $\mathbf{x}'_{\xi,\mathbf{des}}$ and $\mathbf{x}''_{\xi,\mathbf{des}}$.

Up to $n-1$ specifications on ξ (here referred to as $\xi_{\mathbf{spec}}$, which <u>must</u> include any $\xi_{\mathbf{rem}}$ specifications) are written according to Eq. (A-42), in which the matrix $\begin{bmatrix} \mathbf{q}^{\mathrm{T}} \\ \mathbf{F} \end{bmatrix}$ is understood to be full-rank. Thus, for a known and realistic $\xi_{\mathbf{des}}$, $\begin{bmatrix} \mathbf{q_{des}}^{\mathrm{T}} \\ \mathbf{F_{des}} \end{bmatrix}$ and $\begin{bmatrix} \mathbf{q_{rem}}^{\mathrm{T}} \\ \mathbf{F_{rem}} \end{bmatrix}$ together supply sufficient information to determine $\xi_{\mathbf{rem}}$ (or with just as much utility the relative values of $\xi_{\mathbf{rem}}$).

Rearranging the result of Eq. (A-42) to a linear form in which the only variable

quantity is ξ_{des} gives Eq. (A-43), with $df(\xi_{des}) = d - \text{rank}\begin{pmatrix} \mathbf{q}_{des}^{T} \\ \mathbf{F}_{des} \end{pmatrix}$, which equals the

number of independent values of ξ_{des}.

$$
\begin{bmatrix} 0 \\ \xi_{spec} \end{bmatrix} = \begin{bmatrix} \mathbf{q}^{T} \\ \mathbf{F} \end{bmatrix} \xi
$$

$$
= \begin{bmatrix} \mathbf{q}^{T} \\ \mathbf{F} \end{bmatrix} \mathbf{I}_n \xi
$$

$$
= \begin{bmatrix} \mathbf{q}^{T} \\ \mathbf{F} \end{bmatrix} \begin{bmatrix} \mathbf{D}_{\xi}^{T} & \mathbf{R}_{\xi}^{T} \end{bmatrix} \begin{bmatrix} \mathbf{D}_{\xi} \\ \mathbf{R}_{\xi} \end{bmatrix} \xi \qquad\qquad \text{(A-42)}
$$

$$
= \begin{bmatrix} \mathbf{q}_{des}^{T} & \mathbf{q}_{rem}^{T} \\ \mathbf{F}_{des} & \mathbf{F}_{rem} \end{bmatrix} \begin{bmatrix} \xi_{des} \\ \xi_{rem} \end{bmatrix}
$$

$$
= \begin{bmatrix} \mathbf{q}_{des}^{T} \\ \mathbf{F}_{des} \end{bmatrix} \xi_{des} + \begin{bmatrix} \mathbf{q}_{rem}^{T} \\ \mathbf{F}_{rem} \end{bmatrix} \xi_{rem}
$$

$$
\begin{bmatrix} \mathbf{q}_{des}^{T} \\ \mathbf{F}_{des} \end{bmatrix} \xi_{des} = \begin{bmatrix} 0 \\ \xi_{spec} \end{bmatrix} - \begin{bmatrix} \mathbf{q}_{rem}^{T} \\ \mathbf{F}_{rem} \end{bmatrix} \xi_{rem} \qquad\qquad \text{(A-43)}
$$

As outlined above for specifying $\mathbf{x}_{\xi,des}$ ($\chi_{\xi,des}$), an independent subset of ξ_{des} and

ξ_{rem} must exist; that is, Eq. (A-44) must hold, where $\mathbf{q}_{des}^{*}$ and $\mathbf{F}_{des}^{*}$ are the sub-vector and

sub-matrix of $\mathbf{q}_{des}$ and $\mathbf{F}_{des}$, respectively, obtained by removing columns corresponding

to the dependent (i.e., unspecified) ξ_{des}. Additionally, the elements of ξ_{des} must be non-

negative, with the possible exception of ξ_{OH^-} or ξ_{H^+}, which may be negative based on

the chosen sign conventions for indicating H^+/OH^-.

$$
\text{rank}\begin{pmatrix} \mathbf{q}_{des}^{T} \\ \mathbf{F}_{des} \end{pmatrix} = \text{rank}\begin{pmatrix} \mathbf{q}_{des}^{*}{}^{T} \\ \mathbf{F}_{des}^{*} \end{pmatrix} \qquad\qquad \text{(A-44)}
$$

For convenience, we set $\mathbf{\Lambda} = \begin{bmatrix} \mathbf{q_{des}}^T \\ \mathbf{F_{des}} \end{bmatrix}$ and $\lambda = \begin{bmatrix} 0 \\ \xi_{spec} \end{bmatrix} - \begin{bmatrix} \mathbf{q_{rem}}^T \\ \mathbf{F_{rem}} \end{bmatrix} \xi_{rem}$ to give Eq. (A-45).

$$\mathbf{\Lambda}\xi_{des} = \lambda \qquad (A\text{-}45)$$

Combining Eq. (A-26) with Eq. (A-45) gives Eq. (A-46), in which

$$\mathrm{df}\left(\mathbf{x_{\xi,des}}\left(\xi_{tot,des}\right)\right) = \mathrm{df}\left(\xi_{des}\right) = d - \mathrm{rank}\left(\begin{matrix} \mathbf{q_{des}}^T \\ \mathbf{F_{des}} \end{matrix}\right), \ \mathrm{df}\left(\mathbf{x_{\xi,des}}\right) = d - \mathrm{rank}\left(\begin{matrix} \mathbf{q_{des}}^T \\ \mathbf{F_{des}} \end{matrix}\right) - 1, \text{ and}$$

$\mathrm{df}\left(\xi_{tot,des}\right) = 1$. Consequently, $\xi_{tot,des}$ may, in some cases, be required to vary with $\mathbf{x_{\xi,des}}$

depending on the specifications in $\mathbf{F_{des}}$. For example, a row of 1's in $\mathbf{F_{des}}$, $\mathbf{1}_d^T$, mandates

that $\xi_{tot,des}$ be constant for all possible $\mathbf{x_{\xi,des}}$; the absence of the $\mathbf{1}_d^T$ row relaxes this

restriction, yet the presence of other constraints in $\mathbf{F_{des}}$ will impose other requirements

for $\xi_{tot,des}$ and $\mathbf{x_{\xi,des}}$. The constraint of Eq. (8-9) is one such example in which a row of

$\mathbf{F_{des}}$ possesses two 0's and two 1's, and ξ_{spec} is 750 mM, and other similar constraints are

presented in the discussion of Figure 8-20. Since $\xi_{tot,des}$ depends on the values of $\mathbf{x_{\xi,des}}$,

Eq. (A-40) cannot simply be substituted into Eq. (A-46) to establish convexity.

$$\mathbf{\Lambda x_{des}}\left(\xi_{tot,des}\right) = \lambda \qquad (A\text{-}46)$$

Rather, attention is turned to Eq. (A-45) with which we analyze the convexity of

ξ_{des} instead of $\mathbf{x_{\xi,des}}$. Although each element of ξ_{des} is mathematically unbounded, there

is some physical limit on its possible values. Assuming that physically possible, distinct

values of ξ_{all}—and thus ξ_{des}—may be chosen within these limits, say ξ'_{des} and ξ''_{des}, the

convexity of ξ_{des} may be established by inserting Eq. (A-47) into Eq. (A-45) [in place of

Eq. (A-40) into (A-46)]. Eq. (A-48) displays the result.

Thus, it is the *product* of $\mathbf{x}_{\xi,\mathbf{des}}(\xi_{tot,des})$, and *not* $\mathbf{x}_{\xi,\mathbf{des}}$ alone, that is convex whenever $\xi_{\mathbf{des}} \subset \xi$ (i.e., ionic elements are removed from the design, so $r > 0$).[63]

However, the convex combination may be written as in Eq. (A-49), with the $\xi'_{tot,des}$ and $\xi''_{tot,des}$ each depending on $\mathbf{x}'_{\xi,\mathbf{des}}$ and $\mathbf{x}''_{\xi,\mathbf{des}}$, respectively.

$$\xi'''_{\mathbf{des}} = \eta\xi'_{\mathbf{des}} + (1-\eta)\xi''_{\mathbf{des}}, \ 0 \le \eta \le 1 \tag{A-47}$$

$$
\begin{aligned}
\lambda &= \Lambda\xi'''_{\mathbf{des}} \\
&= \Lambda(\eta\xi'_{\mathbf{des}} + (1-\eta)\xi''_{\mathbf{des}}) \\
&= \eta\Lambda\xi'_{\mathbf{des}} + (1-\eta)\Lambda\xi''_{\mathbf{des}} \\
&= \eta\lambda + (1-\eta)\lambda \\
&= \lambda
\end{aligned}
\tag{A-48}
$$

$$\mathbf{x}'''_{\xi,\mathbf{des}}\xi'''_{tot,des} = \eta[\mathbf{x}'_{\xi,\mathbf{des}}(\xi'_{tot,des})] + (1-\eta)[\mathbf{x}''_{\xi,\mathbf{des}}(\xi''_{tot,des})] \tag{A-49}$$

Since $\mathbf{x}_{\xi,\mathbf{des}}$ is multiplied by the scalar $\xi_{tot,des}$, the experimental design can still be based on systematic variations in $\mathbf{x}_{\xi,\mathbf{des}}$ (e.g., by convex combinations discussed in Section A.5.5), but each $\mathbf{x}_{\xi,\mathbf{des}}$ will possess a (possibly) unique $\xi_{tot,des}$, which must be determined according to any constraints or specifications made on ξ. This is why the total amount of ions transferred to the coiled wire filament in the study on spore DPA methylation was not constant (see Section 0 and Figure 8-11).

Knowing $\xi_{tot,des}$ requires specification of at least one value of an element of ξ (or a combination of elements) and some relationship between them. There must be at least one nonzero value of $\xi_{\mathbf{spec}}$ and at least one row of $\mathbf{F}$ capturing a relationship between

---

[63] The expression $a \subset b$ denotes that a is a proper subset of b.

ξ_{des} and ξ_{rem}. The result of Eq. (A-50) may be useful for determining $\xi_{tot,des}$ if constraints in the form of a sum of some elements of ξ_{des} are given, as was the case in Eq. (8-9), the constraint imposed on the methyl donors in the spore DPA methylation study described in Section 8.2.1. [Note: in Eq. (A-50) the integers represented by j need not be consecutive, but the integers employed must be consistent between x_{ξ,des_j} and ξ_{des_j}].

$$x_{\xi,des_i} = \frac{\xi_{des_i}}{\xi_{tot,des}}$$

$$\sum_j x_{\xi,des_j} = \sum_j \left(\frac{\xi_{des_j}}{\xi_{tot,des}} \right), \text{ where } 1 \le j \le d$$

$$= \frac{1}{\xi_{tot,des}} \sum_j \xi_{des_j} \tag{A-50}$$

$$\Rightarrow \xi_{tot,des} = \frac{\sum_j \xi_{des_j}}{\sum_j x_{\xi,des_j}}$$

A.5.3 Convex hull and extreme points

Recall that S_{des} is the set of all feasible values of $\mathbf{x}_{\xi,des}$. The requirements for convexity of S_{des} having been established, the interior and boundaries of S_{des} are now considered. The *convex hull* of S_{des}, $\text{conv}(S_{des})$, is the minimal convex set of points $\mathbf{x}_{\xi,des}$ and $\xi_{tot,des}$ (i.e., ξ_{des}) that contain S_{des}. It can be understood as the envelope that contains all $\mathbf{x}_{\xi,des}$ within S_{des}, or the boundary of what belongs to S_{des} and what does not. With mixtures experiments involving finite sets of FCs, $\text{conv}(S_{des})$ is a *polytope* [469].

Extreme points are a finite set of points that comprises the convex hull. They may be envisioned as the vertices of a convex polytope. Formally, a point $\mathbf{x}_{\mathbf{ex}}$ is an extreme point of S if, for no pair of distinct points, $\mathbf{x}'$ and $\mathbf{x}''$ in S, is it ever true that $\mathbf{x}_{\mathbf{ex}} = \eta\mathbf{x}' + (1-\eta)\mathbf{x}''$ [385]. Thus, no convex combination of two distinct points in S can ever produce an extreme point. Determining the extreme points of S_{des} is of interest because any interior point of S_{des} may be described as convex combinations of its extreme points (or some appropriately-selected subset thereof [470, 471]; further details are given by Carathéodory's Theorem [469]).

A.5.4 Simple algorithms for identifying extreme points

Extreme points may be determined in various ways for a set of charged FCs, each having advantages and disadvantages. **The two approaches presented here are <u>ONLY</u> for Eq. (A-51), a specific, limited case of Eq. (A-43)**.

$$\mathbf{q_{des}}^{\mathrm{T}}\boldsymbol{\xi_{des}} = 0 \qquad\qquad (\text{A-51})$$

Thus, $\boldsymbol{\xi_{rem}}$ serves as a basis for computing the possible values of $\boldsymbol{\xi_{des}}$ [and hence $\mathbf{x}_{\boldsymbol{\xi},\mathbf{des}}\left(\xi_{tot,des}\right)$] that comprise $\mathrm{conv}(S_{des})$. This set, being finite, is denoted by $\boldsymbol{\Xi}$ (capital Xi) and is subscripted as either $\boldsymbol{\Xi_c}$ or $\boldsymbol{\Xi_q}$ depending on the method by which is computed (detailed below). Each row of $\boldsymbol{\Xi}$ contains the concentrations of a single extreme point, $\boldsymbol{\xi_{des}}_{ex}^{\mathrm{T}}$.

Useful note: if a mixture is to be acidic, it is convenient to add to the subscript an a (e.g., $\boldsymbol{\Xi_{q,a}}$, $S_{q,a}$, $\boldsymbol{\xi_{q,a}}$), and if it is to be basic, a b (e.g., $\boldsymbol{\Xi_{q,b}}$, $S_{q,b}$, $\boldsymbol{\xi_{q,b}}$).

A.5.4.1 Method 1

The composition of each stock solution may constitute an extreme point, for if it is the only item added to a mixture, its constituents are the only FCs and will have the highest physically possible mixture values. (Problems with this approach will be discussed later.) Additionally, because H^+ and OH^- cannot be present simultaneously, the acid-base neutralization reaction necessitates considering binary combinations of stock solutions if one is acidic and the other basic. This set of possible mixture values is designated as $\text{conv}(S_c)$, or in matrix notation, Ξ_c, where the latter is a w x d matrix containing the w mixture fraction values comprising $\text{conv}(S_c)$.

Scheme 5 is a pseudocode algorithm used to compute $\text{conv}(S_c)$, given as Ξ_c (Ξ_c). $\delta_{H/OH}$ (δ_H_OH) is the row index of Φ (Φ) corresponding to H^+/OH^-; s_{H^+} (s_H) reveals the *sign* convention for indicating H^+ in Φ (i.e., whether H^+ is indicated by +1 or −1 in Φ); and *ab* (ab) indicates whether the set is to represent an acidic or a basic mixture (acidic = +1, basic = −1).

Lines 3-15 identify pairs of acid/base compounds (by comparing the charges of their $\delta_{H/OH}$ row elements), compute the relative ratio between the two, (α), required to neutralize them, and multiply the opposite conjugate acid/base salt(s) by α^{-1} to finally obtain the appropriate stoichiometry between the two conjugate portions. Lines 16-23 identify neutral salt stock solutions. Lines 24-36 identify basic (25-29) or acidic (30-34) stock solutions according to the conventions provided in Table A-2 using the inputs Φ and s_{H^+}.

In Scheme 5, $\mathbf{\Omega}$ (Ω) becomes an h x n matrix, with h being the number of sets of FCs produced by the algorithm, and n the number of FCs. All elements of $\mathbf{\Omega}$ are zeroes unless otherwise specified by the algorithm. Since the FC concentrations are unknown, the values in $\mathbf{\Phi}$ (along with α) are utilized to produce relative stoichiometric relationships for each row in $\mathbf{\Omega}$. Once $\mathbf{\Omega}$ has been defined, it is reduced to an h x d form, $\mathbf{\Omega}_{des}$, possessing only the d elements (its columns) that are included in the design by multiplying it by $\mathbf{D}^T$ [line 38; $t()$ is the transpose operator]. Conversion of $\mathbf{\Omega}_{des}$ into mixture fractions, $\mathbf{\Xi}_c$, requires dividing each row of $\mathbf{\Omega}_{des}$ by the row's sum, $\mathbf{\omega}_{des}$ [line 39; $one(d)$ is a d x 1 vector of 1's]. However, before the division is carried out, any zeroes-only-valued rows of $\mathbf{\Omega}_{des}$ and $\mathbf{\omega}_{des}$ are removed to avoid division errors (lines 40-50). Each row of the k x d matrix $\mathbf{\Omega}_{des2}$ (note $k < h$) is divided by the corresponding element of the k-element $\mathbf{\omega}_{des2}$ to determine the k x d $\mathbf{\Xi}_c$ (lines 51-55).

Lines 56-84 remove any duplicate rows in $\mathbf{\Xi}_c$ that occur whenever there are two or more ways to get the same final salt from a given set of stock solutions (e.g., Na_2SO_4 may be obtained either as pure Na_2SO_4, by mixing equimolar $NaHSO_4$ and $NaOH$, or mixing 1 mole H_2SO_4 with 2 moles $NaOH$). Lines 56-67 compare row pairs i and j (where $j \geq i$) to find instances where rows are equal. Equality is determined by computing the sum of the absolute value differences between column elements and comparing this sum against a non-zero tolerance, in this case, 10^{-6} (zero is not used because rounding errors may produce non-zero results where a zero would be expected). $\mathbf{P}$ (P) is an upper triangular matrix with a diagonal of ones. Any column of $\mathbf{P}$ having more than a single one represents a duplicate row entry in $\mathbf{\Xi}_c$ and is identified by summing each column of

P using lines 68-78. If the sum of the column is 1, the row is either the first of a series of

duplicates or is not duplicated at all. The indices of unique rows of Ξ_c are stored in the

w-element variable `keep`, which is used to transfer the unique rows from Ξ_c to the

variable, Ξ'_c (Ξ'_c; lines 79-84). Finally, Ξ'_c is renamed to Ξ_c (line 85) and output

from the function.

Scheme 5. Pseudocode for Method 1: Computing the mixture fraction-based convex hull using single or binary combinations of stock salts solutions.

```
1       Function Ξ_c(Φ(m,n),δ_H_OH,s_H,ab,D(d,n))
2          h=1
3          for i from 1 to m-1
4             if Φ(δ_H_OH,i)≠0 then
5                for j from i+1 to m
6                   if Φ(δ_H_OH,i)*Φ(δ_H_OH,j)<0 then
7                      α=-Φ(δ_H_OH,j)/Φ(δ_H_OH,i)
8                      for k from 1 to n
9                         Ω(h,k)=Φ(k,i)+(1/α)*Φ(k,j)
10                     next k
11                     h=h+1
12                  end if
13               next j
14            end if
15         next i
16         for i from 1 to m
17            if Φ(δ_H_OH,i)=0 then
18               for k from 1 to n
19                  Ω(h,k)= Φ(k,i)
20               next k
21               h=h+1
22            end if
23         next i
24         for i from 1 to m
25            if (Φ(δ_H_OH,i)*s_H<0 AND ab<0) then
26               for k from 1 to n
27                  Ω(h,k)=abs(Φ(k,i))
28               next k
29               h=h+1
30            if (Φ(δ_H_OH,i)*s_H>0 AND ab>0) then
31               for k from 1 to n
32                  Ω(h,k)=abs(Φ(k,i))
33               next k
34               h=h+1
35            end if
36         next i
37         h=h-1
```

Scheme 5 — *Continued*.

```
38        Ω_des=Ω*t(D)
39        ω_des=Ω_des*one(d)
40        k=1
41        for i from 1 to h
42           if ω_des(i)>0 then
43              ω_des2(k)=ω_des(i)
44              for j from 1 to d
45                 Ω_des2(k,j)= Ω_des(i,j)
46              next j
47              k=k+1
48           end if
49        next i
50        k=k-1
51        for i from 1 to k
52           for j from 1 to d
53              Ξ_c(i,j)=Ω_des2(i,j)/ω_des2(i)
54           next j
55        next i
56        for i from 1 to k
57           for j from i to k
58              dum=0
59              for l from 1 to d
60                 dum=dum+abs(Ξ_c(i,l)-Ξ_c(j,l))
61              next l
62              if dum < 10^-6 then
63                 P(i,j)=1
64              else P(i,j)=0
65              end if
66           next j
67        next i
68        w=1
69        for i from 1 to k
70           dum2=0
71           for j from 1 to k
72              dum2=dum2+P(i,j)
73           next j
74           if dum2=1 then
75              keep(w)=i
76              w=w+1
77           end if
78        next i
79        w=w-1
80        for i from 1 to w
81           for j from 1 to d
82              Ξ'_c (i,j)=Ξ_c(keep(i),j)
83           next j
84        next i
85        Ξ_c=Ξ'_c
86     Output Ξ_c
87     End
```

Table A-2. Truth table to determine whether a given pure component is acidic or basic in Scheme 5.

$\Phi_{\delta_{H/OH},i}$	q_{H^+}	$\Phi_{\delta_{H/OH},i}q_{H^+}$	salt acidity/basicity
+	+	+	acid
+	−	−	base
−	+	−	base
−	−	+	acid

A.5.4.2 Method 2

Each possible pair of *oppositely charged* FCs combined stoichiometrically in such a way so as to produce a neutral molecular salt represents an extreme point, as do lone *uncharged* FCs. This set is designated $\text{conv}(S_q)$, or in matrix notation, Ξ_q, which is a k x d matrix.

Scheme 6 is a pseudocode algorithm for (1) determining single neutral ξ_i elements or pairs of charged elements, ξ_i and ξ_j, that form a neutral compound and for (2) using those, along with $\mathbf{D}$, to compute the extreme points, Ξ_q (Ξ_q), that constitute $\text{conv}(S_q)$ for acidic or basic mixtures. Important: recall that $\mathbf{q}$ was defined for either an acidic or a basic mixture, and whichever the value of q_{H^+/OH^-} (that is, the element of $\mathbf{q}$ corresponding to acid or base) will determine whether Ξ_q is acidic or basic.

Ω (Ω) is a matrix, each row having either paired charged or single uncharged FC elements (determined from $\mathbf{q}$). As previously, unless specified otherwise by the algorithm, all elements of Ω are zero-valued. First, each neutral pair of FCs is identified via lines 3-11. Since the FC concentrations are unknown, one FC is arbitrarily assigned a value of 1 (line 6), and the other item is determined based on the stoichiometry required for making the overall charge of the pair equal to zero (line 7). All uncharged FCs are

assigned a default value of 1 (lines 12-17). Once the h x n matrix $\mathbf{\Omega}$ has been defined, it is reduced to an h x d form, $\mathbf{\Omega}_{\mathbf{des}}$, possessing only the d elements (its columns) that are included in the design by multiplying it by $\mathbf{D}^{\mathrm{T}}$ [line 19; t() is the transpose operator]. Conversion of $\mathbf{\Omega}_{\mathbf{des}}$ into mixture fractions, $\mathbf{\Xi}_{\mathbf{q}}$, requires dividing each row of $\mathbf{\Omega}_{\mathbf{des}}$ by the row's sum, $\mathbf{\omega}_{\mathbf{des}}$ [line 20; one(d) is a d x 1 vector of 1's]. However, before the division is carried out, the zeroes-only-valued rows of $\mathbf{\Omega}_{\mathbf{des}}$ and $\mathbf{\omega}_{\mathbf{des}}$ are removed to avoid division errors (lines 21-31). Each row of the w x d matrix $\mathbf{\Omega}_{\mathbf{des2}}$ (note $w < h$) is divided by the corresponding element of the w-element $\mathbf{\omega}_{\mathbf{des2}}$ to determine the w x d $\mathbf{\Xi}_{\mathbf{q}}$ (lines 32-36), which is the output of the function (line 37). $\mathbf{\Xi}_{\mathbf{q}}$ consists of w unique, charge-balanced FC pairs or single uncharged FC entities that comprise $\mathrm{conv}(S_{des})$.

Scheme 6. Pseudocode for Method 2: Computing the mixture fraction-based convex hull using all possible combinations of FCs.

```
1       Function Ξ_q(q(n),D(d,n))
2          h=1
3          for i from 1 to n-1
4             for j from i+1 to n
5                if q(i)*q(j) <0 then
6                   Ω(h,i)=1
7                   Ω(h,j)=-q(i)/q(j)
8                   h=h+1
9                end if
10            next j
11         next i
12         for i from 1 to n
13            if q(i)=0
14               Ω(h,i)=1
15               h=h+1
16            end if
17         next i
18         h=h-1
19         Ω_des=Ω*t(D)
20         ω_des=Ω_des*one(d)
21         w=1
22         for i from 1 to h
23             if ω_des(i)>0 then
```

Scheme 6 — *Continued*.

```
24              ω_des2(w)=ω_des(i)
25              for j from 1 to d
26                  Ω_des2(w,j)= Ω_des(i,j)
27              next j
28              w=w+1
29           end if
30        next i
31        w=w-1
32        for i from 1 to w
33           for j from 1 to d
34               Ξ_q(i,j)=Ω_des2(i,j)/ω_des2(i)
35           next j
36        next i
37     Output Ξ_q
38     End
```

A.5.4.3 Comparison of Methods 1 and 2

Ξ_c from Method 1 is not guaranteed to contain only extreme points, while Ξ_q

from Method 2 is. This problem occurs in Method 1 whenever any one of the m precursor

salts included in the m columns of $\mathbf{\Phi}$ in Scheme 5 may be obtained by convex

combinations of other salts. For example, with the system H_2SO_4, $NaHSO_4$, Na_2SO_4, and

NaOH, Scheme 5 deems $NaHSO_4$ as an extreme point [Eq. (A-52)], when in fact this

compound may be obtained by blending equimolar amounts of Na_2SO_4 and H_2SO_4 or

equimolar NaOH with H_2SO_4. Illustrated numerically, in Eq. (A-52), row 2 may be

obtained by multiplying rows 1 and 3 each by 1/2 and adding the result (a convex

combination). Thus, $NaHSO_4$ does not represent an extreme point on the convex hull.

The results of Method 2 [Eq. (A-53)] give proper values for the extreme points with the

present example.

However, although Method 2 produces the entire set of theoretically possible

extreme points, one or more of these may be physically unrealizable because some of the

mixture values belonging to S_q may not be achievable with the available stock solutions. For example, if the only stock solutions are H_2SO_4 and $NaHSO_4$, these two salts constitute the only extreme points and become (correctly) the output of Method 1 [Eq. (A-54)].

$$\mathbf{\Xi_{c,a}} = \begin{array}{c|ccc} & Na^+ & SO_4^{2-} & H^+ \\ \hline Na_2SO_4 & 2/3 & 1/3 & 0 \\ NaHSO_4 & 1/3 & 1/3 & 1/3 \\ H_2SO_4 & 0 & 1/3 & 2/3 \end{array} \tag{A-52}$$

$$\mathbf{\Xi_{q,a}} = \begin{array}{c|ccc} & Na^+ & SO_4^{2-} & H^+ \\ \hline Na_2SO_4 & 2/3 & 1/3 & 0 \\ H_2SO_4 & 0 & 1/3 & 2/3 \end{array} \tag{A-53}$$

$$\mathbf{\Xi_{c,a}} = \begin{array}{c|ccc} & Na^+ & SO_4^{2-} & H^+ \\ \hline NaHSO_4 & 1/3 & 1/3 & 1/3 \\ H_2SO_4 & 0 & 1/3 & 2/3 \end{array} \tag{A-54}$$

Since Method 2 interprets the FCs from H_2SO_4 and $NaHSO_4$ as being H^+, Na^+, and SO_4^{2-}, it predicts that these may be combined to produce H_2SO_4 and Na_2SO_4 [same result as Eq. (A-53)]. Since no physical combination can make Na_2SO_4, the method fails.

In conclusion, each method has an "Achilles heel" that will cause it to fail in some circumstances. It is recommended that the experiments be designed with solutions that truly form extreme points, in which case Method 1 (Scheme 5) will not fail. The Scheme 5 and Scheme 6 algorithms either need to be modified in order to avoid these pitfalls or the user must be able to recognize and correct problems contained in their outputs.

Algorithms exist that identify extreme points given inequality constraints on $\mathbf{x}$ (for example, see CONVRT, XVERT, XVERT1, and CONSIM algorithms plus MIXSOFT mixture DOE software package [27, 28]). However, this author is unaware if

they are set up to handle information in the form of stock solution concentrations and volumes, specifications on an aggregate solution's desired properties, etc. It is more likely that established computer programs are set up in a more general manner, which requires the user to do the tedious transformations and computations necessary to convert between $\mathbf{c_0} + \mathbf{v_0}$, $\mathbf{x_{\xi,des}} + \xi_{tot,des} + v_{tot}$, etc.

A.5.5 Practical convex combinations of extreme points

Having Ξ allows any physically realistic value of $\mathbf{x_{\xi,des}}$ and $\xi_{tot,des}$ to be readily specified by some convex combination of the former. Revisiting the definition of extreme points, an alternative expression for Eq. (A-36) is Eq. (A-55), where $\boldsymbol{\eta}$ is a w x 1 vector and Ξ is the w x d convex hull matrix indicated previously (i.e., either Ξ_c or Ξ_q), formed according to Eq. (A-56) (i.e., by stacking transposed $\mathbf{x_i}$ from $\{\mathbf{x_1}, \ldots, \mathbf{x_w}\}$).

$$\mathbf{x_{conv}} = \boldsymbol{\eta}^T \Xi, \ \mathbf{1}_w^T \boldsymbol{\eta} = 1, \ \eta_i \geq 0 \ \forall \ \eta_i \in \boldsymbol{\eta} \tag{A-55}$$

$$\Xi = \begin{bmatrix} \mathbf{x_1}^T \\ \vdots \\ \mathbf{x_w}^T \end{bmatrix} \tag{A-56}$$

Any set of s points inside the convex hull Ξ may be generated from its inner product with the w x s matrix of s convex multipliers, $\mathbf{H}$ (capital eta) [Eq. (A-57)]. $\mathbf{X_{conv}}$ is an s x d matrix, each row of which is a different point within the design space. Eq. (A-58) indicates the relationship between $\boldsymbol{\eta}$ and $\mathbf{H}$.

Figure A-3 and Figure A-4 display a series of convex combinations of the coordinates corresponding to Ξ, the extreme points (vertices) forming the convex hulls

275

of an equilateral triangle and a square, respectively. Indicated within these figures are the convex multiplier matrices, $\mathbf{H}$, placed over the corresponding polygon and uniquely identified by roman numerals. Note that the sum of a given row of any $\mathbf{H}$ is always one (the requirement for convex multiplication).

$$\mathbf{X}_{\mathbf{conv}} = \mathbf{H}^{\mathrm{T}}\mathbf{\Xi} \tag{A-57}$$

$$\mathbf{H} = \begin{bmatrix} \mathbf{\eta}_1 & \cdots & \mathbf{\eta}_s \end{bmatrix} \tag{A-58}$$

The coordinates of each set of points in a given triangle or square (Figure A-3 and Figure A-4, respectively) are computed by Eq. (A-57). In the lower left corners are lattices obtained when the indicated convex multipliers were utilized (e.g., in Figure A-3, the points in the lower left triangle were computed by $\mathbf{H} = \begin{bmatrix} \mathbf{H}_{\mathrm{I}} & \mathbf{H}_{\mathrm{III}} & \mathbf{H}_{\mathrm{IIV}} & \mathbf{H}_{\mathrm{V}} \end{bmatrix}$).
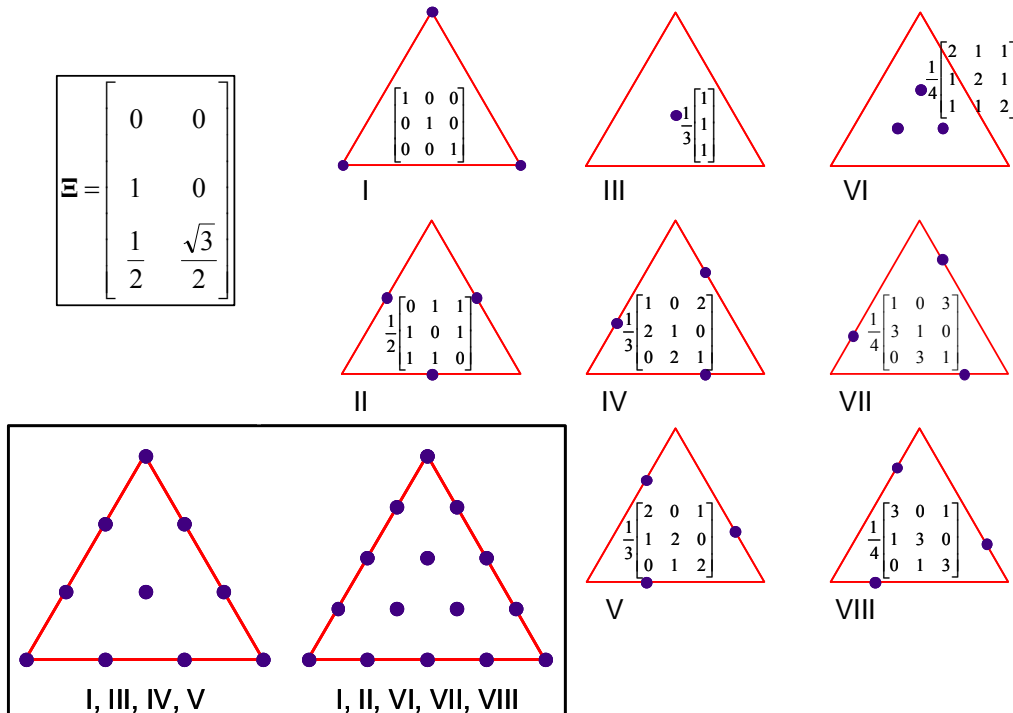
Figure A-3. Illustration of convex combinations of the coordinates of the vertices of an equilateral triangle.

276
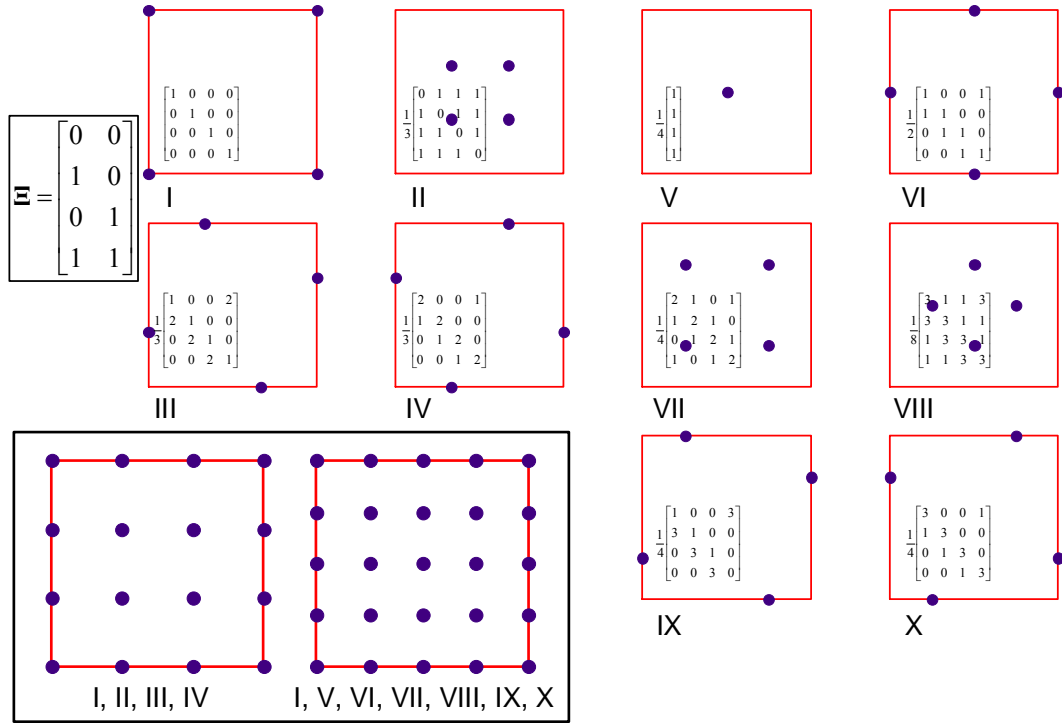
Figure A-4. Illustration of convex combinations of the coordinates representing the vertices of a square.

Appendix B   Displaying mixtures in 2-D and 3-D

The approach underlying visual representation of mixtures data is to employ a simplex, which is an n-dimensional analogue of a triangle. Since mixture fractions must sum to one, an n-dimensional simplex is capable of representing the relative proportions of $n + 1$ components. Hence, a 1-dimensional line (e.g., an x-axis), a triangle, and a tetrahedron may describe binary, ternary, and quaternary systems, respectively. The relationship between mixture fraction, $\mathbf{x_{mix}}$, and a corresponding point, $\mathbf{p}$, in 2-D x-y coordinates of a triangle or in a 3-D x-y-z coordinate system of a regular tetrahedron are presented.

B.1   2-D triangles (for ternary mixture)

Figure B-1 displays a single point (labeled as $\mathbf{p}$) for the single mixture fraction, $\mathbf{x_{mix}}$, which is located within an equilateral triangle whose vertices are given as points $\mathbf{a}$, $\mathbf{b}$, and $\mathbf{c}$. Visually, since $\mathbf{p}$ is closest to vertex $\mathbf{a}$ and furthest from vertex $\mathbf{c}$, it is readily concluded that the composition is mostly A, some B, and relatively little C (where A, B, and C are some measurable quantity associated with the mixture).

Table B-1 contains the x-y coordinates the vertices of Figure B-1, with point $\mathbf{a}$ located at the origin (0,0). In this table, ε represents an arbitrary quantity used as a basis for sizing the triangle (typically $\varepsilon = 1$). In addition to points $\mathbf{a}$, $\mathbf{b}$, and $\mathbf{c}$, Table B-1

includes points labeled **a'**, **b'**, and **c'**, each of which is the point that bisects the face

directly opposite its corresponding vertex in the triangle.
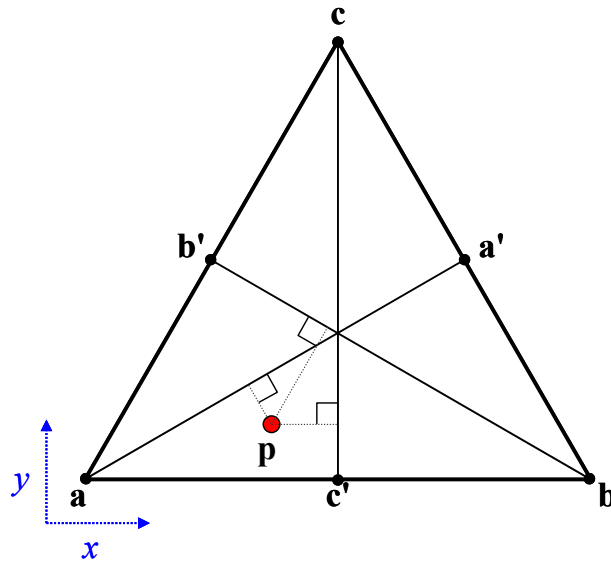
Figure B-1. Ternary mixture diagram with a point, p, representing a mixture composition.

Table B-1. *x-y* coordinates for triangle mixture shown in Figure B-1.

Point	*x*-coordinate	*y*-coordinate
a	0	0
b	ε	0
c	$\dfrac{\varepsilon}{2}$	$\dfrac{\varepsilon\sqrt{3}}{2}$
a' (= 1/2**b** + 1/2**c**)	$\dfrac{3\varepsilon}{4}$	$\dfrac{\varepsilon\sqrt{3}}{4}$
b' (= 1/2**a** + 1/2**c**)	$\dfrac{\varepsilon}{4}$	$\dfrac{\varepsilon\sqrt{3}}{4}$
c' (= 1/2**a** + 1/2**b**)	$\dfrac{\varepsilon}{2}$	0

Taken one at a time, the fractional distance along each of the lines **a'a**, **b'b**, and **c'c** (i.e., fractional distance from a vertex to an opposite face) is the mixture fraction of the corresponding component. That is, the first component of the mixture, $x_{\text{mix,a}}$, represents the fractional distance along line **a'a** (ditto for $x_{\text{mix,b}}$ and **b'b**, and $x_{\text{mix,c}}$ and **c'c**). Figure B-2 represents this aspect visually for lines **a'a** and **b'b**. (Line **c'c** is not included because in 2-space, only 2 non-collinear lines are required to define a single point.)
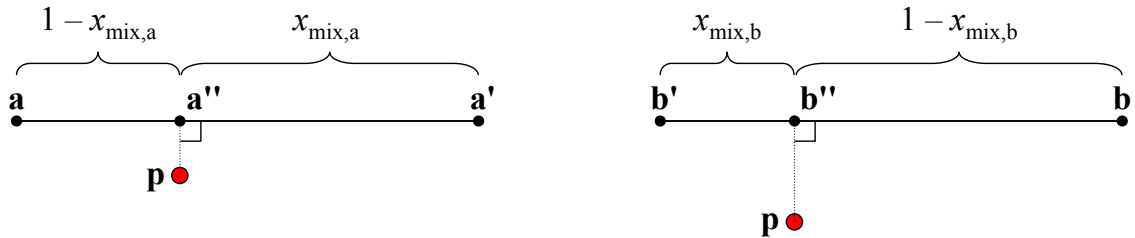
Figure B-2. Illustration of how a mixture point, p, may be located by a convex combination of the endpoints, a and a', and b and b'.

The actual *x-y* coordinates of **p** are obtained using an $n-1$ subset of $\mathbf{x_{mix}}$. Since each mixture component is represented by the fractional distance from a base of the triangle to the opposite vertex (i.e., $x_{\text{mix,a}} = \dfrac{\mathbf{a'a''}}{\mathbf{a'a}}$ or $x_{\text{mix,b}} = \dfrac{\mathbf{b'b''}}{\mathbf{b'b}}$ in Figure B-2), a line drawn from **p** to **a''** (or **b''**) must be perpendicular to line **a'a** (or line **b'b**). The fact that the dot product of orthogonal (perpendicular) vectors is zero is used to set up a system of linear equations to solve for the *x-y* coordinates of **p** based on the requirement that **pa''** $\perp$ **a'a** and **pb''** $\perp$ **b'b**.

The dot product of component A is given by Eq. (B-1), or equivalently, Eq. (B-2). $\mathbf{a''}$ is found from the convex combination of points $\mathbf{a}$ and $\mathbf{a'}$ [Eq. (B-3)], which is substituted into Eq. (B-2) to give Eq. (B-4).

$$\langle (\mathbf{a} - \mathbf{a'}), (\mathbf{a''} - \mathbf{p}) \rangle = 0 \tag{B-1}$$

$$0 = (\mathbf{a} - \mathbf{a'})^{\mathrm{T}} (\mathbf{a''} - \mathbf{p}) \tag{B-2}$$

$$\mathbf{a''} = x_{\mathrm{mix,a}} \mathbf{a} + (1 - x_{\mathrm{mix,a}}) \mathbf{a'} \tag{B-3}$$

$$\begin{aligned} 0 &= (\mathbf{a} - \mathbf{a'})^{\mathrm{T}} \left((x_{\mathrm{mix,a}} \mathbf{a} + (1 - x_{\mathrm{mix,a}}) \mathbf{a'}) - \mathbf{p} \right) \\ &= (\mathbf{a} - \mathbf{a'})^{\mathrm{T}} \left((x_{\mathrm{mix,a}} (\mathbf{a} - \mathbf{a'}) + \mathbf{a'}) - \mathbf{p} \right) \end{aligned} \tag{B-4}$$

Eq. (B-4) is rearranged into a form with $\mathbf{p}$ on one side [Eq. (B-5)]. The equivalent treatment is given to component B to give Eq. (B-6).

$$\begin{aligned} (\mathbf{a} - \mathbf{a'})^{\mathrm{T}} \mathbf{p} &= (\mathbf{a} - \mathbf{a'})^{\mathrm{T}} (x_{\mathrm{mix,a}} (\mathbf{a} - \mathbf{a'}) + \mathbf{a'}) \\ &= x_{\mathrm{mix,a}} (\mathbf{a} - \mathbf{a'})^{\mathrm{T}} (\mathbf{a} - \mathbf{a'}) + (\mathbf{a} - \mathbf{a'})^{\mathrm{T}} \mathbf{a'} \end{aligned} \tag{B-5}$$

$$(\mathbf{b} - \mathbf{b'})^{\mathrm{T}} \mathbf{p} = x_{\mathrm{mix,b}} (\mathbf{b} - \mathbf{b'})^{\mathrm{T}} (\mathbf{b} - \mathbf{b'}) + (\mathbf{b} - \mathbf{b'})^{\mathrm{T}} \mathbf{b'} \tag{B-6}$$

Eqns. (B-5) and (B-6) are combined into Eq. (B-7), which is now full-rank, allowing for direct solution of $\mathbf{p}$ [Eq. (B-8)]. Note again that only two of the three elements of $\mathbf{x}_{\mathrm{mix}}$ were used since the third was not independent of the other two because of the requirement that the mixture fractions sum to 1.

$$\begin{bmatrix} (\mathbf{a} - \mathbf{a'})^{\mathrm{T}} \\ (\mathbf{b} - \mathbf{b'})^{\mathrm{T}} \end{bmatrix} \mathbf{p} = \begin{bmatrix} x_{\mathrm{mix,a}} (\mathbf{a} - \mathbf{a'})^{\mathrm{T}} (\mathbf{a} - \mathbf{a'}) \\ x_{\mathrm{mix,b}} (\mathbf{b} - \mathbf{b'})^{\mathrm{T}} (\mathbf{b} - \mathbf{b'}) \end{bmatrix} + \begin{bmatrix} (\mathbf{a} - \mathbf{a'})^{\mathrm{T}} \mathbf{a'} \\ (\mathbf{b} - \mathbf{b'})^{\mathrm{T}} \mathbf{b'} \end{bmatrix} \tag{B-7}$$

$$\mathbf{p} = \begin{bmatrix} (\mathbf{a} - \mathbf{a'})^{\mathrm{T}} \\ (\mathbf{b} - \mathbf{b'})^{\mathrm{T}} \end{bmatrix}^{-1} \left(\begin{bmatrix} x_{\mathrm{mix,a}} (\mathbf{a} - \mathbf{a'})^{\mathrm{T}} (\mathbf{a} - \mathbf{a'}) \\ x_{\mathrm{mix,b}} (\mathbf{b} - \mathbf{b'})^{\mathrm{T}} (\mathbf{b} - \mathbf{b'}) \end{bmatrix} + \begin{bmatrix} (\mathbf{a} - \mathbf{a'})^{\mathrm{T}} \mathbf{a'} \\ (\mathbf{b} - \mathbf{b'})^{\mathrm{T}} \mathbf{b'} \end{bmatrix} \right) \tag{B-8}$$

The numbers (*x-y* coordinates of vertices and midpoints of a triangle) from Table B-1 are substituted into Eq. (B-8) and simplified to give Eq. (B-9). Again, **p** possesses the *x-y* coordinates for a triangle of the form described above, given $\mathbf{x_{mix}}$. Also, only *two* (of three total) mixture components are required since this ternary mixture only possesses two degrees of freedom. Note that $x \neq \mathbf{x_{mix}}$; the former is a Cartesian coordinate; the latter is a mixture fraction.

$$\mathbf{p} = \begin{bmatrix} \dfrac{\varepsilon}{2}\left(1 - x_{mix,a} + x_{mix,b}\right) \\ \dfrac{\varepsilon\sqrt{3}}{2}\left(1 - x_{mix,a} - x_{mix,b}\right) \end{bmatrix} \tag{B-9}$$

The mixture fraction, $\mathbf{x_{mix}}$, may be computed via Eq. (B-10), a rearrangement of Eq. (B-9), if actual *x-y* coordinates of a point in a ternary mixture diagram are known. Note that $x_{mix,c}$ is found by subtracting $x_{mix,a}$ and $x_{mix,b}$ from 1.

$$\begin{bmatrix} x_{mix,a} \\ x_{mix,b} \end{bmatrix} = \begin{bmatrix} -1 & -\dfrac{\sqrt{3}}{3} \\ 1 & -\dfrac{\sqrt{3}}{3} \end{bmatrix} \begin{bmatrix} \dfrac{x}{\varepsilon} - \dfrac{1}{2} \\ \dfrac{y}{\varepsilon} - \dfrac{\sqrt{3}}{2} \end{bmatrix} \tag{B-10}$$

B.2 3-D tetrahedra (*for plotting a quaternary mixture*)

A tetrahedron is a 3-dimensional simplex that is easily generated by connecting a proper set of four points from a cube (green points in Figure B-3; see Table B-2). The reasoning behind and justification for the derivations used to convert mixture fractions into *x-y-z* coordinates are identical to those discussed for the triangle case just discussed, the only difference being that an additional dimension is added for each computation.
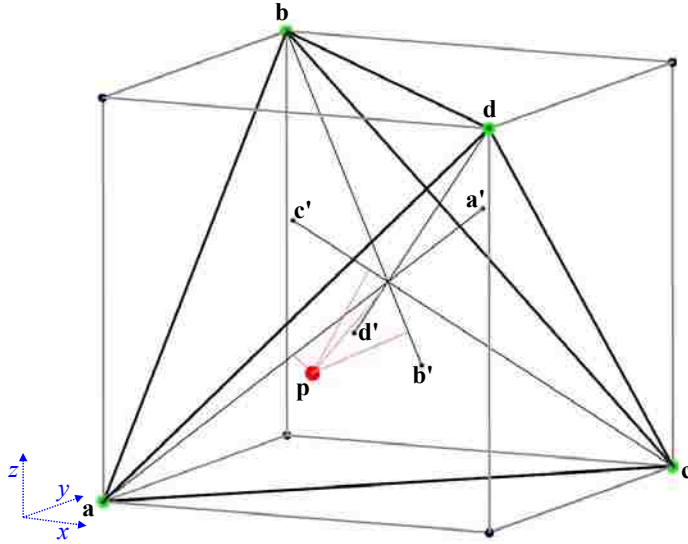
Figure B-3. Illustration of tetrahedron, including rays for each vertex/mixture component and a single experimental point.

The process for converting a vector representing a quaternary mixture to x-y-z coordinates for plotting within a 3-D tetrahedron is identical to that reported above for ternary mixtures, except one additional dimension must be included. Though the details of this process are omitted, the results are given as Eqns. (B-11) and (B-12) (compare these to Eqns. (B-8) and (B-9), respectively).

$$\mathbf{p} = \begin{bmatrix} (\mathbf{a}-\mathbf{a'})^{\mathrm{T}} \\ (\mathbf{b}-\mathbf{b'})^{\mathrm{T}} \\ (\mathbf{c}-\mathbf{c'})^{\mathrm{T}} \end{bmatrix}^{-1} \left(\begin{bmatrix} x_{\mathrm{mix,a}}(\mathbf{a}-\mathbf{a'})^{\mathrm{T}}(\mathbf{a}-\mathbf{a'}) \\ x_{\mathrm{mix,b}}(\mathbf{b}-\mathbf{b'})^{\mathrm{T}}(\mathbf{b}-\mathbf{b'}) \\ x_{\mathrm{mix,c}}(\mathbf{c}-\mathbf{c'})^{\mathrm{T}}(\mathbf{c}-\mathbf{c'}) \end{bmatrix} + \begin{bmatrix} (\mathbf{a}-\mathbf{a'})^{\mathrm{T}}\mathbf{a'} \\ (\mathbf{b}-\mathbf{b'})^{\mathrm{T}}\mathbf{b'} \\ (\mathbf{c}-\mathbf{c'})^{\mathrm{T}}\mathbf{c'} \end{bmatrix} \right) \qquad \text{(B-11)}$$

The numbers (x-y-z coordinates) from Table B-2 are substituted into Eq. (B-11) and simplified to give Eq. (B-12). Again, $\mathbf{p}$ carries the x-y-z coordinates for a triangle of the form described above, given $\mathbf{x_{mix}}$. Also, only *two* (of three total) mixture components are required for its computation since this ternary mixture only possesses two degrees of freedom.

284

Table B-2. *x-y-z* coordinates of points involved in representing quaternary mixtures (see Figure B-3).

Point	*x*-coordinate	*y*-coordinate	*z*-coordinate
a	0	0	0
b	0	ε	ε
c	ε	ε	0
d	ε	0	ε
a' (= 1/3**b** + 1/3**c** + 1/3**d**)	$\dfrac{2\varepsilon}{3}$	$\dfrac{2\varepsilon}{3}$	$\dfrac{2\varepsilon}{3}$
b' (= 1/3**a** + 1/3**c** + 1/3**d**)	$\dfrac{2\varepsilon}{3}$	$\dfrac{\varepsilon}{3}$	$\dfrac{\varepsilon}{3}$
c' (= 1/3**a** + 1/3**b** + 1/3**d**)	$\dfrac{\varepsilon}{3}$	$\dfrac{\varepsilon}{3}$	$\dfrac{2\varepsilon}{3}$
d' (= 1/3**a** + 1/3**b** + 1/3**c**)	$\dfrac{\varepsilon}{3}$	$\dfrac{2\varepsilon}{3}$	$\dfrac{\varepsilon}{3}$

$$\mathbf{p} = \begin{bmatrix} \varepsilon\left(1 - x_{\text{mix,a}} - x_{\text{mix,b}}\right) \\ \varepsilon\left(x_{\text{mix,b}} + x_{\text{mix,c}}\right) \\ \varepsilon\left(1 - x_{\text{mix,a}} - x_{\text{mix,c}}\right) \end{bmatrix} \tag{B-12}$$

As in the two dimensional case above, the mixture fraction, $\mathbf{x_{mix}}$, for a point of known *x-y-z* coordinates within a tetrahedron may be computed via Eq. (B-13)(B-10), a rearrangement of Eq. (B-12). Note that $x_{\text{mix,c}}$ is found by subtracting $x_{\text{mix,a}}$ and $x_{\text{mix,b}}$ from 1.

$$\begin{bmatrix} x_{\text{mix,a}} \\ x_{\text{mix,b}} \\ x_{\text{mix,c}} \end{bmatrix} = \frac{1}{2} \begin{bmatrix} -1 & -1 & -1 \\ -1 & 1 & 1 \\ 1 & 1 & -1 \end{bmatrix} \begin{bmatrix} \dfrac{x}{\varepsilon} - 1 \\ \dfrac{y}{\varepsilon} \\ \dfrac{z}{\varepsilon} - 1 \end{bmatrix} \tag{B-13}$$

Appendix C   MORE INFORMATION ON PARADIGMS A, B, & C

The key studies on reactions active for DPA methylation reported in the body of this dissertation were of acid catalysis in methanolic H_2SO_4 at room temperature (via the tetrahedral mechanism) and of direct methyl transfer in the heated GC inlet (via the S_N2 mechanism). Both of these studies were actually part of a more extensive set of investigations into the "standard" or "reference" protocol that was presented in Section 3.4.1 (Table 3-2), which involves adding methanolic sulfuric acid to spores one minute before adding TMA-OH. These investigations facilitated transitioning from **Paradigms A** to **B** to **C** (see Sections 1.4 and 10.1). **Paradigm A** was discredited by observing how little Me_2DPA is formed after one minute of acid exposure and by noting how rapidly Me_2DPA is hydrolyzed by addition of TMA-OH to the spore suspension, the process being accelerated by solvent evaporation on the wire (details presented in Chapter 5).

A key piece of evidence against **Paradigm B** came from a quick study on CaDPA in the presence of TMA-OH, TMA-MeSO$_4$, and TMA$_2$SO$_4$. The reagents were combined so that 60:1 ratios of TMA$^+$:CaDPA were obtained. The observed relative extents of Me_2DPA conversion were approximately 1:7:2 for TMA-OH, TMA-MeSO$_4$, and TMA$_2$SO$_4$, respectively. Although TMA-MeSO$_4$ possessed twice the total sulfate (as $MeSO_4^-$) compared to TMA$_2$SO$_4$ since the total TMA$^+$ was equal for both experiments, both $MeSO_4^-$ and SO_4^{2-} were in considerable excess relative to CaDPA ($MeSO_4^-$:CaDPA = 60:1 and SO_4^{2-}:CaDPA = 30:1). In both cases, more than sufficient SO_4^{2-} was available

to remove Ca^{2+} from CaDPA. The 3 to 4-fold increase in percent Me_2DPA yield observed

with 60:1 $MeSO_4^-$:CaDPA compared to 30:1 SO_4^{2-}:CaDPA was inconsistent with the

hypothesis that Ca^{2+} was removed by sulfate SO_4^{2-}, thus activating methylation by

TMA^+. Once DPA methylation was observed by the Na^+ salt of $MeSO_4^-$ *without* any

TMA^+ (data not shown), it became clear that $MeSO_4^-$ was an active methyl donor

(**Paradigm C**).

The advent of **Paradigm C** completely altered the interpretation of results for two

extensive thermochemolysis methylation studies involving spores, TMA-OH, and H_2SO_4

in MeOH, which had been conducted under the auspices of **Paradigm B**. For clarity, here

these studies are referred to as **Study I** and **Study II**, and the investigation reported in the

body of this dissertation that focuses on spore DPA methylation is called **Study III**. Due

to the shift in paradigms, **Studies I** and **II** were not discussed in the main body of this

work, but are appended because they provide supportive information.

C.1 Study I

Study I was designed to test two hypotheses: (1) Whether the addition of

methanolic "H_2SO_4" (at the time, $HMeSO_4$ formation was unknown) to spores before

TMA-OH truly improved Me_2DPA yields (presumably by breaking up/permeabilizing

spores in some manner so that the DPA was more free to react with TMA^+); and (2) if the

presence of SO_4^{2-} improved Me_2DPA yields (apparently by Ca^{2+} removal).

The quantitative basis for **Study I** involved holding constant the total quantity of

the ions TMA^+, OH^-, and SO_4^{2-} relative to the amount of spores, with each total ion

concentration being divided into 5 different mixture fractions (hence 5 points in Figure

C-1A). Each mixture point was conducted at 5 different ion:spore molar ratios as follows:

Assuming the total spore count in each Eppendorf tube was 2×10^9 spores, the reagents

were blended so that ratios of 2-, 4-, 6-, 8-, and 10×10^{10} ions:spore were obtained.

However, $MeSO_4^-$ formation occurring during storage of the methanolic H_2SO_4 stock

solution (which at the time was not recognized or followed) would have produced some

$MeSO_4^-$, so the actual mixture composition consisted of TMA^+, OH^-, SO_4^{2-}, and $MeSO_4^-$

. If it is assumed that all sulfate had become $MeSO_4^-$, then the mixture would appear as in

Figure C-1B. The actual mixture was probably some combination of the two that (if

known) could be represented by a tetrahedral diagram.
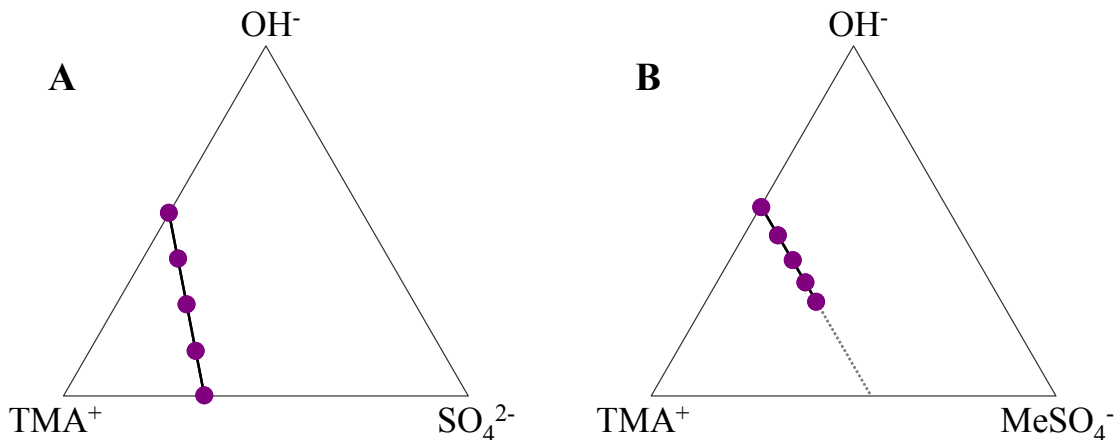
Figure C-1. Intended mixture design space for Study I (A) and possible actual mixture design space assuming complete conversion of H_2SO_4 to $HMeSO_4$ during H_2SO_4 storage (B).

Figure C-2A displays the mixture composition of **Study III** (from Figure 8-4B)

for purposes of comparison with **Study I** along with the possible actual mixture assuming

complete conversion of SO_4^{2-} to $MeSO_4^-$. Figure C-2B is another perspective of Figure

C-1B. Also included as Figure C-1C are data for 4 sets of mixtures experiments

conducted at "low" and "high" total ion concentrations (originally intended to be 2- and

10×10^{10} total ions:spore assuming no $MeSO_4^-$ had formed) with acid either preceding TMA-OH addition to spores by 1 minute or acid and TMA-OH being added simultaneously.

Unfortunately, due to the unquantified $MeSO_4^-$ formation, no definite, consistent basis for comparison exists. With $MeSO_4^-$ formation, the total number of ions:spore was not constant, and neither was the total concentration of methyl donating reagent. The latter quantity is estimated assuming 0.65 µL wire uptake and is indicated in Figure C-1C as nmol quantities of total methyl donor reagent (i.e., $TMA^+ + MeSO_4^-$)on the wire.

Figure C-2. (A) Design space for Study III (see Figure 8-4); (B) possible actual mixture for Study I assuming that all su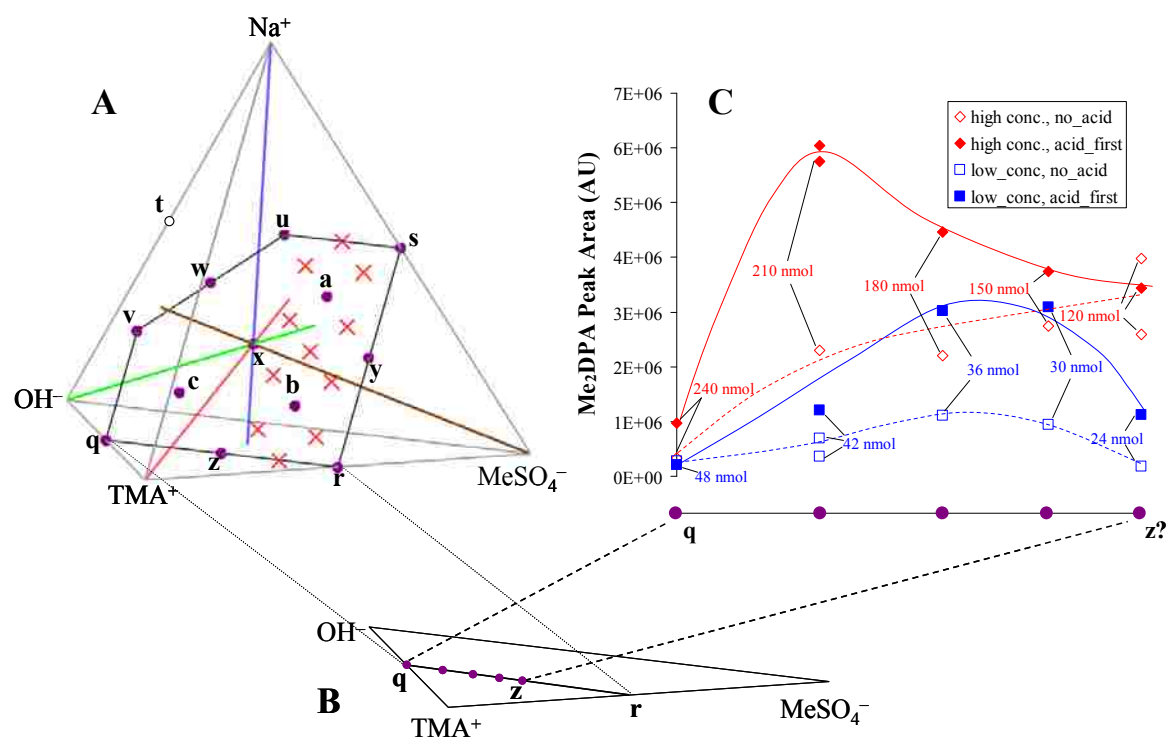lfate was actually $MeSO_4^-$ (see Figure C-1B); (C) experimental Me_2DPA peak area vs. fractional distance along line qz (numbers are nmol of total methyl donor assuming 0.65 µL volume uptake, and curves are a visual interpretation of the data only).

Although in retrospect **Study I** had problems, it provided two key pieces of information: First, it was obvious that addition of H_2SO_4 (and $HMeSO_4$) before TMA-OH significantly improves Me_2DPA yields, apparently by a factor of 1.5-2. Second, TMA-OH alone (point **q** in Figure C-1A-C) is not as effective as a mixture of TMA^+ and sulfuric acid.

C.2 Study II

In addition to the limitations indicated above, **Study I** did not report actual percentage yields of spore DPA. Consequently, **Study II** was conducted to quantify Me_2DPA yields obtained by TMA-OH addition alone (**Study IIa**) and by the combined H_2SO_4 + TMA-OH "reference" protocol (see Table 3-2), which became **Study IIb**. Me_2DPA percent yield was estimated by determining total spore DPA via procedures described in Section 3.4.3. **Study II** was conducted using an Agilent 6890 GC equipped with a flame ionization detector (FID) because it was thought that the nonlinearity in calibration curves seen in the GC-MS instrument (see Section 8.3.2) might be avoided by using the GC-FID instrument. (This hypothesis turned out to be false.) **Study II** also studied both methods' reproducibility.

In the interim between **Study I** and **Study II**, the reaction that produces $HMeSO_4$ during storage of H_2SO_4 in MeOH was discovered, so care was taken to use reagent in which this reaction had gone to completion (as judged by repeated titrations). However, the activity of $MeSO_4^-$ for methylation was *not* recognized until a test was conducted with DPA and $HMeSO_4$ in the absence of TMA^+ (data not shown) *after* **Study II** was complete. Since TMA^+ was thought to be the only active methyl donor, **Study II** utilized

constant total concentration of 500 mM TMA$^+$ as a basis for design. The concentrations of these methods (TMA-OH only vs. HMeSO$_4$ + TMA-OH) are given in Table C-1. Also included in Table C-1 are the linear and nonlinear models' predictions for the overall Me$_2$DPA yield.

The **Study IIa** mixture was identical to point **q** in Figure 8-10 and the **Study IIb** mixture was close to point z in Figure 8-10, prompting the inclusion of the point labeled **z'** in the same figure. The absolute quantities of methyl donors differed among **Study IIa**, **Study IIb**, and **Study III**. Consequently, the results are only approximately comparable. Generally, total DPA conversion averages about 5-10% at point **q** for both studies (Table C-1). The data at point **z** are not much different from point **q**, although the increased yields at **z'** compared to **q** evidently result from acid pre-addition and the presence of MeSO$_4^-$. Although the difference between the responses at points **q** and **z'** is statistically significant (9.1 vs. 14.5%; see Table C-1), overall it is small compared to the differences in the data of **Study III** where Na$^+$ was incorporated as a reagent since the overall yield approached 100% at some mixtures.

In conclusion, with the TMA-OH + HMeSO$_4$ mixtures of **Study I** and **Study II**, approximately 5-15% of the total spore DPA is converted to Me$_2$DPA. Unfortunately, the results of **Study II** are, like those of **Study I**, of limited utility since the basis for measuring reagents (constant TMA$^+$ amount) did not correspond to the actual mechanism (methylation by both TMA$^+$ and MeSO$_4^-$). Although experimental results were obtained using an unsatisfactory experimental design, careful study of the results of the flawed experiments in **Studies I** and **II** guided improved designs for later studies, which ultimately produced more definitive answers (i.e., **Study III**).

Table C-1. Analysis of experimental conditions and resultant Me$_2$DPA peak areas for experiments on spores conducted at points q, z, and z' in Figure 8-10. See text for description of experiments.

Study identity	Mean total spore DPA conc. (mM) or model type	Point q	Point z	Point z' "reference" protocol
"Study II" (an early study on BA spores)	BA: 3.81 ±0.79 mM	**9.1 ±1.2%**$^{\Diamond}$ C_{TMA^+} = 500 mM† $C_{MeSO_4^-}$ = 0 mM Me donor:DPA = 131	*N/A*	**14.5 ±1.7%**$^{\Diamond,\S}$ C_{TMA^+} = 500 mM $C_{MeSO_4^-}$ = 234 mM‡ Me donor:DPA = 193
"Study III" (study on BA and BG spores)	BA: 7.09 ±0.56 mM BG: 5.56 ±0.15 mM	BA = **2.5%**, BG = **6.2%** (mean = **4.4%**) C_{TMA^+} = 750 mM $C_{MeSO_4^-}$ = 0 mM Me donor:DPA = 106 for BA, 135 for BG	BA = **11.4%**, BG = **4.2%** (mean = **7.8%**) C_{TMA^+} = 500 mM $C_{MeSO_4^-}$ = 250 mM Me donor:DPA = 106 for BA, 135 for BG	*N/A*
Models of "Study III"	Model: **lm**	4.1%	11.9%	11.2%
	Model: **nlm_1**	0.1%	8.4%	7.1%
	Model: **nlm_2**	0.1%	9.2%	8.2%

$^{\Diamond}$ Reported errors are 95% confidence intervals on the mean.

§ Spores were exposed to HMeSO$_4$ for 1 minute *before* adding TMA-OH.

† 500 mM methyl donor concentration fixed at 500 mM instead of 750 mM since **Study II** pre-dated knowledge of the methylating activity of MeSO$_4^-$.

‡ The total Me donor concentration in this reference protocol, 734 mM (point **z'** in **Study II**), led to 750 mM as a basis for **Study III**.

Appendix D   PHYSICAL EFFECTS OF ACID TREATMENT ON SPORES

D.1 Facts about spore popping in water

From the literature, it is known that spores, but not vegetative cells, are structurally compromised and sometimes even ruptured when exposed to certain mineral acids [472, 473]. This phenomenon has been termed "acid popping" [474]. During this process, a localized extrusion of spore nuclear material occurs through the structures surrounding the spore core within a few minutes to about half an hour of exposure. Rupture takes place suddenly, without warning, after the spores have been in contact with the acid for times on the order of 1-10 minutes. It occurs at a range of temperatures (e.g., 4, 25, and 60°C [475, 476]). The rate is dependent on spore species [477] and spore strain, perhaps due to differences in coat morphology [478] and/or in the amount of spore cortex [472] or CaDPA. Individual spores in the same culture even respond differently, with all manner of degrees of rupture [479]. Typical effects are presented in Figure D-1: Image A shows an untreated spore and images B, C, and D reveal the extrusion of core contents outward from the center, causing the outer coat to bulge. The core wall (part adjacent to the inner membrane) is convoluted and folded following rupture [480], indicative of its function of exerting an inward force against the core [61, 131].

The spore rupture mechanism has been explained as follows [61, 476]: the penetration of suitable acids into the core causes a rapid transient in osmotic pressure that

results from the dissociation of core CaDPA [and perhaps acid hydrolysis of other complexes] against the surrounding cortex and other spore integuments, through which these ions may yet remain quite impermeable [481]. Apparently, a rapid influx of water from the surrounding aqueous solution occurs, driven by the energy of solvating the "freed" ions and possibly by the increased membrane permeability induced by the strong acid. Only strong acids with a soluble calcium salt [e.g., $CaCl_2$, $Ca(NO_3)_2$, or $Ca(COOH)_2$ from HCl, HNO_3, and formic acid, respectively] cause spore popping [40, 61, 472, 475-477]; acids with insoluble calcium salts [e.g., $CaSO_4$ or $CaHPO_3$, from H_2SO_4 and H_3PO_4, respectively] do not [61, 107, 482, 483].
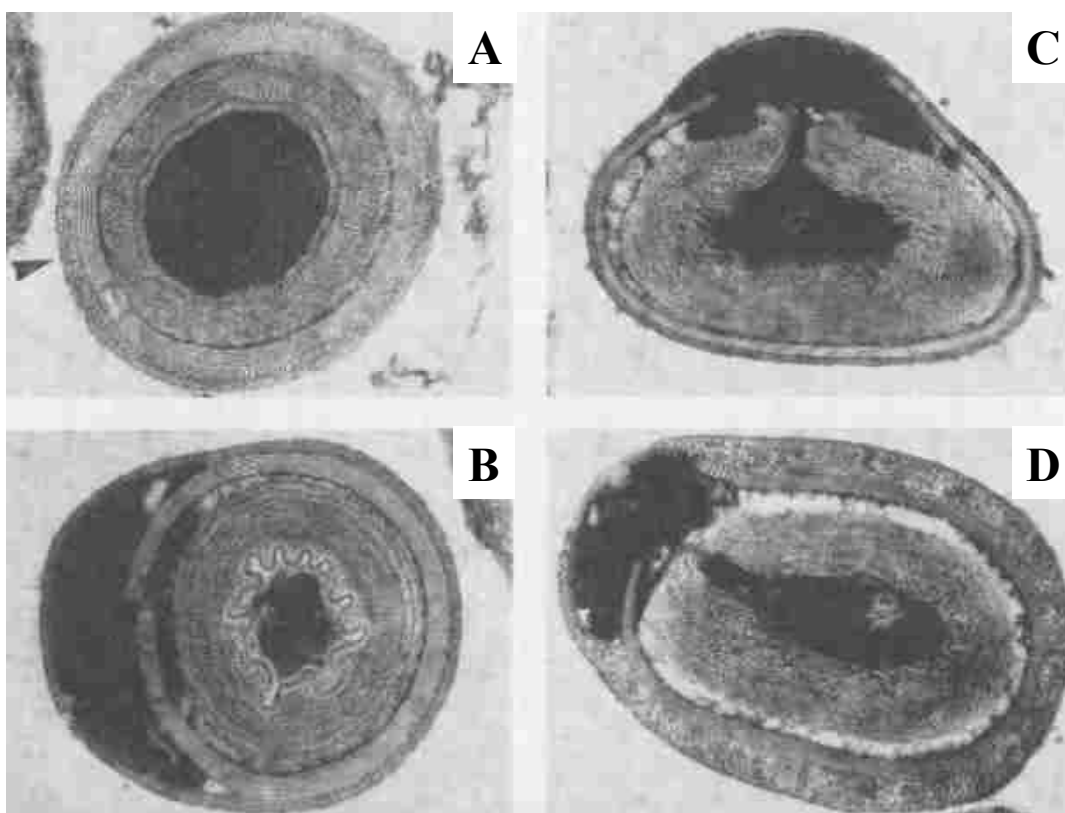
Figure D-1. Sections of *B. acidocaldarius* spores exposed to HCl at pH 0 at 55°C for 60 minutes [480]. See text for details.

Furthermore, only mature, refractile spores that contain CaDPA burst [61, 481]; calcium deficient spores do not [476, 484], nor do germinated spores [475]. Higher acid concentration accelerates the reaction, e.g., spores of *Metabacterium polyspora* explode only 1-2 min after treatment with 2 N HCl, whereas 1 N HCl requires 5-10 min [472].

Just because an acid does not pop spores does not imply that it does no damage to them. For example, the effects of HNO_3, HCl, H_2SO_4, and H_3PO_4 (the order of most to least effective for preparing spores for effective staining prior to visible microscopy) were studied. At room temperature and in 5 min, 12 N HNO_3 and HCl produced "small ruptures…[that] extruded spore material." At the same concentrations and at up to 10 minutes exposure, H_2SO_4 and H_3PO_4 did nothing. Higher concentrations of these latter two acids (28.4 and 44 N, respectively) at higher times (10 min) were required to effect spore destruction, and the effect was different than with HNO_3 or HCl. The resultant spores were enlarged, flattened, and collapsed, appearing like spores do following proteolytic enzymatic digestion [485].

Acid popping has been used to enhance the extraction of material from spores. For example, the tedious procedure of dry rupture of large quantities of spores for releasing a suite of acid-soluble proteins located in the core was avoided by acid popping in 2N HCl either for 30 minutes at 4°C [486] or 20 minutes at 20°C [481]. Exposure to 1 N HCl in water for 90 minutes released DPA and acid-soluble proteins [487].

D.2 Conjectures about spore popping in MeOH

The author was unable to find information discussing the effects of any solvent other than water on spore popping. Since MeOH was employed as the primary solvent for

the studies in this dissertation, a brief discussion about the possibility of acid popping in MeOH is in order.

Methanol, like water, is a polar, protic, hydrogen bonding solvent. However, the substitution of one of water's hydrogens by a methyl group to form MeOH leads to important differences. First, MeOH is larger than water (molecular mass 32 vs. 18 g/mol, respectively), and second, the molecule is less polar. Its dielectric constant is 32.7, while water's is 78.3 [488]. Since a high dielectric constant favors solvated ions [387, 489], ion pairing (e.g., between Ca^{2+} and DPA^{2-}) is much more favorable in MeOH. Hence, osmotic shock to the spore is much *less* likely and thus so is spore popping in this solvent.

Significant destruction of spores in acidic MeOH for several minutes at room temperature is probably unlikely given a few other facts. Chemical activity of H^+ is reduced in MeOH compared to H_2O (see Appendix E). As discussed in Section 9.4, procedures for hydrolysis of various biopolymer-containing materials required high temperatures and hours for complete digestion, and acidic MeOH was described as less effective at cleaving highly ordered polysaccharides than is aqueous acid [433].

Nevertheless, studies summarized in Appendix C provide evidence that $HMeSO_4$ addition to spores 1 minute prior to TMA-OH weakens or permeabilizes them in some manner. Guided by evidence of Setlow *et al.* that acid weakens the inner membrane [107], the author of this dissertation believes that the acid affects the spore's inner membrane, perhaps by modifying proteins therein, which allows for more facile diffusion of CaDPA outward and possibly reagent diffusion inward.

A first simple test of this idea would be to sample (e.g., by LC) the supernatant of spores suspended in a methanolic H_2SO_4/$HMeSO_4$ solution at different time intervals to see how quickly DPA is released under such conditions. Transmission electron microscopy of thin sections of spores thus exposed would assist in determining which structures are damaged most rapidly. However, the results of such studies are not relevant to the current best protocol in which acid-pretreatment is avoided altogether.

Appendix E   DPA PROTONATION BEHAVIOR AND pK$_a$

Many aspects of the physical and chemical behavior of DPA and its derivatives are explained by their protonation behavior. Protonation determines a molecule's (1) overall charge and (2) internal electron density/polarization. As mentioned in Sections 2.2.3.2 and 2.2.5.2, both factors influence reactivity towards methylation, hydrolysis, and other reactions. Additionally, since solubility and multi-phase partitioning behavior depend on charge/extent of ionization, LC retention/separation behavior and uptake by SPME are influenced by protonation. Electrospray ionization efficiency (e.g., in ESI-TOF mass spectrometry) is dependent on the analyte's affinity for protons, which directly influences the instrument's response factor and hence sensitivity. Finally, the polarization of a molecule's electrons affects its spectroscopic behavior in UV-vis absorption, Raman, and NMR spectroscopy. Although changes in these properties may be very useful since they indicate the extent of protonation, chelation, and reaction (e.g., methylation), quantitative errors result if the unknown sample and calibration material are not present in the same matrix. For example, as discussed in Section 8.3.7, the UV absorption of H$_2$DPA is different enough from that of Na$_2$DPA and CaDPA that quantitative discrepancies are observed in solutions of the same concentration. These observations are substantiated by published UV absorption spectra for DPA, which differ at various pH and chelation conditions [181, 428-430].

The purpose of this chapter is to provide quantitative estimates of the protonation of DPA and its methylated derivatives and to use this information as a basis for discussing experimental observations. Even though DPA is the focus, the principles and methods discussed are generally applicable to other molecules.

Because DPA is acidic overall, its (de)protonations and those of its derivatives occur under acidic conditions. Therefore, the properties of solutions acidic in the Brønsted sense (i.e., H^+ concentration exceeds that of OH^-) are discussed rather than properties of basic solutions.

E.1 Review of acid dissociation, pH, and pKₐ

General (de)protonation of a molecule "HA" to form "A" and "H^+" is indicated as a chemical reaction via Eq. (E-1). The notation "H^+" is employed to indicate that some species other than A (typically solvent) is protonated.[64] K_a is HA's acid dissociation constant [Eq. (E-2)], pK_a is the negative logarithm of K_a [Eq. (E-3)], and a denotes activity.

$$HA \leftrightharpoons H^+ + A \tag{E-1}$$

$$K_a = \frac{a_{H^+} a_A}{a_{HA}} \tag{E-2}$$

$$pK_a = -\log\left(\frac{a_{H^+} a_A}{a_{HA}}\right) \tag{E-3}$$

---

[64] In this notation, the charge of HA and its deprotonated form, A, are not given since these charges vary depending on the molecule and in order to conserve space in the equations. However, the charge of A is always one less than HA.

pK$_a$ informs about a molecule's affinity for protons and is related (under isothermal conditions) to $\Delta G°$ of the dissociation [Eq. (E-1)] by a constant as shown by Eq. (E-4). Thus, influences of pK$_a$ are manipulations on $\Delta G°$ "in disguise" [490].

$$\Delta G° = R\,T\,\ln(10)\,pK_a \qquad \text{(E-4)}$$

The definition of molar-based pH, Eq. (E-5), is applied to Eq. (E-3) and the latter rearranged to obtain Eq. (E-6).

$$pH = -\log\left(a_{H^+}\right) \qquad \text{(E-5)}$$

$$pK_a = -\log\left(a_{H^+}\right) - \log\left(\frac{a_A}{a_{HA}}\right) \qquad \text{(E-6)}$$

Because multiple conventions for preparing/measuring solution concentrations exist, activities and hence pH and pK$_a$ values in Eqns. (E-2) through (E-6) must be referenced to the same standard conditions. Molarity and molality are the two convenient standard measurement conventions; accordingly, Eqns. (E-7) and (E-8) apply, where molar and molal activity coefficients and are written as f and γ, respectively, and molar and molal concentrations are indicated by C and m as either variables or subscripts to pH and pK$_a$. The subscripts "A" and "HA" retain the meanings as summarized above.

$$pH_C = pK_{a,C} + \log\left(\frac{f_A\,C_A}{f_{HA}\,C_{HA}}\right) \qquad \text{(E-7)}$$

$$pH_m = pK_{a,m} + \log\left(\frac{\gamma_A\,m_A}{\gamma_{HA}\,m_{HA}}\right) \qquad \text{(E-8)}$$

Note that $pH_C \neq pH_m$ except in very dilute, aqueous solutions, as indicated by Eq. (E-9), where ρ_s^* is the pure, acid-less solvent's density and ρ° is 1 kg/L [491].[65] $pK_{a,C}$ and $pK_{a,m}$ are likewise related [Eq. (E-10)].

$$pH_C = pH_m - \log\left(\frac{\rho_s^*}{\rho^\circ}\right) \tag{E-9}$$

$$pK_{a,C} = pK_{a,m} - \log\left(\frac{\rho_s^*}{\rho^\circ}\right) \tag{E-10}$$

The ratio $\dfrac{C_A}{C_{HA}}$ (identical to $\dfrac{m_A}{m_{HA}}$) indicates the true extent of (de)protonation of species A (e.g., DPA). Although $\dfrac{C_A}{C_{HA}}$ may be directly measured spectroscopically for some cases, it may be inconvenient to do so. However, the ratio may be estimated via pH_C and $pK_{a,C}$ if it is assumed that $\dfrac{a_A}{a_{HA}} = \dfrac{C_A}{C_{HA}}$ (i.e., either $f_A = f_{HA}$ or, even more ideally, $f_A = f_{HA} = 1$, which is approached at low concentrations of A and HA). These assumptions produce the Henderson-Hasselbalch equation, Eq. (E-11), from which the desired quantity, $\dfrac{C_A}{C_{HA}}$, may be estimated by rearrangement to Eq. (E-12).

$$pH_C = pK_{a,C} + \log\left(\frac{C_A}{C_{HA}}\right) \tag{E-11}$$

$$\frac{C_A}{C_{HA}} = 10^{pH_C - pK_{a,C}} \tag{E-12}$$

---

[65] Reference [491] reports Eq. (E-9) incorrectly.

pH has a well-defined theoretical underpinning [e.g., Eq. (E-5)] that is not detectible in practice since a_{H^+} cannot be measured independently from the presence and influence of some counterion. Consequently, the practical basis for pH is usually the difference between potentials generated by a sample and reference galvanic cells sensitive to some elusive feature very closely related to a_{H^+} that is treated as equivalent to H^+ activity [492, 493].

pK$_a$ values have been determined for compounds either experimentally (e.g., via titrations, UV absorbance, capillary electrophoresis, liquid chromatography) and computationally (e.g., using the Hammett and Taft equations or other software packages) [402, 491, 494, 495].

E.1.1 Solvent effects on pH and pK$_a$

Commonly, pK$_a$ and pH are measured or determined in aqueous solutions. However, for Eqns. (E-7) through (E-12) to be valid, the pH measurement must be matched with the corresponding convention of pK$_a$ (indicated by Table E-1). This requirement exists because activities are not equivalent in different solvents. To indicate the solvent type employed, IUPAC [491, 495] recommends labeling pK$_a$ and pH with a left-*super*scripted letter to indicate the media in which they are *measured*, and a left-*sub*scripted letter to indicate to which media they are *referenced*. The letters "w" or "s" are employed to indicate that water or another solvent (other than 100% water) is employed in the pH or pK$_a$ determination. Table E-1 summarizes these conventions.

Table E-1. Scenarios for pH and pK_a.

Sample solution	Reference solution	pK_a value for Eq. (E-7) validity	pH scale
Water	Water	$^w_w pK_a$	$^w_w pH$
Solvent	Water	$^s_w pK_a$	$^s_w pH$
Solvent	Solvent	$^s_s pK_a$	$^s_s pH$

E.1.2 Predicting non-aqueous pK_a values from aqueous data

Published pK_a values are, strictly speaking, valid only for the solvent in which they were measured (often at 0.1 M or 0.1 m total ionic strength in water[66]). pK_a values must be adjusted for different solvent environments. One method for interconversion between $^s_s pK_a$ and $^w_w pK_a$ is via a linear empirical correlation in the form of Eq. (E-13). Parameter values α and β are functional-group-specific. Best-fitting values have been determined as functions of solvent composition for aliphatic and aromatic acids, amines, and pyridyl compounds [262, 263, 491, 495, 496].

$$^s_s pK_a = \alpha \, ^w_w pK_a + \beta \tag{E-13}$$

Conversion between $^s_s pK_a$ and $^s_w pK_a$ is straightforward since the two differ by a constant, solvent-dependent parameter, δ, as shown by Eq. (E-14) [491, 495].

$$^s_w pK_a = ^s_s pK_a + \delta \tag{E-14}$$

Protons have a marked preference for water over methanol [492], which was noted previously to inhibit acid-catalyzed methylation activity (Section 5.2.2). This same

---

[66] For the computations in this appendix, solvent ionic strength is ignored, but solvent identity is not.

feature is responsible for a sharp increase in the pK_a (i.e., $_s^s pK_a > _w^w pK_a$) for acids of all charge types as water concentration becomes low unless the organic solvent with which it is blended is more basic than water [492]. MeOH is more acidic than water, and pyridine less acidic than water. Although the pK_a of pyridine and aliphatic amines change very little when MeOH replaces H_2O as a solvent, pK_a values of carboxylate groups change substantially, increasing by approximately 3-5 units (following an initial decrease [491]).

E.1.3 pH conversions for different solvents

Like for pK_a, approximations to the solvent effects on pH are also possible. For example, Eq. (E-15) is identical in form to Eq. (E-14), so a conventional pH probe referenced to an aqueous solution may be employed for $_w^s pH$ measurements, which are then converted to $_s^s pH$ [491, 495]. As a note of caution, like $_w^w pH$ measurements at the extremes of the pH scale (i.e., <3 and >11), $_w^s pH$ measurements may be influenced appreciably by a non-constant junction potential between the standard and reference cells [492], so $_w^s pH$ measurements must be interpreted carefully.

$$_w^s pH = _s^s pH + \delta \qquad \text{(E-15)}$$

No equation of the form of Eq. (E-13) appears to be available for converting between $_s^s pH$ and $_w^w pH$. One relationship is that of Eq. (E-16), which is an empirical correlation developed between $_w^s pH$ and $_w^w pH$. Here, ϕ, m_{pH}, and d_{pH} are, respectively, the volume fraction of MeOH, the proportionality constant for pH change, and a *buffer-dependent* parameter [495]. Unfortunately, this relationship does not appear to have been

applied to strong acids such as H_2SO_4, and so some other means for determining $_s^s pH$

must be employed.[67]

$$_w^s pH = _w^w pH + m_{pH} \phi^{d_{pH}} \qquad \text{(E-16)}$$

E.1.4 Use of published activity coefficient data to estimate pH

In the absence of direct $_w^w pH$, $_w^s pH$, or $_s^s pH$ measurements, use of actual

physical concentration of dissolved H^+-bearing acid molecules in place of a_{H^+} is *not* a

good approximation for proton activity unless the solution is dilute and contains a strong

acid that dissociates almost completely in the solvent (i.e., K_a is high). There are two

reasons for this. First, the polarity (dielectric constant) of most solvents (including

MeOH) is much lower than the polarity of water, which increases ion pairing and inhibits

acid dissociation. Although an undissociated proton can be catalytically active (e.g., by

hydrogen bonding), its activity in the undissociated state is attenuated significantly.

Second, if the solution possesses a high ionic strength due to the acid or other dissolved

solutes, H^+ activity is also reduced.

Unfortunately, since individual ions' activities cannot be measured independently,

exact values of f_i or γ_i are intractable. H^+ activity in solution may be approximated via

mean ionic activity coefficients, as shown by Eqns. (E-17) and (E-18). The mean ionic

activity coefficients are denoted by $f_\pm$ or $\gamma_\pm$ for molarity or molality, respectively, and

---

[67] A more thorough literature search may turn up more information for pH conversions involving strong acids such as H_2SO_4. Correlations for strong acids have probably not been developed, however, since the main application is liquid chromatography, which does not usually employ strong, non-buffered acids.

the mean ionic concentrations are denoted, in the same order, by $C_{\pm}$ and $m_{\pm}$. Detailed

derivations for these equations and variable definitions are given elsewhere [407, 493].

$$a_{i,C} = f_{\pm}C_{\pm} \tag{E-17}$$

$$a_{i,m} = \gamma_{\pm}m_{\pm} \tag{E-18}$$

Experimentally-determined mean ionic activity coefficients, $f_{\pm}$ and $\gamma_{\pm}$, have

been published for various acids in different solvents, including H_2SO_4 in water and

MeOH. The activity for each ion is thus estimated by using $f_{\pm}$ or $\gamma_{\pm}$ along with Eqns.

(E-17) or (E-18) according to the molar and molal scales, respectively. Consequently, a

means for estimating $_s^s pH$ from the known acid concentration and *mean* ionic activity

coefficient data in the solvent of interest is possible via the mean ionic concentration, $C_{\pm}$

or $m_{\pm}$.

For 1-1 dissociations (e.g., HCl), $C_{\pm}$ or $m_{\pm}$ equal to total HCl molarity (C_{HCl}) or

molality (m_{HCl}). Eqns. (E-19) and (E-20), respectively, are estimates for $a_{H^+,C}$ and $a_{H^+,m}$.

$$a_{H^+,C} \approx f_{\pm}C_{HCl} \tag{E-19}$$

$$a_{H^+,m} \approx \gamma_{\pm}m_{HCl} \tag{E-20}$$

However, for 2-1 dissociations such as with H_2SO_4, Eqns. (E-21) and (E-22)

result because of the convention used to define $C_{\pm}$ and $m_{\pm}$.

$$a_{H^+,C} \approx 4^{\frac{1}{3}} f_{\pm}C_{H_2SO_4} \tag{E-21}$$

$$a_{H^+,m} \approx 4^{\frac{1}{3}} \gamma_{\pm}m_{H_2SO_4} \tag{E-22}$$

Conversions between molarity and molality activities may be necessary because literature activity coefficient values are usually reported as $\gamma_\pm$, while $f_\pm$ values are required for the more convenient measure of molarity. Eq. (E-23) indicates the relationship between $f_\pm$ and $\gamma_\pm$, where ρ_s and ρ_s* are, respectively, actual density of the acidic sample solution and the density of pure solvent without any acid [407] (note $\rho_s = \dfrac{C_i}{m_i}$ and $\displaystyle\lim_{C_i, m_i \to 0} \dfrac{C_i}{m_i} = \rho_s*$, where i indicates any dissolved species).

$$f_\pm = \frac{\rho_s*}{\rho_s} \gamma_\pm \tag{E-23}$$

E.2 Estimates of pH in methanolic H₂SO₄

Shibata *et al.* [497] determined $\gamma_\pm$ at 25°C for 0-70 wt% (0-75 vol%) MeOH in H$_2$O with H$_2$SO$_4$ concentrations ranging from 0-0.5 m (molal), and Hussain *et al.* found $\gamma_\pm$ at 32°C for 100% MeOH and 100% H$_2$O with H$_2$SO$_4$ from 0-4 m. Both studies treated H$_2$SO$_4$ as a 2-1 electrolyte, so Eqns. (E-21) and (E-23) serve as the basis for computation.[68] The estimates for pH$_C$ in 100% MeOH, 100% H$_2$O, and a 69:31 volumetric H$_2$O:MeOH blend (the initial composition of the LC mobile phase) are plotted as functions of molarity in Figure E-1. Activity coefficient values for the MeOH/H$_2$O blend were obtained by interpolation within Shibata *et al.*'s data.

Additionally, the pH$_C$ of H$_2$SO$_4$ in water was estimated from Modro *et al.*'s [498] published approximation to H$^+$ activity, denoted as $a*_{H^+}$ in Eq. (E-24). In that equation,

---

[68] This author is unaware of the impact that partial dissociation of H$_2$SO$_4$ has on the accuracy of this method.

f_{TEA^+} is the activity coefficient of the tetraethylammonium cation (again, activities of individual ions cannot be determined independently from one another and so a_{H^+} does not appear by itself) [498].

$$a*_{H^+} = \frac{a_{H^+}}{f_{TEA^+}} \qquad \text{(E-24)}$$

Also plotted in Figure E-1 are the erroneous pH_C values obtained by assuming ideal solution behavior ($a_{H^+} = C_{H^+}$) for 1-1 and 2-1 dissociations of H_2SO_4; i.e.,

$pH_C = -\log(C_{H_2SO_4})$ and $pH_C = -\log(2C_{H_2SO_4})$, respectively.

None of the foregoing computations for pH_C accounted for solvent autodissociations since all acid concentrations were greater than 5 mM in all cases, which is significantly higher than the H^+ concentration occurring due to autodissociation (i.e., about 10^{-4} mM in neutral water, and somewhat less in MeOH). The consequence of this is that the true inflection point of the pH_C vs. acid concentration curves, which occur on the y-axis, are not apparent in Figure E-1. Had they been included, the pH_C curves would intersect the y-axis at about 7 for water and somewhat greater than 7 for MeOH, all depending on which autodissociation constant is used for each solvent [499].

Several important features are indicated by Figure E-1. First, the "ideal" behavior of a 1-1 dissociating H_2SO_4 solution results in a pH that is approximately 1 unit below the pH computed from $\gamma_\pm$ data in H_2O at H_2SO_4 concentrations exceeding 1 M. At 0.01-0.5 M, the discrepancy in ideal vs. apparent acidity decreases as concentration decreases. These features are qualitatively consistent with expectations about reduced acidity at high H^+ concentration. The pH predicted from Modro *et al.*'s equation is much lower than that

predicted by ideal 2-1 dissociation of H_2SO_4. However, such low "pH" almost certainly

results from the value of f_{TEA^+} being lower than 1. Modro *et al.*'s pH values at 0.5 M

H_2SO_4 merge with the ideal H^+ dissociation curves, and presumably the former would

approach the other aqueous pH measurements/predictions at concentrations below 0.1 M

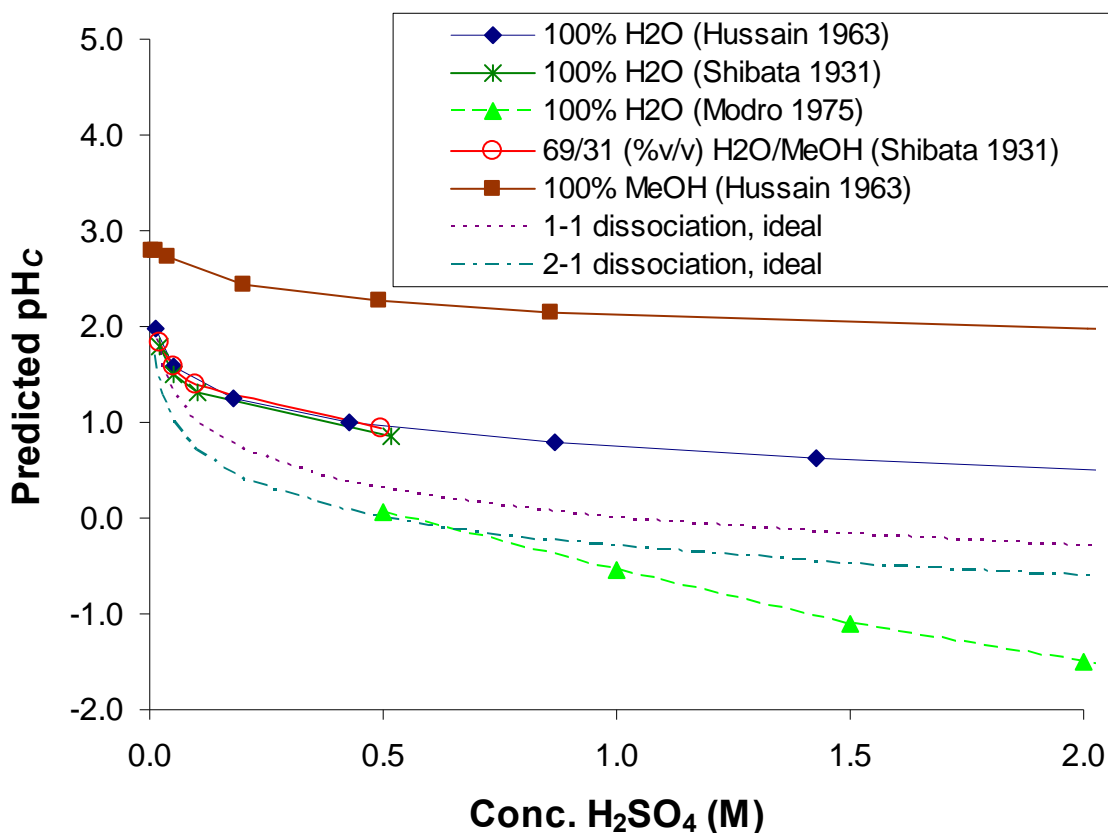H_2SO_4. Unfortunately, these conditions were not studied by Modro *et al.*

Figure E-1. pH vs. molar concentration of H_2SO_4 in H_2O, MeOH, and a H_2O-MeOH mixture (data from [497, 498, 500]).

The agreement in pH_C values from Shibata and Hussain's reported $\gamma_\pm$ values in

100% water is close. In addition, the 31 vol% H_2O prediction is nearly identical to the

100% H_2O cases, indicating that the significant aberrations in pH do not occur at

intermediate MeOH content in acidic aqueous solutions. However, in 100% MeOH, at any given acid concentration H^+ activity is much lower in MeOH than in H_2O and so pH is higher in the former solvent (though pK_a of an analyte may be lower or higher).

It has been noted in other literature [401, 501] that bisulfate (HSO_4^-) hardly dissociates at all in methanolic H_2SO_4 solutions, so the assumption of a 2-1 electrolyte dissociation may be poor for MeOH solutions. In addition, the acid-catalyzed methylation of H_2SO_4 via the reverse of Eq. (4-16) (see also Section 7.1) would have produced the 1-1 dissociating electrolyte $HMeSO_4$. Neither of the above facts were mentioned by either Shibata or Hussain. In the present context where $HMeSO_4$ is desirable as a methylating agent for GC, the acidity of $HMeSO_4$ is probably a better feature to study than H_2SO_4. Additionally, the pH (as with other solution activity parameters) depends on the other ions present in the mixture [e.g., 502]. A rigorous analysis could account for these effects if greater accuracy is required.

In the absence of more definitive information and to avoid more complex computations, the acidity of H_2SO_4 solutions is assumed to be represented by the 2-1 electrolyte dissociation model with the attendant $\gamma_\pm$ values from which pH_C is estimated. This assumption forms the basis for computations now described.

E.3 *Estimating the relative ratios of protonated DPA species*

As indicated in the introduction to this appendix chapter, the (de)protonation of DPA was relevant to the results presented in Chapter 5, namely, the DPA acid-catalyzed methylation studies in 100% MeOH (Sections 5.1 and 5.2) and base-promoted hydrolysis studies in ~5.6 M H_2O in MeOH (Sections 5.3 and 5.4). Furthermore, analytical methods

were impacted by (de)protonation of DPA and its methylated derivatives, including the LC separation, UV absorbance spectroscopy, and electrospray ionization mass spectrometric analysis (see Sections 3.3.2 and 3.4.3). The protonation behavior of DPA in these MeOH-containing solvents must be inferred in some manner since experimental pK_a values for DPA have only been determined in aqueous solutions.

E.3.1 Estimates for pK_a of DPA in MeOH and MeOH-H$_2$O

A series of figures is presented below to illustrate the (de)protonation network of DPA derivatives. Because the discussion considers the multiple protonations that may occur on a given molecule, for convenience the set of protonated forms is indicated by H_nA, where n is an integer from the set {0, 1, 2, or 3}. For example, H_nDPA refers to the collection H_3DPA$^+$, H_2DPA, HDPA$^-$, and DPA^{2-}. Figure E-2 illustrates DPA protonations alongside those of a homologous chemical, isophthalic acid (IPA). Similarly, Figure E-3 and Figure E-4 illustrate the respective (de)protonations of Me$_1$DPA and Me$_2$DPA. (De)protonations of monopicolinic acid (MPA) and benzoic acid (BA) are included in Figure E-5 because these molecules are similar to DPA and IPA. Where published pK_a values are available, they are included in the figures (none were available for Me$_1$DPA and Me$_2$DPA so these values were assumed to be similar to published pK_a values of DPA, MPA, and pyridine). References to these values plus assumed values and estimates for 100% MeOH are included in Table E-4.
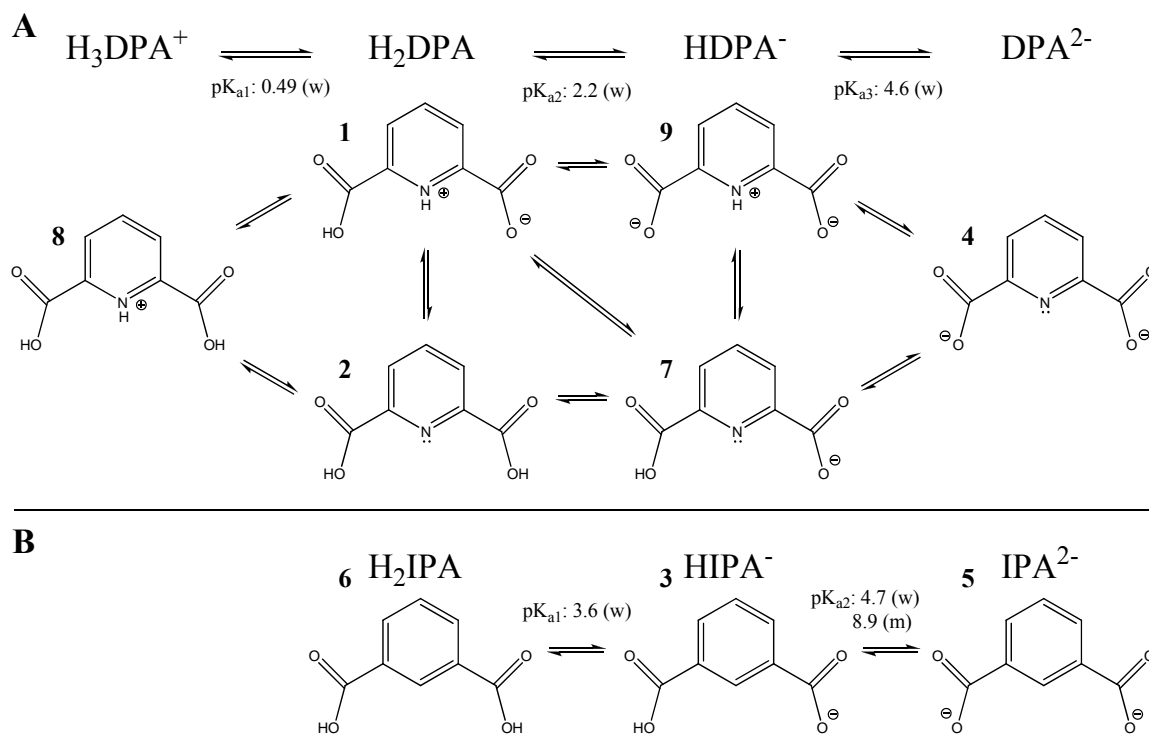
Figure E-2. (De)protonation equilibria of (A) dipicolinic acid (DPA) and (B) isophthalic acid (IPA). Published pK_a values are indicated for water (w) and (if available) methanol (m); see Table E-4.
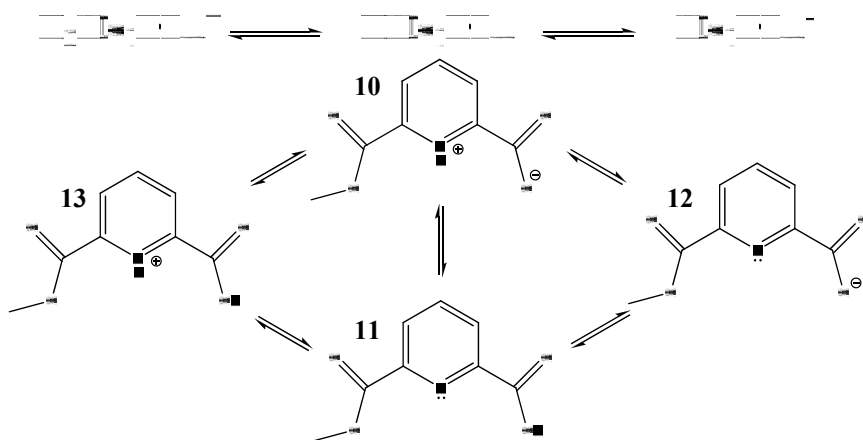

Figure E-3. Possible (de)protonations of the monomethyl ester of dipicolinic acid (Me$_1$DPA).

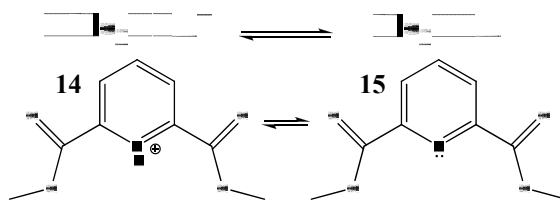**Figure E-4.** (De)protonation of dimethylated dipicolinic acid (Me$_2$DPA).

315

pK$_a$ values alone do not distinguish between pairs of prototropic tautomers of DPA (**1** vs. **2**, and **9** vs. **7** in Figure E-2, or **10** vs. **11** in Figure E-3). Which of these species dominates can be inferred from pK$_a$ data for similar but simpler compounds plus experimental observations, as described below.

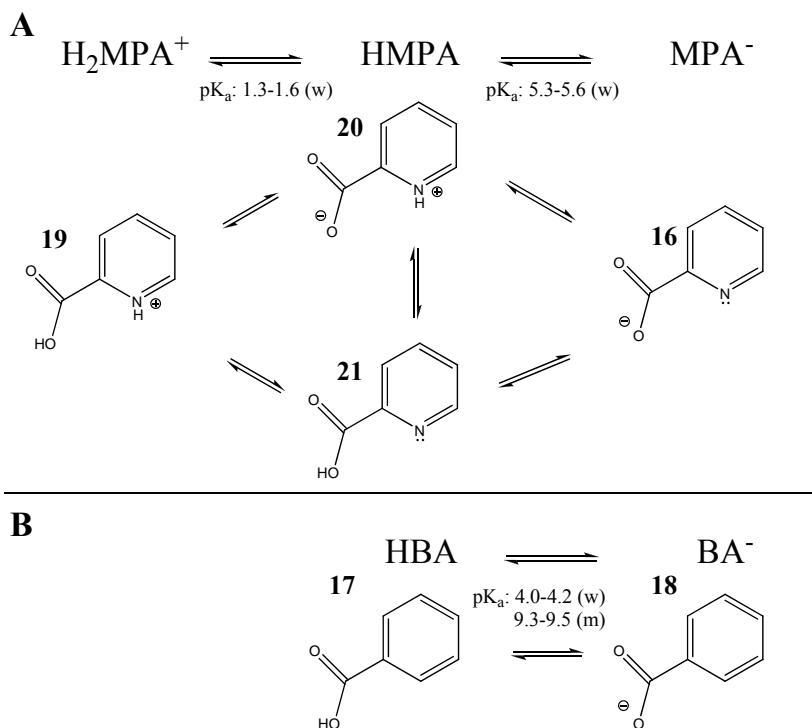**Figure E-5.** (De)protonation equilibria of (A) monopicolinic acid (MPA) and (B) benzoic acid. pK$_a$ values given for water (w) and (where available) methanol (m).

E.3.2 Example computation for the (de)protonation states of DPA

A method is now given for computing the relative abundances of H$_n$DPA. This specific example illustrates a generally applicable approach useful for species that can gain or lose protons.

Eqns. (E-25), (E-26), and (E-27) are, respectively, the deprotonation equilibria of H_3DPA^+, H_2DPA, and $HDPA^-$.

$$H_3DPA^+ \leftrightarrows H_2DPA + H^+ \tag{E-25}$$

$$H_2DPA \leftrightarrows HDPA^- + H^+ \tag{E-26}$$

$$HDPA^- \leftrightarrows DPA^{2-} + H^+ \tag{E-27}$$

Applying the assumptions used to obtain Eq. (E-11) (i.e., $f = 1$ for all species but H^+), Eqns. (E-28), (E-29), and (E-30) result.

$$\frac{C_{H_2DPA}}{C_{H_3DPA^+}} = 10^{pH_C - pK_{a1,C}} \tag{E-28}$$

$$\frac{C_{HDPA^-}}{C_{H_2DPA}} = 10^{pH_C - pK_{a2,C}} \tag{E-29}$$

$$\frac{C_{DPA^{2-}}}{C_{HDPA^-}} = 10^{pH_C - pK_{a3,C}} \tag{E-30}$$

The relative amounts of all four H_nDPA species are estimated by solving Eqns. (E-28), (E-29), and (E-30) simultaneously with Eq. (E-31), which is the material balance on all H_nDPA species.

$$C_{H_3DPA^+} + C_{H_2DPA} + C_{HDPA^-} + C_{DPA^{2-}} = C_{DPA\_tot} \tag{E-31}$$

One convenient method for solving the relative proportions of all H_nDPA species is to linearize Eqns. (E-28) through (E-30) and combine Eqns. (E-28) through (E-31) into an expression of the form $\mathbf{Ax} = \mathbf{b}$, where the matrix $\mathbf{A}$ is given by Eq. (E-32), the unknown concentration vector $\mathbf{x}$ by Eq. (E-33), and the constant vector $\mathbf{b}$ by Eq. (E-34).

Eq. (E-35) then becomes the solution for the equilibrium distribution of H_3DPA^+,

H_2DPA, $HDPA^-$, and DPA^{2-} as a function of pH.

$$\mathbf{A} = \begin{bmatrix} 10^{pH_C - pK_{a1,C}} & -1 & 0 & 0 \\ 0 & 10^{pH_C - pK_{a2,C}} & -1 & 0 \\ 0 & 0 & 10^{pH_C - pK_{a3,C}} & -1 \\ 1 & 1 & 1 & 1 \end{bmatrix} \qquad \text{(E-32)}$$

$$\mathbf{x} = \begin{bmatrix} C_{H_3DPA^+} \\ C_{H_2DPA} \\ C_{HDPA^-} \\ C_{DPA^{2-}} \end{bmatrix} \qquad \text{(E-33)}$$

$$\mathbf{b} = \begin{bmatrix} 0 \\ 0 \\ 0 \\ C_{DPA\_tot} \end{bmatrix} \qquad \text{(E-34)}$$

$$\mathbf{x} = \mathbf{A}^{-1}\mathbf{b} \qquad \text{(E-35)}$$

Setting the total concentration of DPA species, C_{DPA_tot} , equal to 1 concentration

unit (e.g., mM or M) makes the equilibrium concentrations $C_{H_3DPA^+}$, C_{H_2DPA} , C_{HDPA^-} ,

and $C_{DPA^{2-}}$ (i.e., together referred to as $\mathbf{x}$) equal to their relative proportions. Again,

effects of total solution ionic strength are inconsequential since f is assumed to be unity

for all species except H^+ and so total DPA concentration is insignificant.

By this method, Figure E-6 was generated for the DPA, Me_1DPA, and Me_2DPA

protonation behavior on the 0-14 pH scale using nominal values of pK_a for H_3DPA^+,

H_2DPA, and $HDPA^-$ plus estimated pK_a values for $H_2Me_1DPA^+$, HMe_1DPA, and

HMe_2DPA^+. All pK_a values are indicated in Table E-2. Since only $_w^w pK_a$ values were

available from literature,[69] the $_s^s pK_a$ values were estimated by assuming that both the

$_w^w pK_{a1,C}$ and $_w^w pK_{a2,C}$ reflect (de)protonations of the carboxylate groups and $_w^w pK_{a3,C}$

indicate pyridine (de)protonation. These assignments are justified by the $_w^w pK_a$ values

reported for similar compounds (see $_w^w pK_a$ and $_s^s pK_a$ data in Figure E-2, Figure E-3,

Figure E-4, Figure E-5, and Table E-4).

The maximum proportion of each species occurs at a pH value that is near the

mean of the two closest pK_a values for the system. For example, the maximum proportion

of H_2DPA occurs at pH = 1.35, which is the average of pK_{a1} and pK_{a2} of H_3DPA^+ and

H_2DPA, respectively.

Using the foregoing modeling approach, two special cases of acid concentrations

are considered to provide the basis for discussion about DPA protonation in solutions

relevant to some of the studies discussed in this dissertation. Specifically, DPA

methylation was conducted in 100% MeOH in 360 mM H_2SO_4 (see Chapter 5 and Table

5-1), and LC separation was carried out in a solution initially 69 vol% H_2O in MeOH

with 13 mM trifluoroacetic acid, which is *approximated* as 10 mM H_2SO_4. It is

noteworthy, however, that TFA is much weaker than H_2SO_4, so $_s^s pH_C$ of 13 mM TFA

may be significantly higher than that of 10 mM H_2SO_4. The true acidity of TFA in water-

MeOH solutions may be investigated further.

---

[69] These pK_a values were obtained in a variety of solutions, typically at low ionic strengths. The ionic strength has a significant impact on pK_a values: As ionic strength increases, the pK_a values for DPA increase [503, 504], but pK_a values of isophthalic acid decrease [505]. Therefore, the numbers employed for these computations are approximate.

The estimated $^s_s pK_{a,C}$ values for these conditions are listed in Table E-2 and the corresponding $^s_s pH_C$ values for 10 and 400 mM H_2SO_4 in the respective solvents in Table E-3. Also in Table E-3 are the relative fractions of each of the DPA species estimated by the $^s_s pK_{a,C}$ and $^s_s pH_C$ data along Eqns. (E-32) through (E-35). The most abundant H_nDPA species for the given conditions are bolded in Table E-3.
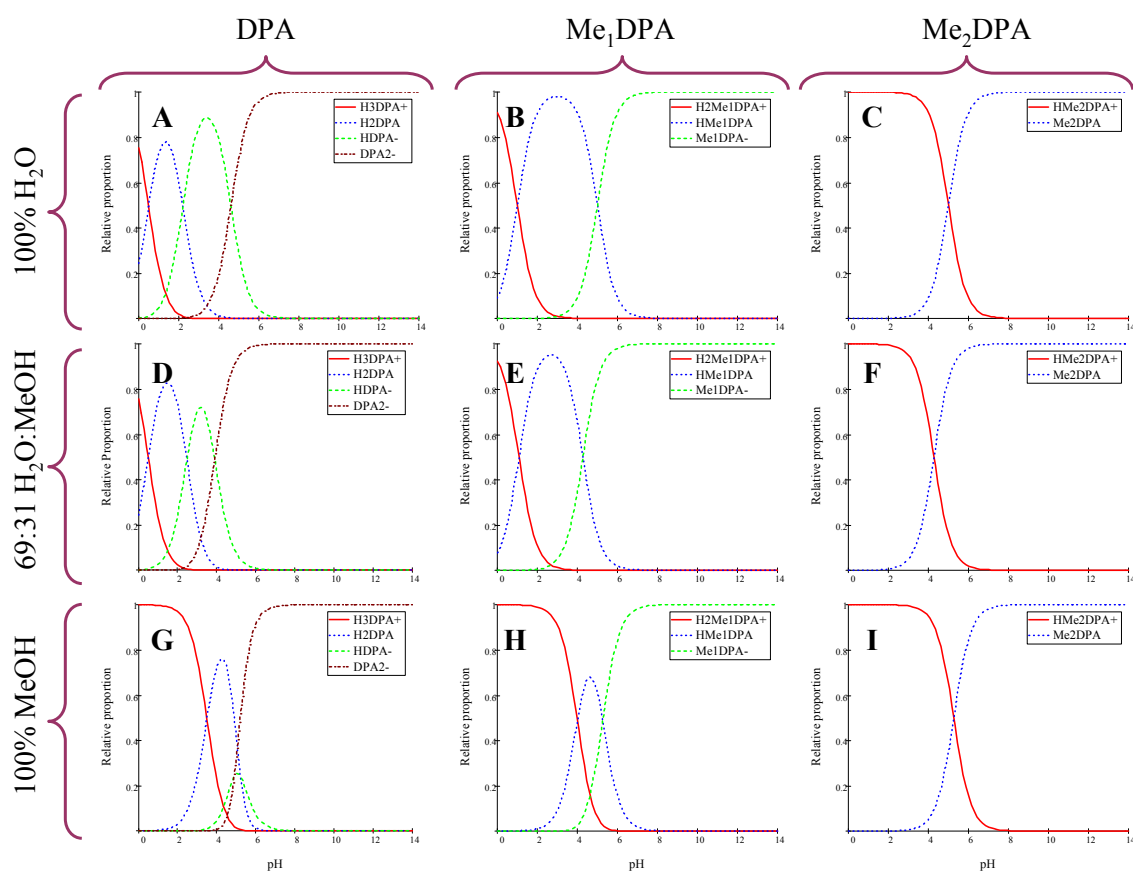
Figure E-6. Relative degrees of protonation as functions of $^s_s pH$ predicted for species from the H_nDPA series (A, D, G), H_nMe_1DPA series (B, E, H), and H_nMe_2DPA series (C, F, I). Solvents are 100% H_2O (A, B, C), 69:31 H_2O:MeOH (in vol%; D, E, F), and 100% MeOH (G, H, I).

Table E-2. $^s_s pK_{a,C}$ values for the DPA derivatives in three solutions with two acid strengths. With H_nDPA, the letters in parentheses indicate whether the predicted (de)protonation occurs on the carboxylate (cb) or the pyridyl nitrogen (pd; see text for further details).

	$^s_s pK_{a,C}$		
	100 % H_2O	69% H_2O	100% MeOH
H_3DPA^+	0.49 (cb)	0.50 (cb)	3.49 (cb)
H_2DPA	2.2 (cb)	2.47 (cb)	4.89[*] (pd)
$HDPA^-$	4.6 (pd)	3.89 (pd)	5.20[*] (cb)
$H_2Me_1DPA^+$	1*	1.1	4
HMe_1DPA	5*	4.3	5.3
HMe_2DPA^+	5*	4.3	5.3

Table E-3. $^s_s pH_C$ values and extents of (de)protonation of DPA, Me_1DPA, and Me_2DPA per the conditions and assumptions of Table E-2. Species of greatest abundance are bolded.

	10 mM H_2SO_4			400 mM H_2SO_4		
	100 % H_2O	69% H_2O	100% MeOH	100 % H_2O	69% H_2O	100% MeOH
$^s_s pH_C$	2.1	2.0	2.8	1.0	1.0	2.3
H_3DPA^+	0.014	0.020	**0.824**	0.206	0.230	**0.938**
H_2DPA	**0.556**	**0.708**	0.175	**0.742**	**0.745**	0.062
$HDPA^-$	**0.429**	0.268	0.001	0.052	0.026	0.000
DPA^{2-}	0.001	0.004	0.000	0.000	0.000	0.000
$H_2Me_1DPA^+$	0.075	0.098	**0.938**	**0.473**	**0.544**	**0.980**
HMe_1DPA	**0.923**	**0.897**	0.062	**0.526**	**0.456**	0.020
Me_1DPA^-	0.001	0.005	0.000	0.000	0.000	0.000
HMe_2DPA^+	**0.999**	**0.994**	**0.996**	**1.000**	**0.999**	**0.999**
Me_2DPA	0.001	0.006	0.004	0.000	0.001	0.001

At a given acid concentration, the model predicts that the most abundant protonated species changes as percent MeOH is increased. For example, at 400 mM H_2SO_4 in 100% H_2O approximately 74% of all H_nDPA exists as H_2DPA, while in 100% MeOH about 94% of H_nDPA is H_3DPA^+.

Table E-4. Select pK$_a$ values for a variety of carboxylic acids and pyridyl compounds from both the literature and computations. Values marked with an asterisk (*) are estimates from the 100% H$_2$O values according to Rosés *et al.* [495].
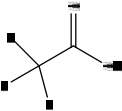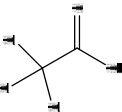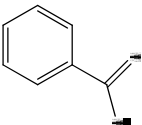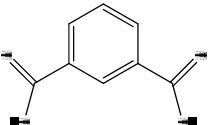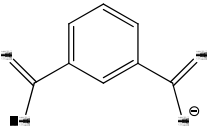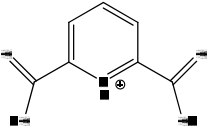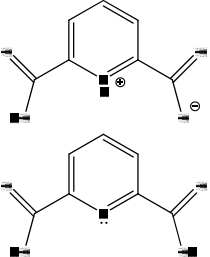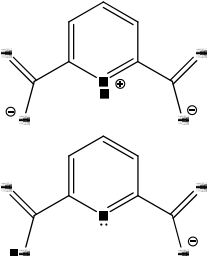
Species	Structure	100% H$_2$O ($_w^w$pK$_{a,C}$)	100% MeOH ($_s^s$pK$_{a,C}$ assumed)
Acetic acid		4.75 [262, 263, 506]	9.6 [262, 263]
Trifluoroacetic acid		0.52 [506]	5.6*
Trichloroacetic acid		0.55 [263]	5.59 [263]
H-BA (Benzoic acid)		4-4.2 [402, 507, 508]	9.3-9.5 [262, 263, 508]
H$_2$-IPA (pK$_{a1}$ of isophthalic acid; **6→3** in Figure E-2)		~3.6 [509-511]	6.6*
H-IPA$^-$ (pK$_{a2}$ of isophthalic acid; **3→5** in Figure E-2)		~4.7 [509-511]	8.9 [508]
H$_3$-DPA$^+$ (pK$_{a1}$ of DPA; **8→1+2** in Figure E-2)		0.49 [309]	3.5*
H$_2$-DPA (pK$_{a2}$ of DPA; **1+2→9+7** in Figure E-2)		~2.2 [74, 173, 307-309]	5.2*
H-DPA$^-$ (pK$_{a3}$ of DPA; **9+7→4** in Figure E-2)		~4.6 [74, 173, 307, 308]	4.9*

Species	Structure	100% H$_2$O ($_w^w$pK$_{a,C}$)	100% MeOH ($_s^s$pK$_{a,C}$ assumed)
H$_2$-Me$_1$DPA$^+$ (pK$_{a1}$ of Me$_1$DPA; **13→10+11** in Figure E-3)		~1 (assumed)	~4*
H-Me$_1$DPA (pK$_{a2}$ of Me$_1$DPA; **10+11→12** in Figure E-3)		~5 (assumed)	~5.3*
H-Me$_2$DPA (**14→15** in Figure E-4)		~5 (assumed)	~5.3*
H$_2$-MPA$^+$ (pK$_{a1}$ of monopicolinic acid; **19→20+21** in Figure E-5)		1.3-1.6 [503, 512, 513]	4.3-4.6*
H-MPA (pK$_{a2}$ of monopicolinic acid; **20+21→16** in Figure E-5)		5.3-5.6 [503, 512, 513]	8.3-8.6*
Pyridine		5.2-5.3 [262, 263, 512]	5.4 [262, 263]

E.4 Discussion of DPA (de)protonation behavior

E.4.1 High DPA acidity

Most published pK$_a$ values for DPA indicate that the first and second observed

deprotonations occur with respective pK$_a$ values of around 2.2 and 4.6. Since these

numbers are close to the pK$_a$ values of the DPA homologue IPA (pK$_a$ of 3.6 and 4.7, respectively; see Figure E-2), it was initially assumed that (de)protonation of DPA is similar, with two proton exchanges occurring between the two carboxylates and the solvent. The reduced pK$_a$ values of DPA relative to IPA were believed to result from the electronegative nitrogen in the aromatic ring. However, this perspective was discovered to be incorrect. Not only might N withdraw electrons by induction, its free electron pair has a high proton affinity, which greatly influences (de)protonation behavior. The protonation of the pyridyl nitrogen adds positive charge that compensates for loss of H$^+$ from a carboxylate, further withdrawing electrons from the carbonyl carbon and perhaps stabilizing the negative carboxylate by forming an internal hydrogen bond (see Figure E-7), although this internal bond formation remains to be validated.
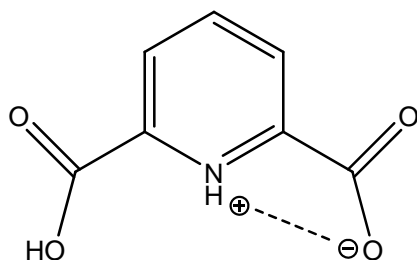
Figure E-7. Possible hydrogen bonding within a DPA molecule.

In short, the presence of N in the aromatic ring greatly increases the acidity of DPA's carboxylate groups. As pH is increased, DPA loses its hydrogens from both carboxylate ions *before* losing its pyridyl hydrogen.[70] This conclusion is supported by

---

[70] The presence of cations, especially multivalent ones with which DPA forms chelates, may influence this trend as well as affect the reactivity of DPA.

published information about proton exchange behavior of H_nMPA, where the first (de)protonation is on the carboxylate group (**19** → **20** in Figure E-5), and the second to loss of H^+ by N (**20** → **16** in Figure E-5) [503]. Therefore, in H_2O at the pH range of ~2 to ~5, H_1MPA is zwitterionic [503].

E.4.2 Influence of pK_a and pH on LC retention times

The same LC method was used for both the acid-catalyzed methylation and the base-promoted hydrolysis studies, but in the latter the DPA and Me$_1$DPA peaks shifted to lower retention times (*cf* Figure 5-1 and Figure 5-4, which are reproduced below along with the total ion mass spectra as Figure E-8 and Figure E-9). In fact, in the hydrolysis study, DPA and the solvent peak co-eluted. Since the injected mixture (10 μL of 334 mM MeO$^-$ + OH$^-$) possessed much more base than the mobile phase did acid,[71,72] DPA and Me$_1$DPA were deprotonated (negatively charged) as they passed through the column, causing them to elute early, giving them non-Gaussian peak shapes, and (following the electrospray ionization process) strongly attenuating the response factor of the mass spectrometer (compare top portions of Figure E-8 and Figure E-9). The reason for the shoulder in the Me$_1$DPA peak in Figure E-9 is unknown but may be related to the presence of both HMe$_1$DPA and Me$_1$DPA$^-$.

---

[71] At 0.1% v/v (13 mM) TFA in 31 vol% MeOH/H_2O, the lowest possible ^w_wpH is ~2 = $-\log(0.013$ M).

[72] A 10 μL volume of 334 mM MeO$^-$ + OH$^-$ requires 260 μL of mobile phase, which is about 64% of the total dead volume of the LC system (400 μL, based on solvent peak holdup time) to neutralize the base, and even more to acidify it sufficiently for near-complete DPA protonation.
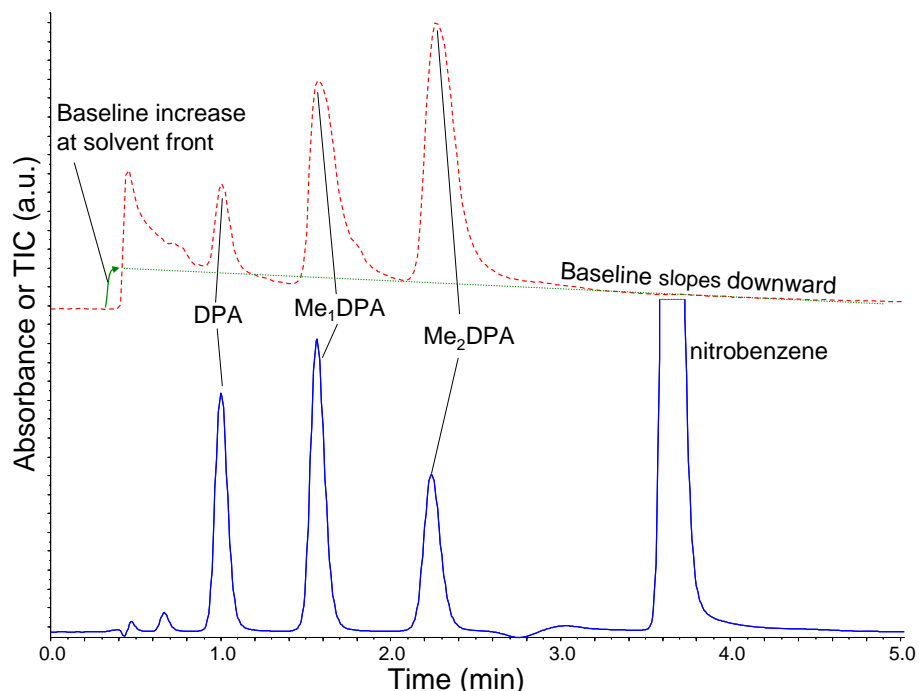
Figure E-8. Total ion count (TIC) chromatogram (red dashed lines) and UV absorbance chromatogram for DPA, Me₁DPA, and Me₂DPA during acid catalyzed methylation study (see Figure 5-1).

The effect of pH on LC retention times is well-documented for weak organic acids, including benzoic acids. Retention times are either quantitatively predicted via known pK_a values, or known retention times are used to estimate the pK_a of an acid [495, 514]. Efforts were not made to correct the separation retention times because a calibration curve produced from diluting known concentrations of DPA in the same basic reaction mixture was linear and furthermore, the three compounds still separated well. Increasing the acid content of the mobile phase in order to neutralize the high sample basicity was not possible since the pH limit of the LC stationary phase is about 1.[73]

---

[73] One must be careful in increasing acid concentration of a mobile phase to correct a problem such as this one since the minimum allowable pH of most silica-based LC stationary phases is ~1 [515].
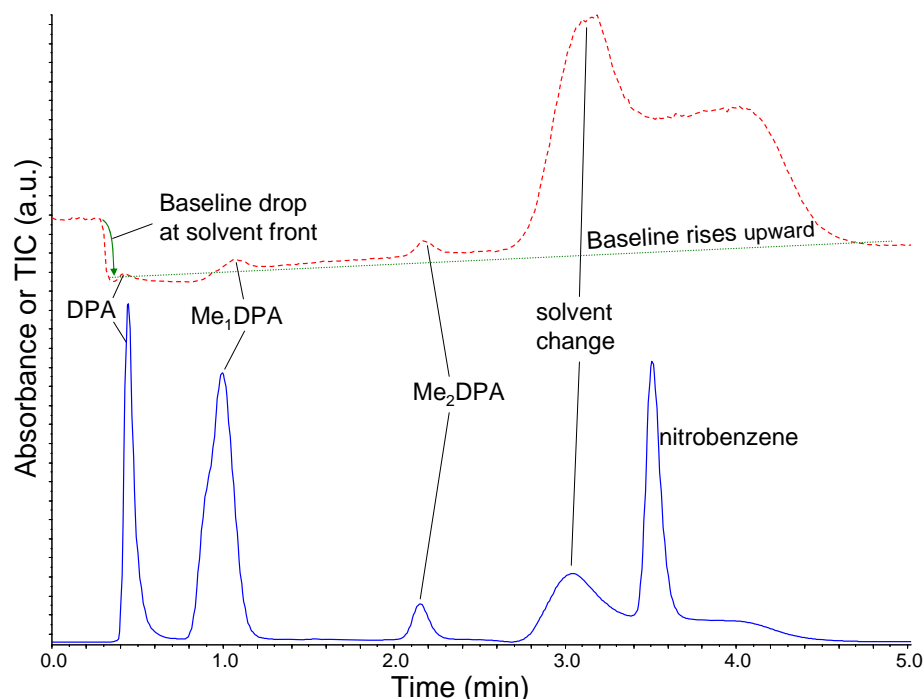
Figure E-9. Total ion count (TIC) chromatogram (red dashed lines) and UV absorbance chromatogram for DPA, Me₁DPA, and Me₂DPA during base promoted hydrolysis study (see Figure 5-4).

E.4.3 Solution pH, pK$_a$ of DPA, and electrospray ionization

The acid-catalyzed methylation study involved injecting H_2SO_4 along with the DPA, Me$_1$DPA, and Me$_2$DPA species in MeOH, while the base-promoted hydrolysis study entailed injecting base ($OH^- + MeO^-$) along with the same intermediates in their deprotonated forms. These two scenarios produced very different responses in the mass spectra of the eluting analytes, which were ionized by positive electrospray ionization (ESI). With H_2SO_4, a high mass spectral signal was observed for DPA, Me$_1$DPA, and Me$_2$DPA compounds. In fact, sulfuric acid's strong acidity caused the entire baseline to increase once the solvent peak (with the acid) eluted from the column. The increased baseline slowly returned to its original position over the course of the run. The baseline

enhancement is understood to result from removal of species from/in the column and/or protonation of contaminants present in the solvent—effects induced by H_2SO_4).

The excess base in the hydrolysis study caused just the opposite effect of H_2SO_4 on the liquid chromatogram (see Figure E-9). At the solvent elution point, the baseline dropped and the DPA, Me_1DPA, and Me_2DPA peak areas/heights were greatly reduced because their acidic protons were removed. The vertical scale of the UV absorbance chromatogram of Figure E-9 is approximately twice that of Figure E-8, yet the TOF-MS peaks of the DPA compounds in Figure E-9 are practically non-existent, even though UV absorbance reveals their presence. The height of the solvent peak in Figure E-9 is approximately 20 times lower than the height of the Me_2DPA peak of Figure E-8! (The quantity of nitrobenzene in the sample of Figure E-8 was much greater than that of Figure E-9, making comparison of this peak unproductive.)

The pattern of DPA (de)protonation indicated at the end of Section E.4.1 is substantiated by these observations. If the pyridyl proton did not exhibit strong binding, then (assuming carboxylate methylation does not significantly alter the pyridyl nitrogen's proton affinity) the Me_1DPA and Me_2DPA would, like DPA, also exhibit weak positive electrospray ionization, which is contrary to actual observations of higher sensitivity to these methyl ester compounds. These facts provide evidence that the first and second deprotonations of DPA (at least in solutions of high water content) are on the carboxylates.

As a result, electrospray ionization of DPA in 13 mM TFA is probably much more efficient in a solvent of lower polarity and reduced proton affinity relative to water (e.g., 100% MeOH). Experiments to confirm this would be easy to conduct.

E.4.4 Acid-catalyzed DPA methylation

Because binding to carboxylate groups is enhanced as the solvent is changed from water to methanol, while binding to basic nitrogens is approximately the same in both solvents, the relative abundance of species **2** and **7** (Figure E-2) is greater in MeOH than in H_2O. In fact, the correlations employed to estimate ${}_s^s pK_{a,C}$ values for the H_nDPA derivatives (see Table E-2 and Table E-3) predict that the order of (de)protonation changes from $\mathbf{8} \leftrightharpoons \mathbf{1} \leftrightharpoons \mathbf{9} \leftrightharpoons \mathbf{4}$ to $\mathbf{8} \leftrightharpoons \mathbf{1} \leftrightharpoons \mathbf{7} \leftrightharpoons \mathbf{4}$ as the solvent is changed from 100% H_2O to 100% MeOH (see ${}_s^s pK_{a,C}$ values in the rows corresponding to H_2DPA and H_1DPA$^-$ in Table E-2 for different solvents).

In an acidic solution, since all species are either positively charged or neutral and since nucleophilic acyl substitution reactions only occur if carboxylic acids are in their acidic form [239], the reactive intermediate of DPA is one of species **8**, **1**, or **2** in Figure E-2. Species **2** can be eliminated from consideration because the ${}_s^s pK_{a,C}$ value of the carboxylate is much lower than pyridine in MeOH; hence, the acid-catalyzed methylation reaction with MeOH occurs either via **8** or **1**. Between these two, **1** (H_3DPA$^+$) is present in much higher abundance based on the information in Table E-3. Consequently, the acid catalyzed methylation reaction, which requires activation of the carboxylate oxygen by its hydrogen bonding to another proton, is inhibited by the positive overall charge of **1**. Likewise, the second methylation probably proceeds via **13** (H_2Me_1DPA$^+$) in Figure E-3, with the same charge inhibition.

Appendix F   DETAILED SPORE GROWTH PROTOCOL

F.1 Day 1: Prepare Leighton-Doi (LD)/Columbia agar media

Note: Steps 1, 2 and 3 may need to be completed only once and the resultant solutions may be stored in a cabinet for future use. Check cabinets first.

1. Prepare agar media

   a. Add 534 mL distilled H_2O to a 1000 mL autoclaved reagent bottle with screw top.

   b. Leighton-Doi agar: Add 4.8 g Leighton-Doi Difco nutrient broth; Columbia agar: add 21 g Difco Columbia broth.

   c. Add 10 g granulated agar to mixture.

   d. Place stir bar into container and mix while heating until boiling rigorously.

   e. Autoclave for 45 min at 15 psi.

2. Prepare steps for salt dextrose solution

   a. Dissolve magnesium sulfate heptahydrate, 5.0 g in 100 mL HPLC H_2O.

   b. Dissolve manganese sulfate monohydrate, 0.4 g in 100 mL HPLC H_2O.

   c. Dissolve ferrous sulfate heptahydrate, 0.06 g in 100 mL HPLC H_2O.

3. Prepare salt dextrose solution

   a. Add 150-160 mL HPLC H_2O to a 250 mL autoclaved screw cap bottle.

   b. Dissolve potassium chloride, 3.8 g in HPLC H_2O.

   c. Dissolve calcium chloride dihydrate, 0.6 g in HPLC H_2O.

   d. Dissolve dextrose, 1.8 g in HPLC H_2O.

   e. Add 1 mL each of 2.1, 2.2, and 2.3 to HPLC H_2O.

   f. Bring the total volume of the HPLC H_2O to 200 mL with additional HPLC H_2O.

   g. Filter sterilize solution through a 0.22 micron Nalgene® filter unit (sterile) inside the laminar flow hood.

   h. Label filter sterilized Nalgene® bottle: salt-dextrose solution for LD broth.

4. Complete salt dextrose agar

    a. While in the hood, add 66 mL salt dextrose to bring the total volume to 600 mL.

    b. Remove from the hood and place in the water bath, bring the temperature to 50°C.

    c. Stir for 1 min to ensure that the mixture is consistent.

    d. Pour agar plates in a clean room.

Procedure: Inoculate LD/Columbia Media for Pure Culture.

1. Prepare isolation plates (isoplates) from freezer stock

    a. Extract bacteria stock solution from freezer.

    b. Inside laminar flow hood, place 10 µL bacteria stock solution in first quadrant of a "normal" Difco Columbia agar plate (without salt dextrose solution) and streak for pure culture, following standard streaking protocol.

    c. Replace freezer stocks.

2. Incubate inoculated isoplates at 37°C for 24 h.

F.2 Day 2: Plate lawns for generating spores

1. Ensure culture is pure.

    a. Gram stain an isolated colony from the isoplate and check for pure culture (follow standard gram staining procedure).

    b. Use a microscope to verify purity (if irregular, contact supervisor).

2. Plate "lawns" using a pure culture from the isoplate.

    a. Inside the laminar flow hood, use a cotton swab (sterile) to collect a section of pure colony from the isoplate.

    b. Make a vertical streak using an inoculated cotton swab along the center of a new salt dextrose agar plate. To reinforce, swab along the entire line 4-5 times.

    c. Rotate the plate 45 degrees to the side and starting from one end, swab across the surface in a side-to-side motion gradually moving downward so that swab makes contact with the entire surface.

    d. Rotating plate back to its original position, swab once more along the centerline several times and in an up and down pattern gradually swab outward towards the left side of the plate.

    e. Repeat previous step, but instead swab towards the right.

    f. Diagonally swab entire plate from one end to the other.

3. Incubate.

   a. Place inoculated plates in a plastic bag and seal using a twist-tie or similar.

   b. Note: There can be more than one plate per bag but they must be of the same bacteria/media.

   c. Place plates in an incubator (32°C or 37°C) for 2 weeks.

F.3 Day 15: Collect spores from lawn plates and prepare for testing

1. Verify that sporulation has occurred.

   a. Remove plates containing "lawns" from incubator.

   b. Take the top plate from each bag and place it under the hood (there should be one plate from each bacteria type/media).

   c. Take a quarter inch sample (using the large end of a sterile inoculating loop) from each plate and suspend it in 1 mL autoclaved HPLC water inside a plastic 25 mL conical tube.

   d. Vortex suspension so that the bacteria are uniform throughout.

   e. Plate 10 µL on a slide for microscopic evaluation.

   f. Note: If sample looks "stringy", then most bacteria are still in a vegetative state and have yet to sporulate completely. Wait 1-2 days and re-check.

   g. Sample should have approximately a 90-95% spore concentration (the other 5-10% being vegetatives).

   h. Note: *Bacillus cereus* does not sporulate well in Columbia agar.

   i. Note: *Bacillus anthracis* Sterne strain turns especially dark when grown in Columbia agar.

   j. Note: *Bacillus thuringiensis* has patchy clear spots when grown in Columbia agar.

2. Collect spores from plates.

   a. Place lawn on a Petri plate rotator inside the laminar flow hood.

   b. Bend the narrow end of a plastic inoculation loop (while still in its sterile package) to form approx. a quarter inch long elbow.

   c. Using the ¼ inch long flat surface of the sterile loop, gently press down on the surface of the plate and slowly spin the rotator.

   d. Start at the center and move elbow outward until you reach the edge of the plate.

   e. After the plate has been cleared, wash spores from loop inside a 50 mL plastic conical centrifuge tube filled with 10 mL sterile HPLC H$_2$O.

f. Note: Spores of the same type and grown in identical media are placed in the same tube.

3. Heat kill vegetative spores and wash.

   a. Heat water bath to 65°C.

   b. Place each of the tubes in the hot water bath for 30 min to kill vegetative cells.

   c. Prepare a screw cap bottle to be used as Sporulation Broth Waste. Label as such.

   d. Verify that the centrifuge is set with the C0650 fixed rotor, time: 10 min, temperature: 19°C, rpm 8000-10,000.

   e. Following the 30 min 65°C bath, centrifuge the conical tubes for 10 min.

   f. Pour off the supernatant (into the waste container) opposite the pellet in one continual motion.

   g. Wash the spores by adding 10 mL of sterile HPLC H_2O to each tube and re-suspending the pellet. Additional sterile HPLC H_2O may be added if the pellet is difficult to re-suspend.

   h. Store the suspension overnight in a refrigerator (~4°C).

F.4 Day 16: Wash spores second time

1. Centrifuge the suspension for 10 min.
2. Pour off supernatant.
3. Re-suspend the pellet in 10 mL of HPLC H_2O -autoclaved.
4. Store the suspension overnight in a refrigerator (~4°C).

F.5 Day 17: Wash spores third time and deliver

1. Washing

   a. Centrifuge the suspension for 10 min.

   b. Pour off supernatant.

   c. Re-suspend the pellet in 5 mL of sterile HPLC H_2O.

   d. Store the suspension overnight in a refrigerator (~4°C).

2. Preparing spores for testing

   a. Place each of the 50 mL tubes under the laminar flow hood.

   b. Vortex each 50 mL tube for 10 s to resuspend settled spores.

c. Using a 1000 µL pipet, aliquot 1 mL from each 50 mL conical tube into 4 small Eppendorf tubes.

d. Label Eppendorf tubes with species name, media type, and growth T.

e. Vortex for 4 min at 1,400 rpm.

f. Using the 1000 µL pipet, remove supernatant from each tube.

g. Place in container and deliver samples to the analytical chemistry lab.

Appendix G   SPORE COUNTING METHODS

Three means of determining the concentration of washed spore suspensions were investigated, namely, colony forming unit (CFU) counting, flow cytometry, and manual counting using a hemocytometer. A single suspension of *B. anthracis* Sterne spores grown at BYU was used for all experiments.

G.1 CFU counting

Multiple solid agar-based growth plates for CFU counting were prepared by dissolving 21 g Difco Columbia broth and 7 g granulated agar in 600 mL of water, autoclaving the mixture, cooling it to approximately 50°C, and then pouring the plates. A series of 10-fold dilutions of spore suspensions in sterile physiological saline solution were prepared. For each dilution, a 1 mL sample was vacuum-filtered through a gridded membrane filter (0.45 μm pore size), the filter was placed atop the agar plate, the plate was incubated for one day at 37°C, and the number of visibly distinct colonies was counted. The plates containing colonies in an easily-counted number (i.e., 10-100) were used for quantitation purposes (too many colonies are difficult to count due to overlapping, and too few reduce the precision of the method). The counts were multiplied by the dilution factor to estimate the concentrations of viable spores present in the original suspension.

The results of the CFU counting study are shown in Table G-1. The row representing the 10^7 dilution factor averaged to be 19, indicating that the concentration of viable spores (and 95% confidence interval) was approximately $1.9 \pm 1.5 \times 10^8$ spores/mL.

Table G-1. CFU counting results for *B. anthracis* Sterne spore suspensions; *NC* = Not Countable.

Dilution factor	Dilution series A		Dilution series B	
	1	2	1	2
10^6	*NC*	*NC*	*NC*	*NC*
10^7	27	27	16	7
10^8	0	2	0	1
10^9	0	0	0	0
10^{10}	0	0	0	0

G.2 Flow cytometry

A BD FACSCanto^{TM} flow cytometer was used at a sample flow rate of 10 µL/min with a counting time of 30 s to explore this method as a rapid means of determining the concentration of diluted samples from stock spore suspensions.

A flow cytometer counts forward and side light scattering events (FSC and SSC, respectively) occurring as a particle-laden fluid stream passes through one or more laser beams. FSC events relate to particle size (volume), while SSC events are dependent upon the internal properties such as internal granularity [516]. The instrument's light detector voltages are adjusted to function for counting particles within a narrow window of size range. Spherical BD FACS 7-color setup beads in 4 and 6 µm sizes (already available in

the lab) were used to verify that the detector voltages were adjusted approximately correctly for counting the 1-μm-sized spores (Figure G-1).[74]

Spores were diluted 100 and 500 times from the original suspension to target approximately 10^6 spores/mL, per the results of the CFU study. Since the spore samples consisted of particles smaller than 4 μm, the detector voltages were adjusted upwards until distinct groupings were observed (labeled "Big" and "Small" in the top part of Figure G-2 because it seemed that there were two "sizes" of spores). These groupings were assumed to capture the 1-μm-sized particles. In all cases, sample collection time was 30 seconds at a flow of 10 μL/min, meaning that 5 μL of spore suspension was sampled per run. The axes of these plots are in arbitrary units that do not correspond directly to size.

Without standard beads sized near the 1-μm spores, it was not possible to know with certainty what the groupings in Figure G-2 represented. An initial best guess was that the group labeled "Little" consisted of single spores, and the "Big" group contained two (or more) spores. Two samples of each dilution were analyzed, and the counts within the boxes designated for each size were converted into a spore concentration for the original sample by multiplying the event count by either 1 or 2 and considering the dilution factor and total volume sampled by the flow cytometer. Table G-2 summarizes the results from this approach. Thus, the average source spore concentration (and 95% confidence interval) was estimated to be 2.12 ±0.58 x10^8 spores/mL.

[74] An old 0.3 μm bead sample was also located, but it had degraded into useless fragments.
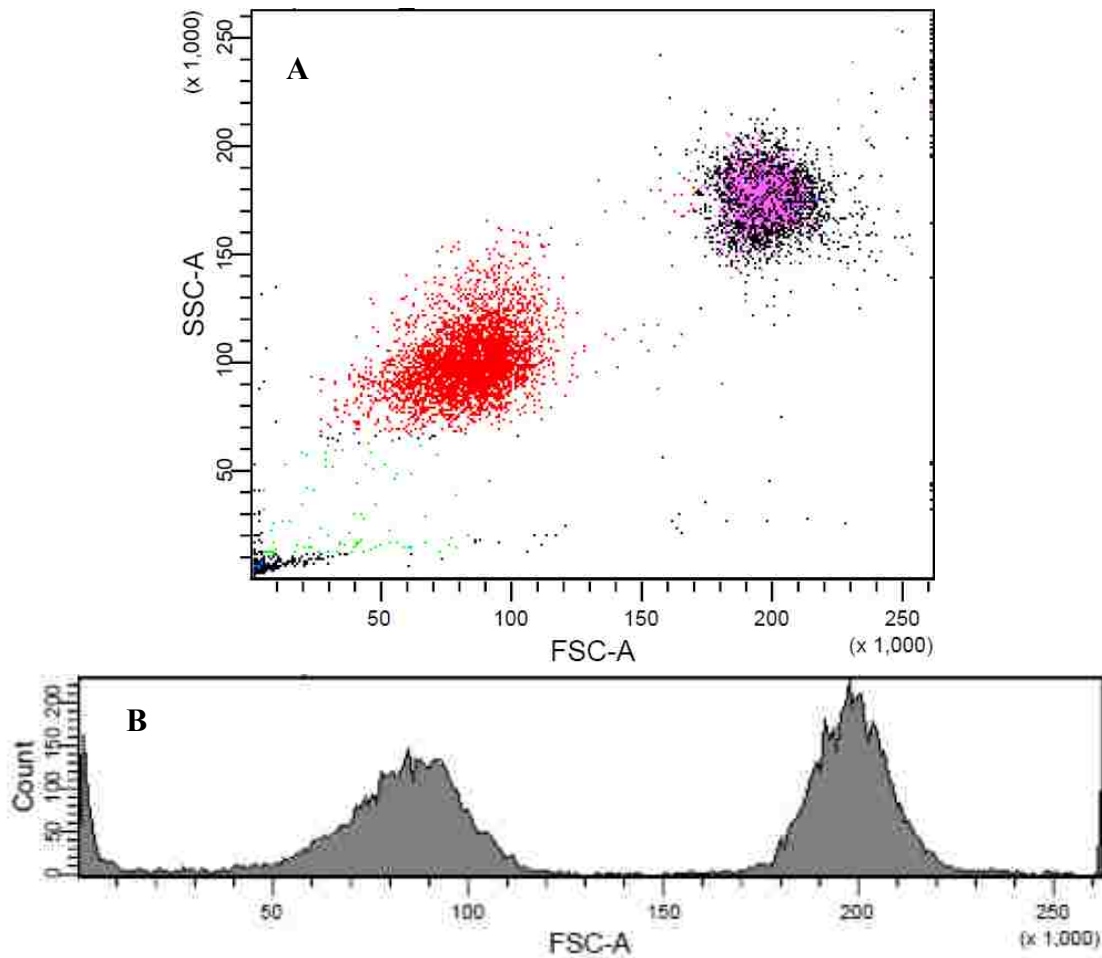
Figure G-1. Optimized flow cytometric analysis of 4 and 6 μm beads.[75] (A): Scatter plot of forward and side scatter events (the different colors in this figure mean nothing for the present discussion) (B): Histogram of forward scatter events (which correspond to particle size). FSC and SSC voltages were 250 and 300 V, respectively.

Since $2.12 \pm 0.58 \times 10^8$ was close to the CFU-counting value of $1.9 \pm 1.5 \times 10^8$ spores/mL and possessed smaller error bars, the flow cytometric method appeared to be an attractive alternative for counting spores. However, closer examination reveals several issues. First, other than the relative positions of the data clusters, the numbers assigned to

---

[75] Color in this figure is misleading. The pink points in the portion of the scatter plot corresponding to the gated portion (not shown) of 6 μm beads labeled with specific fluorophores. Fluorescence events of the 4 μm beads are not indicated by color because they are masked by the "Big" and "Little" selections on the FSC-SSC plot (indicated in Figure G-2 and ensuing discussion).

the putative spore "clumps" (1 vs. 2 spores) had no reliable basis. Second, whether light

scattering events were included or excluding in the total spore count (i.e., the location of

the boxes in the top of Figure G-2) was subjective. Third, the histogram included in the

bottom part of that same figure revealed that the majority of light scattering events were

not captured by the assumed spore populations. The small material was thought to be

spore, cell, and/or residual growth agar debris from scraping spores off growth plates,[76]

but it also may have included spores.
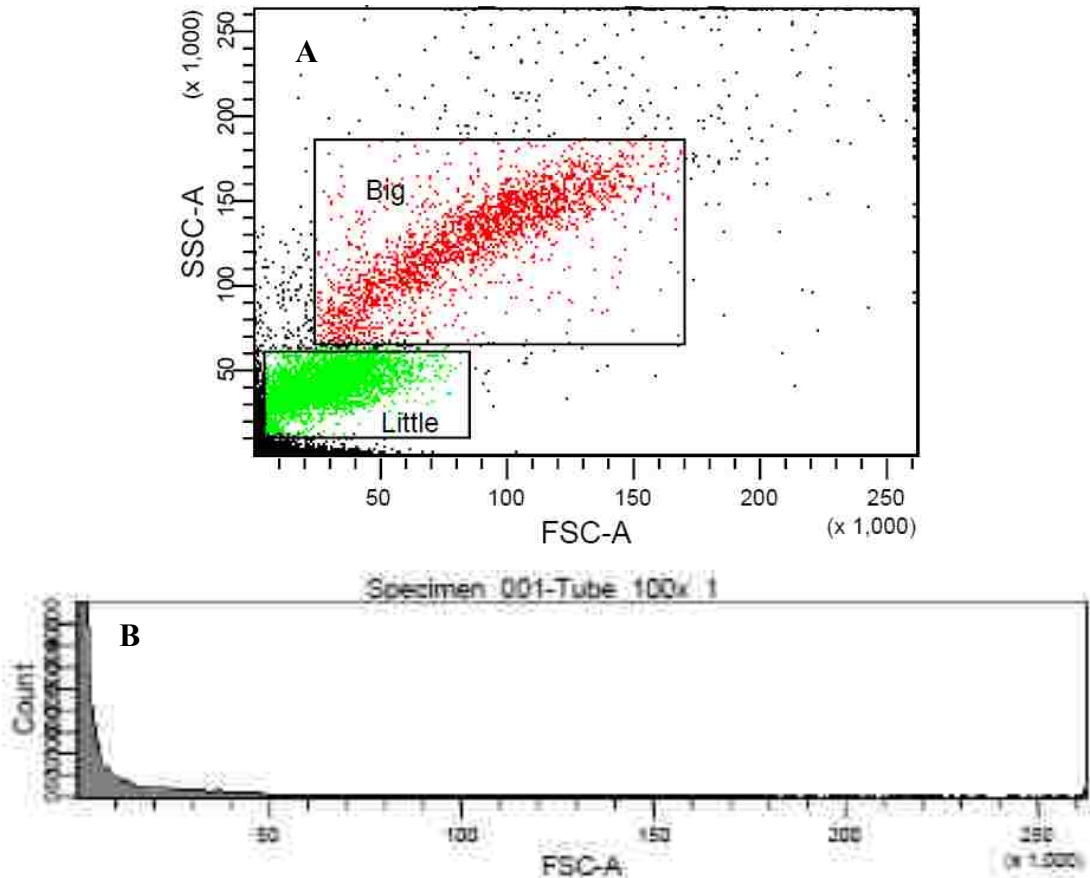
Figure G-2. Flow cytometric analysis of 100-times diluted spore suspension. (A): Scatter plot of forward and side scatter events. (B): Histogram of forward scatter events (which correspond to particle size). FSC and SSC voltages were 550 and 450 V, respectively.

[76] Spore pellets and spore extracts have been slightly brown-colored, indicating the presence of this agar.

Table G-2. Estimated concentration of source spore suspension based on flow cytometry data.

Dilution factor	# counts	Assumed # spores/count	Total # spores in 5 µL volume	spores/mL
100	2386	2	8374	1.67×10^8
	3602	1		
100	2842	2	9924	1.98×10^8
	4240	1		
500	662	2	2354	2.35×10^8
	1030	1		
500	675	2	2481	2.48×10^8
	1131	1		

Fourth, neither of the aforementioned counting methods gave results consistent with measurements of total DPA concentration in the stock spore solution (3.85 ± 0.46 mM, per the previous report). *B. anthracis* spores weigh about 5 picograms [39] and are approximately 10 wt% CaDPA [181, 517]. Using these values plus the molecular weight of CaDPA (205.2 g/mol), the expected concentration of DPA for a spore concentration of 2×10^8 spores/mL is approximately 0.5 mM (converting the observed DPA concentration to spore count gives about 1.6×10^9 spores/mL). Although these computations were not based on actual weight measurements of the *B. anthracis Sterne* spores in question, the observed DPA content was approximately an order of magnitude higher than predicted based on the best available information in the literature.

G.3 Direct count by hemocytometry

A hemocytometer was utilized to visually count the refractile bodies present in a spore suspension. This device is essentially a special microscope slide with a grid of very

fine lines etched into it and a means of suspending a coverslip above the grid at a fixed

distance. The coverslip was first installed and approximately 10 μL of a spore suspension

were drawn into the gap between the facing surfaces of the slide and coverslip by

capillary action; thereby, discrete fixed volumes defined by the borders of the grid are

created. The number of particles (in this case, spores) within a 200 x 200 μm square area

of the grid (4 nL) was counted using the Zeiss Axio Imager.A1 at 400x magnification and

multiplied by the appropriate conversion factor (250,000) to give the spores per mL.

Counting required continual up and down adjustment of the focal plane to visualize all

spores in the area because the distance between the plate and the slide is about 100 μm

and thus the spores reside at the different focal lengths.

The red square overlaid on the left side of the hemocytometer grid in Figure G-3

indicates the area in which spores were counted. Six such areas for each dilution (100x

and 500x; cf. Table G-2) were analyzed, results of which are presented in Table G-3. Any

particle appearing as a refractile body was counted as a spore, even if it was contained

within a larger, non-refractile rod-shaped entity (approximately 1 in 20 of the refractile

bodies appeared in such a form, and many of them were trapped in things granular and

irregular in shape). This method of counting spores averages out to be 5.0 ±0.8 x10^9

spores/mL.

G.4 Conclusions regarding spore counting methods

Three counting methods were used to estimate the stock concentration of *B.*

anthracis Sterne spores, namely, colony forming unit counting, flow cytometry counting,

and direct counting on a hemocytometer. The results were 1.9 ±1.5 x10^8, 2.12 ±0.58

$x10^8$, and $5.0 \pm 0.8 \times 10^9$ spores/mL, respectively. CFU and flow cytometry give spore

concentrations that are order of magnitude lower than the observed amount of DPA

would indicate. Since direct counting is consistent with total observed DPA, it is

concluded that only by direct count can spores be reliably quantified.
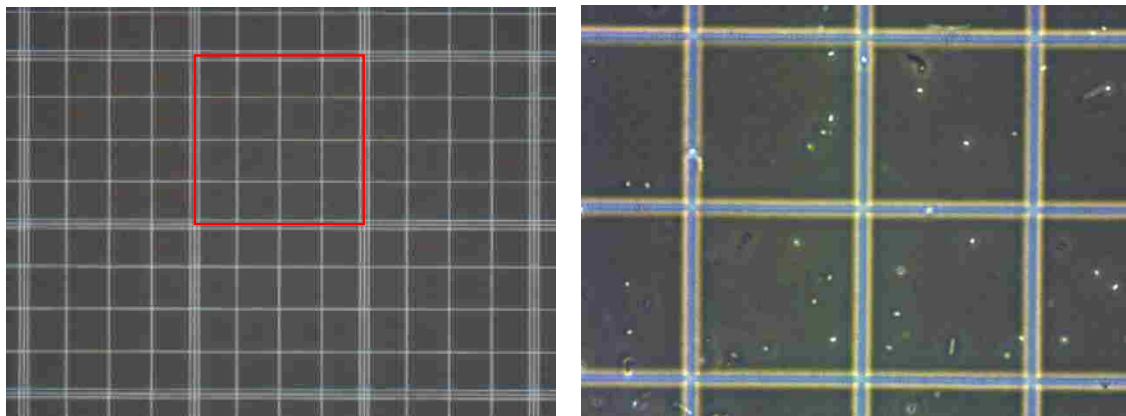
Figure G-3. Light microscopy images of spores on the hemocytometer grid at 100x magnification, phase bright (left) and 400x, phase contrast (right). The red square is 200 μm on a side and defines a volume of 4 nL.

Table G-3. Hemocytometer counts.

Sample ID	100x dilution		500x dilution	
	Raw count	Spores per mL	Raw count	Spores per mL
1	167	4.18×10^9	38	4.75×10^9
2	155	3.88×10^9	57	7.13×10^9
3	151	3.78×10^9	41	5.13×10^9
4	149	3.73×10^9	53	6.63×10^9
5	158	3.95×10^9	45	5.63×10^9
6	170	4.25×10^9	55	6.88×10^9

CFU counting is the most time-consuming counting method. It should accurately

give the concentration of *viable* spores present in a suspension, provided that they remain

separated and don't stick together. Flow cytometry is the most rapid and convenient of the methods since it requires less than 1 minute per sample, but it does not distinguish individual spores from spore clumps or other particles. Addition of beads closer in size to the spores (especially fluorescing beads), adjustment of the fluid sheath flow in the instrument, and/or use of advanced techniques such as spore-specific binding peptides or antibodies [518] would help to clarify this issue. Finally, since hemocytometry is based on direct visual inspection of spores (allowing for assessment of spore sample purity) and is fairly simple and rapid, it is the method of choice for estimating total spore quantities. It does suffer from several drawbacks in that it is tedious, it relies upon human judgment to classify a particle as a spore (although this is greatly facilitated by the spores' bright, refractile appearance in the phase contrast mode), and it does not distinguish viable spores from nonviable ones.

Since one principal objective of this research project is to examine and optimize the yield of the derivatized spore biomarkers for analysis by GC-MS, distinguishing between "live" and "dead" spores is not necessary. Therefore, hemocytometry is recommended for counting spores.